MECHANICAL PROPERTIES OF CARBON/GRAPHITE COMPOSITES

A Thesis presented

for the degree

of

Doctor of Philosophy

by

Gary Savage

Department of Metallurgy and Materials Science,
Imperial College of Science and Technology
University of London.

September, 1986.

For Grandad

CONTENTS

		Page
Abstract		
Section 1	INTRODUCTION	1
Section 2	BASIC PRINCIPLES AND LITERATURE REVIEW	5
2.1.	Examination of Japanese Leads	5
2.2.	Polyfurfuryl Alcohol	11
2.3.	Pyrolysis of Polymers	14
2.3.1.	Pyrolysis of Organic Materials	14
2.3.2.	Carbon Yield of Polymers	19
2.3.3.	Detailed Chemistry of the Pyrolysis of Polyfurfuryl Alcohol	21
2.4.	The Structure of Amorphous Carbon	25
2.4.1.	Changes in the Structure of the Resin during Carbonisation	25
2.4.2.	X-Ray Small Angle Scattering	27
2.4.3.	The Structure of Amorphous Carbon	28
2.4.4.	Higher Temperature Treatments of Vitreous Carbon	34
2.5.	Vitreous Carbon Composites	37
2.6.	Mechanical Properties and their Measurement	43
2.6.1.	Elasticity	43
2.6.2.	Theoretical Strength of Materials	46
2.6.3.	Fundamentals of Fracture Mechanics	47
2.6.4.	Fracture Strength and its Measurement	51
2.6.5.	Fracture Toughness	56
2.6.6.	Fracture Toughness Measurement	62
2.7.	Mechanical Properties of Amorphous Carbon	64
2.7.1.	General Considerations	64
2.7.2.	Elastic Response of Amorphous Carbon	66
2.7.3.	Hardness of Vitreous Carbon	68
2.7.4.	Strength and Fracture	71
Section 3	APPARATUS AND EXPERIMENTAL PROCEDURE	73
3.1.	Materials	73
3.2.	Specimen Production	73
3.2.1.	Casting of the Polymer Resin	73
3.2.2.	Casting Composite Resins	74
3.2.3.	Production of Amorphous Carbon	75
3.3.	Microstructional Analysis	85
3.3.1.	Scanning Electron Microscopy	85
3.3.2.	Pore Size and Distribution Measurement	85
3.3.3.	Density Measurements	87
3.3.4.	Porosity Measurements	87

Page

Section 3 (Cont'd)

3.4. Particle Size Analysis 87
3.5. Microhardness Testing 88
3.6. Mechanical Testing 88

3.6.1. Specimen Preparation 88
3.6.2. Loading Techniques 89
3.6.3. Fracture Strength Determination 89
3.6.4. Fracture Toughness Determination 89

Section 4 RESULTS AND DISCUSSION 97

4.1. Polymer Production 97
4.2. Pyrolysis 97
4.3. Initial Examination of Amorphous Carbon Produced by Pyrolysis of Pure Polyfurfuryl Resin 98
4.4. The effect of Curing Time of the Resin on the Properties of the Resulting Amorphous Carbon 104
4.5. Effect of Curing Temperature on the Properties of Pyrolysed Polyfurfuryl Alcohol 112
4.6. Effect of Catalyst Concentration on the Properties of Pyrolysed Polyfurfuryl Alcohol 119
4.7. Summary of Experiments carried out on Pure Resin 125
4.8. Vitreous Carbon - Graphite Composites 126

4.8.1. Introduction 126
4.8.2. Effect of Volume Fractions of Graphite on the Properties of the Composite 130
4.8.3. Effect of Graphite Particle Size on the Properties of the Composite 141

4.9. Use of Zinc Oxide as a Pore Former in Vitreous Carbon 153

Section 5 CONCLUSIONS AND SUGGESTIONS FOR FURTHER WORK 163

5.1. Conclusions 163
5.2. Suggestions for Further Work 166

APPENDIX 168

A. Statistical Analysis carried out on Mechanical Testing Results 168
B. Computer Program used to Calculate the Properties of Amorphous Carbon 172
C. Calculation of Particle Size Distribution from a Distribution of Section Diameters 182

C.1. Introduction 182
C.2. Saltykov's Method 187
C.3. Computer Program to Perform Saltykov Correction 192

ACKNOWLEDGEMENTS 194

REFERENCES 195

A B S T R A C T

The thesis describes the results of an investigation into the relationship between the microstructure and mechanical properties of an amorphous carbon and amorphous carbon/graphite composites.

Acid catalysed polyfurfuryl alcohol was used to prepare a cured resin from which an amorphous carbon was produced by heating the resin to 1000°C in an inert atmosphere. It was found that many of the properties of the amorphous carbon could be related to the process variables. A study was made of the effects of curing time, curing temperature and catalyst concentration on the carbon yield, the density, the modulus of rupture strength and the fracture toughness of the carbon. Water is a by-product of the polymerisation reaction and the observed porosity of the carbon was found to correlate well with the mechanical properties.

When natural graphite was added to the resin, a strong, tough carbon/graphite composite was produced. Studies were made on the effect of the size of the graphite particles and the amount added to the resin on the resulting mechanical properties. It was found that for a given amount of added graphite, the strength decreased with graphite size, however the toughness reached a maximum value for graphite particles, about 20μm across. An examination of the fractured surfaces of the carbon/graphite composites revealed that the graphite acted as a reinforcing agent by deflecting the propagation of growing cracks. When the graphite exceeded 20μm across, the cracks propagated by passing through the graphite rather than passing round it.

The use of carbon/graphite composites as potential writing materials requires a structure with a high degree of porosity. Experiments have been conducted on the addition of zinc oxide to the batch material to provide porosity in the fired materials. The properties of the porous carbons have been investigated and it has been shown that the ZnO must be extremely well dispersed to produce a fine micro-porous material.

SECTION 1

INTRODUCTION

During the summer of 1977 Imperial College undertook a preliminary examination of some commercially produced sub.mm. pencil leads. The leads were produced in Japan and marketed in the U.K. by the Pentel Company and Berol Ltd. under licence. It was readily established (1) that the pencil leads examined were not of the conventional graphite-clay mixtures traditionally used for pencil lead manufacture, but consisted almost entirely of carbon. A review of the patent literature revealed that many new types of pencil lead based on mixtures of graphite and organic polymers had been patented around that time, particularly by Japanese companies.

At the request of Berol Ltd. the College undertook a research programme to continue the investigation of these new leads and to assist the company in developing its own products in this new field.

Analysis showed that the original leads contained approximately 95 wt% carbon (or other non-crystalline organic material) and that they were composed of approximately 50% of mineral graphite and 50% of carbon from another source. Examination of patent literature and the book "Polymeric Carbon, Glass and Char" (2) showed that a large range of organic polymers and resins may be pyrolised to give amorphous or glassy carbons by heating in a controlled atmosphere to about 1000°C. Continued heating to 2000°C or above can sometimes produce carbon fibres of high modulus.

Pyrolysis to 1000°C, however, is capable of producing fibres with an amorphous structure and a moderate tensile strength. The process is accompanied by a considerable volume contraction, for example, up to 60% for the pyrolysis of a phenolic resin to 1200°C. One would therefore expect such a product to be fairly porous.

It was concluded, from optical and scanning electron microscopy, x-ray difraction and weight loss data, that the Japanese leads were made by pyrolising a mixture of mineral graphite and an organic polymer or resin. There was no way in which the original organic resin could be identified as pyrolysis completely destroys its nature.

A wide range of phenolic and thermosetting resins were investigated as precursors for the production of sub.mm. leads (3). The extrusion of compositions based on these resins mixed with graphite produced leads which were able to be converted almost entirely to carbons by heating to high temperatures in an inert or reducing atmosphere. Compositions based on phenolic resins were found to be unsatisfactory due to swelling and fusion of adjacent leads during processing, and porosity which results from the evolution of gas during curing and the initial stages of firing (4). On the otherhand, considerable success was achieved with leads based on polyfurfuryl alcohol resins. It is possible to extrude and fire these leads to give a good finish, strength and promising writing properties. The effect of composition and heat treatment on the properties of the fired leads were investigated and it was found that the Modulus of Rupture strength was as good as, if not better than, those of the Japanese competitors.

For this reason, then, it was decided to press on with the work and attempt to produce a commercially viable product based on polyfurfuryl alcohol/graphite compositions.
The aim of this present work is to attempt to understand the factors affecting the strength of polymer leads by an investigation of the mechanical properties of the pyrolised polymer and polymer/graphite composites.

Mechanical failure of amorphous materials is almost completely controlled by brittle fracture. This means that the failure occurs with negligible plastic deformation, without prior warning (due to the very rapid rates of crack propagation) and involves low energy absorption.

The mechanical properties of pyrolised polymer and polymer/graphite composites are discussed in terms of their fracture strength and toughness, these parameters being defined on the basis of the flaw concept which was introduced by A.A. Griffith in 1920 (5). Analytical solutions for the fracture strength and toughness are available for several different test-piece geometries. Generally the specimens used in the determination of fracture toughness contain an initial crack and it is assumed that no growth occurs prior to catastrophic failure. It is standard procedure to accept as valid any fracture toughness test on a brittle material if there is a linear relationship between load and displacement up to the point at which failure occurs i.e., the assumption is made that no sub-critical crack growth takes place.

Since fracture toughness is a material constant, providing the standard procedure is observed, the values obtained for any given material ought to be independent of the test geometry.

The techniques used in this work to measure the fracture strength and toughness of the polyfurfuryl alcohol/graphite material will be the beam and Single Edge Notched Beam geometries respectively. These have been chosen because of their relative simplicity to set up and operate and because they are believed by many workers (6) to be the most reliable. In the S.E.N.B. tests, each of the test-pieces contains a pre-determined flaw in the form of a blunt machined notch. Fracture strength and toughness results will be compared with fabrication parameters and microstructural analysis of the material in an attempt to establish the relationships.

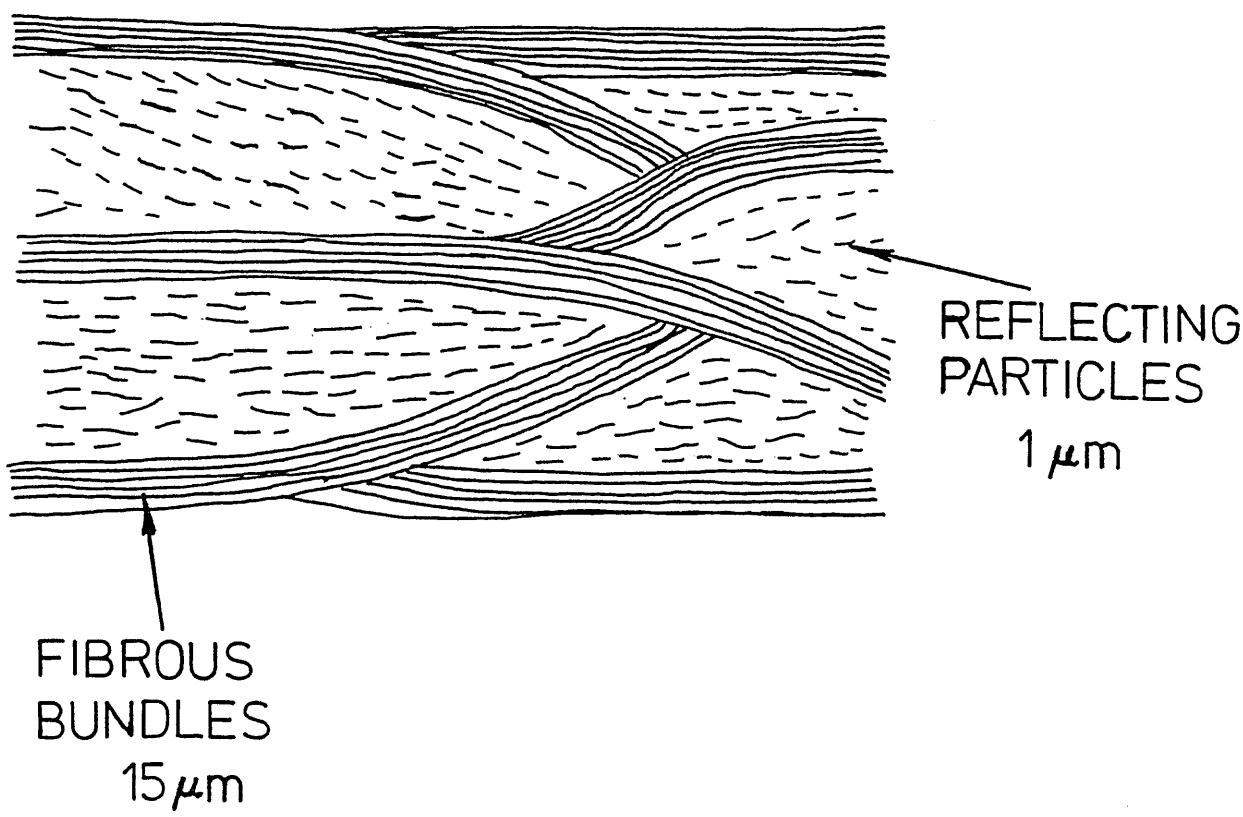
SECTION 2

BASIC PRINCIPLES AND LITERATURE REVUE

PRODUCTION, STRUCTURE AND PROPERTIES OF AMORPHOUS CARBON

2.1. Examination of Japanese leads

Samples of the sub mm leads marketed by Berol and those of Pentel were examined using optical microscopy. Both samples showed a highly oriented structure with fibres running parallel to the axis of the lead. At magnifications of 400 times or greater, bundles of fibres approximately 15 μm in diameter were clearly visible, with highly reflecting particles of 1 μm or less sandwiched between the bundles. The small particles were thought to be graphite flakes. An examination of the fractured ends of leads showed no sign of micro-fibrils, such as would have been expected if high tensile fibres had been incorporated in the lead.



The two types of leads showed minor differences indicating that although similar in nature they were not identical material.

Scanning electron microscopy of the surface of longitudinally fractured leads supports the evidence obtained from the optical examination. The longitudinally crushed leads show a highly oriented structure along the axis of the lead. However, there is no direct evidence of individual fibres in the material. At high magnifications, small particles appear embedded in a matrix.

The differences between Berol and Pentel leads were slight, from which one can draw the conclusion that the processes of manufacture must have been similar. X-Ray powder diffraction, used to determine the crystalline phases present, showed graphite to be the major phase in both samples. A number of very weak extra diffraction lines were observed indicating 1 to 2% of an additional phase or phases. The samples were subsequently calcined in air for 72 hours at 700°C to remove all traces of graphite and organic matter (1).

Sample	Initial Weight	Weight of residue	% Loss
Berol	0.0386g	0.0022g	94.3
Pentel	0.0442g	0.0019g	95.7

In each case the residual ash was a pale chocolate colour. X-Ray examination showed no trace of graphite but both ash samples contained quartz and another phase, thought to be sanidine $(Na,K)Al\ Si_3O_8$.

It can be seen that the Japanese leads contain approximately 95wt% carbon (or other non-crystalline organic material). The carbon could be of several types since the presence of mineral graphite is shown by the presence of silicates in the calcined residues. Mineral graphite is assumed to contain approximately 92wt% carbon, which indicates that the leads were composed of approximately 50% of mineral graphite and 50% of carbon from another source. The microscopic analysis would suggest that the 'other' source of carbon is an amorphous product of the pyrolysis of an organic material. This suggested that the leads were made by pyrolising a mixture of mineral graphite and an organic polymer or resin.

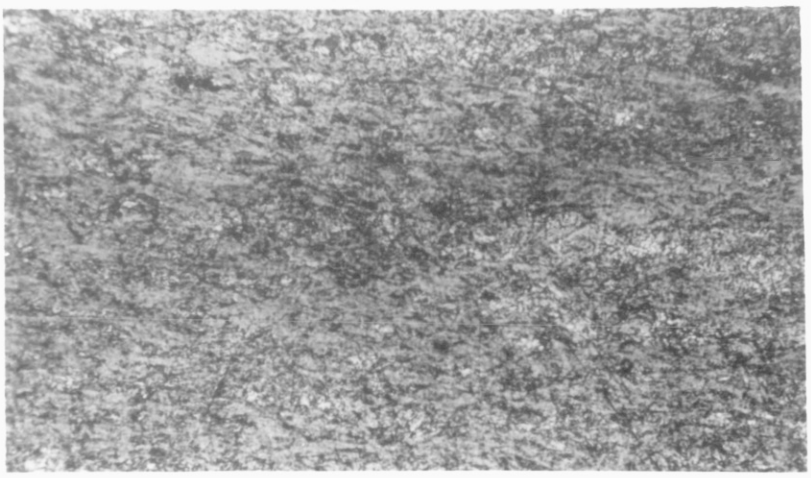


Fig. 2.1 x 250

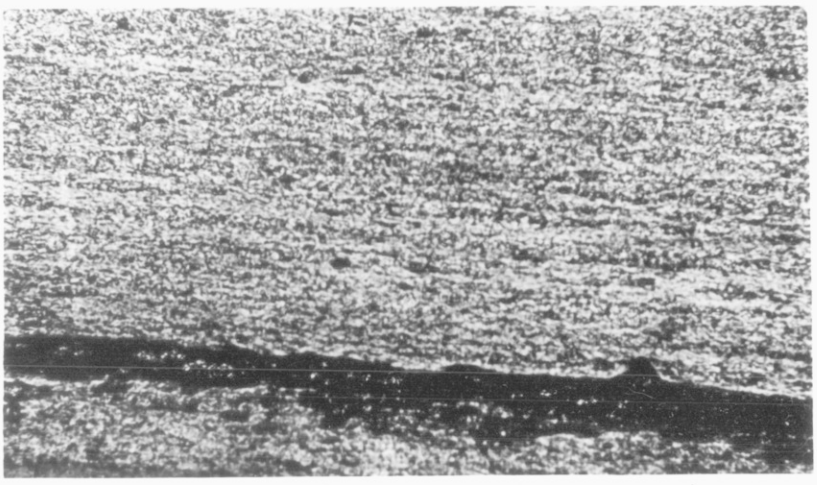


Fig. 2.2 x 300

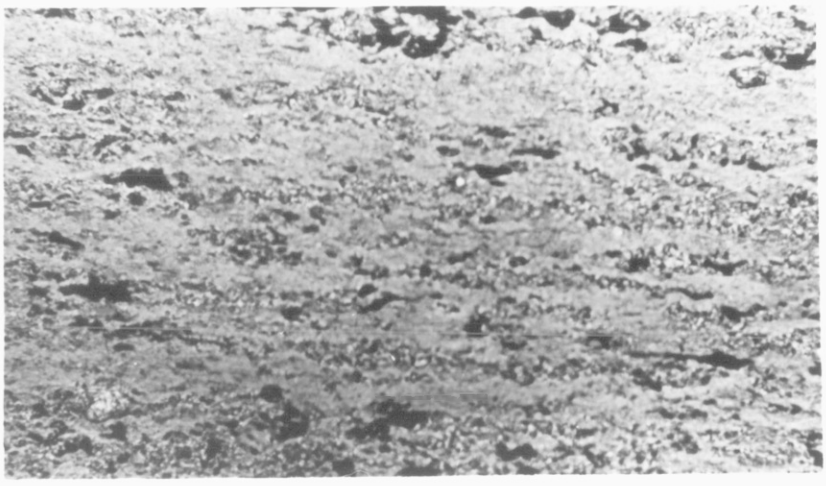


Fig. 2.3 x 380

Figs. 2.1 to 2.3

Optical micrographs of Japanese sub mm leads showing their highly oriented structure of fibres running parallel to the lead and small graphite particles.

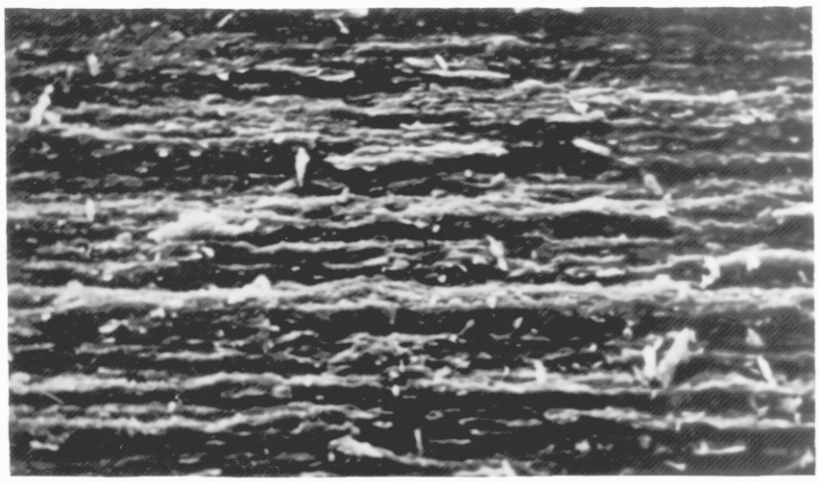


Fig. 2.4 x 200



Fig. 2.5 x 1000



Fig. 2.6 x 5000

Figs. 2.4 to 2.6

Scanning electron micrographs of longitudinally fractured sections of Berol leads.



Fig. 2.7 x 500



Fig. 2.8 x 1000

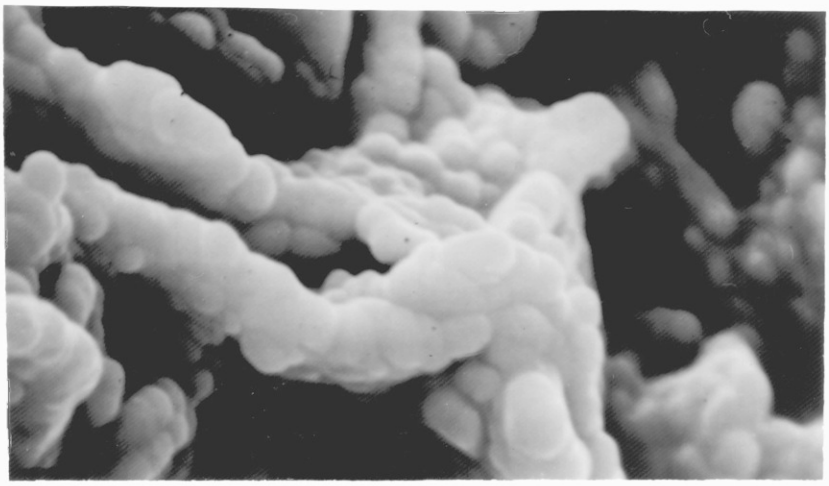


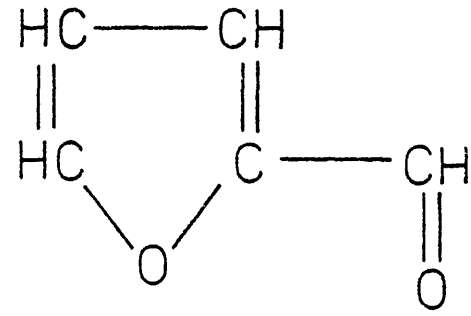
Fig. 2.9 x 5000

Figs. 2.6 to 2.9

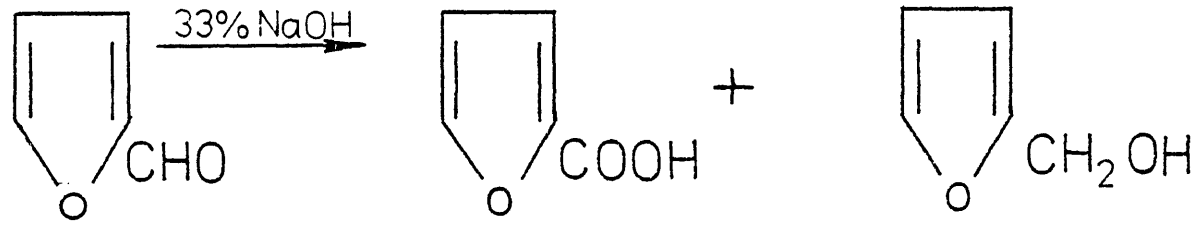
Scanning electron micrographs of twist fractures from Berol leads.

2.2 Polyfurfuryl Alcohol

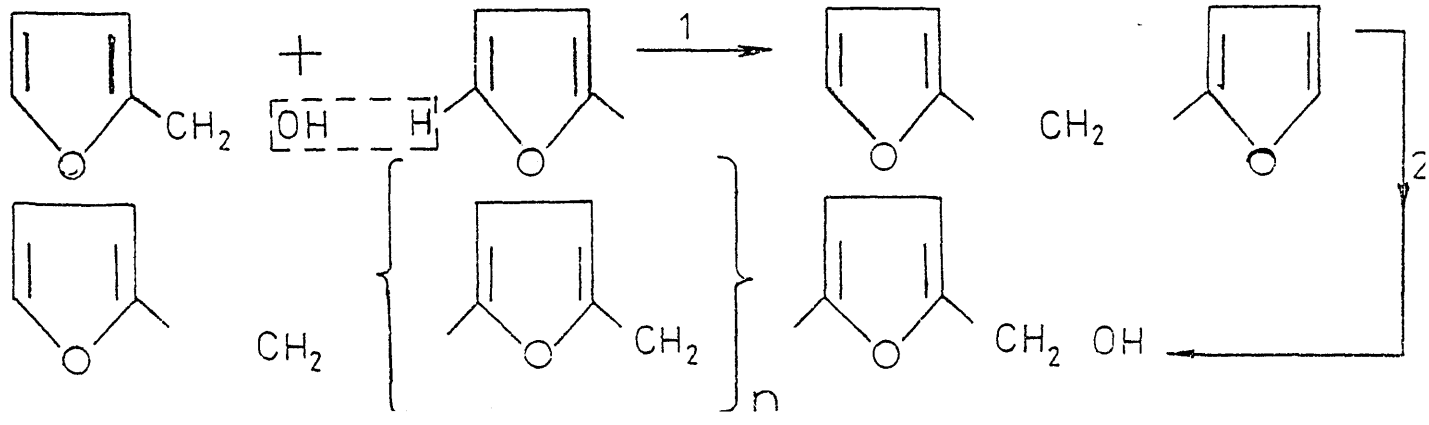
Furfuryl alcohol is made from furan,



which is derived from waste vegetable matter (7). The compound is produced on a large scale from oathulls which gives a 10% yield when obtained as a by-product in the manufacture of Quaker Oats (8).



Furan resins (9) are produced by the resinification of furfuryl alcohol in the presence of an acid catalyst, usually with heat, until the desired degree of polymerisation is achieved. The polymerisation, which is exothermic, produces a thermosetting resin. Heat is required before the process will commence and the reaction can be stopped at any point by cooling the resin and catalyst mixture. The chemical reaction involves the alcohol group from furfuryl alcohol and an active hydrogen from the ring of an adjacent molecule to give difurfuryl alcohol. Intermolecular dehydration (stage 1) is followed by formation of a linear polymer (stage 2) and the final reaction stage, again in the presence of an acid catalyst, produces a highly crosslinked, infusible resin (10).



Commercial furfuryl alcohol resins, such as that supplied by Berol Ltd for the present work, are low viscosity liquids which have been produced by the action of heat and an acidic catalyst on furfuryl alcohol. In order to get a storage - stable product, the acid catalyst is neutralised before a viscous stage is reached which would prevent effective neutralisation. As a result, the commercial product still contains large amounts of unreacted furfuryl alcohol monomer.

The thermosetting of the liquid intermediate resin is accomplished by the addition of an acidic catalyst, usually followed by the external application of heat. In the thermosetting process, any monomeric furfuryl alcohol present will largely be polymerised (condensed), with the splitting out of water which will vapourize under the prevailing conditions. A small amount of the furfuryl alcohol undoubtedly will vapourise and be lost before it can be chemically condensed. Both the water and the furfuryl alcohol vapours will tend to create porosity in the thermoset product which, of course, is undesirable. The obvious remedy is to use liquid resins which have been partially polymerised and, therefore, will give only small amounts of water and furfuryl alcohol vapours during the thermosetting step. This will, of course, cause an increase in viscosity of the resin making it more difficult to use so a compromise must be struck between the ease of use and the porosity of the cured and polymerised material (11).

Furfuryl alcohol has been termed a 'reactive' compound (12).

The patent literature describes a great number of the catalysts used to resinify F.A. Mineral acids, strong acids,Lewis acids and acyl halides are very active. Industrially, control of the exothermic reaction is achieved by regulation of catalyst concentration and temperature. The mechanism of resinification has been inferred, in part at least, by identification of the intermediate products formed. The initial and predominant reaction is intermolecular dehydration (see p.11). This leads to higher molecular weight condensation products in which furan rings are linked together by methylene bridges in a linear chain. To a small extent, furfuryl ether is also formed. Formaldehyde, resulting from thermal decomposition is always found in the reaction mixture. Some hydrolytic fission can also be inferred based on infra-red evidence.

Experimental evidence (13) indicates that formaldehyde formed during resinification may, under appropriate conditions, recondense with the intermediate products, and this is one way by which the chains can become chemically cross linked. Finally, cross linking may occur by a mechanism involving the nuclear double bonds during the later curing stages. This explains the high degree of chemical inertness of the thermally set resin. Fig 2.10 illustrates the linkages most likely present in cured F.A. polymers; it is not intended to represent the unit polymer itself.

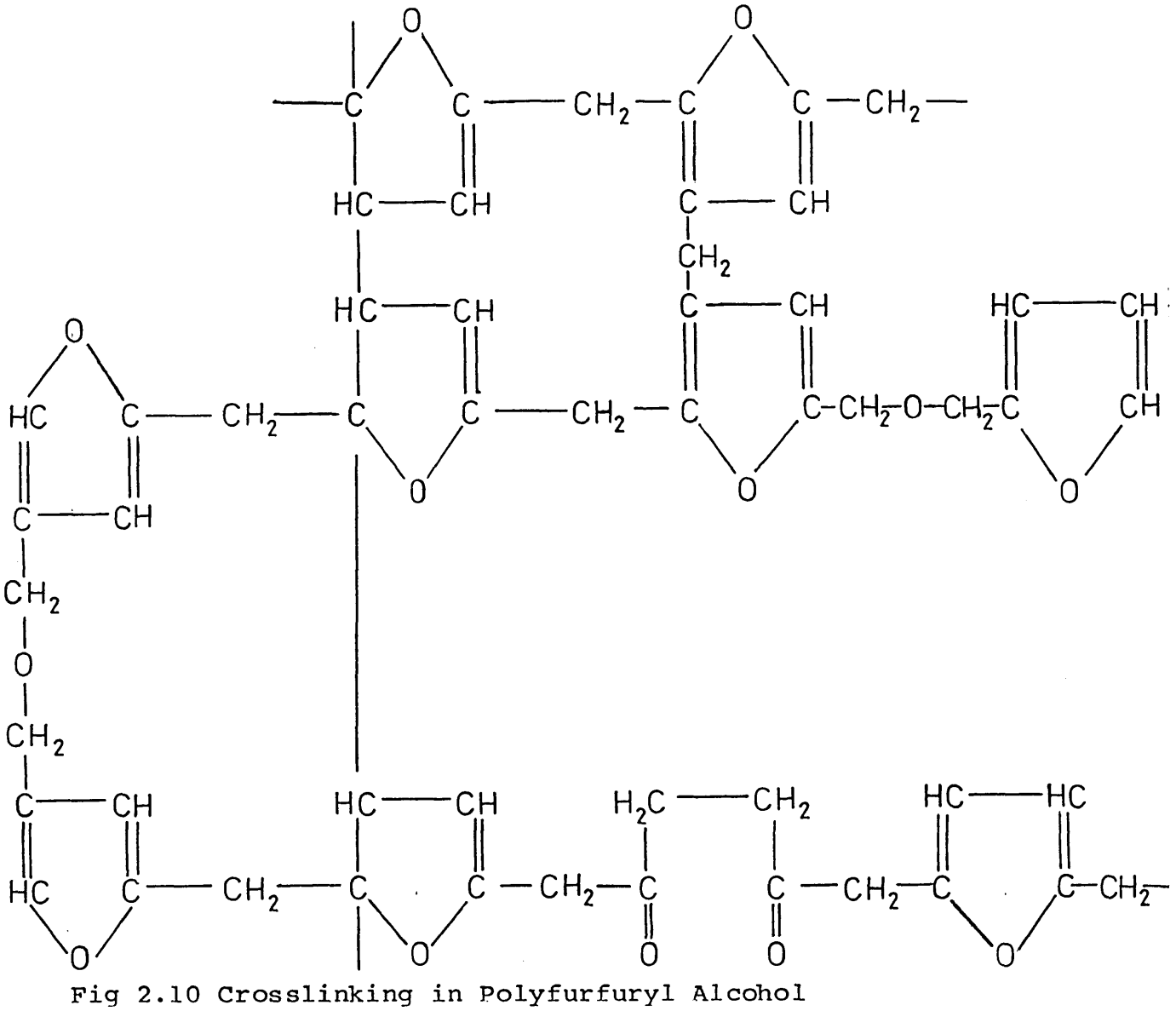


Fig 2.10 Crosslinking in Polyfurfuryl Alcohol

2.3 Pyrolysis of Polymers

2.3.1 Pyrolysis of organic materials

It has been known (14) for over 80 years that the thermal decomposition of hydrocarbons upon a hot surface tends to deposit carbon of a more or less graphitic nature. This was the 'glance' coal of the early electrical brush manufacturers or Foucault's 'deposited carbon from gas retorts' (15).

Retort carbon, or 'glance' coal, is a dense form of carbon produced by the deposition of carbon in the upper part of the retorts during the manufacture of coal and water gas.

Because of its high price and difficulty of manufacture, retort carbon only found use in the electrical industry where its properties could best be exploited. Horton (16) studied the kinetics of "pyrolytics" formed during oxidation and other workers such as Brown and Watt (17) reported on the preparation of pyrolytics by the breakdown of hydrocarbon gases at various temperatures. The dependence on temperature of the density of the carbon deposited from methane was reported (18) and the electrical and thermal properties of similar materials from benzene have been studied (19).

Workers then began to turn their attention towards carbons produced from the breakdown of larger organic compounds, the pyrolysis temperatures being 1000 - 1500°C. Pirani and Fehse (20) studied the properties of carbons produced at 1500°C and 2000°C. Carbon fil aments were heated in carbon tetrachloride, benzene hexachloride and petroleum spirit at various temperatures. Crystalline deposits of graphite were formed.

Further developments in the field of pyrolytics occured with the production of glass-like carbon by the thermal decomposition of 3-dimensionally crosslinked polymers (21) 'Glass-like', or 'amorphous' carbon appeared as commercially available products in the early sixties under the designations of 'glassy-carbon' and 'Vitreous-carbon' (22-25). Most scientific investigations were concerned with the properties of this special form of carbon whereas only a few papers dealt with the formation of glass-like carbon from well defined raw materials.

Davidson and Losty (26) developed a process by which masses of cellulose fibres were agglomerated and carbonized to form electrically conducting glassy carbon artefacts with almost zero-permeability to all gases and the ability to withstand savage chemical attack and very high temperatures. Phenol formaldehyde polymers are cited as starting materials for vitreous carbon (24, 25). Otani (27) used PVC "pitch" crosslinked by oxygen and Bradshaw (28) described the formation of glass-like carbons from aromatics. Ishikawa (29) prepared amorphous carbon from polyfurfuryl alcohol resins.

Generally, when polymers are heated in an inert atmosphere reactions take place initially within the C-C chain. These intramolecular reactions result in one of three possibilities:

(i) The chains degrade into small molecules and the products are evolved as gases leaving little or no carbon behind. An example of this behaviour is shown by polyethylene.

(ii) The chains collapse to form aromatic lamellae and so move into a plastic phase from which the lamellae stack above each other to form spherulitic liquid crystals - the so-called 'mesophase' (30). The result is a crystalline anistropic coke which on heating to 2700°C will soften to a graphite material, an example of a polymer exhibiting this behaviour is Polyvinyl Chloride.

(iii) The chains remain intact and merely coalesce with neighbours; the material does not pass through a plastic or liquid state. The final char is isotropic if the precursor material is isotropic and can be anisotropic if the precursor material is anisotropic. In both cases the material is not graphitizable when heated to 2700°C and remains relatively hard. An example of this is polyvinylidene chloride.

If pure polymers are used, the carbons produced in cases (ii) and (iii) form distinct groups with very different properties. However, if we incorporate such carbons as carbon black and graphite, composite materials with intermediate properties are apparent which makes the grouping difficult. The mechanisms of pyrolysis and carbonization are not fully understood because it is very difficult to determine the crystallographic and chemical structure of intermediates existing during the carbonization process.

In general, when polymers of type (iii), of which polyfurfuryl alcohol is an example, are pyrolised the following stages of structural changes are noted.

1. The pre-carbonization stage: The materials turn black at an early stage, usually at the very beginning of a regime of rapid weight loss, or during pre-oxidation when linear conjugated carbon - carbon systems start to form. All loose molecules such as excess monomer or solvent are volatilised.

2. The carbonization regime: This is a regime of rapid weight loss, typically between 300 and 500°C in which oxygen, nitrogen and chlorine etc., are removed. The back-ground absorption in the infra-red gradually increases as the conjugated systems get longer. At any given temperature the process may be stopped, the time taken to achieve a weight loss characteristic of the temperature being of the order of minutes. This is ascribed to the increasing difficulty in eliminating molecules as strain energy is built up in the polymeric network with the increase in crosslinking between chains. The result is a loose network of linear conjugated systems which are isolated electronically from each other.

3. Dehydrogenation: at the end of stage 2 the material still contains typically, one hydrogen for every two carbon atoms, which corresponds to the formula of an aromatic ladder polymer. Thus there exists a third regime between 500 and 1200°C in which hydrogen is gradually eliminated, the hydrogen:carbon ratio being a characteristic of a given heat-treatment temperature. The electrical conductivity increases rapidly as separate conjugated systems become interconnected to form a conducting network. The density, hardness and stiffness increase, the damping and permeability decrease.

2.3.2 Carbon yield of polymers

The carbon yield of a polymer can be found by heating a known weight of the polymer in an inert atmosphere at a given temperature, and weighing the carbon residue. The carbon yield is then the ratio of the amount of the carbon residue to the initial weight and the conversion efficiency is the ratio of the weight of carbon in the residue to the amount of carbon in the original resin.

Many long chain polymers breakdown completely into gaseous products. Madorsky (31) showed that polyethylene at one extreme and PTFE at the other leave no carbon residue. Polyvinyl fluoride $(CH_2\ CHF)n$ and polytrifluoroethylene $(CHF\ CF_2)n$ also leave very little residue, but $(CF_2\ CH_2)n$ leaves 30% carbon residue by weight which accounts for all the carbon originally present in the polymer.

Mackay (32) determined the carbon yield for a whole range of polymers (cf. Table 1) and came to the conclusion that carbon yield cannot be predicted. Linear polymers such as polystyrene or poly-p-xylene, even though having a high degree of aromacity, give low carbon yields. Linear polymers of polyfurfuryl alcohol and polyphenylene oxide with aromatic groups inter-spersed with ether linkages provide good carbon yields. Conversion efficiency for PFA, for example, was a high 90.5%.

Carbon yield does not seem to be influenced by whether the polymer is thermoplastic or thermosetting, linear or crosslinked, but whether it is capable of cyclization, ring fussion or chain coalescence at the onset of carbonization.

In general, the resins should have a high degree of aromacity and high molecular weight. There should be no more than one carbon atom between aromatic rings, because chain scissions will take place leading to volatilazation of the fragmental parts - witnessed in a low yield from poly-p-xylene.

Nitrogen should be in the ring structure and not in the chain. For example, polybenzimidazole is more stable and provides higher carbon yields than amine-cured epoxy resins. Other elements such as sulphur do not affect the stability of the polymers but do result in lower carbon yields and low conversion efficiency. All phenolic polymers except those in which the para position is blocked by either a phenyl or methyl group are good carbon forming materials.

Polymeric precursors	Carbon yield (%)	
Coal tar pitches	50	High Yields
Petroleum fractions	Variable	
Polyvinyl chloride	42	
Phenol-formaldehyde	52	
Epoxidized Phenol-formaldehyde	50	
Phenol-benzaldehyde	37	
Oxidized polystyrene	55	
Polyfurfuryl alcohol	50	
Polyvinyl alcohol	50	
Polyacrylonitrile	44	
Polyvinylidene chloride	25	
Cellulose	20	
Polybutylene Rubber	10	Moderate Yield
Cellulose acetate	10	
Melamine formaldehyde		
Polyvinyl acetate		Negligible Yields
Ethyl cellulose		
A typical Epoxy resin		
Acrylonitrile - styrene co-polymer		
Polystyrene	5	
Polyamides		
Polyisobutylene		
Polyethylene		
Polymethylmethacrylate		

Table 2.1. Carbon yields of various polymeric precursors (2).

2.3.3 Detailed Chemistry of the Pyrolysis of Polyfurfuryl Alcohol

Data for the determination of the chemistry of pyrolysis are provided by thermo-gravimetric analysis (T.G.A.), thermo-volumetric analysis (TVA), differental thermal analysis (DTA), analysis of gaseous products, and by arresting the pyrolysis at various stages to analyse the residue. The techniques and the results on the thermal degradation of organic polymers are described by Madorsky (33).

Rather variable data on carbon yields resulting from the pyrolysis of polyfurfuryl alcohol are reported in the literature. Fitzer and Schafer (34), employing heating rates of both 12 and 30°C/hr for temperatures up to 1000°C obtained a 61% carbon yield, whereas Ozanne (35) using a heating rate of 150°C/hr to 900°C observed only 50%. On the other hand O'Neil et al (36) using heating rates between 420 and 540°C/hr to a final temperature of 950°C found a high carbon residue of 59%. These differences are thought to be caused by a difference in the amount of crosslinkage in the resins tested (34).

On the basis of all the data available the mechanism for the pyrolysis of polyfurfuryl alcohol (I) is shown in Fig 2.11. The primary pyrolysis product is water, being formed from the free hydroxyl groups. Subsequently the methylene bridges rupture, forming CH_4 as a by-product, and the furan ring is opened (II). The latter process is recognised by the release of carbon monoxide, carbon dioxide and again water. It is not possible to give a definite formulation of the intermediate stages. According to the observed CO formation the furan ring is stable up to approximately 275°C.

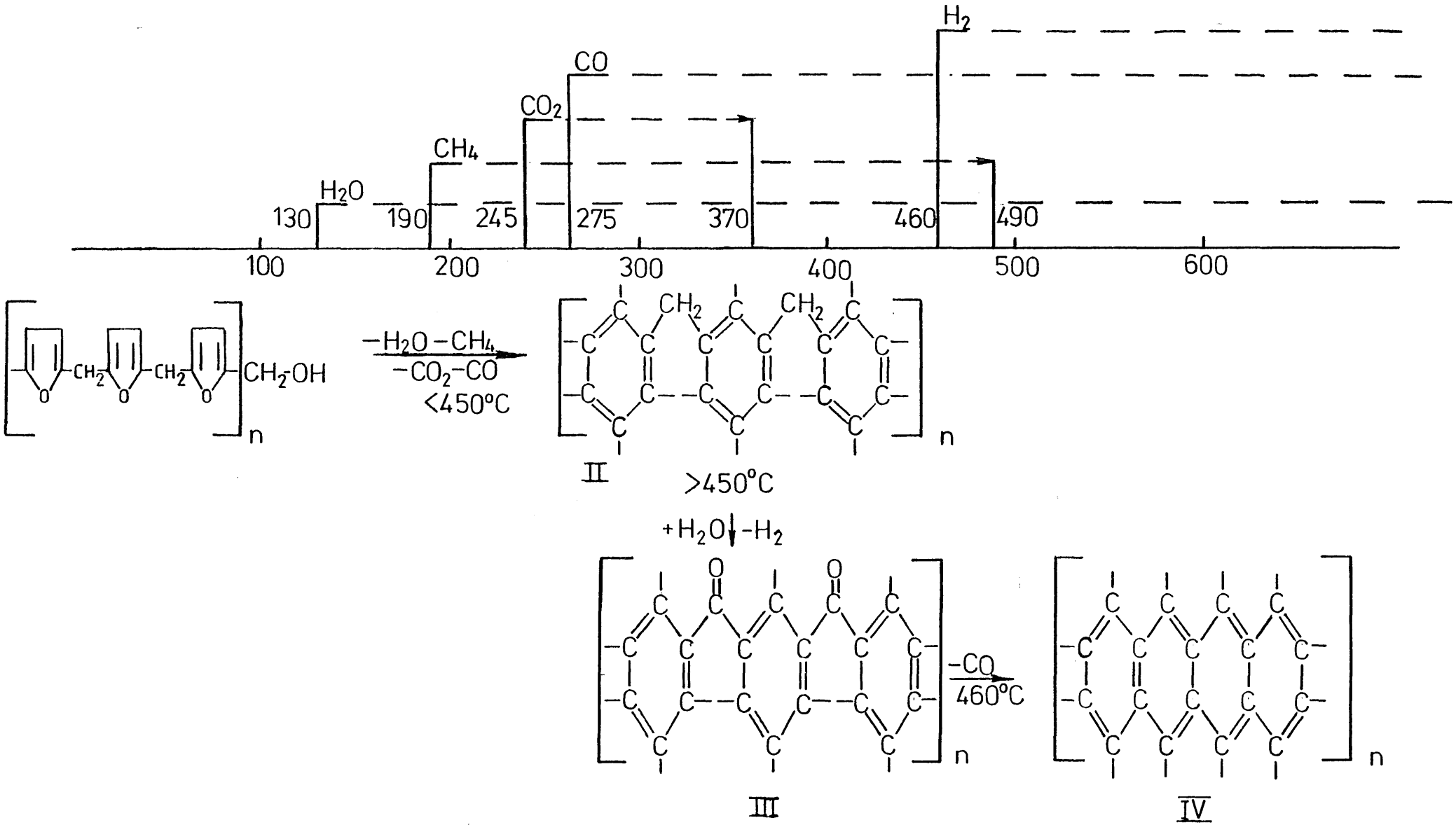


FIG. 2.11 THE PYROLYSIS CHEMISTRY OF POLYFURFURYL ALCOHOL.

Between 300 and 400°C the ir. band of the C-O-C bond of the furan ring, at a wave length of 5.85 μm, loses its intensity, due to the rupture of the furan ring. In the gas analysis, this temperature is characterized by a maximum in the first carbon monoxide formation as well as by release of water. A quantitative calculation reveals that, taking into account the hydroxyl group decomposition to water, half the furan ring oxygen must be released as water. The other half is liberated as carbon monoxide.

At 400°C, new ir. bands begin to appear which indicate the beginning of a build up of aromatic systems. These aromatic systems are formed spontaneously from the fragments of the furan rings. They have also been identified by Braun (37) using Diamond's X-ray profile analysis.

At temperatures above 450°C a reaction of pyrolysis water with remaining methylene bridges occurs ((III) in fig 2.11). This secondary reaction to form alkanone groups is readily recognised from the decrease in the formation of water above 450°C. In the same temperature range, the formation of methane ceases because of the oxidation of the methylene bridges and significant amounts of hydrogen are released. Above 460°C the carbonyl groups liberate carbon monoxide, leading to a highly unsaturated aromatic C-H residue (IV) capable of forming crosslinked aromatic systems.

During pyrolysis polyfurfuryl alcohol exhibits around 20% linear shrinkage (34). This shrinkage corresponds to the known behaviour observed during the production of commercial amorphous carbon products (38).

The density of the carbon produced is 1.55 g cm^{-3}. When comparing this bulk density with that of graphite (2.267 gcm^{-3}) a difference of 30% appears which must be attributed to a different structutal arrangement (cf. section 2.5). Transmission electron microscopy does not reveal any pores. X-ray small angle scattering carried out on a sample heat treated to 1200°C revealed a uniform porosity of approximately 25Å (39). It has also been shown (34) that a variation of the degree of crosslinking in the starting materials will affect the consecutive chemical steps of the decomposition and the formation of gaseous by-products. A decrease in the amount of crosslinking will diminish the carbon yield in the residue by promoting the formation of low molecular weight compounds.

2.4 The Structure of Amorphous Carbon

2.4.1 Changes in the structure of the resin during carbonisation

Klug and Alexander (40) used X-ray diffraction and infra-red spectroscopy to follow the changes in structure during carbonization in polymeric systems. The original precursors were all polymeric resins with a structure difficult to analyse. The X-ray diffraction patterns of resins heat treated to temperatures up to 300°C were identical to those of the same resins at room temperature, from which they concluded that the structure of the resin does not change significantly up to this temperature. As the temperature was increased, from 350 towards 500°C, the X-ray diffraction peaks became broader and more assymetric. Infra-red spectroscopy suggested the formation of intermolecular cross-links as the chain polymer is converted into a narrow ribbon of aromatic molecules linked with carbon - carbon bonds. Very little change occurred in the diffraction pattern on increased heating to 1000°C. It appeared therefore, that the structure of the final carbon was essentially only a minor modification of the material produced at 500°C.

Some workers have suggested the presence of small regions of three-dimensionally ordered material within the vitreous carbon. It is postulated, that there are minute areas where the carbon ribbons will condense sufficiently to produce small crystallites with a graphite layer structure. However, very little information on this has been published and no-one has ever reported crystallites of a significant size or number.

Fishbach and Kotlensky (41) and Noda and Inagaki (42, 43) showed that graphitization, that is to say the development of a graphite-like layer structure, proceeds in glassy carbon with increasing heat treatment. However the small crystallite sizes observed in the commercial vitreous carbons studied (largest crystallite size observed after heat treatment to 3000°C was $<85\text{Å}$) suggested that three-dimensional ordering does not take place. In fact, no (hkl) lines are generally detected by X-ray diffraction even after the most prolonged annealing i.e. the structure of the material is essentially random.

The resin heat-treated to 500°C consists of narrow ribbons of condensed aromatic molecules which are tangled and coiled in a complicated manner: these ribbons are linked with modified methylene bridges which results in a three-dimensional network structure. Pyrolysis above 500°C involves the removal of hydrogen which gradually releases the internal strain energy in the narrow ribbons. However, this relaxation is restricted by the strong bonds between the ribbons.

X-ray profiles of systems heat-treated above 500°C show strong small-angle scattering which indicates that the material contains a large proportion of fine pores. This occurs because the tangled and highly strained ribbons cannot fill space efficiently. Optical microscopy cannot detect any macroscopic pores and there is no evidence of texturing. Polarized light microscopy and X-ray diffraction texture studies do not reveal any anisotropy which infers that the narrow ribbons of aromatic molecules are not drawn straight and parallel in a certain direction but are quite randomly orientated.

2.4.2 X-ray small angle scattering

Small angle X-ray scattering arises from the presence of heterogeneities in solid matrices (44). This type of analysis is ideal for glassy carbons since although they are impermeable to gases, their low densities suggest they are very porous. Amorphous carbon shows pronounced scattering of X-rays at small angles which is attributable to fluctuations of the electron density on a larger scale than that of interatomic distances (45). Guinier and Fournet plotted the Logarithm of the X-ray scattering intensity (I) against the square of the scattering angle (E). The slope was given by $-4\pi^2R^2/3\lambda^2$, where λ is the X-ray wavelength and R the radius of gyration of the scattering particles or voids. This law is obeyed by systems containing particles or voids of approximately equal size in a homogeneous matrix.

Such measurements were made by A.C. Craievich (2) using specimens of a phenolic resin pyrolysed to various temperatures between 500 and 1000°C.

Heat-treatment temperature/°C	Density/gcm^{-3}	Radius/Å of pores
500	1.14	-
600	1.17	4.2
700	1.26	4.7
800	1.43	7.0
900	1.52	7.9
1000	1.55	8.4

Table 2.2: The variation of pore size and density with the temperature of pyrolysis of a phenolic resin.

He found that in all cases a linear portion of the Guinier plot was measurable between E = 1° and E = 2.3°. For E <1° the slope of the curves increased very rapidly. This was attributed to the presence of larger voids with diameters greater than 500Å or, perhaps, because the voids are very very flat oblate ellipsoids. Jenkins and Walker (46) obtained similar results and noted that the size distribution of micropores is very narrow.

Table 2.2 shows the variation of the radius of pores with heat-treatment temperature, together with the density of the carbon. It can be seen that increases in R correlate with increases in density; this is possibly because dehydration draws together the microfibrils during the pyrolysis regime eliminating a substantial proportion of small voids to leave a residual population of voids with an average diameter of 8.4Å.

2.4.3 The structure of amorphous carbon

Studies of the process of carbonization suggest that glassy carbon consists of condensed aromatic ribbon molecules, randomly oriented and tangled in a complicated manner. The high resistance to graphitization of glassy carbon shows that the configuration of these ribbons is very stable. Several questions arise on the detailed structure of glassy carbon; firstly, whether the structure is two-dimensional as in graphite or three-dimensional as in a glass, and secondly, whether the fully formed

amorphous carbon contains the tetrahedral sp^3 hybrids (in which all four bonding electrons are absorbed into four evenly spaced orbitals) in addition to trigonal sp^2 hybrids (in which three electrons are absorbed in a symmetrical planar hybridized orbital system, the extra electron being in the free p state and available for forming a subsidiary π bond).

The possibility of carbon being present in diamond-like structures of tetrahedral carbon atoms is discussed by Ergun and Tiensuu (47), Ergun and Alexander (48) and Kakinoki et al (49). The presence of such structures is taken as an explanation for the extreme resistance of glassy carbons to graphitization. Noda and Inagaki (43) carried out electron diffraction work in which they claimed that diamond and graphite are present in equal amounts. Furukawa (50) criticized this view and proposed a cubic model with an average co-ordination number for each atom and a mixture of single, double and triple bonds to produce a three-dimensional network.

Kakinoki (51) modified the model of Noda and Inagaki with the addition of oxygen bridges between trigonal and tetrahedral carbon. From their studies of the specific heat of glassy carbon, Takahashi and Westrum (52) proposed that the material is essentially two-dimensional. Halpin and Jenkins (53) found that glassy carbon has a layer structure formed by the stacking of aromatic molecules.

It is possible to view directly the essential layer structure in glassy carbon with an electron microscope if the magnification and resolving power are sufficiently high. Low resolution electron micrographs of amorphous carbon show that the edges consist of a network of strings or microfibrils, the thickness of which is about 30Å. Each string is considered to be a stack of graphite-like ribbon molecules. It is also possible to make out micropores created when the strings form a network structure. The diameter of the pores has been estimated to be between 5 and 10Å, comparable to that calculated from X-ray small angle scattering.

High resolution electron microscopy, employing the phase contrast technique, carried out by Jenkins et al (54) showed that only short range order exists in the structure. The system is made up of stacks of two-dimensional ribbon-like molecules, reminiscent of fibrils in crystalline polymers. The fibrils are randomly orientated and tangled in a complicated manner. The height of a stack of ribbon-like molecules was estimated to be up to 40Å. Electron micrographs of the surface of the material show the continuity of the microfibrils to form loops projecting from the surface. Orientation is random and fracture occurs at the interfibrillar boundary. No loose ends are apparent, which would explain the chemical inertness of glassy carbon. In the interior, the material retains its essential randomness and microfibril continuity. There are indications that the width of the layers can be quite large locally.

This is attributed to the presence of many confluences in the ribbon network where neighbouring ribbons merge to form a much wider ribbon locally.

Perret and Ruland (132) suggested that the cavity-aperture system is a direct result of stacks of ribbon-shaped carbon layers. Points of close approach of the ribbons create the apertures. The changes observed during the development of the pore structure (as observed by Craievich and Jenkins and Walker) are most marked between 970 and 1500°C and thought to be due to the final stages of chemical degradation of the carbonized polymer. Using wide angle X-Ray scattering, Wignalls and Pings (133) showed that the basic atomic arrangement within the ribbons was that of hexagonal graphite-like sheets with no graphitic registration between the sheets. Ergun and Schehl (134) made a detailed analysis of the Fourier transforms of the ($|k$) reflections and deduced that the hexagonal rings are severely distorted making it virtually impossible to define the two dimensional lattice. They were further able to show that while stacking of the layers is extensive, it is faulty with a mean spacing between faults of $\simeq$ 21Å. Ergun (135) used a profile matching technique to show that there is a large amount of strain in the material because of folds in the ribbon structure. These folds constitute faults in the two-dimensional lattice.

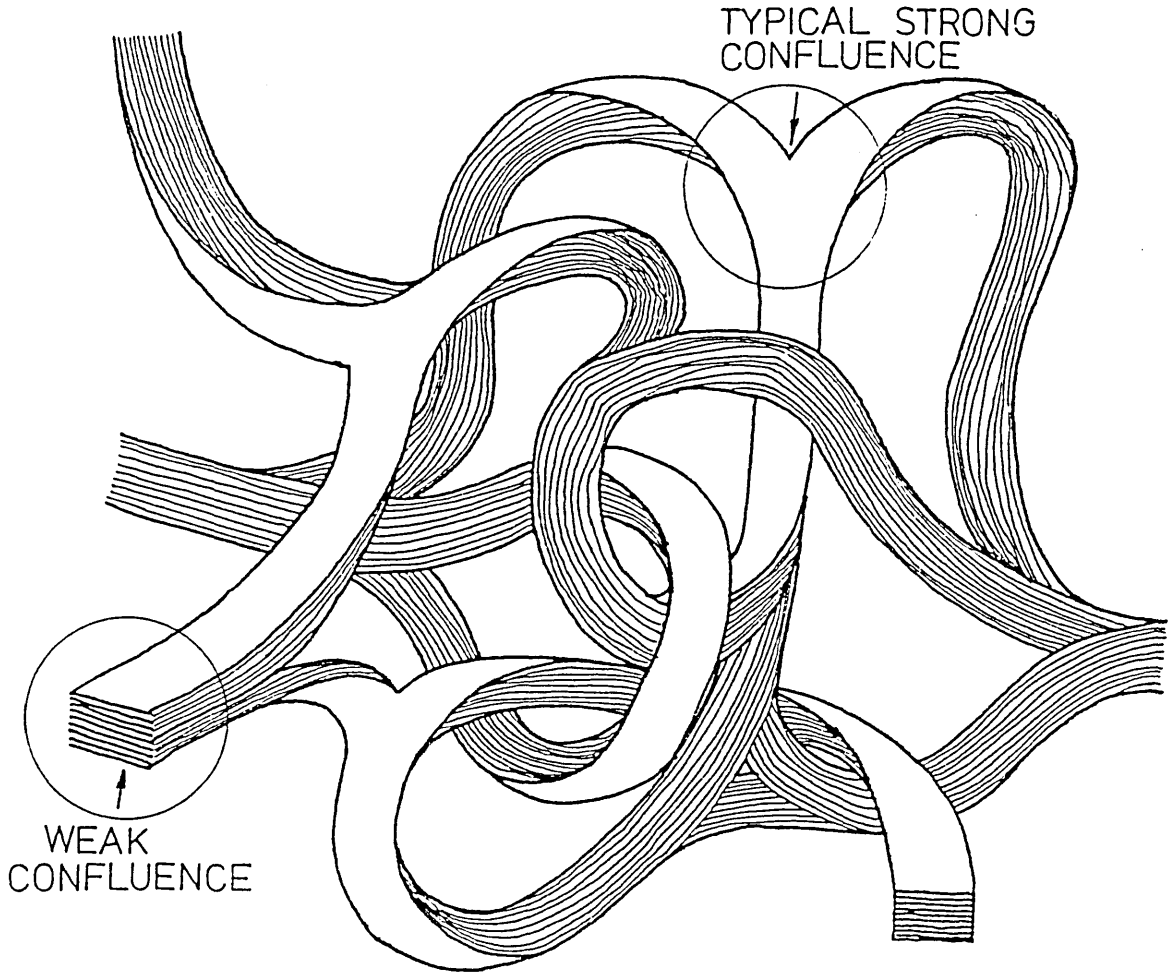


Fig 2.12

A schematic structural model for amorphous carbon[2].

Considering all the information available, a three-dimensional structural model for isotropic glassy carbon is shown in Fig 2.12. This is a highly simplified version as in reality the fibrils are packed much more closely together to form a tighter mass. There are two types of confluences illustrated within the network of microfibrils. Strong

confluences occur where ribbons merge into each other, and weak confluences where ribbons overlap.

It can be assumed, then, that the production of disordered amorphous carbon by the heat treatment of thermosetting polymers, in the region between 400 and 1000°C, proceeds by the progressive coalescence of stabilised polymer chains. This defines the carbonization process. The final structure is laid down at the start of the coalescence, but is only attained progressively as the temperature is raised because of the increasing difficulty in ordering as the mechanism proceeds. This difficulty can be attributed to the competition between adjacent polymer chains, thus hampering the attainment of the final condensed structure.

The glassy carbon residue from the pyrolysis has a microstructure which is lath-like and contains a significant volume of micropores as indicated by its low density of around $1.5 g cm^{-3}$. The material is non-graphitizing, characterized by interlayer separation (d_{002}) always larger than that of graphite (55). Although amorphous carbon contains a large volume of pores, they are neither observed by scanning electron microscopy nor by conventional gas absorption methods of characterization (21). Both N_2 condensation and BET absorption measurement indicate negligible pore surface area ($<10 m^2 cm^{-3}$) showing that the pores are not interconnected (56). Small angle X-Ray scattering and lattice image studies showed that the microstructure has a heterogeneity associated with porosity on the scale of a nanometre.

2.4.4 Higher Temperature Treatments of Vitreous Carbon

The density of glassy carbon decreases when it is heated above its process temperature of 1000°C. The decrease is greater the more the heat treatment temperature exceeds the process temperature (56, 57). Fischbach and Rorabaugh (58) experimented on several different glassy carbon materials and concluded that 80 to 90% of the density decrease resulted from volume expansion and the remainder was attributed to weight loss. They suggested that the volume expansion resulted from internal pressure generated by the continued evolution of volatile pyrolysis products and, perhaps, the release of absorbed material within the closed pore system. Thus, for slow heating rates and/or thin samples, there is enough time for the gases to diffuse out as they are generated, so that the increase in internal pressure and the associated volume increase is small. On the other hand, at high heating rates, or with thick samples, pressure large enough to cause a large volume increase or fracture would be generated. Bragg and Bose (59) obtained similar results but argued that although the gas pressure model for the density decrease in glassy carbon can operate, it does not account for all of the decrease because the pyrolysis is virtually complete at the processing temperature. They hypothesized that the density decrease is due to the volume expansion of pores caused by anisotropic lattice thermal strains. A rough calculation of the thermal stresses within the material at high temperature showed the same order of magnitude as the failure stress of

graphite in the presence of 10Å Griffith flaws - comparable to the size of the pores present. They concluded that the coarsening of porosity was due to the rupture of pore edges due to thermal stress, which also explained why the change is not reversible on cooling.

From their experiments, Saxena and Bragg (55) showed that the evolution of the structure of glassy carbon with increased heat treatment temperature goes through three different stages. Up to 1500°C the material undergoes a settling down process, with the completion of dehydrogenation thought to occur at around 1500°C (60). The second region is characterized by a constant value of d_{002} of 3.44Å and involves a relief of the internal stress within the structure. Fischbach (61), in his creep studies on vitreous carbon, noted that, as a result of shrinkage during pyrolysis, the material has high internal stresses which are relieved slightly with higher heat treatment temperatures. Also, while trying to intercalate glassy carbon with K in a gaseous atmosphere, the material was reduced to a fine powder. The explanation proposed was the presence of intense frozen stresses within the carbon which were abruptly relieved (62). In the third stage the structure slowly evolves toward the ideal graphite structure and limited graphitization takes place. Even at 2800°C, however, the value of d_{002} is 3.40Å which is still significantly larger than the ideal 3.35Å. It would appear that the material is metastable in its disordered form. Thermodynamic evidence for this has been given in the work of Das (63).

Mehrotra et al (64) summarised the higher temperature behaviour of vitreous carbon with the following conclusions. The density and weight of glassy carbon decrease, with increase in heat treatment temperature, while the volume increases. The weight loss reaches a plateau at around 2000°C, while the density decrease and volume increase show a quadratic temperature dependence. Typical values of density decrease, weight loss and volume expansion at 2700°C are 12.4, 1.9 and 10.2% respectively. The weight loss is not the major cause of density decrease and is thought to occur due to the release of residual hydrogen. The density decrease is shown to be mainly due to volume expansion that can be attributed to gas pressure for heat treatment temperature up to 1600°C and to relief of thermal stress above 1600°C. The mechanism responsible for the permanent dimensional change is suggested to be ratchet-like (65), wherein the new microstructure formed during heating is not rearranged during cooling.

2.5 Vitreous Carbon Composites

Commercial glassy carbon products are generally fabricated from a mixture of carbonaceous filler such as petroleum coke, pitch coke, natural graphite, etc., and a carbonaceous binder eg. coal tar pitch or polyfurfuryl alcohol (66). The mixture, after being shaped by compression moulding, extrusion or some other forming process into an artefact of the desired shape and size, is fired in a non-oxidising atmosphere to produce a rigid carbon product (67). Watt et al (68) used natural graphite and polyfurfuryl alcohol to manufacture carbon artefacts for use as high temperature heat exchangers with very low permeability to gases for the nuclear industry. This work was also applied to impermeable crucibles, heat exchangers and electrodes for the chemical and metallurgical industries. Glassy carbon artefacts have also found employment in the defence industry (11), electronics (69) and bioreplacements (70, 71, 72) to name but a few.

The characteristics of carbon/carbon composites of this type are determined both by their micro and macrostructure. The microstructure depends mainly on the types of materials used as the filler and binder, and their relative proportions. The macrostructure affects many of the properties which are important to industry, such as density and strength etc., and is determined by the selection of the conditions of preparation. A great deal of investigation has been done into the microstructure of carbons but very little concerning the macrostructure, except the work by Mrozowski (73) and his collaborators (74, 75, 76).

A formed carbon mixture before heat treatment is called 'green'. The mixture of the green carbon determines the phenomena during the following processes and the properties of the final product. The most effective factor determining the nature of the green carbon is the binder content. Okada and Takeuchi (67) were able to show that the strength of polyfurfuryl alcohol/natural graphite composites exhibits a maximum for a definite binder content. Moreover, knowing that the density of the material depends on its binder content, they were able to use their results to illustrate the usefulness of Mrozowski's theoretical formula relating mechanical strength and binder content:-

$$S = S_o d_o^{y}(d - d_o) \qquad (2.1)$$

where S = Strength of composite

S_o = Strength of filler

d_o = filler density

$(d - d_o)$ = density of binder

y = empirical factor found from exptl. data.

Using differential thermal analysis, Wewerka, Walters and Moore (77) showed how the integrity of the composite is improved with increase of binder resin polymerization (viscosity), indicting that beneficial effects should result by using binder resin of the highest practical degree of polymerization. Dickinson and Wewerka (78) studied polyfurfuryl alcohol as a binder. Using gel permeation chromatography, they were able to characterize the complex

structures of the resins in terms of molecular size distributions. A binder resin will affect the properties of the composite directly by virtue of its interaction with filler particle surfaces and by its behaviour during carbonisation, and also indirectly by affecting fabrication variables such as the ease of mixing the binder with the filler and the pressure required for extrusion. They were able to show that certain physical characteristics of acid-polymerised furfuryl alcohol resin binders, such as their viscosities and molecular size distributions, can greatly affect the extrusion and physical properties of composites made from them. The mechanical and physical properties of the composite can be improved by polymerising the resin to an optimum viscosity if compatible with fabrication conditions. This optimum occurs because, although a high binder viscosity is preferred, if the viscosity is too high it can lead to cracking during heat treatment. The monomer content should be kept to a minimum and polymerisation conditions chosen such as to result in a narrow molecular size distribution.

Further work by Dickinson and Wewerka compared acid and γ alumina polymerised furfuryl alcohol as binders in Carbon Reinforced Carbon (CRC) composites (79). They found that the acid polymerised binder was better for two reasons; (1) it had a narrower molecular size distribution and (2) it contained a relatively large amount of small polymerisable molecules. Thus, they were able to show that not only is it necessary for a superior binder resin to have a suitable

molecular size distribution, the resin must also be composed of low mw. molecules that are capable of further polymerisation during heat treatment, otherwise, sample integrity will be damaged by the volatilisation of an excessive amount of small molecules during the curing and carbonization of the resin.

An investigation of synthetic binders for carbon and graphite by Riesz and Susman (80) showed that during thermal degradation a binder should provide a maximum degree of surface reactivity in order to establish an intimate degree of contact with the filler, which enables the binder to form continuous inter-particulate bridges; it is for this reason that polyfurfuryl alcohol possesses such excellent binding properties. Winslow, Matreyek and Yager (81) carried out a detailed analysis of several binders and suggested that furfuryl alcohol may develop its binder properties as a result of its unusually high carbon to hydrogen ratio following thermal degradation.

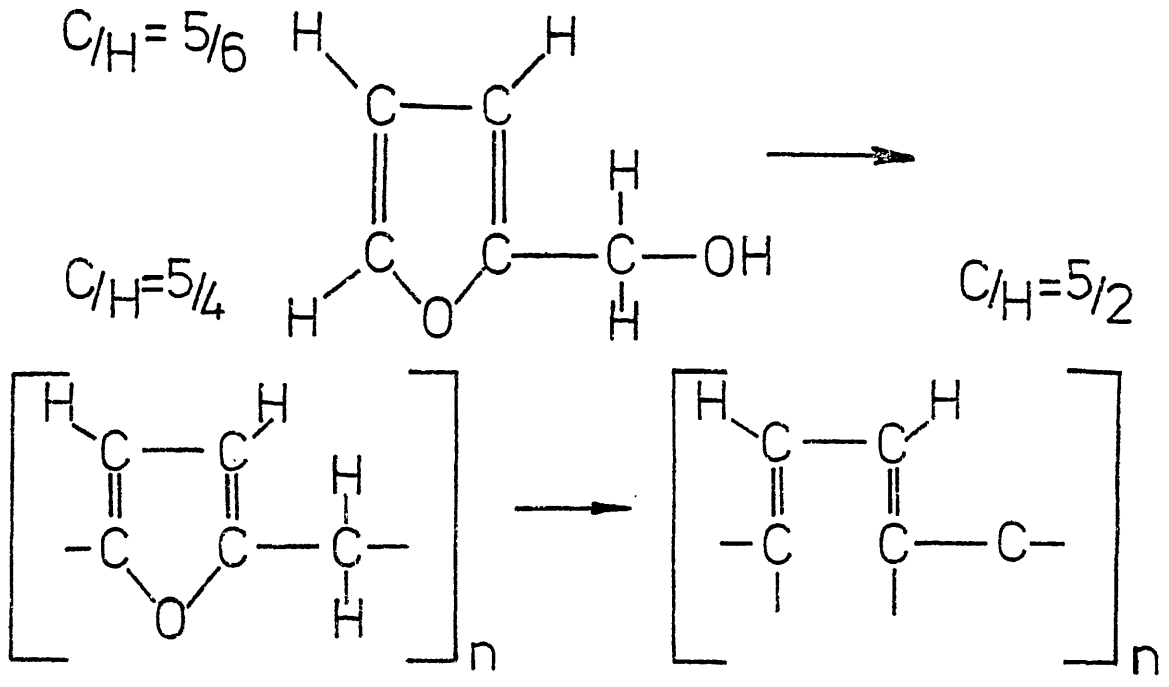


Fig 2.13 C/H ratio of furfuryl alcohol, polymer and pyrolysis residue.

While this is an over-simplification, it is evident that a highly reactive carbonaceous residue is formed which can become integral with the bulk carbon structure.

It has been observed (21) that addition of natural graphite as a filler increases the bulk density of glassy carbon after heat treatment. However, the permeability is increased. Fig 2.14 depicts the density during heat treatment for a pure furfuryl alcohol resin and a resin containing 10% of natural graphite filler. The dotted line represents the density calculated under the assumption of simple mixing. As can be seen, the actual density during carbonization is lower. This behaviour can be explained by assuming that the shrinkage of the resin is hindered by the incompressible filler. After heat treatment a very high density was found.

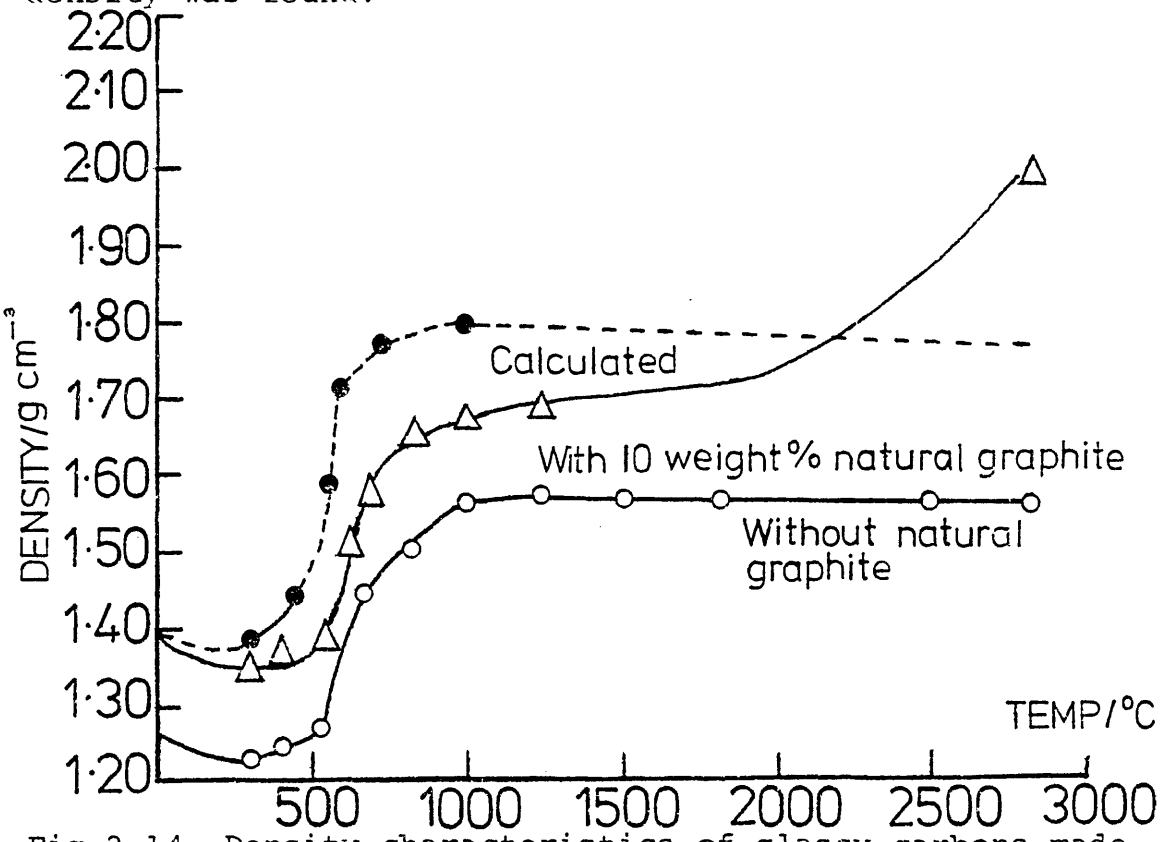


Fig 2.14 Density characteristics of glassy carbons made from pure furfuryl alcohol and resin filled with 10% natural graphite as compared to the calculated density.

Kamiya and Inagaki (82) measured thermal expansion along the c-axis of natural graphite flakes embedded in glassy carbon in order to estimate the stress caused by the large difference in thermal expansion coefficients of natural graphite and glassy carbon. Scanning electron micrographs of natural graphite/glassy carbon composites showed that the natural graphite flakes adhere tightly to the glassy carbon matrix and there are no obvious voids around the flakes. The thermal expansion of the natural graphite was found to be surpressed when the flakes were embedded in glassy carbon. The observed behaviour is caused by the constraint of the large c-axis expansion of the natural graphite flake by the smaller, isotropic expansion of the glassy carbon matrix. The large shrinkage of resins during carbonization is thought to assist the stress accumulation at the boundaries between the flakes and the matrix. The stress created may promote graphitisation of the glassy carbon and consequently become relaxed after heat treatment above 1800°C. An abrupt graphitisation of nongraphitising carbons such as glassy carbon has been noted under high pressures (greater than $300MNm^{-2}$) (60, 83). The reported fact that glassy carbon is graphitised in the regions around the graphite flakes (21) can be explained by the stress accumulation showed by Kamiya and Inagaki.

2.6 Mechanical Properties and their Measurement

The mechanical properties of a material determine the limitations for structural applications when the material is required to sustain a load (84).

2.6.1 Elasticity

When a load is applied to a material, deformation occurs due to a slight change in spacing between atoms. The load is defined in terms of stress σ and expressed in units of Mega-Newtons per square metre (MNm^{-2}). The deformation is defined in terms of strain ϵ and calculated as the ratio of extension to original length i.e.

$$\epsilon = \frac{\Delta l}{l} \qquad (2.2).$$

It is generally expressed as a ratio or a percentage. The amount and type of strain depends on the atomic bond strengths, the applied stress and temperature. Up to a certain stress limit for each material the strain is reversible; i.e., when the stress is removed, the atomic spacing returns to its original state and the strain falls to zero. This phenomena is known as elastic deformation. The stress and strain are related by a simple proportionality constant. For tensile stress,

$$\sigma = E\epsilon \qquad (2.3).$$

The proportionality constant is called the modulus of elasticity or Young's modulus (E). At a certain stress,

which depends on the material, the strain stops being reversible and one of two things can happen. The material will either yield and undergo irreversible (plastic) deformation or fracture will occur.

At ambient and intermediate temperatures, glassy carbon behaves elastically with no plastic deformation up to fracture, as illustrated in Fig. 2.15. This is known as "brittle" or "linear elastic" fracture and is the most critical characteristic that must be considered in design for load bearing applications.

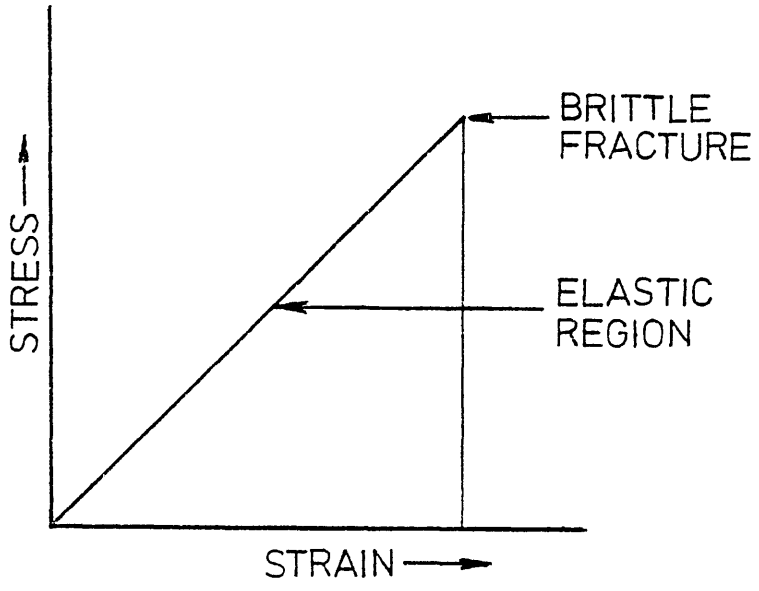


Fig. 2.15. Linear elastic stress - strain relationship.

As shown in equation (2.3) the modulus of elasticity E is the proportionality constant relating elastic stress and strain. It is best thought of in terms of the amount of stress required to produce unit elastic strain and therefore a measure of the stiffness of the material.

$$E = \frac{\sigma}{\epsilon} \qquad (2.4).$$

If E is considered on the atomic level in terms of tensile stress, the stronger the bonding, the greater the stress required to increase the interatomic spacing and the higher will be the value of E. Ceramic materials with strong covalent bonding have the highest E values, e.g. diamond, BN and SiC, and those with weak ionic bonding, such as NaCl, have much lower E values. Bond strength, and thus E, varies in different crystallographic directions. In an extruded or fibrous material in which the polymer/carbon chains are arranged in an axial direction, the Young's Modulus will be very much greater in this direction than any other. In the case of amorphous carbon, the covalent bonding, and hence E, is much greater in the ribbon axis. When an amorphous carbon is formed simply by pyrolysing the cured resin it is isotropic, because of the random ribbon orientation. If, however, the resin is extruded prior to firing this anisotropy must be taken into account in design work.

Composite materials which are made up of more than one phase have a modulus which is intermediate between the moduli of the constituents. The modulus of the composite can be estimated using the law of mixtures:

$$E = E_a V_a + E_b V_b \qquad (2.5)$$

where E_a and E_b are the elastic moduli of the constituents, and V_a and V_b are the volume fractions.
This is a simplified relationship and suitable only for rough estimates.

Porosity also affects Young's Modulus, resulting always in a decrease. Mackenzie (85) derived a relationship for estimating the modulus of porous materials:

$$E = Eo(1-1.9P + 0.9P^2) \qquad (2.6)$$

Eo = elastic modulus of non porous material

P = volume fraction of pores

This relationship is valid for materials containing up to 50% porosity and having a Poisson's ratio of 0.3. Poisson's ratio (ν) is the ratio of thickness decrease to length increase due to a tensile stress:

$$\nu = \frac{-\Delta t/t}{\Delta l/l} \qquad (2.7)$$

Where t = thickness

l = length

The method most commonly used to measure Young's Modulus involves the direct measurement of strain as a function of stress. When the results are plotted E can be calculated from the slope of the elastic portion of the curve.

2.6.2 Theoretical Strength of Materials

The term "strength" of a material is very ambiguous. It is generally used to describe the stress at which some change occurs in the material and as such requires a

modifier to be specific e.g. tensile strength, compressive strength, bend strength, fracture strength etc.

The "theoretical strength" of a material is defined as the tensile stress required to break atomic bonds and pull a structure apart. Orowan (86) derived the following equation for estimating theoretical strength under tensile loading.

$$\sigma_{th} = \left(\frac{E\gamma}{a_o} \right)^{\frac{1}{2}} \qquad (2.8).$$

Where σ_{th} = theoretical strength

E = Young's Modulus

γ = fracture surface energy

a_o = inter-atomic spacing

The theoretical strength for ceramic materials varies, typically, from 0.1 to 0.2E. There is a large discrepancy between the theoretical fracture strengths and the measured fracture strengths (generally around 0.001 to 0.002E) of practical engineering ceramics (87). The reason for this is that most structural materials contain flaws or cracks that are introduced either during fabrication or service. The presence of these flaws results in a localised concentration of the applied stress.

2.6.3 Fundamentals of Fracture Mechanics

Under various combinations of static and alternating loads, and a reactive environment, the flaws in a material may grow slowly and stably. Unstable fracture will occur in a structure when a flaw has reached a critical size.

The original analysis of the critical stress to propagate cracks was carried out by Griffith and published in two classic papers (5, 88). The essential feature is the balance between the energy required to form two new fracture faces and the released elastic strain energy. Crack tip processes and micromechanism of crack advance are not considered.

Consider the total change in energy (ΔW) when a crack of length 2a is introduced into an infinite plate of unit thickness which is subjected to an applied stress σ .

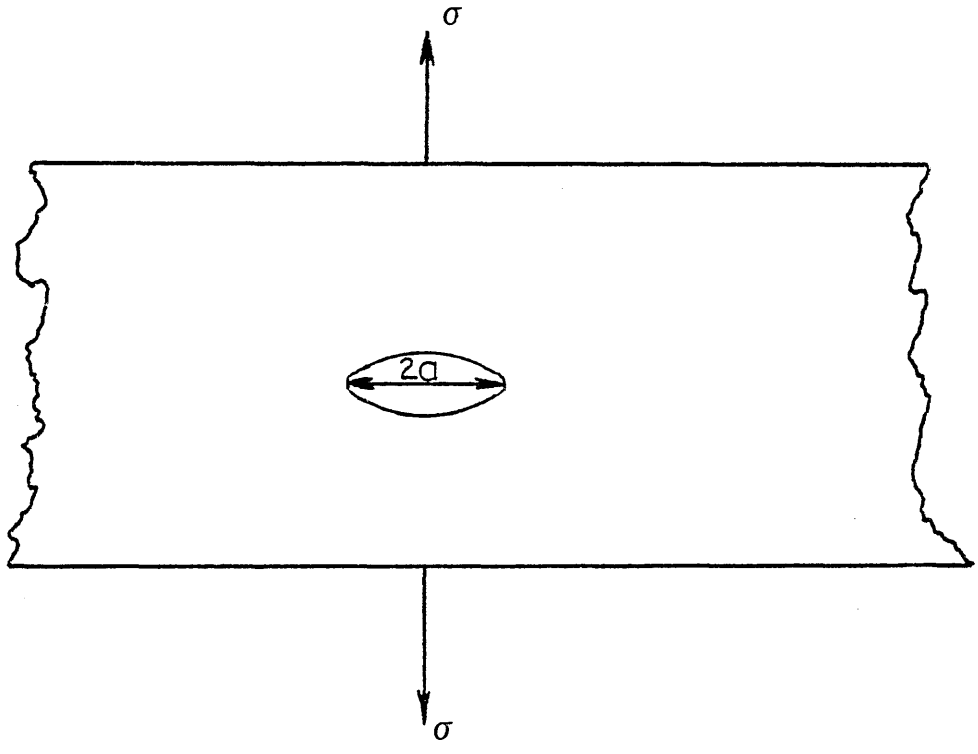


Fig. 2.16 Thin crack under uniaxial tension (model used in Griffith analysis)

then, $\Delta W = U + S$

where U = Elastic energy out (2.9).

S = energy in

S is the energy required to create two crack surfaces having surface energy γ_s per unit area:

$$S = 4a\gamma_S \qquad (2.10).$$

U is the decrease in elastic strain energy arising from the unloading of the material is the vicinity of the crack:

$$U = \frac{-\sigma^2\pi \cdot a^2}{E'} \qquad (2.11).$$

Where E' = E (Young's Modulus) for plane stress

$= \frac{E}{1-\upsilon^2}$ for plane strain (υ = Poisson's Ratio)

For unstable crack propagation, one needs to consider the change in W as a function of crack length. If $\frac{d\Delta W}{da} \leqslant 0$ unstable crack propagation will occur. Therefore for instability

$$\frac{du}{da} + \frac{dS}{da} \leqslant 0 \qquad (2.12).$$

i.e. $$\frac{-2\sigma^2\pi a}{E'} + 4\gamma_S \leqslant 0$$

in the limiting condition: (2.13).

$$\sigma_f = \left(\frac{2E'\gamma_s}{\pi a} \right)^{1/2}$$

where σ_f is the applied stress required for fracture to occur.

i.e. $$\sigma_f \propto \frac{1}{\sqrt{a}} \quad (2.14).$$

for all brittle materials.

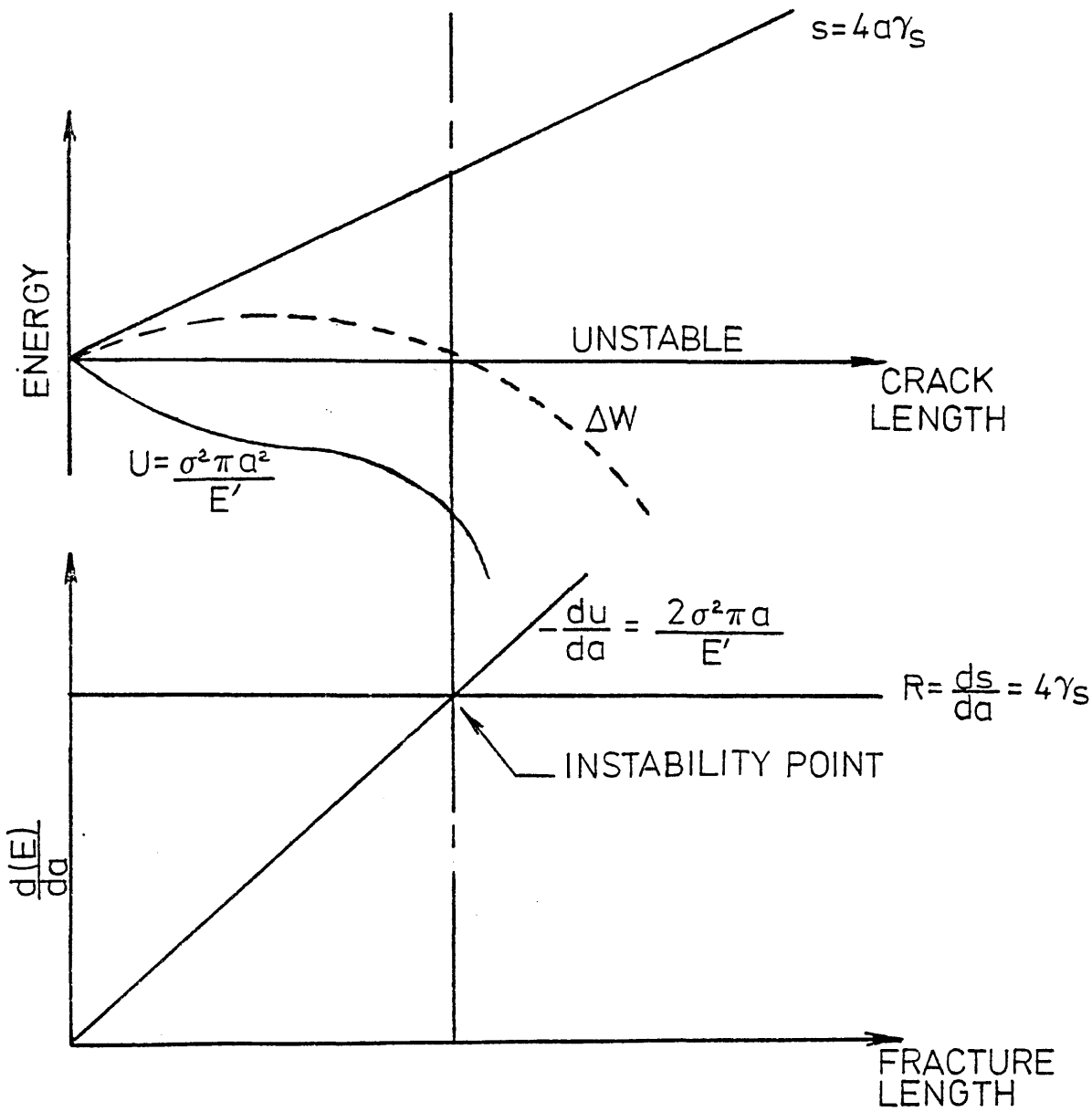


Fig. 2.17 Griffith criteria for unstable crack growth (fracture)

Equation (2.13) was later modified by Irwin and Orowan (89) to the form:

$$\sigma_f = \frac{1}{Y}\left(\frac{2E'\gamma_i}{a}\right)^{1/2} \qquad (2.15)$$

where γ_i = effective surface energy for fracture initiation

Y = a geometrical constant

2.6.4 Fracture Strength and its Measurement

The fracture strength (σ_f) of brittle materials is discussed generally in terms of the modified Griffith equation (2.15). The relevant parameters are those that affect γ_i and a. The microstructural dependence of γ_i varies from one material to the next. The flaw size, a, has a direct influence on the strength, as is illustrated in the equations. The strength of a material decreases as the flaw size increases. For most materials, the flaw size is related to the pore and grain sizes. The effect on strength is determined by the largest flaw. Thus the relative size of grains and pores, or other flaws, will dictate which of these is important.

The strength of a brittle material is generally characterised by bend testing (90), in which the specimen is broken in a 3 or 4-point loading system. Since the compressive strengths of brittle materials are much greater than tensile strengths, failure in bending will be due to tensile stresses. The test specimen can have a circular, square, or rectangular cross-section, provided it is uniform along the complete length. Such a specimen is relatively easy to fabricate.



Fig. 2.18 Schematic diagram of Bend Tests.

The bend strength is defined as the maximum tensile stress at failure and is referred to as the modulus of rupture (MOR). The bend strength (S) for a rectangular test specimen can be calculated using the general flexure stress formula:

$$S = \frac{Mc}{I} \qquad (2.16).$$

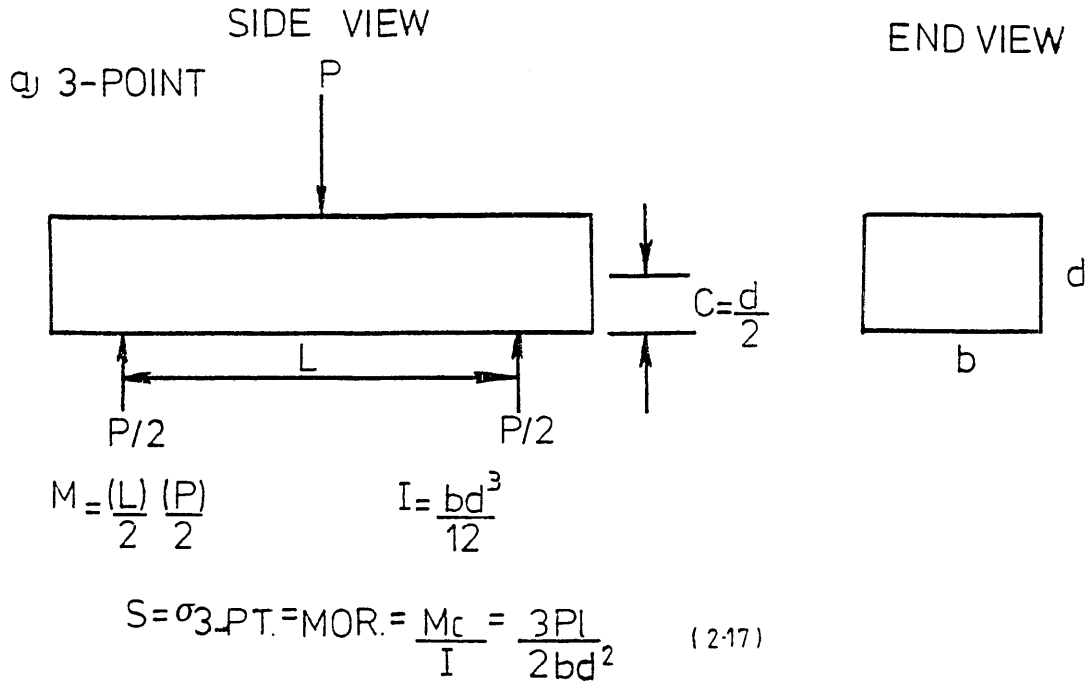
where M = moment

C = distance from neutral axis to tensile surface

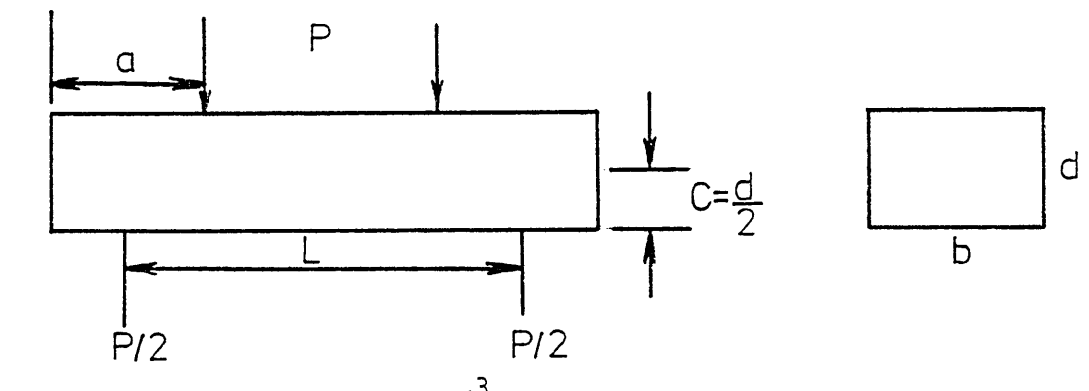
I = moment of inertia

For a rectangular test specimen $I = \frac{bd^3}{12}$ and $C = \frac{d}{2}$

where d is the thickness of the specimen and b is the width. Fig. 2.19 illustrates the derivation of the 3 and 4 point flexure formulae for rectangular bars.



$$S=\sigma_{3\text{-PT.}}=MOR.=\frac{Mc}{I}=\frac{3Pl}{2bd^2} \qquad (2.17)$$



$$S=\sigma_{4\text{-PT.}}=MOR=\frac{Mc}{I}=\frac{3Pa}{bd^2} \qquad (2.18)$$

Fig. 2.19 Derivation of 3 and 4-point flexure formulae for a rectangular bar.

The strength data is relatively straight forward to obtain, but there is a severe limitation on the use of MOR data obtained for ceramics: the measured strength will vary significantly depending on the size of specimens and whether it is measured in 3 or 4-point bending.

The stress distribution for 3 and 4-point bending is shown in Fig. 2.20 after Benham (91). In the case of 3-point, the peak stress occurs only along a single line on the surface of the test bar opposite the point of loading. The stress decreases linearly along the length of the bar and into the thickness of the bar, reaching zero at the bottom supports and at the neutral axis, respectively. The probability of the largest flaw in the specimen being at the surface along the line of peak stress is very low. Therefore, the specimen will either fracture at a flaw smaller than the largest flaw or in a region of lower stress, whichever one satisfies equation (2.13) first. The MOR measured in a 3-point bend test does not reveal the strength limit of the material, or even the local stress and flaw size that caused fracture. All it reveals is the peak stress on the tensile surface at the time of fracture.

4-point bending tests yield lower strength values for a given material than does 3-point. Fig. 2.20 (b) illustrates the stress distribution in a 4-point bend specimen. The peak stress is present over the area of the tensile face between the load points. The tensile stress decreases linearly from the surface to zero at the neutral axis and from the load points to zero at the bottom supports. The area and volume under peak tensile stress or near-peak tensile stress is much greater for 4-point bending than for 3-point bending, and thus the probability of a larger flaw being exposed to a high stress is increased.

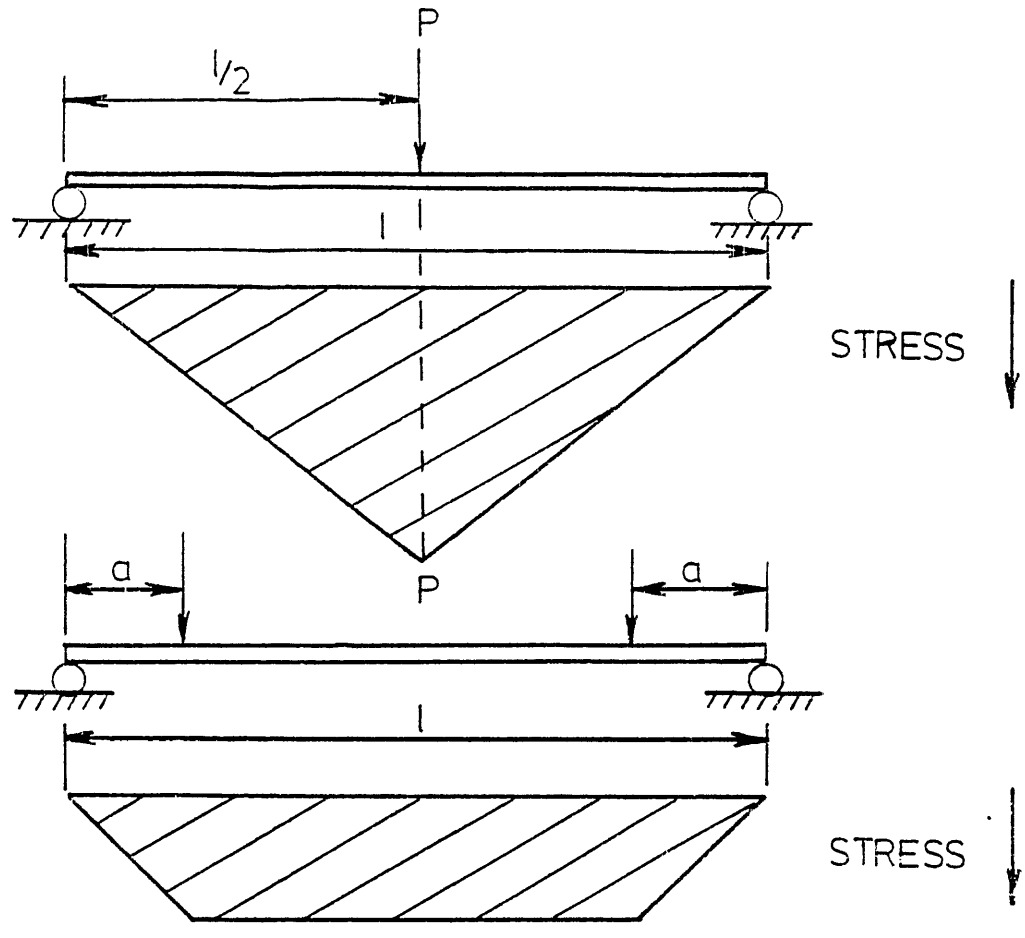


Fig. 2.20 Comparison of the tensile stress distributions for (a) 3-point and (b) 4-point bend tests.

It would appear, then, that a 4-point test is far superior to 3-point and should always be used in preference. However, in its defence, the 3-point test is much easier to set up and less time consuming in alignment. Errors can be reduced by statistically analysing a large number of specimens and, as the errors are roughly the same in each test, 3-point results are very useful for comparative work. Also, in many cases 3-point loading is the closest approximation to that which will be endured when the material is in use.

2.6.5 Fracture Toughness

Stress concentrations at crack tips are caused by the presence of cracks in the material under stress. Fracture will occur when the stress at the tip of a crack, which was initially stable, has reached a critical value or when a propagating crack has grown to a critical size. Hence, the fracture toughness of a material is a measurement of its resistance to failure in the presence of a crack. This parameter is sometimes referred to as "notch brittleness" (92). Brittle materials are indicated by a low value of fracture toughness. The most widely used approach for finding the fracture toughness of a material is via:

The Stress intensity Factor K

1. Elastic Stress Concentration

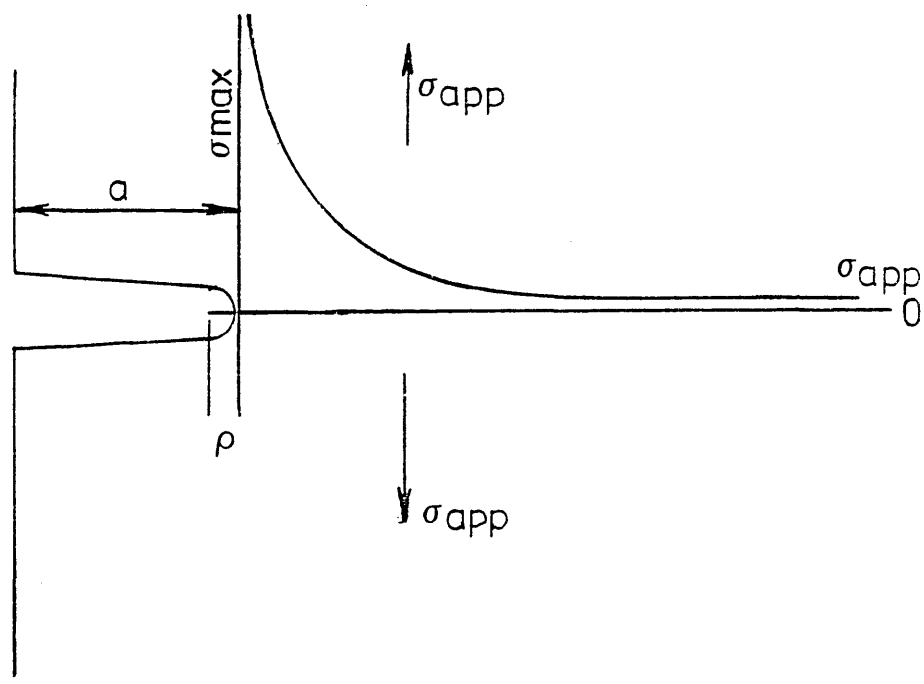


Fig. 2.21 Stress concentration at a surface flaw under a tensile stress.

The maximum stress at the tip of an elliptical notch of depth a and crack root radius ρ , under an applied stress σapp was analysed by Inglis (93). σmax is given by

$$\sigma max = \sigma app\left(1 + 2\sqrt{a/\rho}\right) \qquad (2.19).$$

For sharp cracks $a \gg \rho$

$$\sigma max = 2\ \sigma app\ (a/\rho)^{1/2} \qquad (2.20).$$

For fracture to occur in an ideal brittle material, a second condition is necessary in addition to the Griffith energy requirement. The maximum stress must reach the theoretical strength of the material to provide the mechanism for fracture. Using the Orowan estimate for the theoretical strength (2.8) and equating this to σmax gives for the failure stress:

$$\sigma_f = \left(\frac{E\gamma\rho}{4a_0 a}\right)^{1/2} \qquad (2.21).$$

From (2.20), for very sharp cracks when $\rho \to 0$ σmax should tend to infinity. For most materials, however, deformation with plastic blunting occurs at the crack tip and the maximum stress concentration is thereby reduced. In the limiting case, because the crack passes between adjacent planes of atoms, a reasonable estimate for the smallest possible value of the crack tip radius is half the inter-atomic spacing. Substitution for this in (2.21) gives the second necessary condition for fracture:

$$\sigma_f = \left(\frac{E\gamma}{8a}\right)^{1/2} \qquad (2.22).$$

However, for many materials, fracture is not associated with the attainment of a critical value of tensile stress. For this reason, σmax does not provide a reliable basis for the avoidance of brittle fracture.

ii. Elastic Stress-field around an Infinitely Sharp Crack

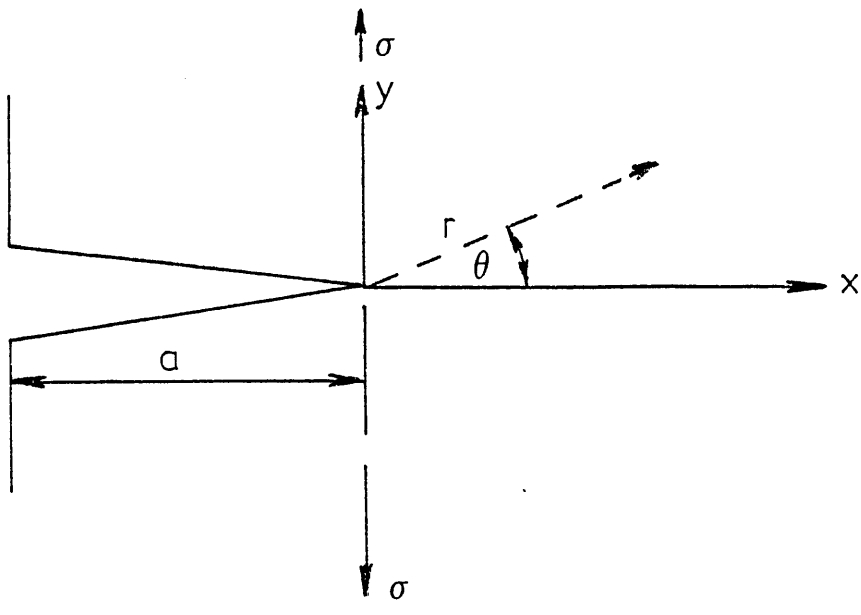


Fig. 2.22 Definition of the co-ordinate system for stress in the vicinity of a sharp crack.

Under the influence of a remote stress σ, the elastic stresses close to the tip of the crack of length a are given by:

$$\sigma_y = \sigma\left(\frac{a}{2r}\right)^{1/2} \cos\left(\frac{\theta}{2}\right)\left[1+\sin\left(\frac{\theta}{2}\right)\sin\left(\frac{3\theta}{2}\right)\right] \qquad (2.23)$$

$$\sigma_x = \sigma\left(\frac{a}{2r}\right)^{1/2} \cos\left(\frac{\theta}{2}\right)\left[1-\sin\left(\frac{\theta}{2}\right)\sin\left(\frac{3\theta}{2}\right)\right]$$

For plane stress (thin sheet) $\sigma_z = 0$

For plane strain (thick sheet) $\sigma_z = \upsilon(\sigma_x + \sigma_y)$

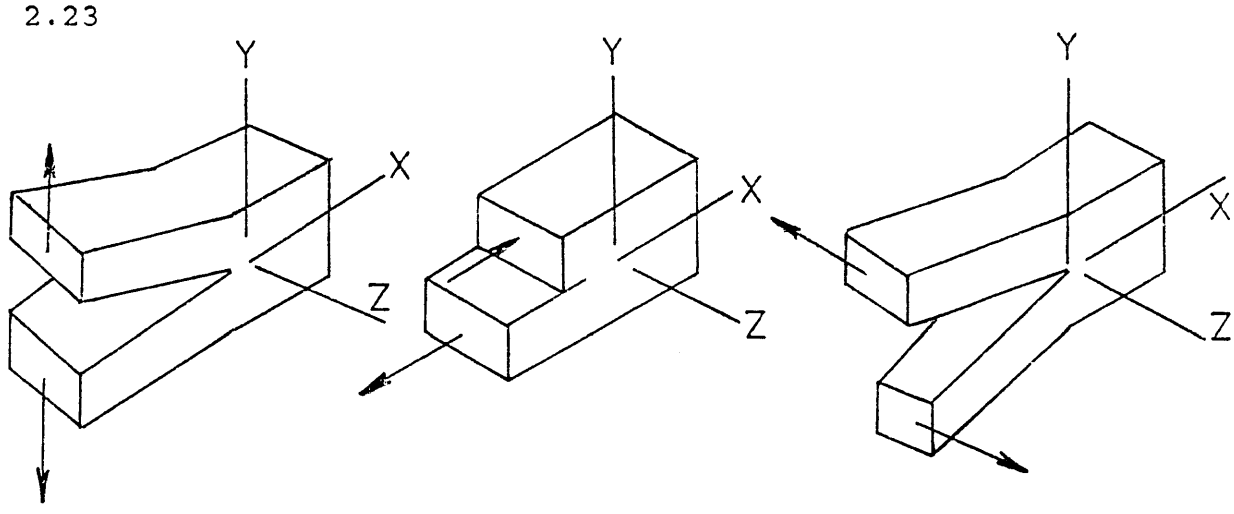
in the plane of the crack $\theta = 0$

Therefore $$\sigma_y = \sigma_x = \sigma\left(\frac{a}{2r}\right)^{1/2} = \sigma\left(\frac{\pi a}{2\pi r}\right)^{1/2} \qquad (2.24)$$

$$= \frac{K_I}{2\pi r} \qquad (2.25)$$

where $K_I = \sigma(\pi a)^{1/2}$ (2.26)

K is called the stress intensity factor, the subscript I indicates that the crack extends under the influence of a tensile stress normal to the crack plane. There are two other opening modes due to shear as is illustrated in Fig. 2.23



MODE I K_I MODE II K_{II} MODE III K_{III}

Fig. 2.23 Stress intensity factor notations for various displacement modes.

K is independent of r and is determined only by the crack length and the remote stress. It is a single parameter which completely specifies the amplitude of the stress field in the vicinity of the crack tip.

iii. Critical Stress Intensity K_c

The only parameter which distinguishes one crack situation from another is K. Therefore, if fracture is controlled by conditions in the vicinity of the crack tip, failure must be associated with the attainment of a critical stress intensity K_c.

Therefore at fracture; $K_c = \sigma_f (\pi a_c)^{1/2}$ (2.27)

where σ_f is the critical value of applied stress required to fracture a specimen containing a defect of length a, or alternatively, a_c is the critical defect size for a constant applied stress σ_f. K_c is a macroscopic criterion for failure. It makes no assumption about the precise mechanism of fracture. Whether it requires a critical stress, strain or energy release rate need not be specified. K is a stress field parameter independent of the material. K_{IC} is a characteristic material property and is called the "Plane Strain Fracture Toughness." One advantage of measuring K_{IC} is that the value may be used to compare the basic toughness of different materials (94). Equation (2.27) is only valid for an infinite plate of an ideally elastic material containing a central crack of length 2a. For the general case of a crack in a material having finite dimensions:-

$$K_{IC} = Y \sigma_f (a)^{1/2} \qquad (2.28).$$

Where Y is a geometric factor dependent on the dimensions of the component and the shape of the crack. Y can be calculated from the appropriate elasticity equations given by Paris and Sih (95).

iv. Thickness Effect

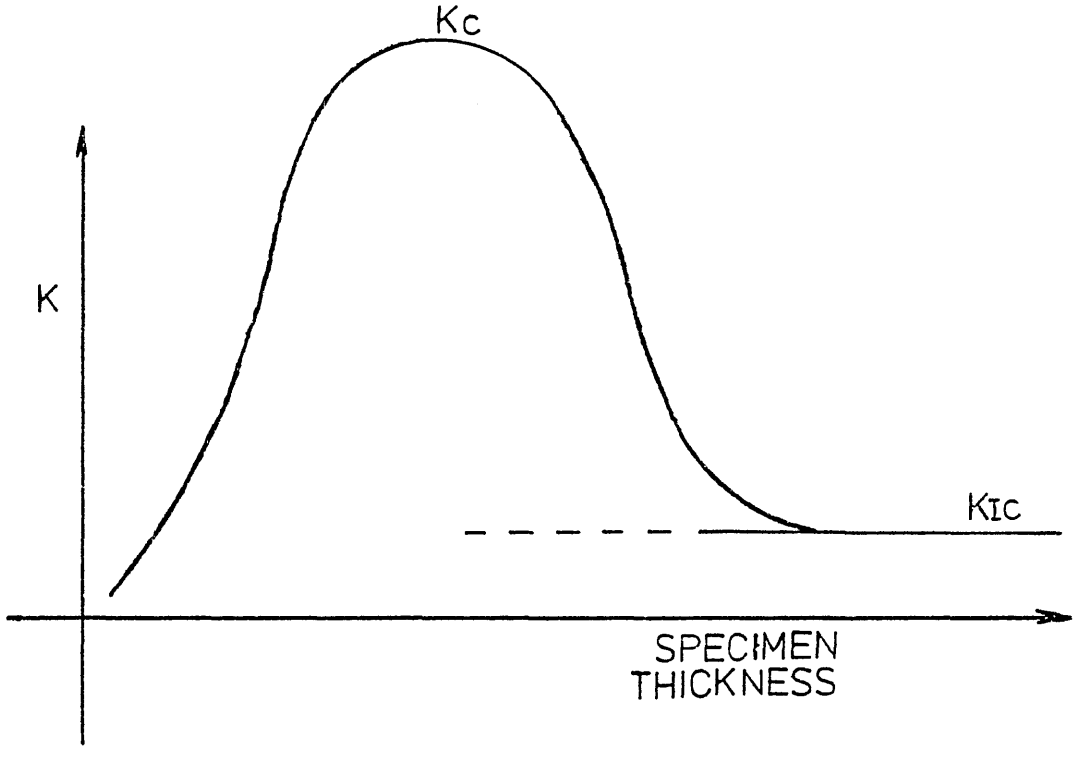


Fig. 2.24 Variation of K with specimen thickness.

The "plane strain fracture toughness", K_{IC} , is a true material property. Providing plane strain conditions prevail, it is independent of specimen dimensions. This requires a sufficiently large specimen thickness which is usually taken as:

$$b > 2.5(K_{IC}/\sigma y)^2 \qquad (2.29)$$

where b = specimen width

σy = material yield strength

Because of the limited plasticity, the ratio K_{Ic}/σ_y is generally very very small for brittle materials such as vitreous carbon and so the thickness constraint is nearly always satisfied. Indeed, the only thickness constraint that usually needs to be imposed is that the section is large enough to be microstructurally representative of the material (96). The limited plasticity also leads to ideal behaviour for fracture mechanics measurements, i.e. no deviations from linearity occur.

For sections thinner than the minimum thickness for plane strain, increasing amounts of through-thickness deformation take place, and K_C increases steadily until a maximum plane stress value is reached. Fracture then occurs on planes of maximum shear stress, inclined at 45° to the thickness direction. For design purposes, the plane strain toughness K_{Ic} is usually employed because it represents the most severe stress concentration which would be experienced in service.

2.6.6 Fracture Toughness Measurement

Test specimens with a rectangular cross-section may be machined from ceramic specimens. While the process may be time consuming, it is easier to fabricate beam specimens than those with circular cross-section. Fracture toughness measurements may be made by introducing a notch, with a diamond saw, into one surface to a depth of approximately half the thickness of the sample, known as a single edge notched beam specimen (SENB). The specimen may then be tested in 3-point bending. The arguments mentioned earlier

(section 2.6.4) against 3-point bending do not apply since the machined flaw is so much larger than any inherent flaws it is the only one which can initiate fracture. If a notch is sawn in a very brittle material a certain amount of crack growth at the notch tip occurs, so the crack length is generally measured after the test is complete using a travelling microscope. K_{IC} is calculated by substituting for σ_f, found from equation (2.17), into (2.28).

$$K_{IC} = y\left(\frac{3Pla^{\frac{1}{2}}}{2bd^2}\right) \qquad (2.30)$$

2.7. Mechanical Properties of Amorphous Carbon

2.7.1. General Considerations

The carbonisation of certain cross-linked polymers, under carefully controlled conditions, yields a non-graphitising carbon material which, on account of its non-crystalline, isotropic structure, is referred to as Amorphous Carbon. Because of its high lusture and similarity to glass in both appearance and fracture, the material is also known as Vitreous Carbon (97).

Vitreous or Amorphous Carbon, then, is the glassy appearing carbonaceous residue from the pyrolysis of a polymeric resin precursor (98). The material is typified by a low density of around 1.5 gcm^{-3} (99). A variety of defects identified in the material have been attributed to residual impurities that are presumably present in the parent polymer (100). The presence of these defects is thought to be responsible for the highly variable strengths observed in amorphous carbon. The fracture strength is found to vary depending on the quality and heat-treatment temperature of the material. Fractographs of amorphous carbon which had failed in three point bending (which is generally accepted as the most useful method of measuring the mechanical properties of the material) show a smooth, featureless, concoidal fracture surface similar to that of glass (101).

The mechanical properties of amorphous carbon are directly related to their structure which consists of a three-dimensional network of aromatic ribbons with three types of bonding therein. Between closely spaced parallel

ribbons only weak Van der Waal's forces exist, which can be neglected. Within the ribbons, because of its extremely stiff covalent characteristic, the C-C bond is the stiffest component of the system. However, this is only noticed with a high degree of preferred orientation as is the case in carbon fibres. In a random configuration of ribbons, the response to an applied stress is related mainly to the ease of rotating ribbon segments with respect to their environment and is resisted by carbon bonding between the ribbons.

Considering its isotropic, non-crystalline structure, the Young's Modulus, as well as the hardness, of glassy carbon is very high. This is due in the main to the presence of stable inter-fibrillar cross-links which prevent aromatic ribbon molecules in the fibrils from shearing past each other (69). As a result of its hardness, relatively high strength and chemical inertness to body fluids (102) amorphous carbon has found itself employed as a structural material for biomedical applications (103). However, the material is somewhat limited when load bearing is required because of its extreme brittleness (104). Vitreous carbon is much stronger than most other carbons or graphites. It has a hardness value of between 6 and 7 on Mohs' scale. When using the Vickers Diamond Indentation equipment, the indentation disappears almost as soon as the pressure is relieved, suggesting that the material retains some of its elastic properties after heat treatment (105).

The hardness and high strength of the material suggest that the structure includes some tetrahedral cross-links between the hexagonal layers. This is considered likely in view of the presence of such cross-links in the starting material and the isotropy of properties irrespective of the method of fabrication of the polymer precursor. The inter-fibrillar cross-links are strained, and so are less thermally stable than the graphite trigonal bond within the ribbons. They are thus progressively ruptured at high temperatures and thought to be responsible for viscoelastic behaviour observed at about 2500°C (101).

2.7.2 Elastic Response of Amorphous Carbon

Fischbach (106) and Taylor and Kline (107) reported room temperature Young's Modulus measurements on amorphous carbon at different heat-treatment temperatures. Values varied between 26 and 29 GNm^{-2}. These results indicated a consistent decrease in modulus with increase of heat-treatment temperature above 1000°C. The values quoted are relatively high for an isotropic, low density carbon. The superior stiffness of glassy carbon is attributed to the strong boundary restraint at the edges of the component ribbons and strong interlamellar bonding up to heat-treatment temperatures of 2000°C (108). Andrew and Sato (109) showed that as the heat-treatment temperature of the material increases above 1500°C the modulus decreases.

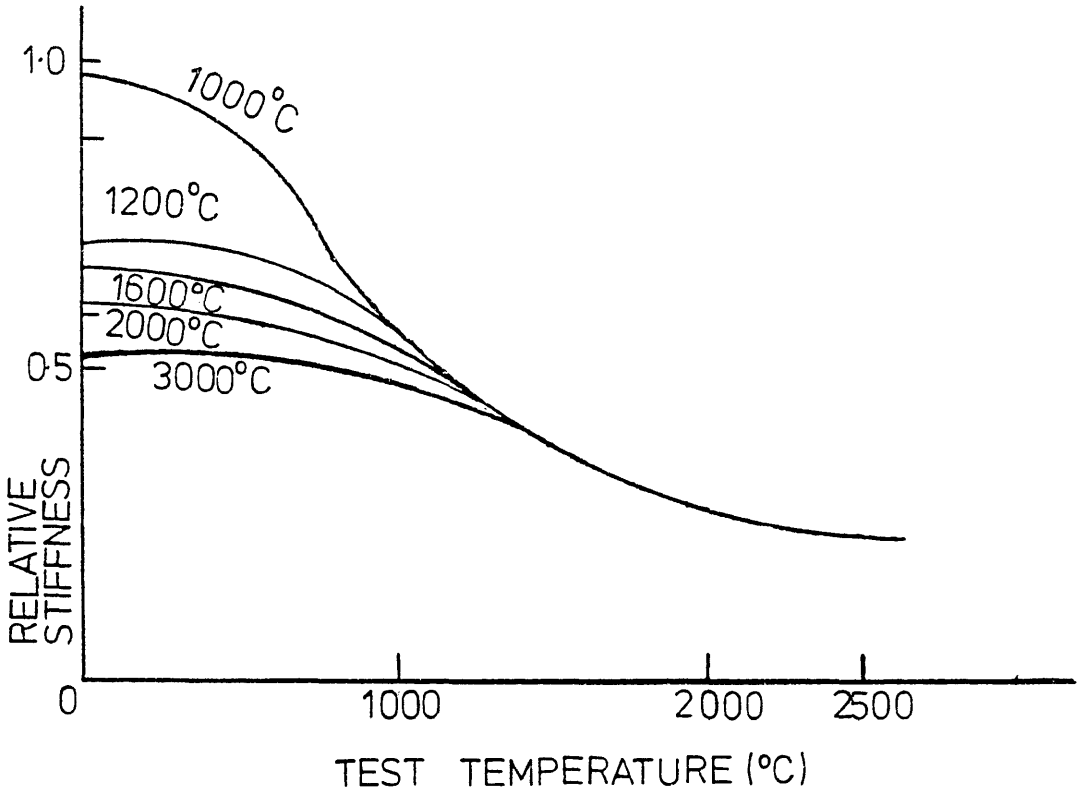


Fig 2.25 Variation of relative stiffness with test temperature in glassy carbons heat-treated from 1000 to 3000°C (After Andrew and Sato (109)).

Up to a heat-treatment temperature of 1500°C the Young's modulus of glassy carbon increases rapidly. For heat treatment above 1500°C the elastic modulus decreases considerably as interfibrillar cross-links are progressively ruptured.

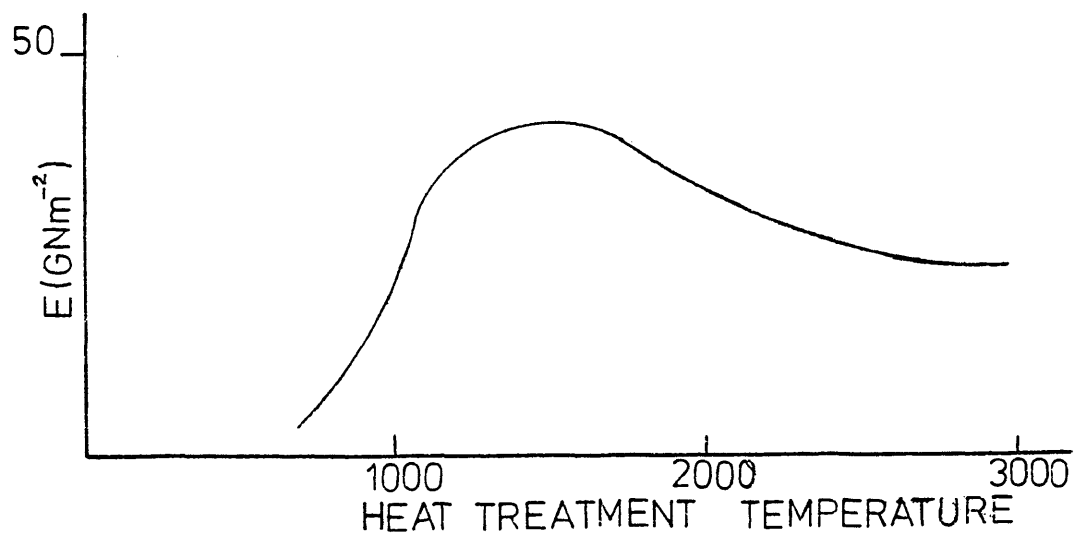


Fig 2.26 Variation in Young's Modulus of glassy carbon for pyrolysis to 3000°C.

The absence of a positive temperature coefficient in the Young's modulus of glassy carbon indicates the absence of interlamellar microcracks, which would tend to be filled in as the temperature is raised. The differential movement between material above and below the cracks is inhibited so the material stiffens as a result. This absence of interlamellar microcracking is probably due to the very small layer sizes and high degree of cross-linking.

Fischbach (106) has shown that at high temperature (above 2000°C) it is possible to cause plastic deformation in amorphous carbon which produces structural anisotropy in the material and can be detected by magnetic susceptibility measurements. He also showed that 7% elastic recovery is possible. It appears that above 2000°C the material becomes viscoelastic. 2500°C can be regarded as a 'glass transition point' by analogy to the behaviour of low temperature polymers. This plasticity is accompanied by an increase in open porosity.

2.7.3. Hardness of Vitreous Carbon

Vitreous Carbon is a very hard and brittle material, it will scratch most forms of siliceous glass and can be cut only with a diamond tool, or an ultrasonic technique (109). Hardness and resistance to deformation are sensitive to the amount of cross-linking between chain polymers and between the aromatic ribbon molecules. It is therefore possible to deduce the carbonization mechanism and the structure of the resulting amorphous carbon from hardness measurements on resin carbonized at various temperatures.

The hardness of the material can be determined using a Vickers micro-hardness testing machine. The Diamond Pyramid Hardness (DPH) number is determined from the average length of the two diagonals in the indentation of a four sided diamond pyramid under an applied load of, typically, 100 g. Kawamura (110) found that the DPH is a useful measure of the Young's modulus of glassy carbon. He found that the relationship between Young's modulus and DPH is linear, intersecting both axes at zero.

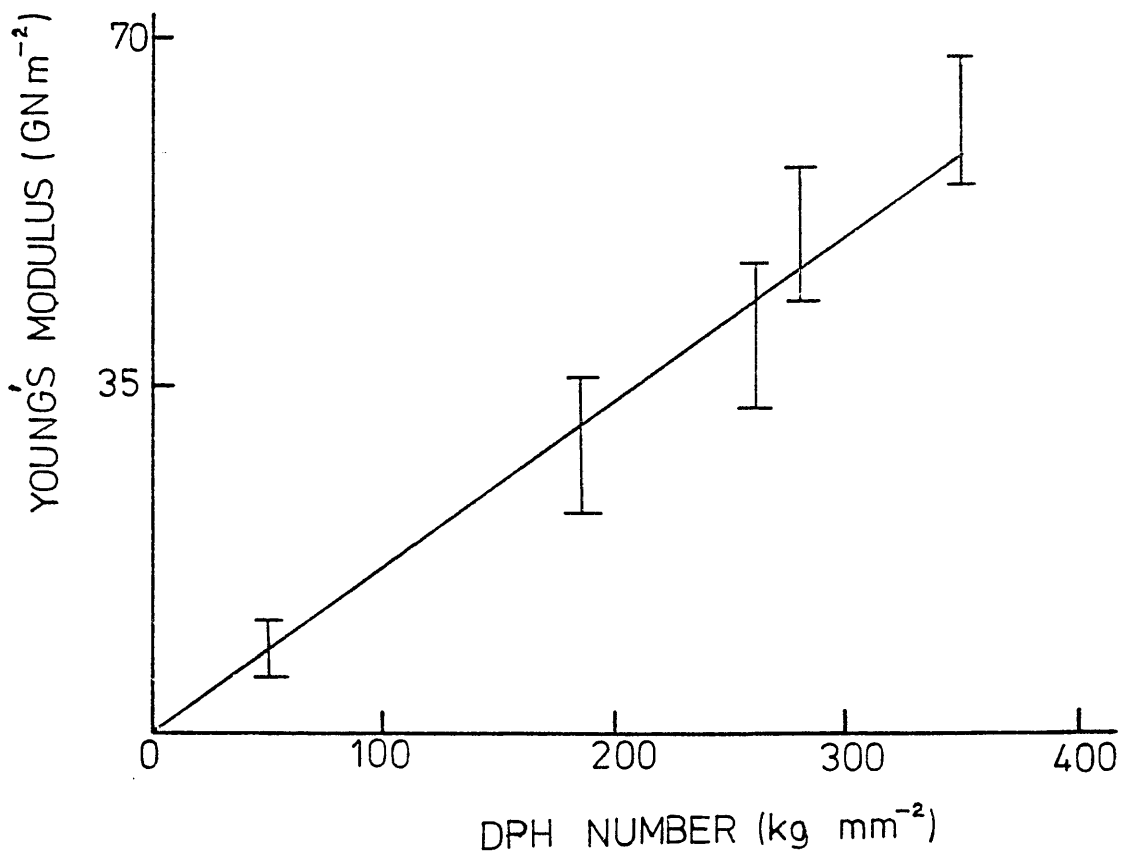


Fig 2.27 Variation of Young's modulus with DPH number for a range of glassy carbons subjected to various heat treatment temperatures (after Kawamura (110)).

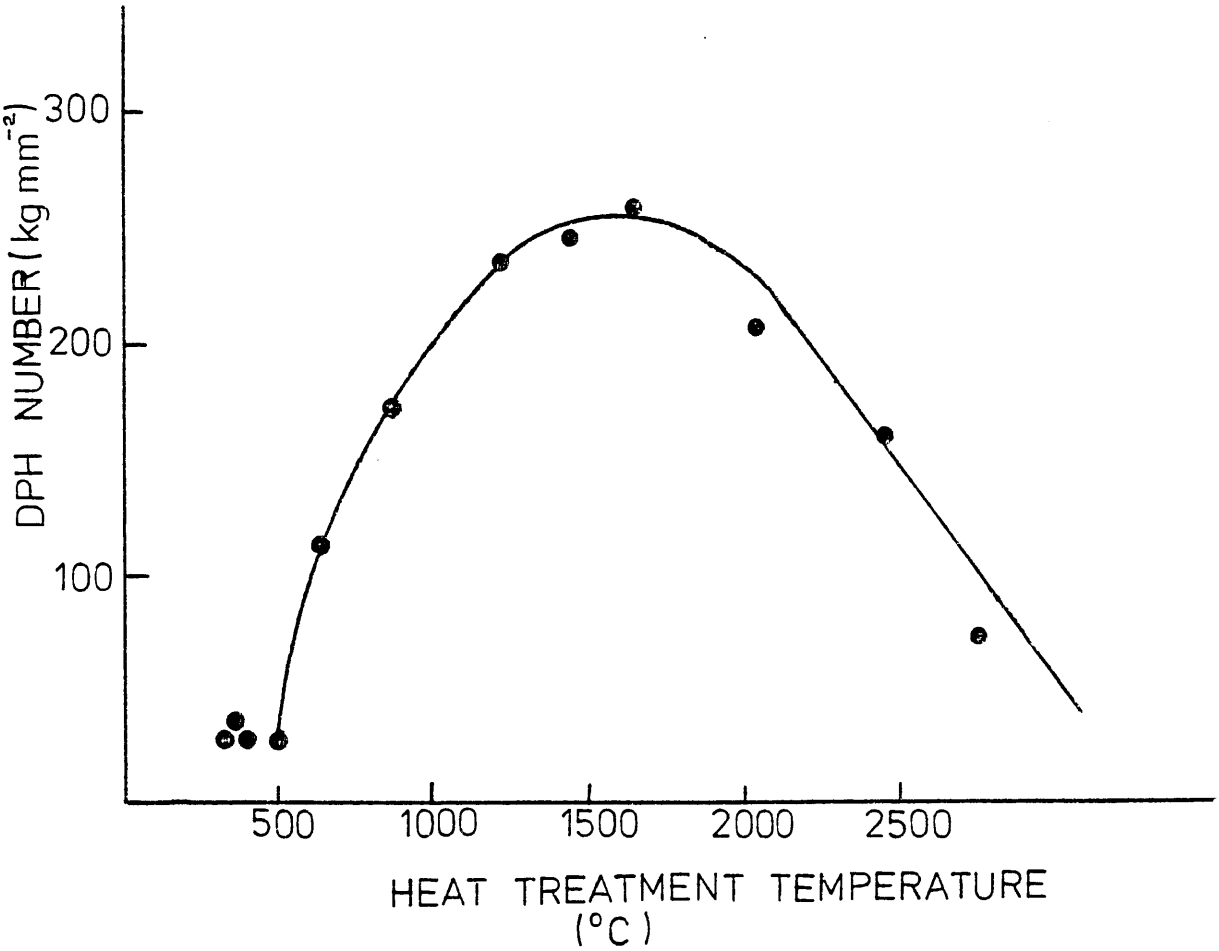


Fig 2.28 Shows the variation of DPH number of glassy carbon as a function of the heat treatment temperature.

The increase in hardness after heat treatment to 350°C supports the conclusion, deduced from infra-red spectroscopy studies, that intermolecular cross-links are formed between the chain polymers at that temperature. Infra-red spectroscopy results also suggest that aliphatic ether linkages are ruptured between 350 and 500°C resulting in a more open structure. This would explain the decrease in hardness within this temperature range.

The rapid increase in hardness on annealing above 500°C is due to the formation of inter-ribbon cross-linking. The decrease in hardness above 1500°C is thought to occur due to the breaking of these inter-ribbon cross-links allowing the release of internal strain energy in the tangled ribbons, leading to a decrease in the intermolecular forces and the associated hardness.

2.7.4 Strength and Fracture

The strength of amorphous carbon is structure sensitive and varies with density, degree of cross-linking and preferred orientation etc. (111). Strength is also sensitive to defects.The effect of defects is much more pronounced in glassy carbon than other materials, because of its inability to relax the stress build-up at inhomogeneities.

Fischbach and Kotlensky (41) measured the tensile and structural properties of amorphous carbon and showed that the strength decreases with increased test temperature. Sato and Asakura (112) measured the strength of glassy carbon as a function of heat treatment temperature; their results are presented in Table 2.3.

Test	Heat Treatment Temperature/°C	Average Value /MN m^{-2}	Standard Deviation/MN m^{-2}
Compression	1000	369	130
	2000	200	43
	3000	95	15
Flexion	1000	165	64
	2000	132	27
	3000	121	30

Table 2.3 Compressive and flexive strengths of glassy carbon (round bar specimens - after Sato and Asakura (112)).

Their results show that heat treatment above 1000°C drastically lowers the strength of glassy carbon. Johnson (113) showed that defects, such as voids and inclusions, in the precursor are carried over into the resulting carbon. Voids and cracks are also produced by the increased internal gas pressure during carbonization. As a result, it is not possible to make large bulk samples of glassy carbon without producing macropores and microcracks. The presence of these inhomogeneities in the structure would go some way in explaining the scatter generally observed in the strength measurements.

It is generally accepted that the strengthening and stiffening of vitreous carbon up to 1000°C is due to the increase in cross-linking between ribbon units. When some of the inter-ribbon cross-links are broken by high temperature heat treatment the apparent crystallite size within the material increases gradually, accompanied by a release of internal strain energy in the aromatic molecules. Increase in crystallite size makes crack propagation easier. The severence of inter-layer cross-links, in particular, promotes such crack propagation leading to a fall in strength at high temperatures.

SECTION 3

APPARATUS AND EXPERIMENTAL PROCEDURE

3.1 Materials

The raw material used for the production of the amorphous carbon in this study was "Qua-Corr Furan Resin No. 1001", a partially polymerised furfuryl alcohol resin having an average molecular weight of the dimer unit. The resin is manufactured by the Chemicals Division of the Quaker Oats Corporation. The catalyst employed was a saturated solution of zinc chloride in water (50:50 by weight) which is known as a Lewis acid. The graphite used in the composites was mineral graphite which had been sieved into 'nominal' size distributions and was supplied by Berol Ltd. via several commercial producers. The zinc oxide used as a pore former was BDH "Analar" grade.

3.2 Specimen Production

3.2.1 Casting of the Polymer Resin

Several methods of producing the polymerised resin have been investigated. The one which proved to be the most successful was as follows:-

The resin and catalyst were vigorously mixed in a disposable plastic cup. The amount of catalyst added was recorded as a weight %. After approximately 15 minutes stirring the resin and catalyst were adjudged to be properly mixed, and were put into a vacuum disiccator and evacuated for 1½ hours to remove air bubbles due to mixing. After

this period the vacuum pump was switched off and the mixture allowed to stand for a further hour under vacuum. The catalysed resin was carefully poured into a silicone rubber mould. The mould and contents were then placed inside an oven at the required temperature for the required time of curing. The temperature of the oven was controlled to ± 1°C. The moulds were made to the dimension 102 x 52 x 12mm. The inner surface of the moulds were produced to a high standard by forming over a metal former machined to a high finish with tolerances of ± .01mm. Before the resin was added, the moulds were sprayed with P.T.F.E. which acts as a release agent.

When the prescribed curing time was complete, the mould was removed from the oven and allowed to cool. The cured polymer block could then easily be prised from the mould. 1mm was machined off each face of the block to ensure that is was perfectly regular. The machined block was cut into beams 6mm wide (± .25mm) to produce specimens ready for heat treatment.

3.2.2 Casting Composite Resins

Graphite or zinc oxide powders were added by weight % to the resin to produce composites. Graphite loadings of up to 10%, and all the specimens using zinc oxide, were made by mixing by hand. The resin and powder were placed in a glass beaker and stirred vigorously for 30 minutes with a spatula. This mixture was then evacuated in a desiccator as in section 3.2.1. The catalyst was added after evacuationand the remainder of the preparation identical to that used for the resin alone.

When the amount of graphite was greater than 10% the viscosity of the mix is too high for it to be mixed by hand. The resin and graphite were placed in the Z - blade mixer belonging to Berol Ltd. and mechanically mixed for 2 hours whilst being continually evacuated. The catalyst was added after this period and the mixing continued for a further two hours. The 'green' composite was then poured into silicone rubber moulds to be cured and machined as before.

3.2.3 Production of Amorphous Carbon

To produce amorphous carbon, which is strong, and with a fine grained porosity, required a very slow heating rate from room temperature upwards. The furnace used for the initial investigation into the processing of the polymer was the one originally designed and built for the heat treatment of sub. mm. leads. This proved, however, to have too small a capacity for producing the large number of specimens required for mechanical testing. This and other fabrication problems necessitated the designing and building of a new, larger and improved heat treatment furnace with modified gas purification.

The pyrolysis was performed in an inert atmosphere of high purity Argon (3 ppm. oxygen). Previous work had found that even with an oxygen partial pressure as low as this, some carbon was lost due to oxidation. Also there was a tendency for the gas to contain a small amount of moisture, probably left over from when the cylinder was cleaned. To combat this, the Argon from the cylinder was further purified by pre-drying and removal of the residual oxygen

prior to being introduced into the heat treatment furnace. A flow diagram explaining the gas purification system is shown in Fig. 3.1.

(i) Argon Pre-Treatment

After release from the cylinder the argon was dried by passing through a series of 3 standard drying columns employing a molecular sieve. The gas was then fed into the pre-treatment furnace for deoxygenation.

The Furnace consisted of a horizontal, 430 mm. long, alumina winding tube. The tube was wound with Kanthal A1 resistance wire. A mullite reaction tube, 590 mm. long, with cones ground on either end was placed inside the winding tube. Connections to the gas supply were made via standard pyrex cones. The control thermocouple (chromel-alumel) was placed in the centre of the furnace between the winding and reaction tubes. The reaction tube was filled with titanium granules and maintained at 900°C throughout the processing of the polymer specimens in order to act as a 'getter' for the residual oxygen in the argon. The furnace is shown in Fig. 3.2, the temperature was maintained by a CAL model 6103 controller.

(ii) Carbon Heat-Treatment Furnace

The furnace consisted of a 900 mm alumina reaction tube held in a horizontal position within the furnace. Heat was supplied by eight "Crusilite" elements surrounding the reaction tube. The elements are connected as two groups of four in series, with the two groups being connected in parallel with each other. Connections to the gas supply are made via water-cooled brass end-caps employing "O" ring

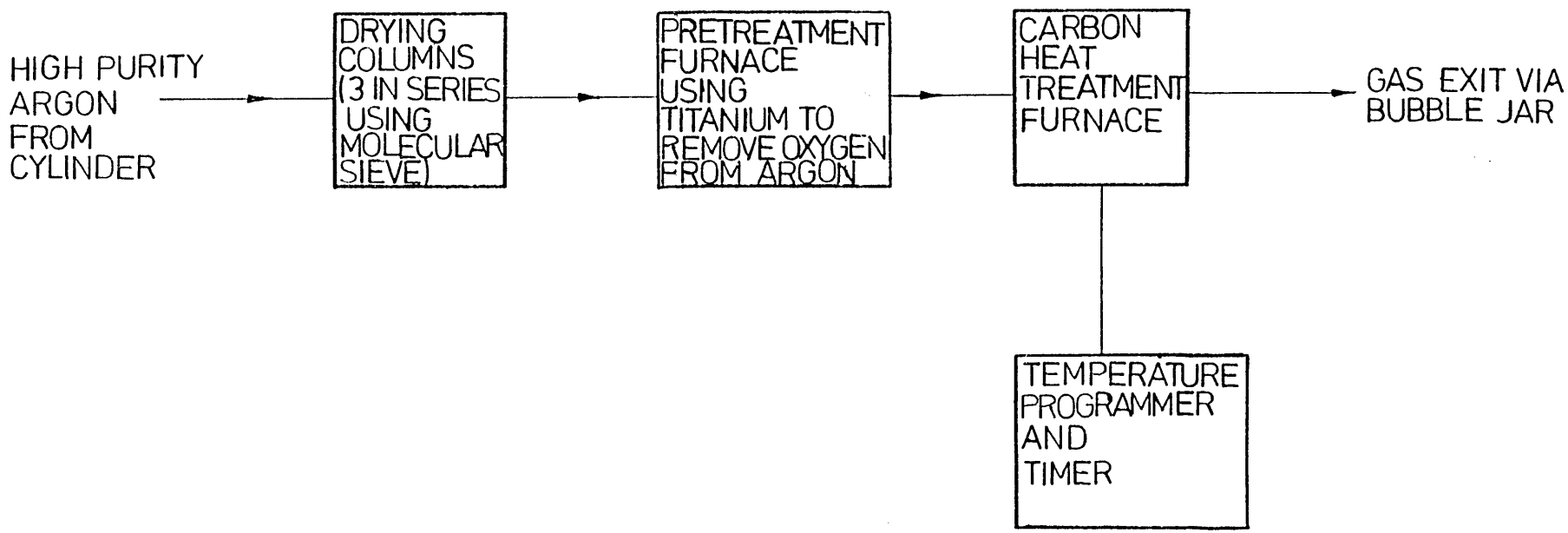
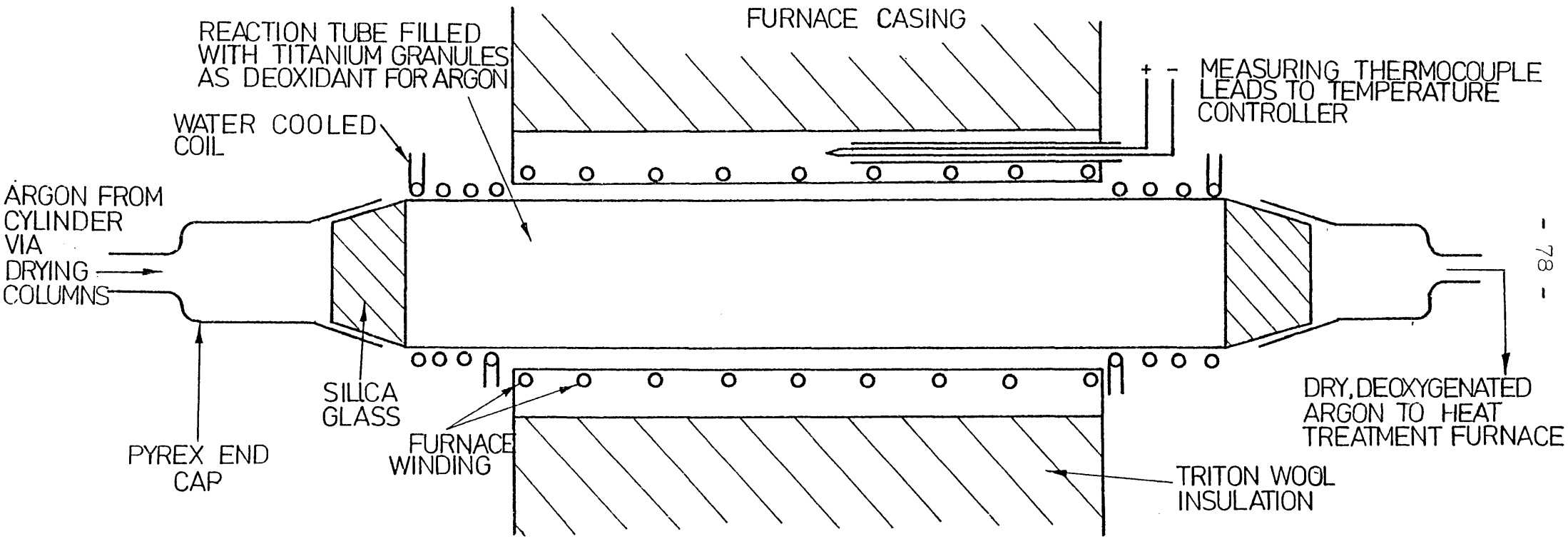


FIG. 3·1. FLOW DIAGRAM SHOWING THE STAGES IN THE PURIFICATION OF THE ARGON SUPPLY.

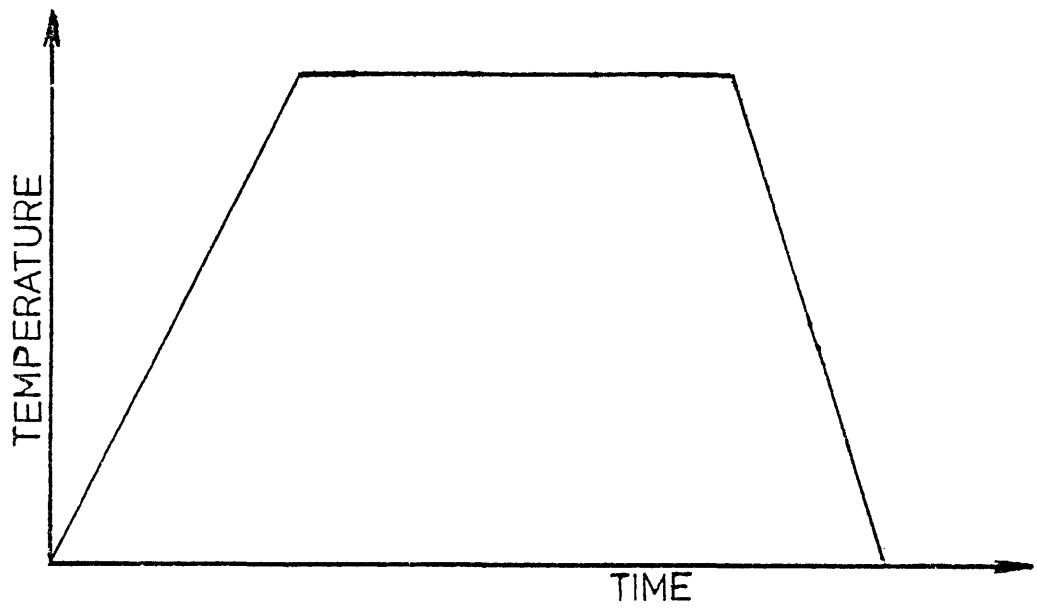


Winding Tube	Alumina	430 mm Long	35 mm Dia.	
Reaction Tube	Mullite	590 mm Long	27 mm Dia.	Ends ground to accept standard B 24 ground glass socket.
Furnace Winding	Kanthal	18 swg wound over 12 inches at 12 TPI.		
Winding Resistance	29 Ohms.			

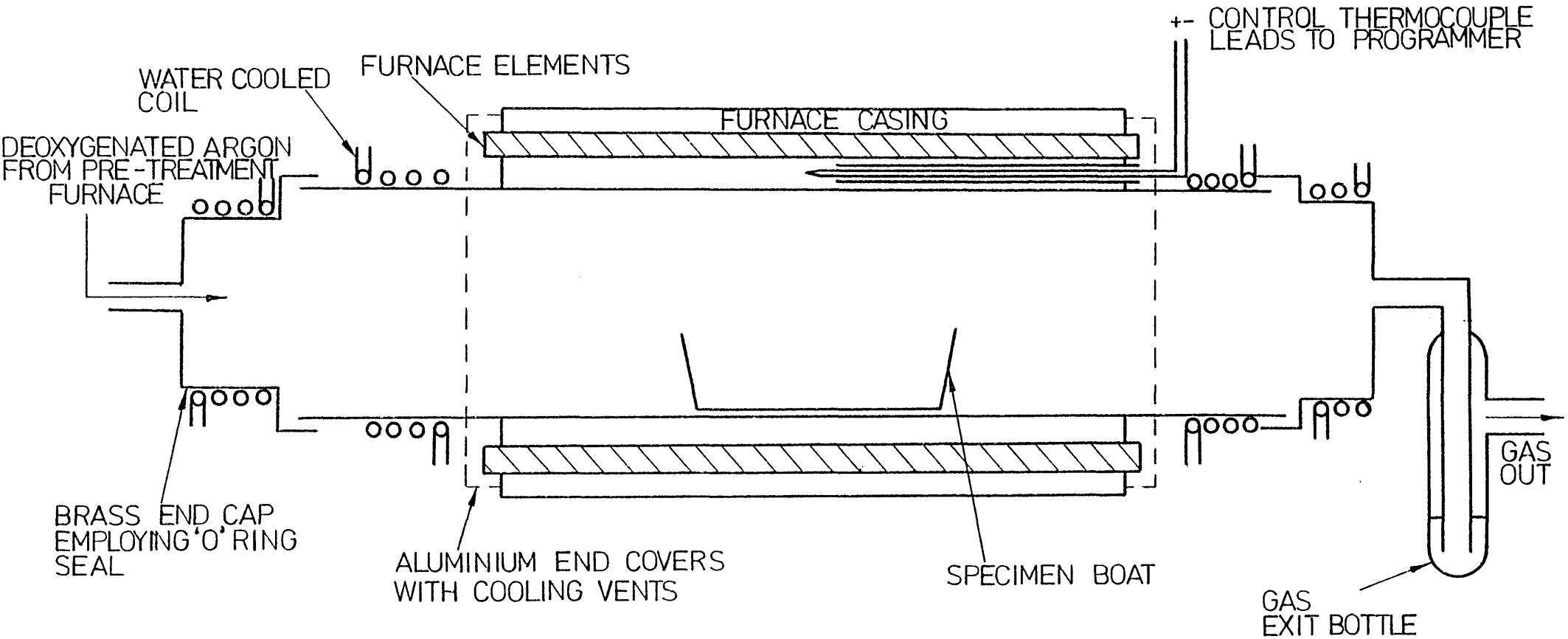
Fig. 3.2 Argon Pretreatment Furnace

seals. The control thermocouple (Pt/Pt 10% Rh) was situated between the reaction tube and elements. A re-crystallised alumina specimen boat, capable of holding 20 beam specimens 5 cm. in length could be placed inside the hot zone of the furnace. The furnace is illustrated in Figs. 3.3 and 3.4.

The temperature of the furnace was controlled by a Eurotherm controller (Type PID 070) and the heating or cooling rates by a Eurotherm programmer (Type 125), an auxiliary unit (Type 126) and a timer (Type 200). Such a system provides a very flexible heat-treatment profile with linear heating or cooling rates from 2° to 99°C per hour (0.02 mV to 0.99 mV per hour). The programme profile used in this study is shown below:-

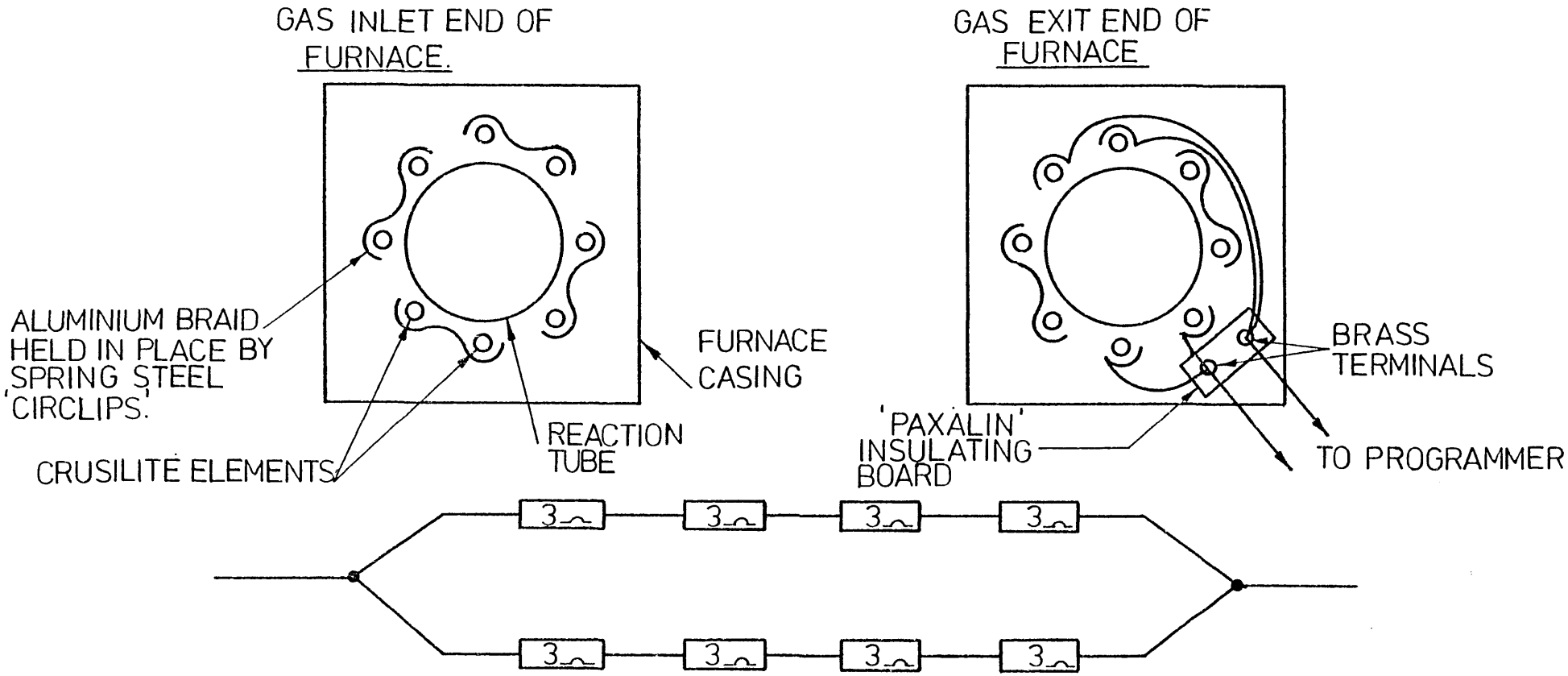


A wiring diagram for the controller, programme units and furnace is shown in Fig. 3.5. Generally there was only a 3 or 4° difference between the sample and thermocouple temperatures during a heating and cooling cycle and this was reduced still further during a hold period. A photograph of the processing apparatus is shown in Fig. 3.6.



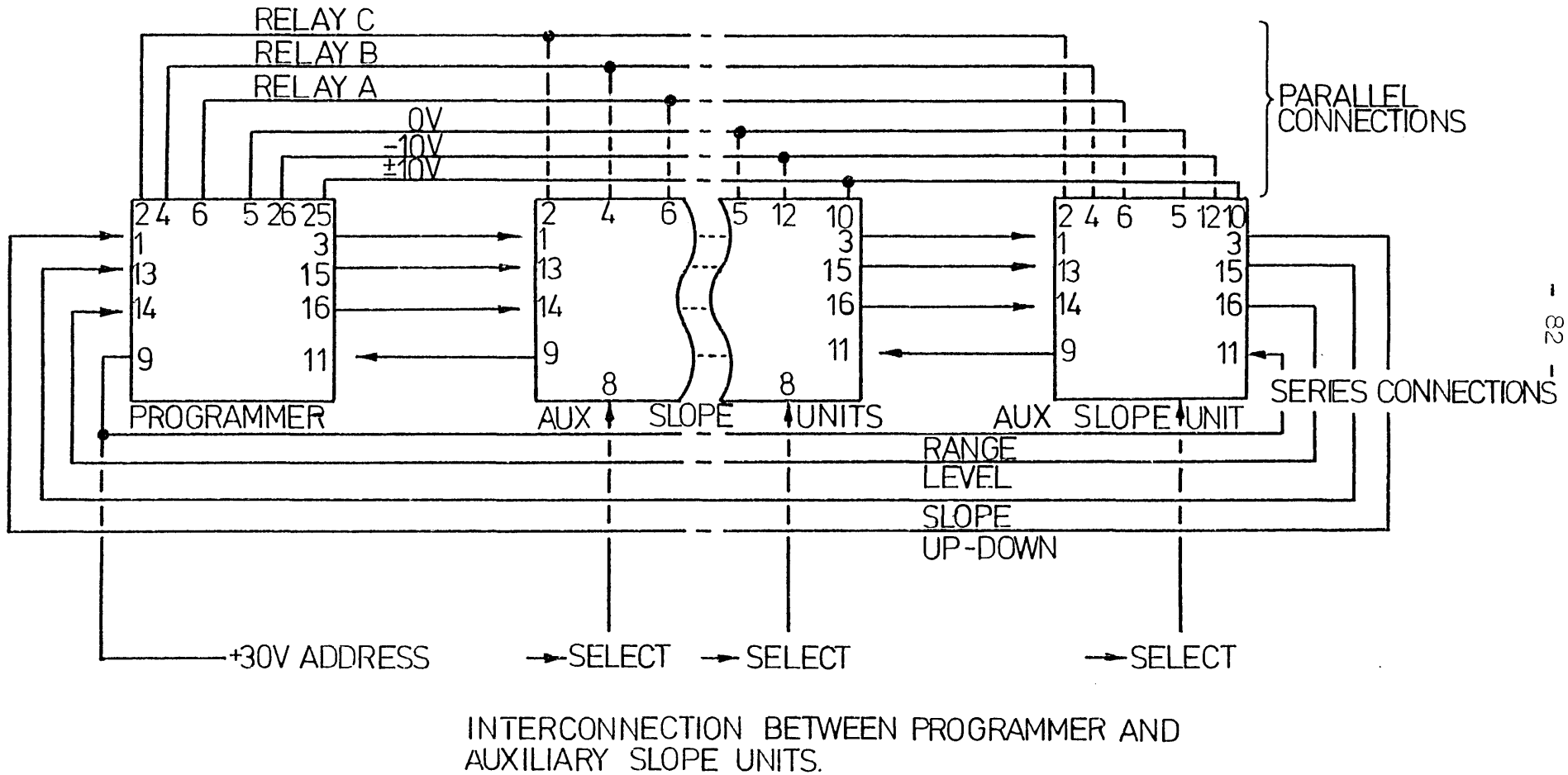
Reaction Tube	Alumina 900 mm Long 50 mm Dia.
Furnace Elements	Crusilite Elements (8) each of 3 Ohms Resistance
Furnace Resistance	6 Ohms.

Fig. 3.3 Carbon Heat Treatment Furnace



The eight crusilite elements are connected in two groups of four in series and the two groups in parallel with each other.

Fig. 3.4 Wiring Diagram of Carbon Heat Treatment Furnace Elements



INTERCONNECTION BETWEEN PROGRAMMER AND AUXILIARY SLOPE UNITS.

Fig. 3.5 Circuit diagram for furnace, controller, programmer, auxiliary unit and timer.

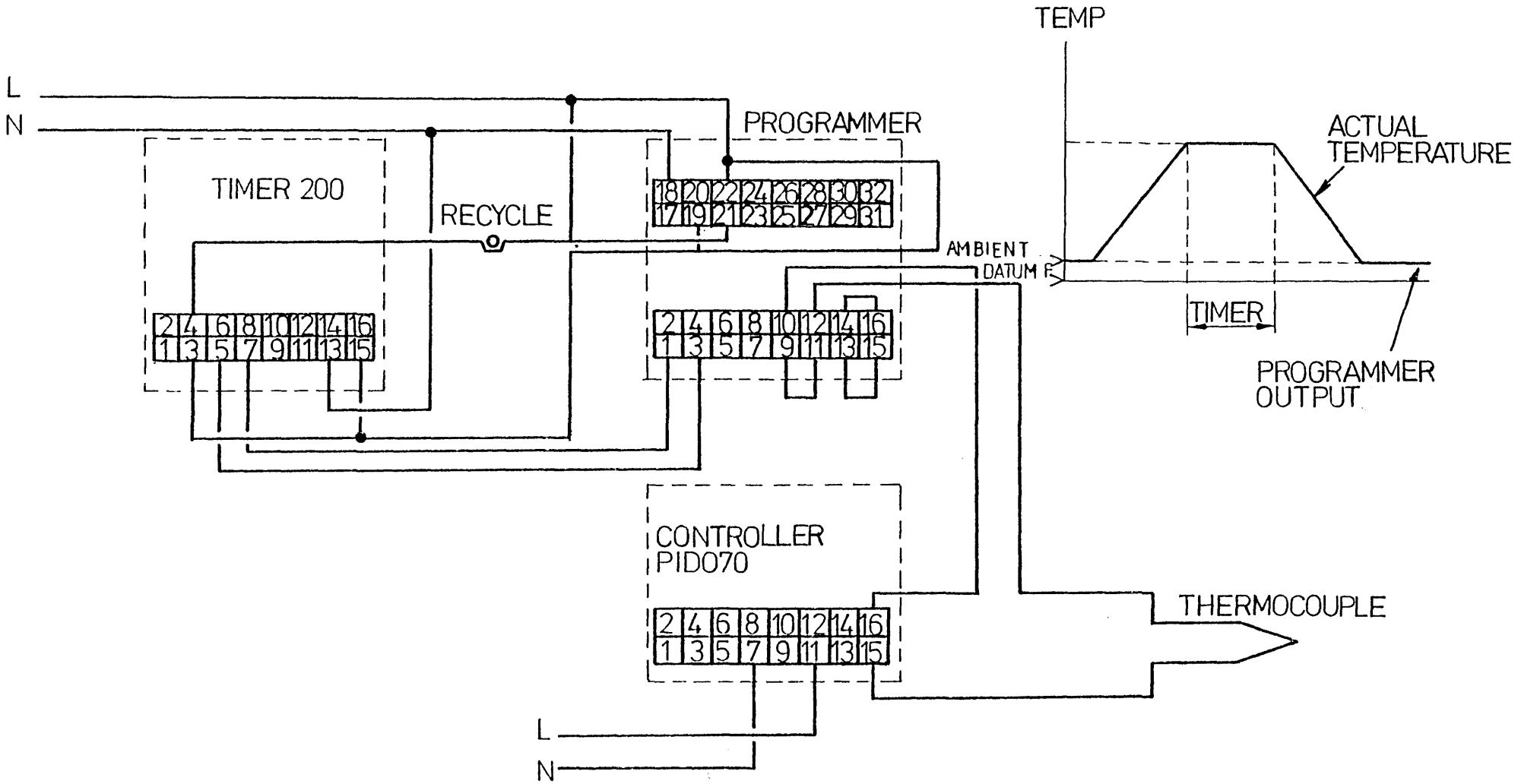

L
N
TIMER 200
RECYCLE
PROGRAMMER
18 20 22 24 26 28 30 32
17 19 21 23 25 27 29 31
2 4 6 8 10 12 14 16
1 3 5 7 9 11 13 15
AMBIENT
DATUM P
TEMP
ACTUAL
TEMPERATURE
TIMER
PROGRAMMER
OUTPUT
CONTROLLER
PID070
THERMOCOUPLE
L
N

Fig. 3.5 (Cont'd)



Fig. 3.6 The apparatus used in the production of amorphous carbon.

3.3 Microstructural Analysis

3.3.1 Scanning Electron Microscopy

Fracture faces were prepared from pyrolysed beam specimens which had failed under a mechanical bending load. The specimens were cleaned in alcohol and mounted on standard aluminium stubs using Rawlplug "Durofix" adhesive. A small amount of "Silver Dag" was used to produce a good electrical contact between stub and specimen which prevented charging of the specimen in the electron beam. Specimens were cut from broken beams using a diamond saw and mounted in a mixture of epoxy resin and natural graphite (approximately 10% graphite to prevent charging in the SEM) with the cut surface uppermost. The exposed surfaces were then polished using an Engis Ltd., "Kent Mk. 2A" automatic polishing machine with 6, 3, 1 and .25 μm diamond impregnated laps. Powder samples were mixed with ethanol to form a slurry. A dropper was used to introduce a small amount of slurry onto an aluminium stub. The ethanol was allowed to evaporate and the powder made to adhere to the stub by sputtering with a 200Å layer of gold.

3.3.2 Pore Size and Distribution Measurement

Analysis of porosity in the amorphous carbons was carried out using a Bausch and Lomb "Omnicon 3000" image analyser interfaced with a Data General "Nova 4" mini-computer. Scanning electron micrographs of polished surfaces were enlarged to around 10" x 8" for analysis. The instrument identified different phases by differences in contrast but the contrast in the photographs was insufficient for accurate measurement. This problem necessitated the production of replicas of the micrographs an example of which is shown in Fig. 3.7.

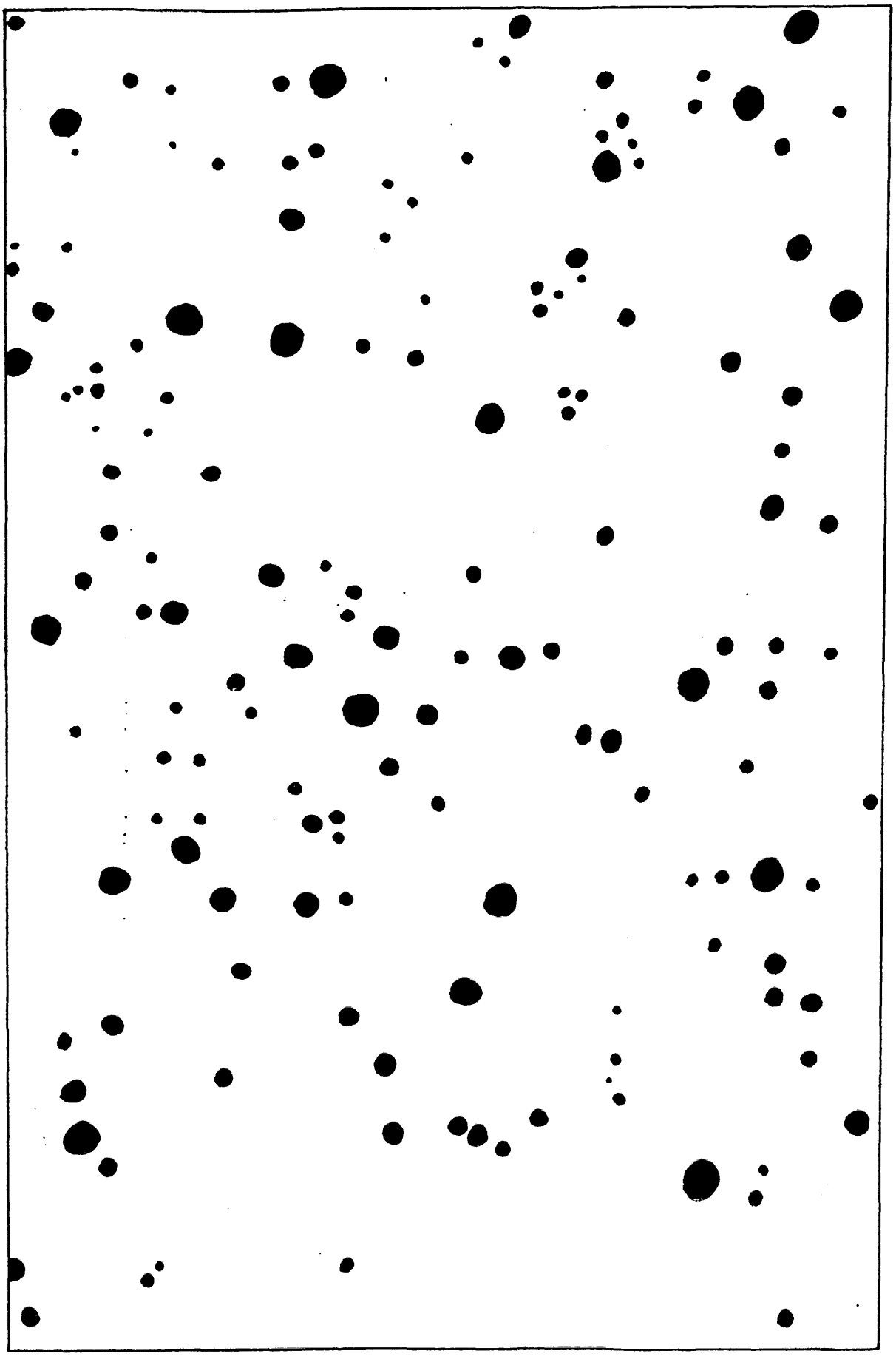


Fig. 3.7 Example of Electron Micrograph replica used in porosity analysis

The image analyser was programmed to measure % porosity, maximum pore size, mean pore size and plot the pore size distribution in the form of a histogram.

3.3.3 Density Measurements

The volume of the bulk specimen was found using a water displacement technique. The weight was found on a balance reading to ± 1 x 10^{-4}g. The bulk density of the amorphous carbon was calculated from;

$$\rho = \frac{m}{v} \qquad (3.1)$$

where ρ = density, m = mass, v = volume.

3.3.4 Porosity Measurements

The porosity of the material was calculated from its density data using the following relationship:

$$\% \text{ porosity} = \frac{100\ (\rho_t - \rho_b)}{\rho_b} \qquad (3.2)$$

where, ρt is the theoretical maximum density of the material (taken as that of a mechanically ground powder sample = 1.635 gcm^{-3}) and ρb is the bulk density.

3.4 Particle Size Analysis

The particle size distributions of the graphite and zinc oxide powders added to the resin were measured using a Malvern "3600 Particle Size Analyser". The instrument consists of a laser source, sample cell (containing a dispersion of the particles in a liquid such as water,

acetone etc.,) and an array of concentric diodes to detect diffracted light, all mounted upon an optical bench. The signal from the diode array is analysed by a modified Commadore PET micro computer. The particles in suspension diffract the light through an angle θ , the smaller the particle the greater is θ . The angle of diffraction is therefore related to particle size and the intensity of diffracted light at any given angle is related to the proportion of particles of that size in the sample. The diffracted light is collected and focused upon the array by a lens system which is interchangeable depending upon the required range of particle sizes.

3.5 Microhardness Testing

The hardness of the material was determined using a 'Leitz micro-hardness' testing machine. The D.P.H. number was determined from the average length of the two diagonals in the indentation of a four sided diamond pyramid under an applied load of 200g. The specimens tested were the polished faces set in epoxy resin used in porosity analysis. A mean value from 10 impressions was taken and the specimens were sputtered with a 200Å layer of gold prior to testing to improve reflectivity and ease measurement of the diamond impressions.

3.6 Mechanical Testing

3.6.1 Specimen Preparation

The surfaces of specimens "as-removed" from the furnace were sufficiently smooth (average flaw size $<50\,\mu m$) such that no special treatment was required for specimens used in fracture toughness measurements because of the presence of machined, cut notches. Unnotched specimens used

for MOR tests were, however, subjected to surface preparation using 800 grade SiC paper prior to testing.

3.6.2 Loading Techniques

All tests were performed in air using a Universal Instron machine for loading the specimens. A compression-tension load cell with a maximum loading capacity of 1 KN was used. The loading jig consisted of an upper ram, which was attached to the load cell, and specimen mount which was fixed to the Instron cross head. With the specimen in position, load was applied when the specimen mount was driven against the upper ram via the cross head movement.

3.6.3 Fracture Strength Determination

The modulus of rupture tests were carried out using the 3-point bend jig shown in Figs. 3.8 and 3.10. The specimens, 4 x 6 x 40 mm. in size, were loaded between three parallel tungsten carbide rods so that the upper rod was situated exactly in the middle of the two lower supporting rods, which were 3 mm. in diameter, and fixed in grooves machined on the upper ram and the specimen mount. The specimens were broken using a 35 mm. span. The modulus of rupture values were calculated using equation 2.17.

3.6.4 Fracture Toughness Determination

Fracture toughness parameters may be determined by the analytical methods in which the stress intensity factor (K_{Ic}) is measured. The test geometry used in this work was that of the Single Edge - Notched Beam, the solution of which was that obtained from the appropriate modified Griffith equation (95) in which K_{Ic} is expressed as a function of applied load, crack size and sample dimensions. The critical stress intensity was then calculated from the

critical load at failure. The specimen geometry and recommended proportional dimensions for SENB specimens in 3-point bending are shown in Fig. 3.9. These specimens are compact and of simple geometry and hence are relatively easily and readily prepared. The size of specimen used was 6 x 4 x 40 mm. A blunt notch of length 'a', approximately half the width of the specimen was introduced midway along the specimens' length.

The sawn notches were made using a Capco diamond cutting machine in which the specimen was moved against a high speed (4000 rpm) diamond blade of 0.25 mm. cutting thickness. Because the material is so brittle a special jig had to be designed and built to hold the specimens rigid while the notches were cut. Fig. 3.10 shows the drawings used in making the jig and Fig. 3.11 the jig and cutting machine in use. The specimen movement was stopped once the desired notch depth was achieved and had to be reversed manually. Honilo 43 - red oil flowed on the cutting point in order to lubricate and cool the blade.

The SENB specimens were tested in the 3-point rig used in the modulus of rupture test using a 24 mm. span. They were loaded so that the upper rod was situated in the same plane as the notch in the middle of the two lower supporting rods (Ref. Fig. 3.8). The fracture toughness (K_{IC}) was calculated from equation 2.30. The dimensional calibration factor (y) accounts for allowed variations in the ratio of crack length/specimen depth. The values of y were calculated from the expression given by Srawley and Brown

(114) and are plotted in Fig. 3.13

for $\frac{\text{span}}{\text{depth}} = 4$

$$y = 1.93 - 3.07\left(\frac{a}{d}\right) + 13.66\left(\frac{a}{d}\right)^2 - 23.98\left(\frac{a}{d}\right)^3 + 25.22\left(\frac{a}{d}\right)^4 \qquad (3.3)$$

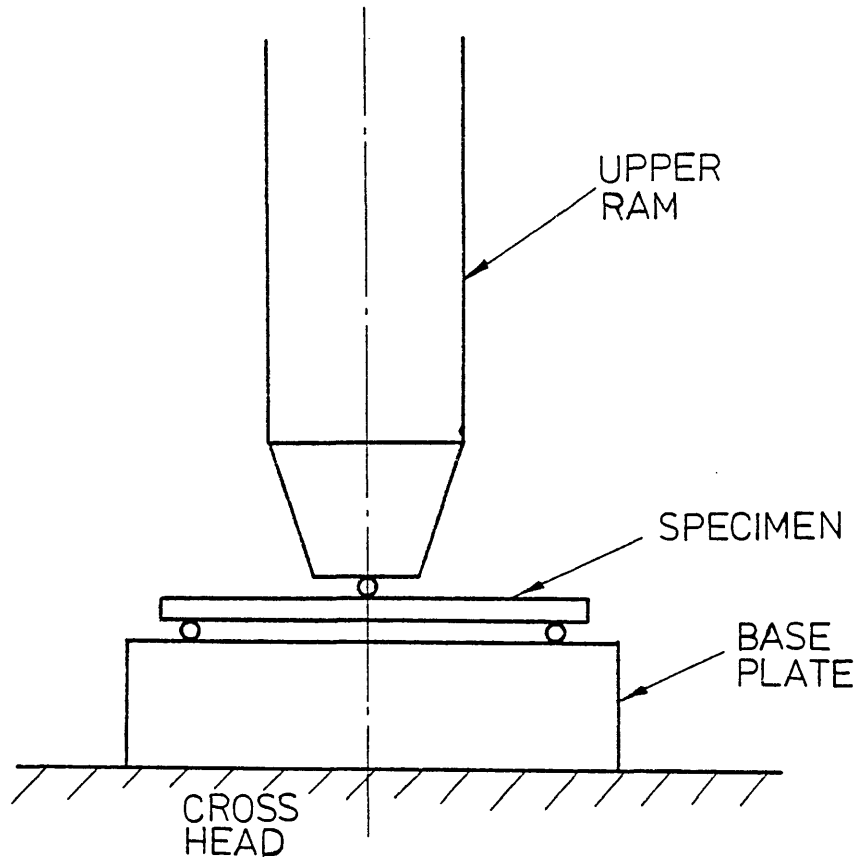
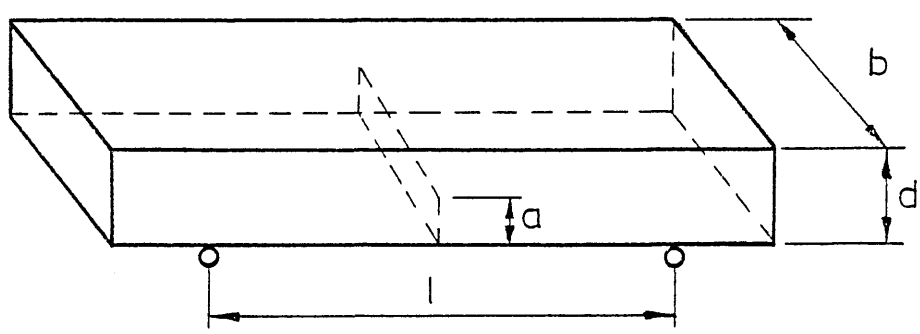


Fig. 3.8 The 3-point bending jig.



$$\cdot 45 \leqslant \frac{a}{b} \leqslant \cdot 55$$

$$\frac{b}{d} \approx \cdot 5$$

$$l \geqslant 4d$$

NOTCH WIDTH $\leqslant \frac{1}{16} d$

Fig. 3.9 The S.N.E.B. specimen and the recommended dimension proportional relations.

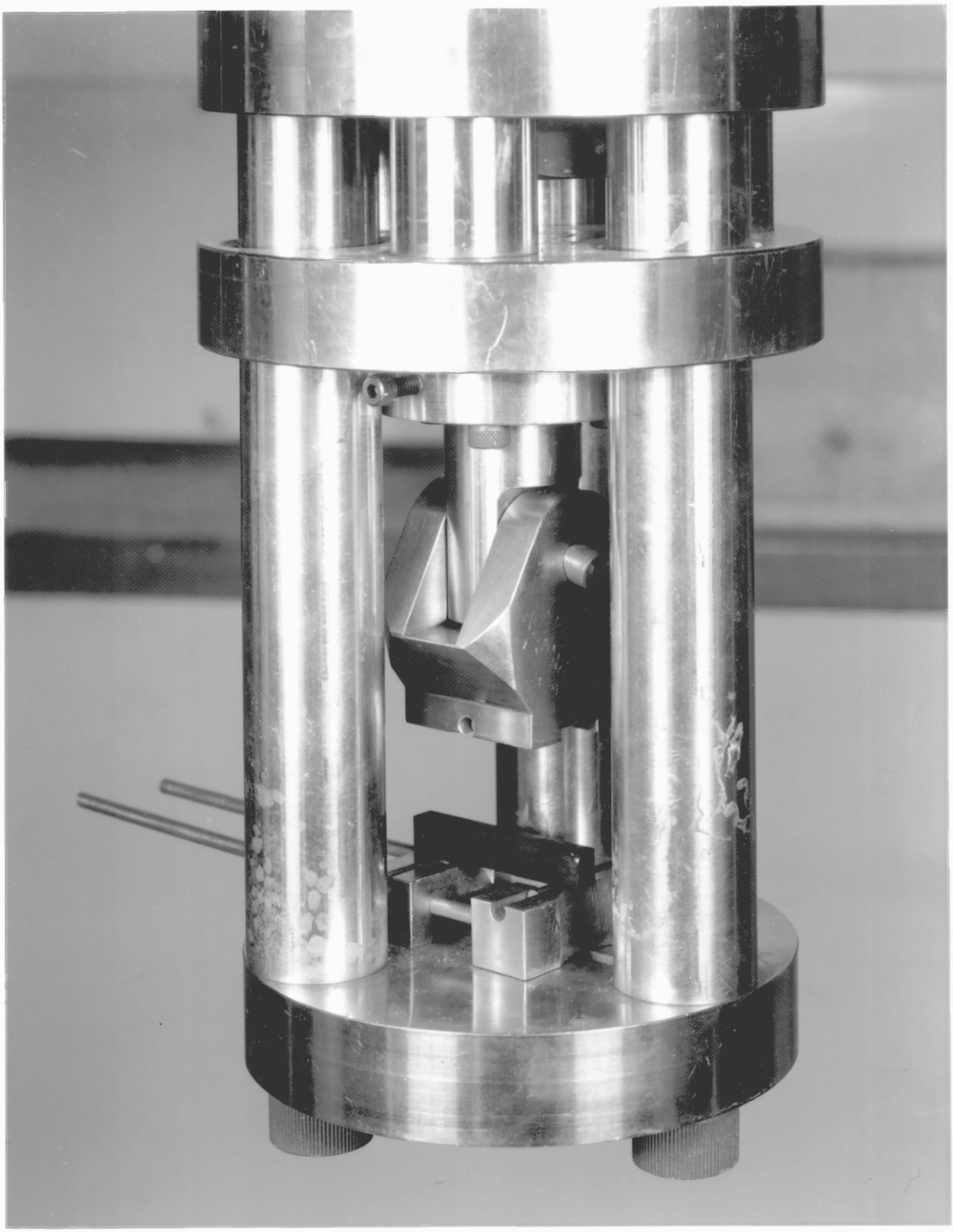
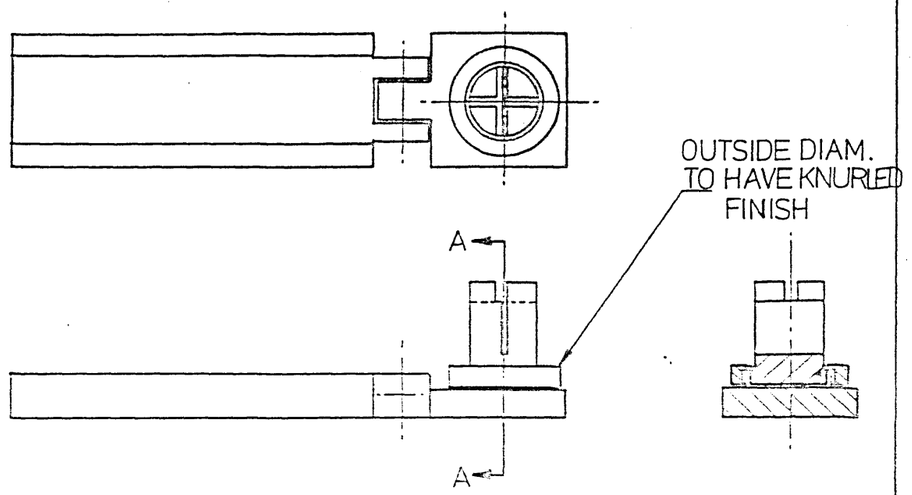
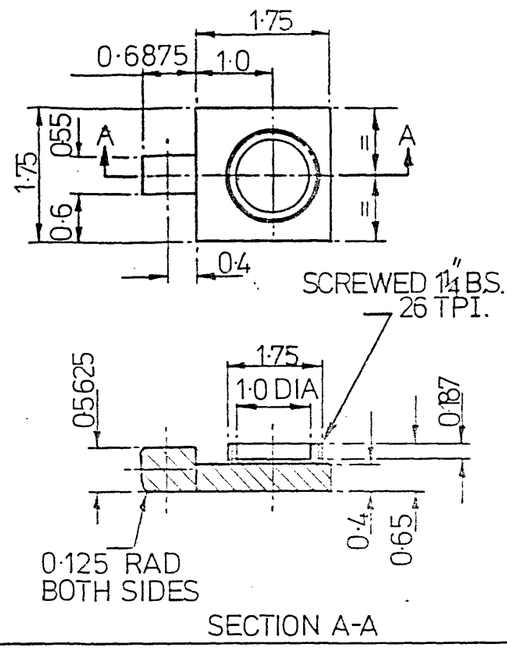
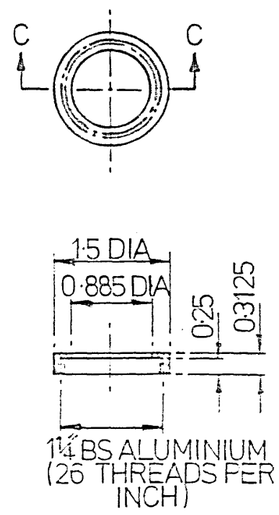
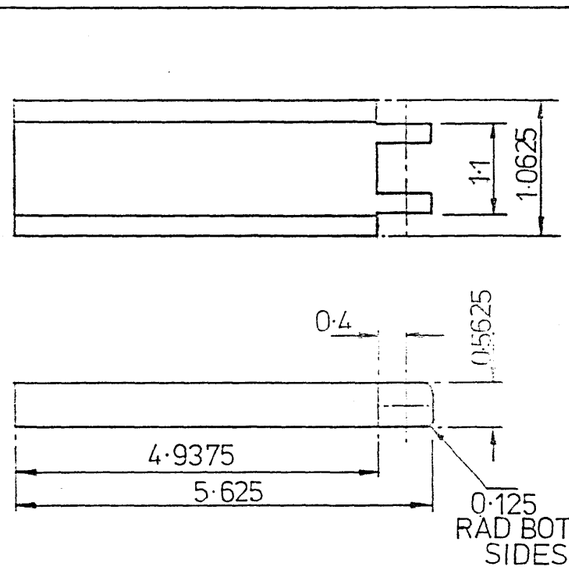


Fig. 3.10 3-point bend jig used in the strength and toughness testing of amorphous carbon.









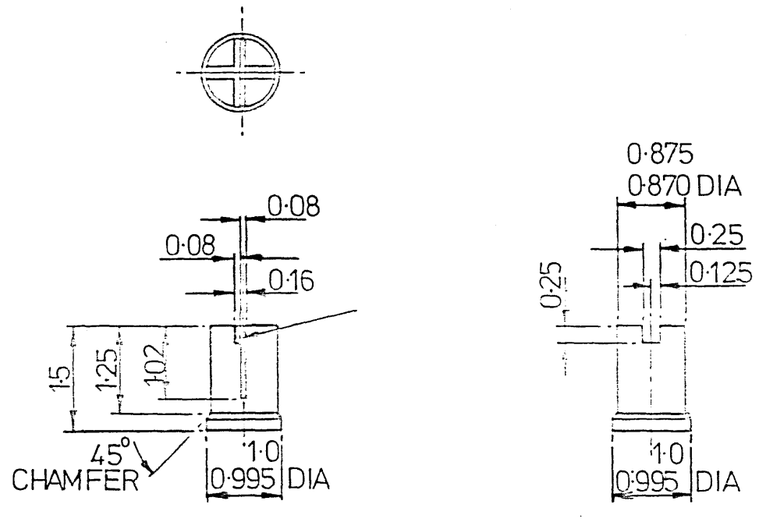


FIG. 3·11 JIG USED TO SUPPORT BEAM SPECIMENS DURING NOTCH CUTTING



Fig. 3.12 Apparatus used to cut notches in specimens for Fracture Toughness Tests.

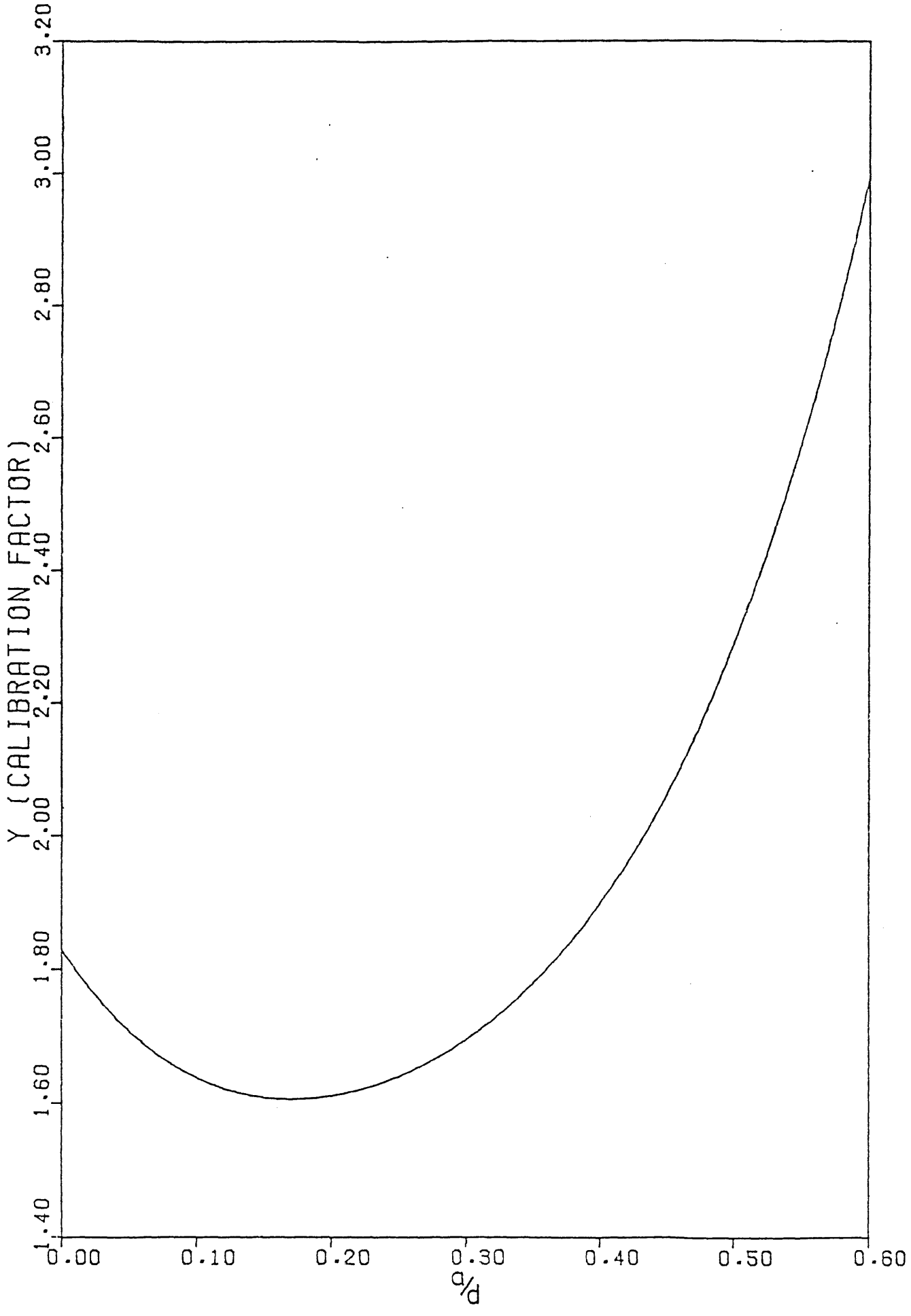


Fig. 3.13 y = Calibration for bend specimens.

SECTION 4

RESULTS AND DISCUSSION

4.1. Polymer Production

Sample preparation using silicone rubber moulds proved to be very successful and a series of batches were produced using different curing conditions, catalyst concentrations and amounts of composite constituents. It was not possible to cure the resin at temperatures below 60°C because the polymerisation kinetics were too slow. Above a curing temperature of 100°C the resin blocks were of very poor quality due to large trapped air bubbles. This occurred because the polymerisation proceeds too quickly at higher temperatures. The surface of the resin solidified before the water vapour produced during the reaction was able to escape. Resins produced in the range 60 - 100°C were of good quality with very few trapped air bubbles and easily converted into the beam geometry required for heat treatment/mechanical testing.

4.2. Pyrolysis

To produce specimens of an acceptable standard for use in bend tests, a considerable amount of work was required in order to modify the heating programme previously used in the processing of sub. mm. pencil leads to make it suitable for the more difficult task of pyrolysing the beam specimens. Initially, there were severe problems with specimens disintegrating on heating due to the internal stresses set up around trapped air bubbles and other irregularities as the

temperature was raised. This was combatted by slowing down considerably the heating and cooling rates. The programme finally used involved heating from ambient to 1000°C (10.2mV) at 50°C per hour (0.4mVhr^{-1}) holding for 10 hours and cooling at 133°C per hour (0.99mVhr^{-1}). The carbon produced maintained the regular geometry and smooth surface of the precursor. Approximately 20% linear shrinkage was observed and 50% by volume. Carbon yields generally varied between 50 and 60%.

4.3. Initial examination of amorphous carbon produced by pyrolysis of pure polyfurfuryl alcohol resin

An initial investigation of the amorphous carbon produced by the method devised for this work was carried out on resin cured at 80°C for 24 hours using 3% catalyst by weight, as this was believed by previous workers (115) to produce the best results. Table 4.1 lists the properties of the amorphous carbon.

Property	Value
Carbon yield	56.48%
Linear shrinkage	19.74%
Volume shrinkage	48.32%
Bulk density	1.523 gcm^{-3}
Porosity*	7.354%
Hardness	264 VPN
Maximum pore size	7.99μm
Mean pore size	4.70μm
Modulus of Rupture	14.42 MNm^{-2}
Fracture toughness (K_{Ic})	0.293 MNm$^{-3/2}$

* calculated from eqn. 3.2

Table 4.1 Properties of amorphous carbon produced by pyrolysing pure polyfurfuryl alcohol resin at 1000°C.

The carbon produced is of very good quality, even when compared to many commercially available products, having a density of 1.523 gcm^{-3}. It is very hard (264 VPN) and fairly strong for this type of material, with an MOR of 14.42MNm^{-2}. Fig 4.1 shows a general SEM view of a fracture face from a sample broken in bending. The fracture is initially flat at the edges of the specimen moving into a concoidal fracture surface at the centre. This is typical of brittle failure in a glassy material. Fig. 4.2, a higher magnification micrograph of the concoidal fracture area, shows some evidence of microcracking in what is otherwise a very featureless picture, indicating the extreme brittleness of the material. The brittleness is further illustrated by the very low value of fracture toughness observed, K_{IC} = 0.293$MNm^{-3/2}$.

It can be seen from the micrographs that failure in the material was initiated at interior spherical pores. Micrographs of these pores, which appear to be uniformly distributed within the material, are shown in Figs. 4.3 and 4.4. The very rounded nature of the pores suggests that they were produced by the evolution of water vapour during curing and the initial stages of firing rather than as a result of high temperature heat treatment. That is to say, they appear to be a consequence of the method of production and not intrinsic to the material.

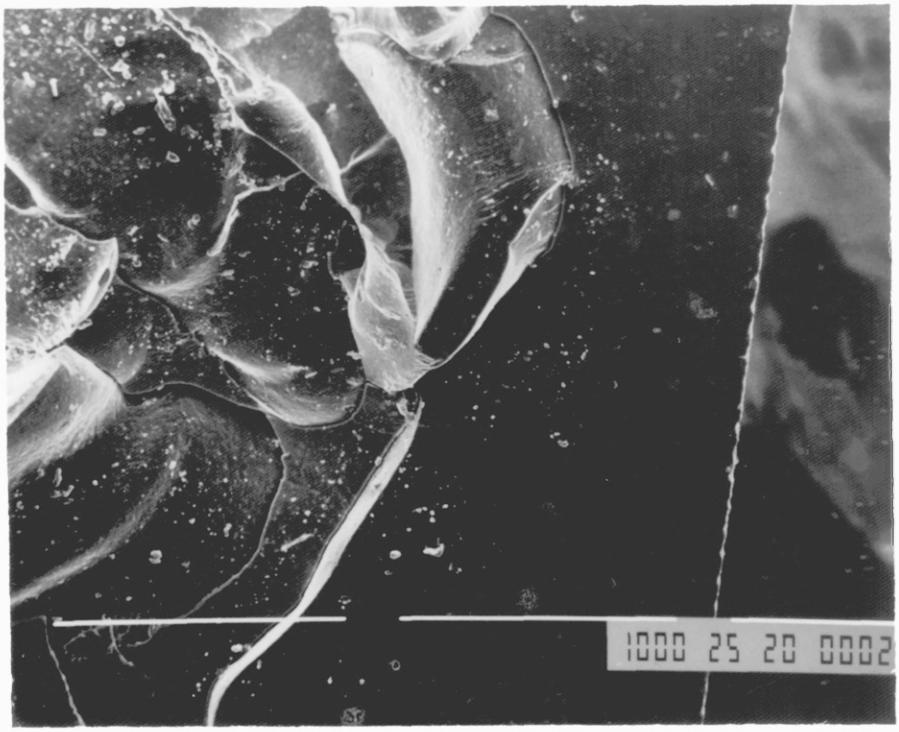


Fig. 4.1 Fracture face of amorphous carbon sample showing initially flat fracture spreading into concoidal area (x35)

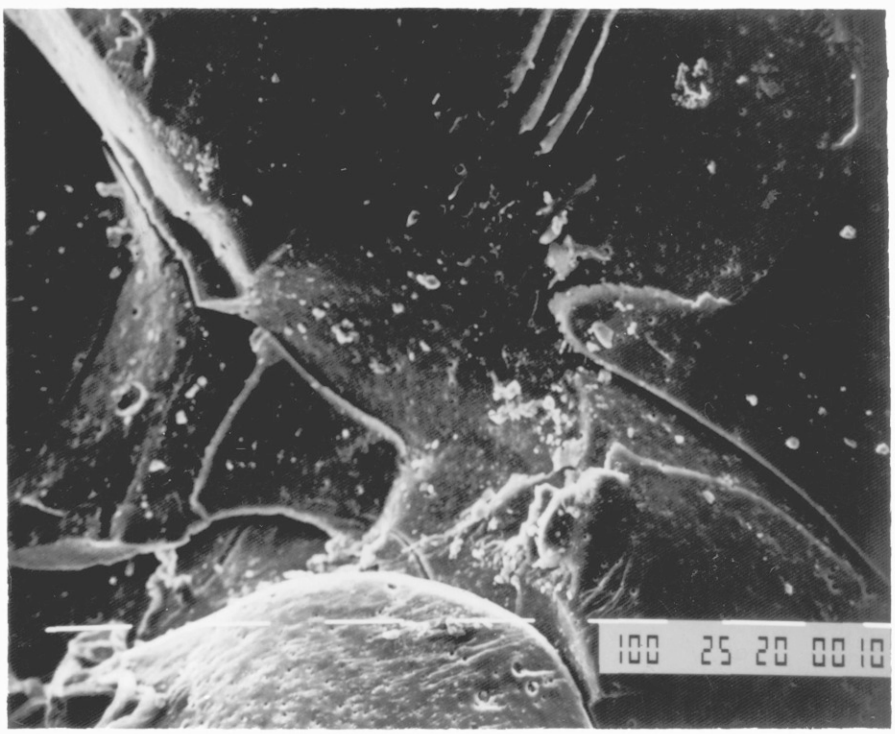


Fig. 4.2 Micrograph of concoidal fracture area showing evidence of microcracking (x100)

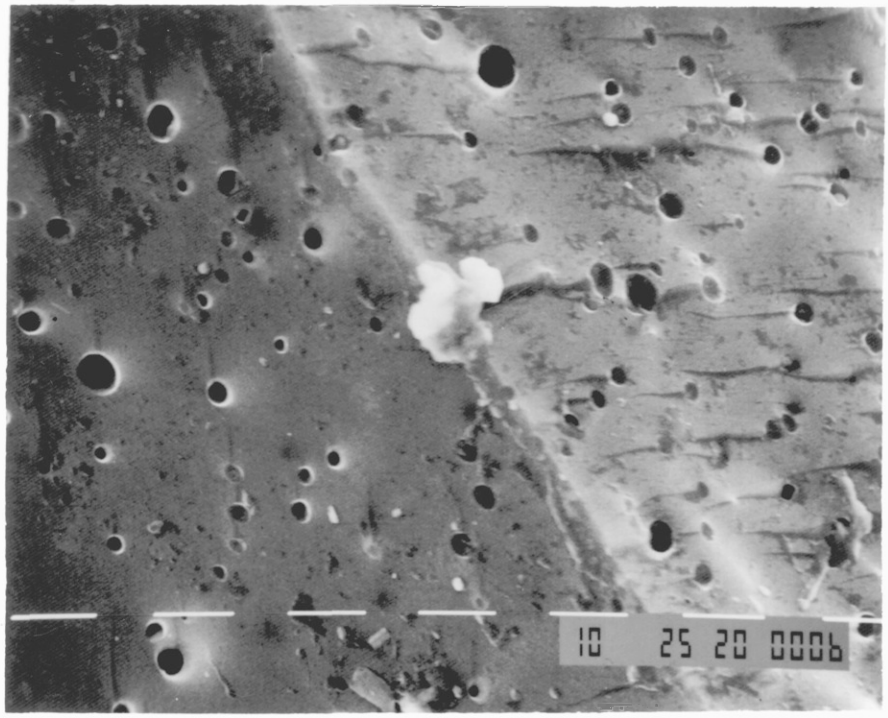


Fig. 4.3 Rounded, fine grained porosity in amorphous carbon (x1000)

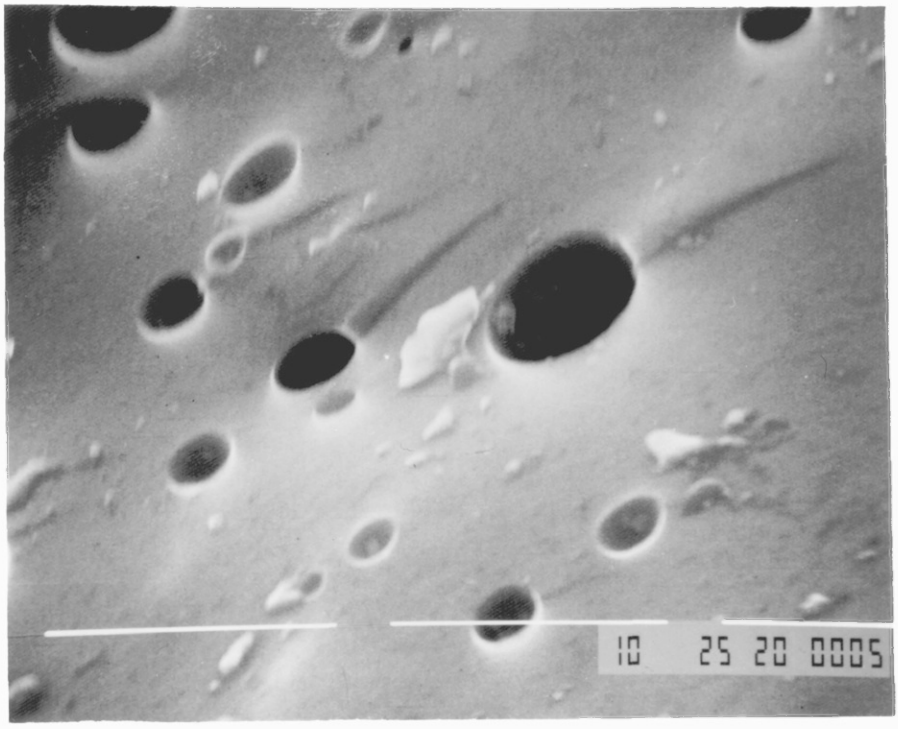


Fig. 4.4 As above (x3500)

Evidence that the material retains some of its elastic properties after heat treatment was shown during hardness testing. When an impression was made using a diamond, a small cross-shaped crack was made by the point of the indentor which was surrounded by a diamond shaped impression. This outer impression started to disappear almost as soon as the pressure was removed, making quick measurement a necessity! This phenomenon has also been reported by Cowlard and Lewis (105).

The literature survey and scanning electron microscope studies suggest that there are essentially two types of porosity present in the material. Firstly, an Angstrom scale porosity can be discerned using X-Ray small angle scattering and high resolution transmission electron microscopy. This results from the structure of the material. The random chain network cannot fill space efficiently and produces this small scale porosity which can therefore be thought of as inherent to the material. Secondly, there is a uniformly distributed micron-scale porosity. These pores are very rounded (roughly spherical in shape) and, as such, appear to have been formed by the evolution of water vapour during an early stage of production.

The pore sizes measured from micrographs by the image analyser are not the true pore sizes and therefore have to be corrected. Since the true pores are spherical and the pore sizes are measured by generating random chords, sections through them rarely pass through the diameter.

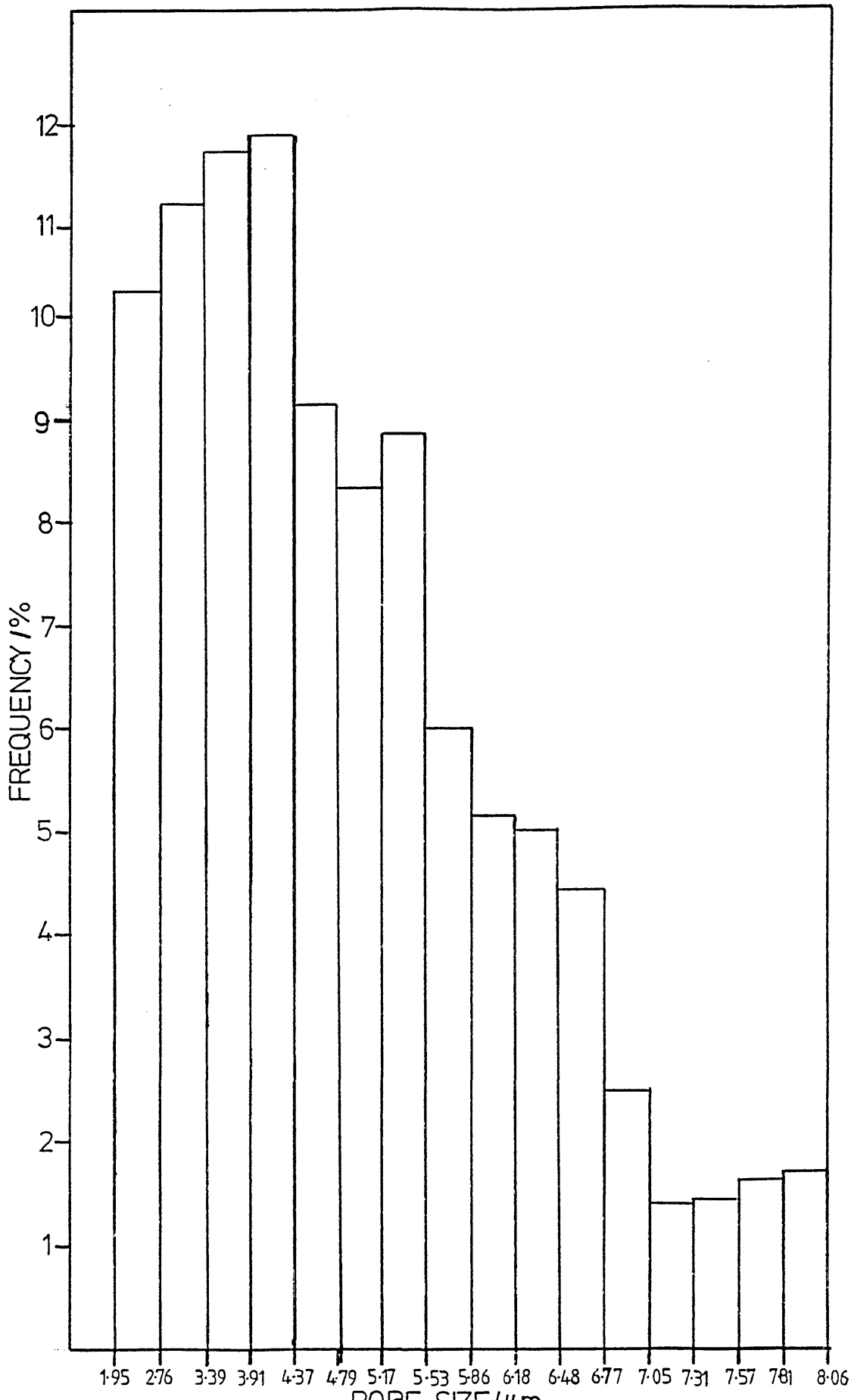


FIG.45. PORE SIZE DISTRIBUTION IN AMORPHOUS CARBON.

The "apparent" pore size may, however, be corrected to the actual pore size using Saltykov's Method (116). Fig. 4.5 shows the distribution of the pores within the material. The pores are distributed over a fairly narrow range between 1.9 and 8μm with the distributon skewed towards the smaller sizes. The largest pore observed was 7.99μm and the mean pore size 4.7μm. Although porosity in a material is detremental to the strength because of the stress concentrations created, Rautavuori and Tormala (117) have suggested that porosity in amorphous carbon is essential in production as it allows the escape of pyrolysis gases. Assuming that the maximum theoretical density of the material approximates to that of a finely ground powder sample, the carbon produced contained approximately 7½% porosity.

4.4 The effect of curing time of the resin on the properties of the resulting amorphous carbon

A series of polymer batches were prepared and fired in which the time of curing was varied from 8 to 72 hours, while the temperature of curing and catalyst concentration remained constant at 80°C and 3% by weight respectively. The polymer samples varied in resilience from being rubber-like to gradually becoming hard and glassy as the curing time was increased. It therefore seems a reasonable assumption that the curing time is an approximate measure of the degree of polymerisation. The effect of curing time/degree of polymerisation of the resin upon the properties of the resulting carbon are shown in Tables 4.2 and 4.3.a and b and figs. 4.6 through 4.10.

The carbon yield, hardness, modulus of rupture and fracture toughness of the material initially increased rapidly with curing time and then tailed off to a plateau at around 48 hours. The increase in carbon yield occurred because some of the low molecular weight chains or unreacted monomer in the partially polymerised resin were driven off during pyrolysis, along with non-carbonaceous side groups. As the curing time was increased the chains became longer and more and more 3-dimensionally cross-linked and so less carbon was driven off. Kawamura (110) has shown that Young's modulus and hardness of vitreous carbon are related, and so an increase in stiffness due to increased cross-linking is to be expected. The increase in cross-linking also makes the propagation of cracks through the material more difficult and as a result improved the strength and toughness.

The amount of shrinkage decreased linearly (it would appear) with increasing curing time. This suggests that the carbon chains alter their configuration slightly to take up the space vacated by molecules which have been driven off, as the bulk density was not observed to vary. The maximum and mean pore sizes and pore size distributions do not seem to vary with curing time which shows that the pores are not produced by molecules driven off during the pyrolysis process.

Batch Number	Time of Curing/ Hours	Carbon Yield/%	Linear Shrinkage/ %	Volume Shrinkage /%	Bulk Density /gcm^{-3}	Calculated Porosity/ %	Measured Porosity/ %	Maximum Pore Size /μm	Mean Pore Size/ μm	Hardness /VPN
1	8	51.42	19.92	51.65	1.52	7.01	4.44	8.43	4.66	207
2	16	55.32	19.88	50.83	1.53	6.42	4.32	8.54	4.91	226
3	24	56.48	19.74	48.32	1.52	6.85	4.59	7.99	4.70	264
4	48	57.35	19.63	44.92	1.52	6.79	4.61	8.69	4.82	304
5	72	57.42	19.44	43.18	1.52	7.03	4.45	7.84	4.73	305

TABLE 4.2

The effect of curing time at 80°C on the physical properties of pyrolysed polyfurfuryl alcohol.

NOTES

a. Calculated Porosity obtained using Eqn. (3.2)
b. Measured Porosity found using image analyser.

Batch Number	Modulus of Rupture/MNm^{-2}	Standard deviation /MNm^{-2}	90% confidence interval/MNm^{-2}
1	10.01	2.96	±1.01
2	11.58	3.19	±1.09
3	14.42	3.56	±1.21
4	15.21	3.8	±1.16
5	15.40	3.10	±1.06

a. Modulus of rupture

Batch Number	K_{Ic} /$MNm^{-3/2}$	Standard deviation /$MNm^{-3/2}$	90% confidence interval/$MNm^{-3/2}$
1	0.220	0.033	0.012
2	0.264	0.033	0.011
3	0.293	0.029	0.009
4	0.383	0.039	0.014
5	0.386	0.037	0.012

b. Fracture toughness

Table 4.3 The variation of mechanical properties of amorphous carbon with curing time of the resin precursor.

The results show that the mechanical properties of vitreous carbon are improved with increased viscosity (degree of polymerisation) of the resin precursor. This is not completely true however, as there is an optimum resin viscosity as reported by Dickinson and Wewerka (78).

There are two reasons for this. Firstly, the improvements in mechanical properties tailed off tc a plateau as the polymerisation approached completion, and secondly, if the degree of cross-linking is too great the rigidity of the resin causes the build up of large thermal stresses which can lead to catastrophc failure. This was illustrated by a batch polymerised for 168 hrs. at 80°C which completely disintegrated on firing.

It was noted that there was generally a difference of about 2.5% between the measured and calculated porosities. The measured porosity, obtained using the image analyser, is the amount of μm scale porosity produced by the evolution of water vapour and low molecular weight chains during curing and the initial stages of heat treatment. The calculated porosity is the larger of the two because it also includes some of the Å-scale porosity which is inherent to the structure of the material. The calculated value is not an absolute measure of the porosity in the material because it is a comparison with a powder density and not even the most severe grinding to a fine powder can eliminate all of these ultra-small pores. It is, however, useful in comparative work since the standard is always the same.

The significant scatter observed in the modulus of rupture results is due to irregularities in the structure such as microcracks and pores and also because of the problems mentioned earlier (section 2.6.4) causing difficulties in measuring MOR accurately in 3-point bending.

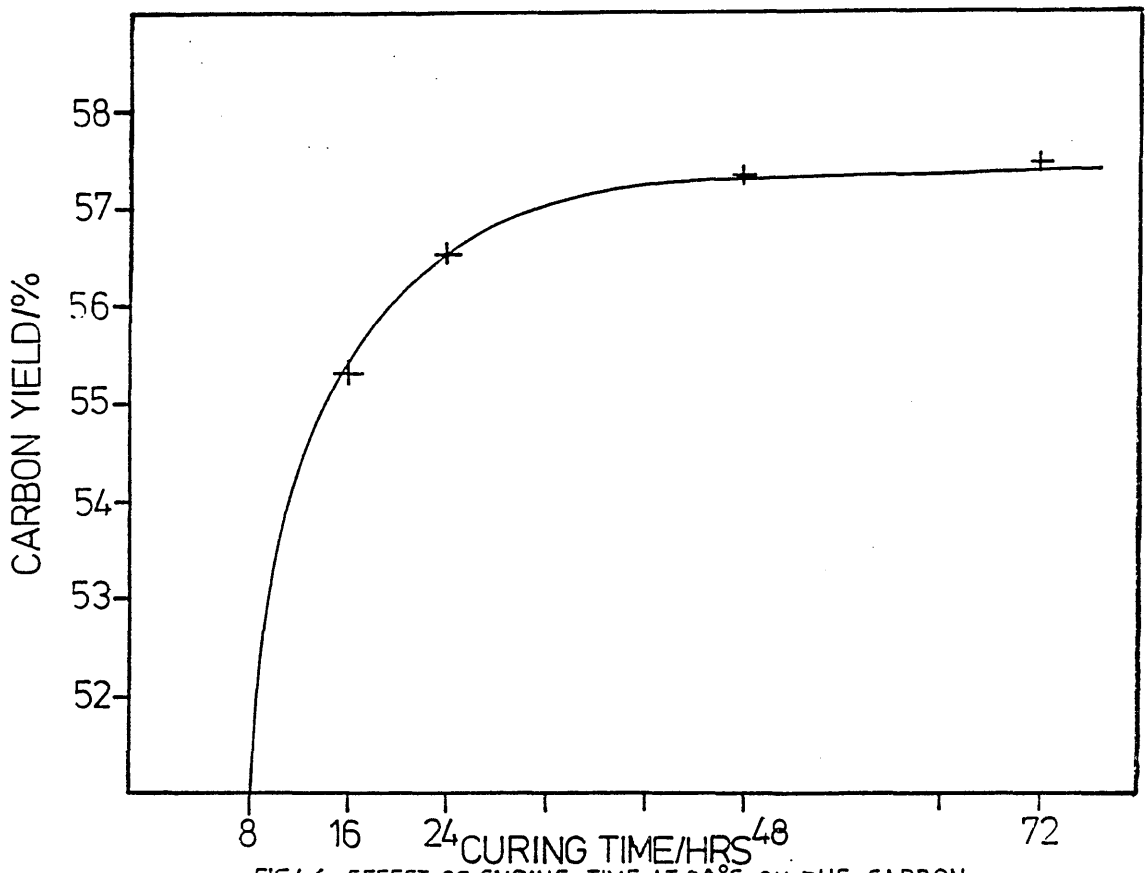


FIG.4·6. EFFECT OF CURING TIME AT 80°C ON THE CARBON YIELD FROM PYROLYSED POLYFUFURYL ALCOHOL.

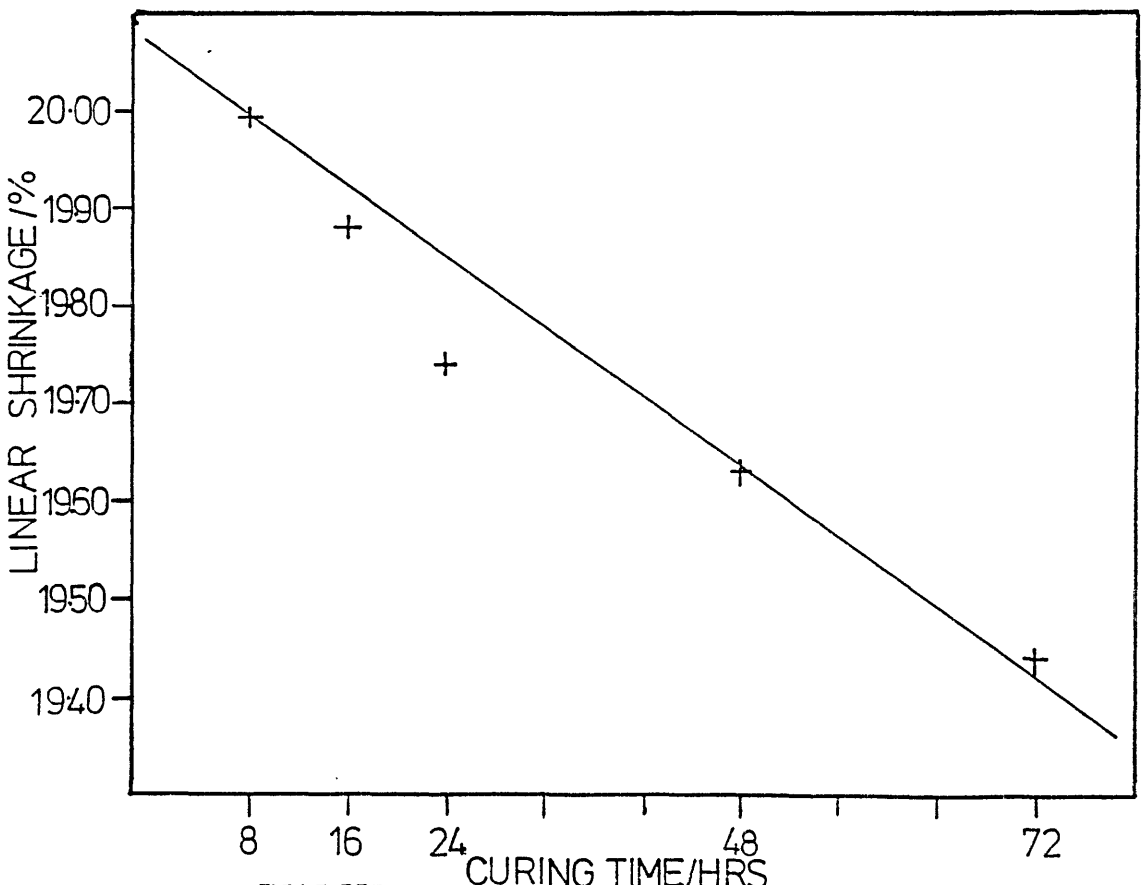


FIG 4·7. EFFECT OF CURING TIME AT 80°C ON THE LINEAR SHRINKAGE FOLLOWING THE PYROLYSIS OF POLYFUFURYL ALCOHOL.

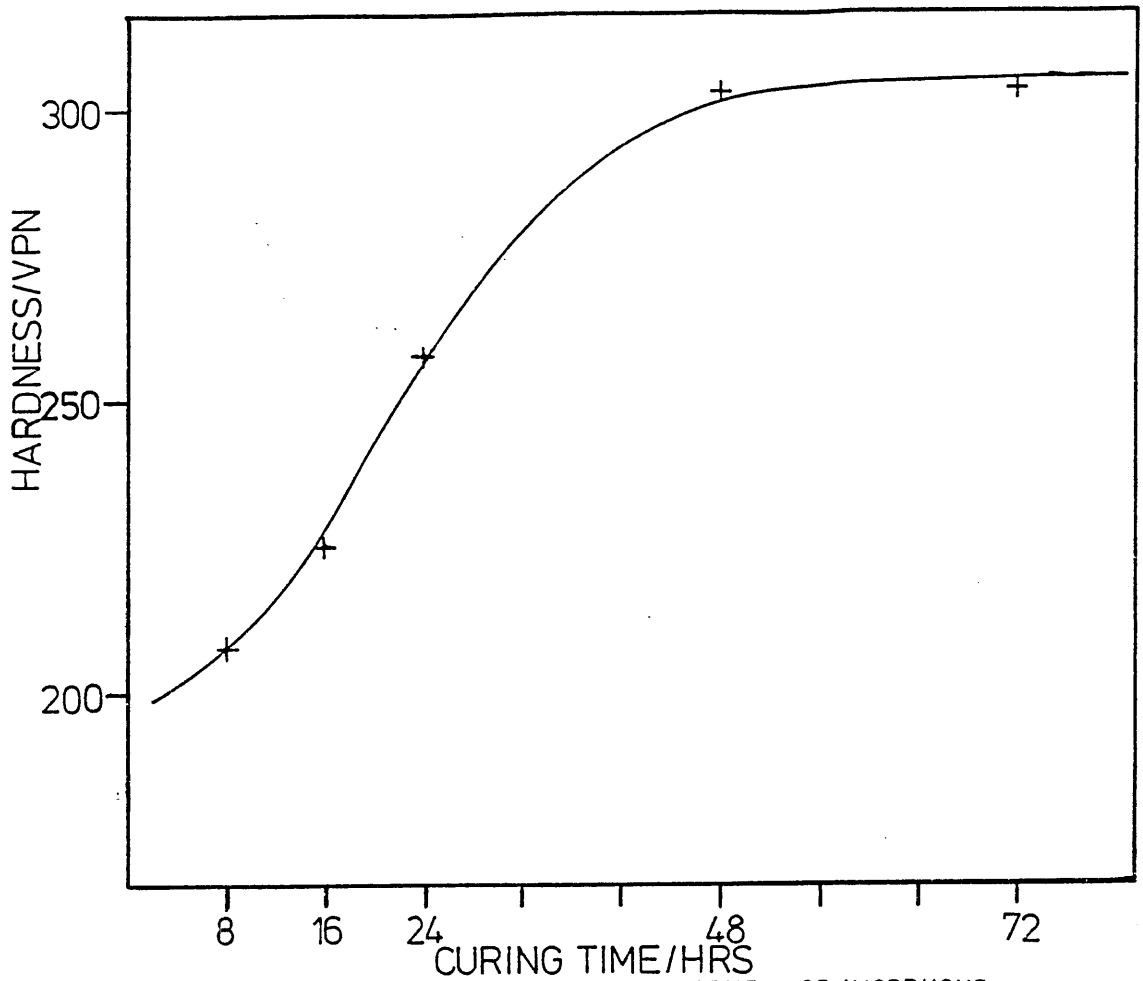


FIG.4·8 EFFECT OF RESIN CURING ON THE HARDNESS OF AMORPHOUS CARBON.

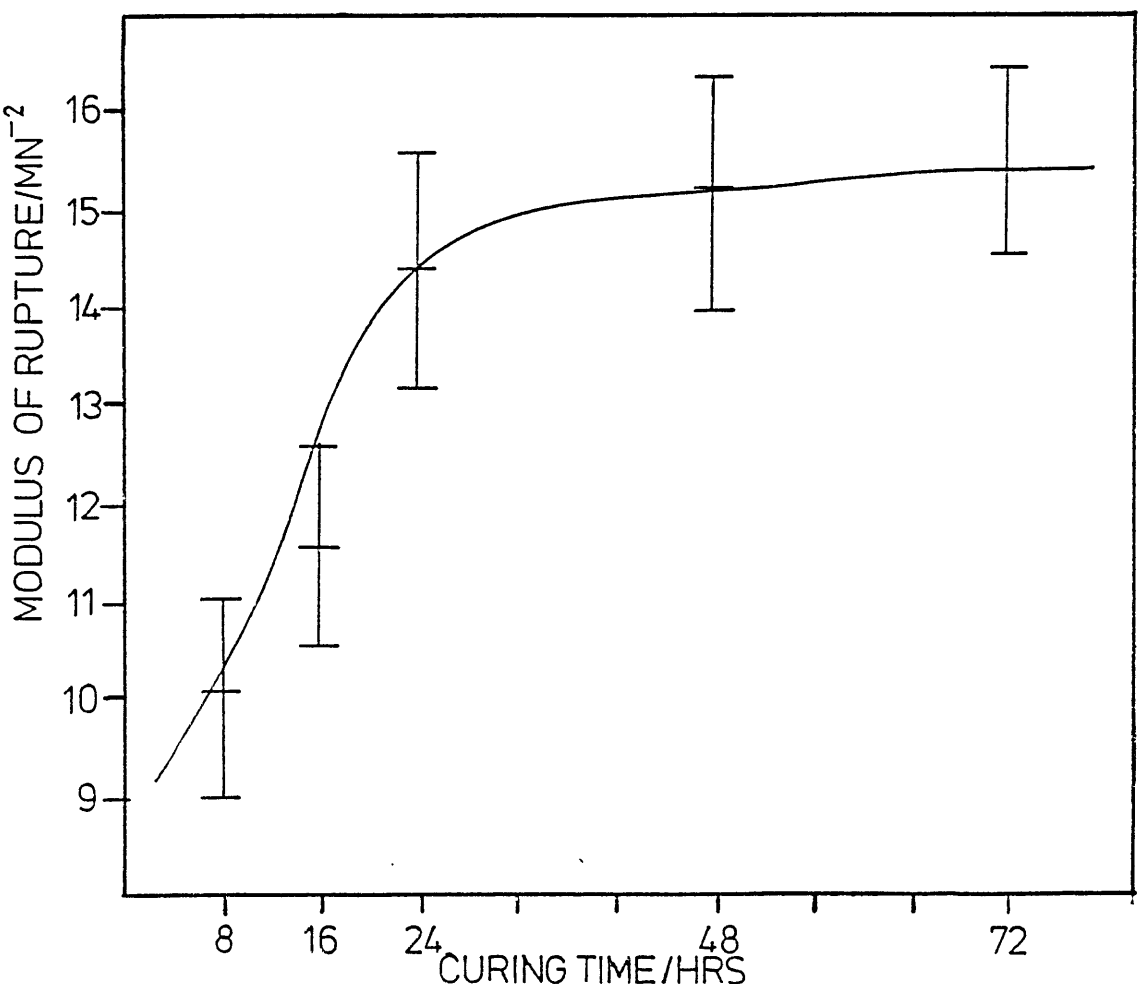


FIG.4·9 EFFECT OF RESIN CURING TIME ON MODULUS OF RUPTURE OF PYROLYSED POLYFURANOL

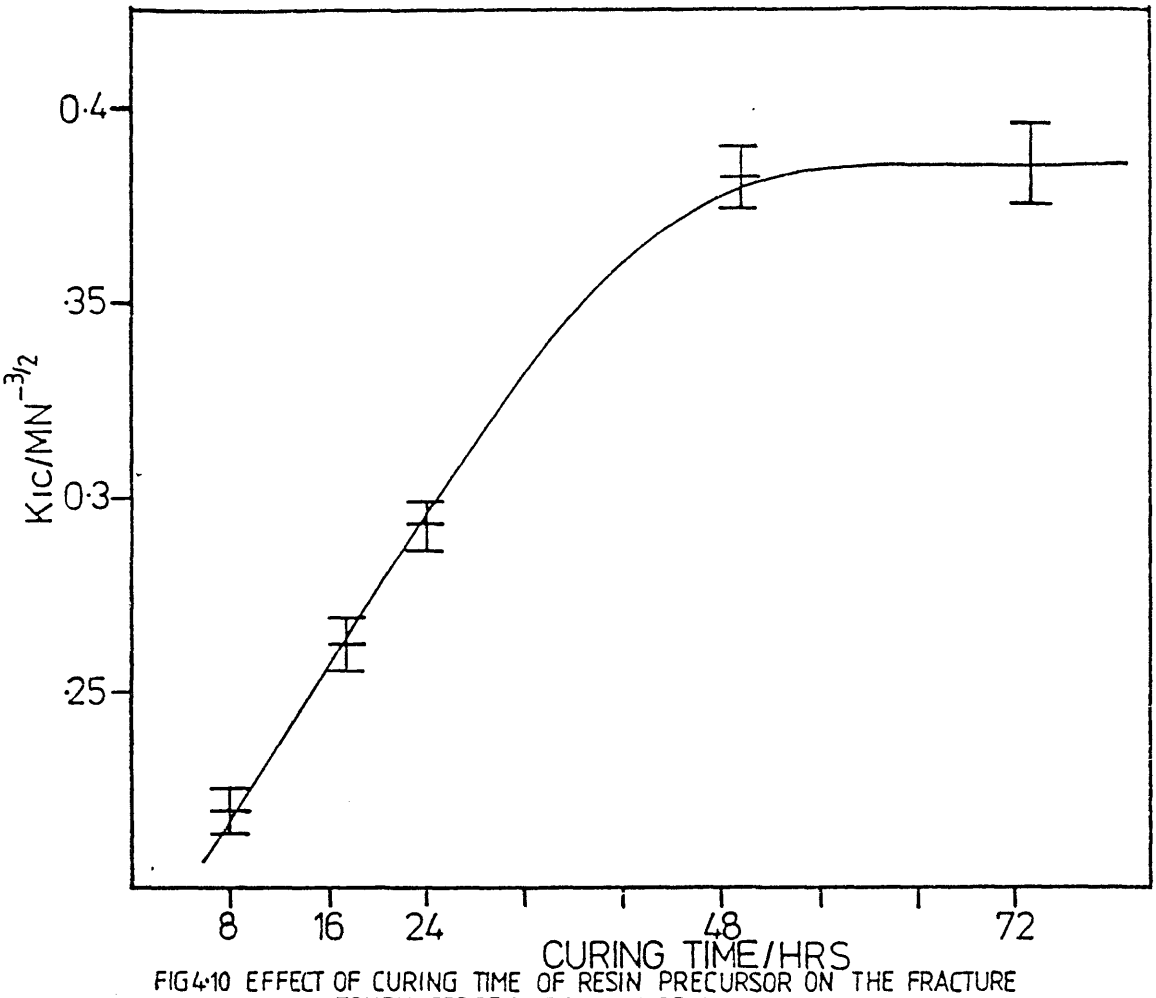


FIG4·10 EFFECT OF CURING TIME OF RESIN PRECURSOR ON THE FRACTURE TOUGHNESS OF VITREOUS CARBON.

The spread of results about the mean varies between 20 - 30%. Improvements in the mechanical properties of the carbon are associated with improvements in the integrity of the precursor and thus explain the decrease in scatter of results as the strength and toughness increased. The variation in K_{1c} measurements was much less (10 - 15%) and shows that this is much more of a material property and, therefore a more accurate representation of the mechanical properties.

4.5 Effect of curing temperature on the properties of pyrolysed polyfurfuryl alcohol

Batches 6, 7, 3, 8 and 9 represent a series of experiments in which the catalyst concentration and length of cure were kept constant (3% and 24 hours respectively) and the temperature of curing varied from 60 - 100°C. The results, which appear in Tables 4.4 and 4.5 and Figs. 4.11 through 4.15, show that the strength and toughness rise to a maximum at around 80°C and then fall away sharply as the temperature is increased. The explanation for this is that below 80°C the resin was still only partially polymerised after 24 hours and some low molecular weight material lost during firing as illustrated by the low carbon yields from batches 6 and 7. Above 80°C a "ripening" of the porosity was observed.

The amount of measured porosity remains the same but the maximum and mean pore sizes were increased as shown in Figs, 4.14 and 4.15. It appears that the increased temperature acts as a driving force for the diffusion of water vapour through the curing resin and the larger pores grew at the expense of the small ones.

The dramatic fall off in strength and toughness occured because the flaw size in the material was effectively increased by the ripening of porosity. One anomoly in the results can be seen in the hardness values. The hardness rose with curing temperature up to a maximum at 80°C and then fell away. The increase with temperature is expected due to the increased degree of cross-linking which makes the material stiffer. One would expect hardness to decrease with an increase in the amount of porosity but in this case the amount of porosity remained the same, only its size was changed.

Batch Number	Time of Curing/ Hours	Carbon Yield/%	Linear Shrinkage/ %	Volume Shrinkage/ %	Bulk Density /gcm^{-3}	Calculated Porosity/ %	Measured Porosity/ %	Maximum Pore Size /μm	Mean Pore Size/ μm	Hardness /VPN
6	60	54.25	18.62	50.19	1.52	6.42	3.48	8.31	4.79	232
7	70	56.32	19.02	47.54	1.52	7.03	4.61	8.40	4.61	248.5
3	80	56.48	19.74	48.32	1.52	6.85	4.59	7.99	4.70	264
8	90	56.40	19.81	48.87	1.51	7.50	4.71	10.57	5.76	242
9	100	56.44	19.83	49.16	1.52	6.83	4.35	11.15	6.18	208

TABLE 4.4

Effect of curing temperature on the properties of pyrolysed polyfurfuryl alcohol

NOTES

All samples cured for 24 hours, catalyst concentration constant at 3% (by weight).

Batch Number	Modulus of Rupture/MNm^{-2}	Standard deviation /MNm^{-2}	90% confidence interval/MNm^{-2}
6	12.33	3.57	±1.22
7	13.85	3.47	±1.19
3	14.42	3.56	±1.21
8	10.66	2.70	±1.32
9	7.30	3.33	±1.01

a. Modulus of rupture

Batch Number	K_{1c} /$MNm^{-3/2}$	Standard deviation /$MNm^{-3/2}$	90% confidence interval/$MNm^{-3/2}$
6	0.235	0.033	±0.011
7	0.262	0.033	±0.012
3	0.293	0.029	±0.009
8	0.221	0.034	±0.012
9	0.158	0.026	±0.010

b. Fracture toughness

Table 4.5 Effect of curing temperature of resin precursor on the mechnical properties of vitreous carbon.

In 1974 Zarzycki (118) carried out an experiment in which he measured the Young's modulus of a glass containing a dispersed second phase of amorphous spherical particles. He found that, if the volume fraction of the second phase remained constant, the Young's Modulus decreased as the texture of the structure coarsened. This phenomena can be related to changes observed in the hardness of vitreous carbon if it is assumed that the spherical pores can be considered as a second phase within the glassy material.

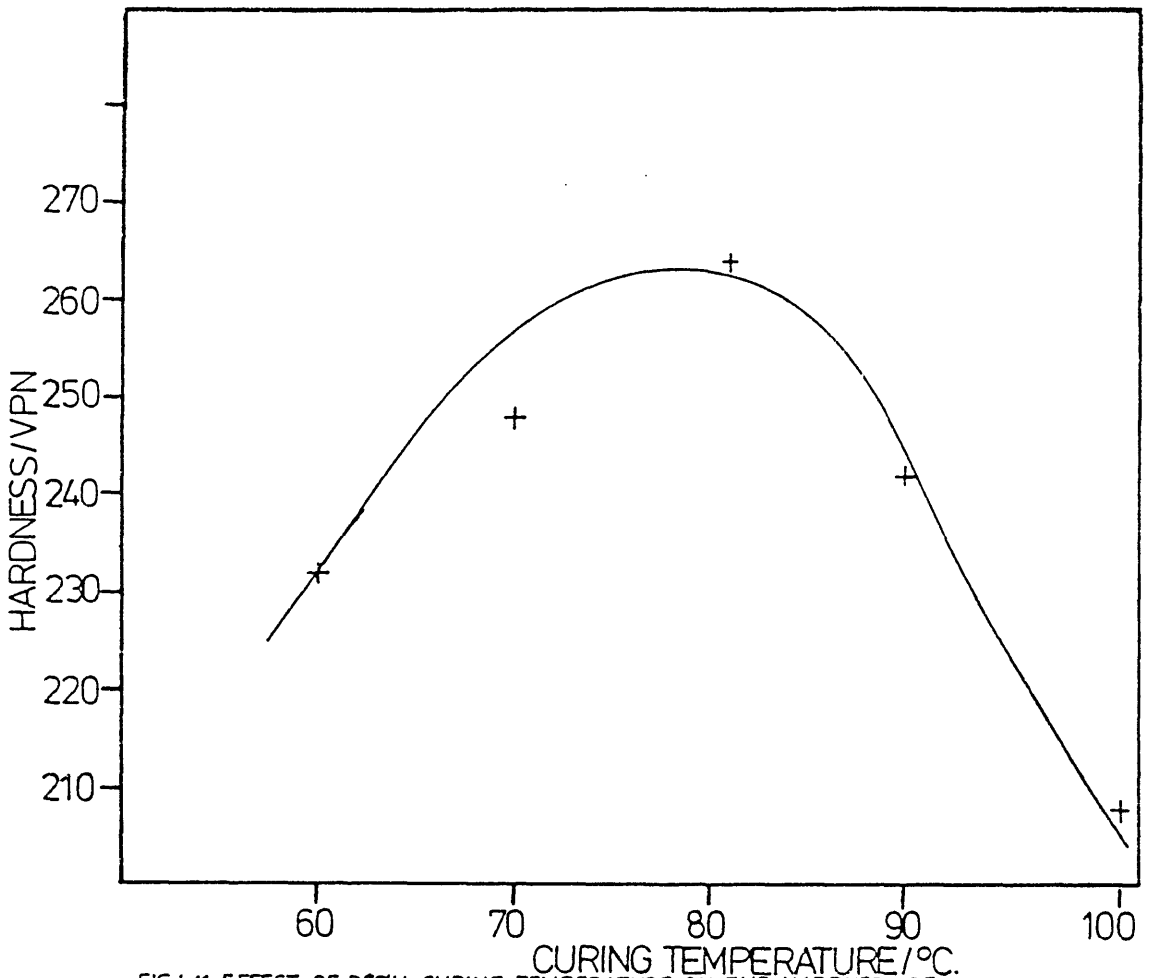


FIG 4·11 EFFECT OF RESIN CURING TEMPERATURE ON THE HARDNESS OF AMORPHOUS CARBON

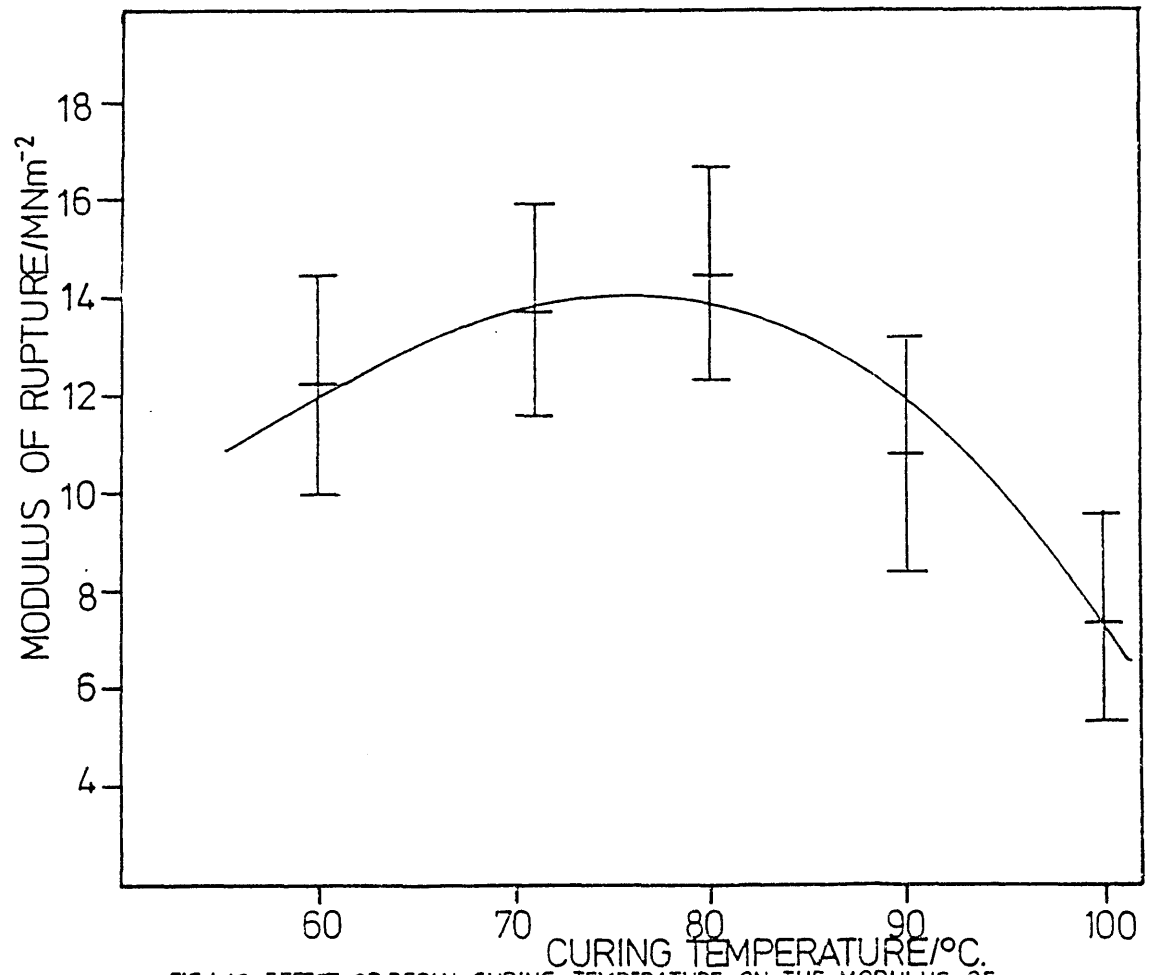


FIG 4·12 EFFECT OF RESIN CURING TEMPERATURE ON THE MODULUS OF RUPTURE OF PYROLYSED POLYFURANOL.

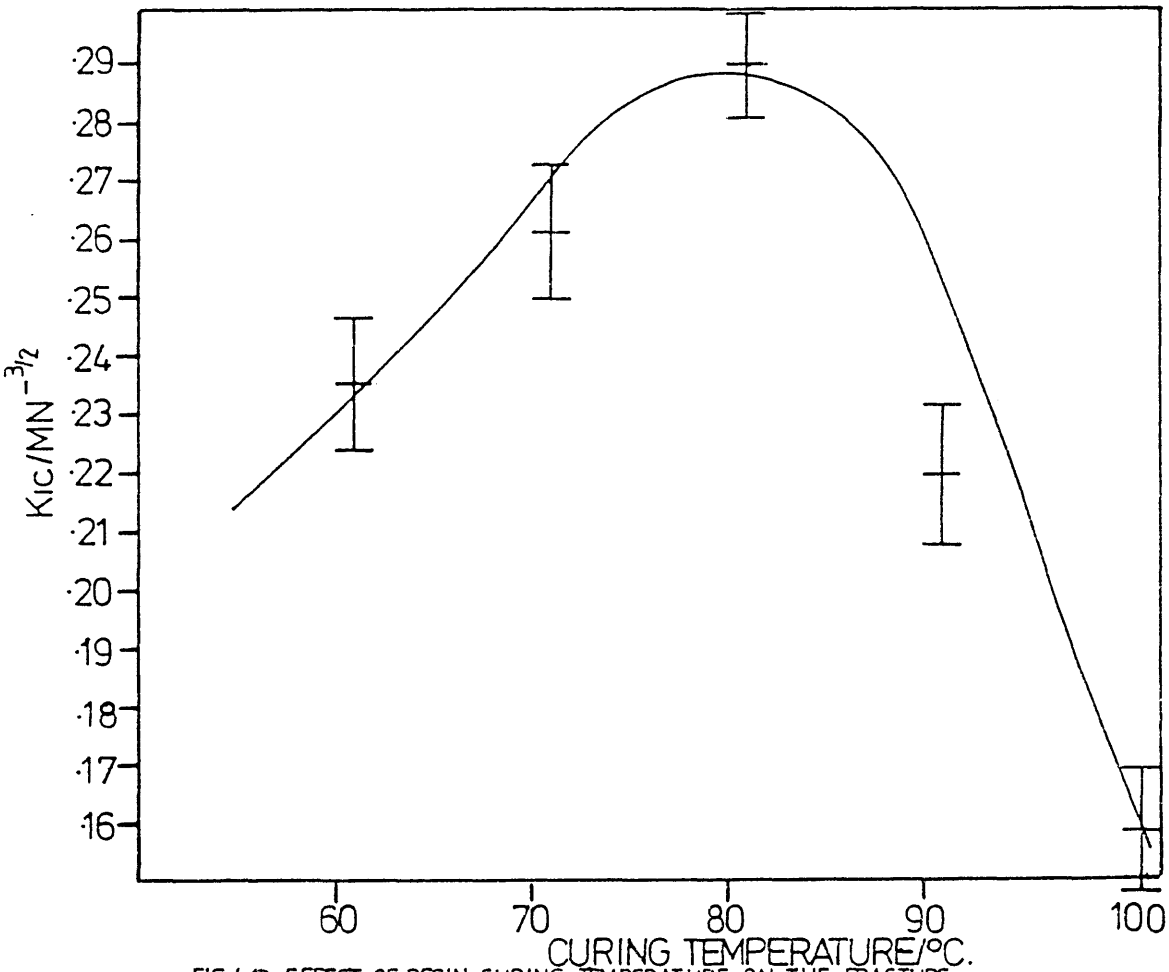
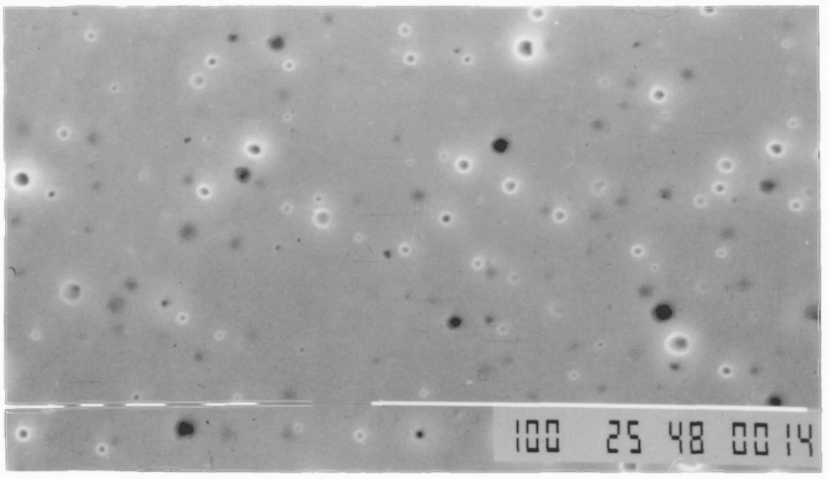
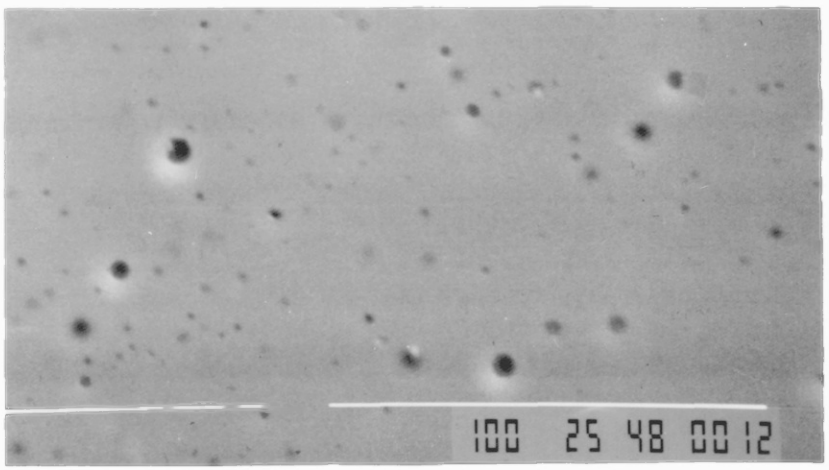


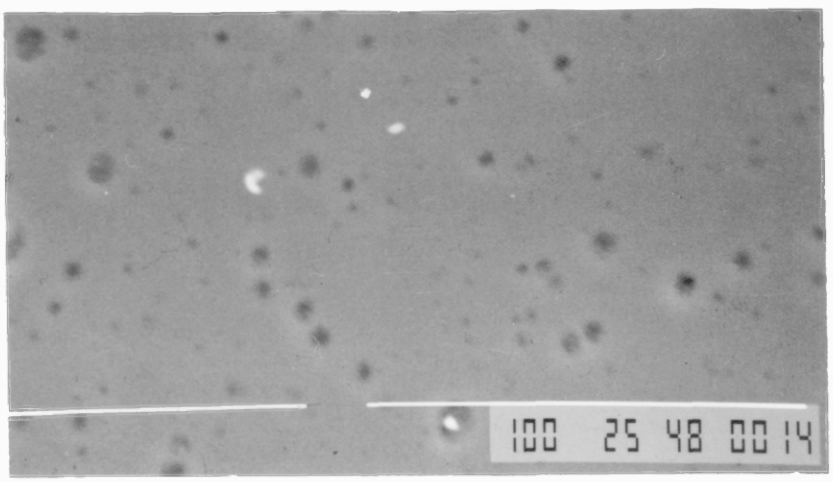
FIG 4·13 EFFECT OF RESIN CURING TEMPERATURE ON THE FRACTURE TOUGHNESS OF AMORPHOUS CARBON.



a. 80°C



b. 90°C



c. 100°C

Fig. 4.14 Electron micrographs showing the effect of resin curing temperature on the microstructure of amorphous carbon.

100μ

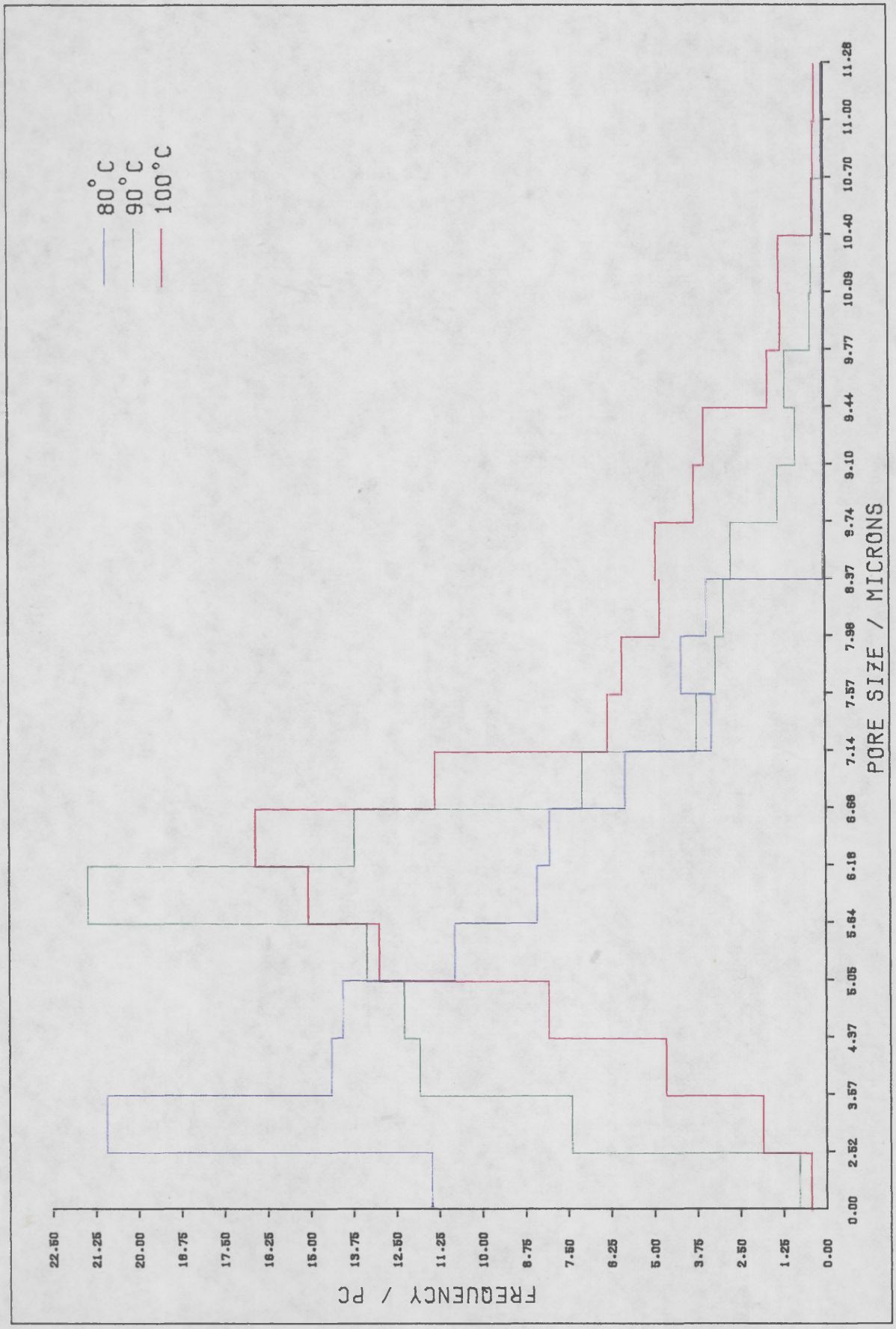


FIG 4·15 EFFECT OF CURING TEMPERATURE OF RESIN PRECURSOR ON THE PORE SIZE DISTRIBUTION IN VITREOUS CARBON.

4.6 Effect of catalyst concentration on the properties of pyrolysed polyfurfuryl alcohol

To assess the effect of catalyst concentration the temperature and length of cure were kept constant at 80°C and 24 hours and the catalyst concentration varied from 1 to 9%. The results appear in Tables 4.6 and 4.7 and Figs. 4.16 through 4.20. Introduction of more catalyst also increased the amount of water introduced into the resin. This water would be driven off during the early stages of curing leading to a lower bulk density and increased porosity. If the amount of porosity in the material is increased the propagation of cracks becomes easier and leads to a reduction in strength and toughness. Increased porosity also caused a decrease in hardness. One can think of the hardness of a material as a measure of its Young's modulus. A porous material can be thought of in terms of a composite between the material and a gas. In other words, we are considering a composite between two materials, one of which has, effectively, no strength or stiffness. If the volume fraction of pores is increased the modulus will fall, according to a first approximation, by the law of mixtures. The carbon yield was observed to decrease with increased catalyst concentration (fig. 4.16). This occured because the amount of non-carbonaceous material in the resin was increased. The zinc chloride volatilizes at high temperature and there must also have been some residual water in the resin driven off during the early stages of heat treatment to account for the reduction in carbon yield.

Batch Number	Catalyst Concentration /%	Carbon Yield/%	Linear Shrinkage/ %	Volume Shrinkage/ %	Bulk Density /gcm^{-3}	Calculated Porosity/ %	Measured Porosity/ %	Maximum Pore Size /μm	Mean Pore Size/ μm	Hardness /VPN
10	1	59.80	19.56	49.37	1.56	4.62	1.49	7.18	4.77	309
3	3	56.48	19.74	48.32	1.52	6.85	4.59	7.99	4.70	264
11	5	56.00	18.52	52.35	1.50	9.34	6.41	8.40	4.83	254
12	7	54.62	18.46	54.14	1.45	11.31	7.98	8.07	4.26	196
13	9	52.81	19.09	54.59	1.43	12.54	10.38	7.14	4.68	165

TABLE 4.6

Effect of Catalyst concentration on the properties of pyrolysed polyfurfuryl alcohol

NOTES

All samples cured for 24 hours at 80°C

Batch Number	Modulus of Rupture/MNm^{-2}	Standard deviation /MNm^{-2}	90% confidence interval/MNm^{-2}
10	17.13	3.33	±1.01
3	14.42	3.56	±1.21
11	11.48	1.97	±0.66
12	8.88	3.05	±1.04
13	7.05	2.79	±0.95

a. Modulus of rupture

Batch Number	K_{IC} /$MNm^{-3/2}$	Standard deviation /$MNm^{-3/2}$	90% confidence interval/$MNm^{-3/2}$
10	0.357	0.032	±0.010
3	0.293	0.039	±0.013
11	0.243	0.029	±0.009
12	0.196	0.037	±0.013
13	0.156	0.037	±0.010

b. Fracture toughness

Table 4.7 Effect of catalyst concentration in resin precursor on the mechanical properties of amorphous carbon.

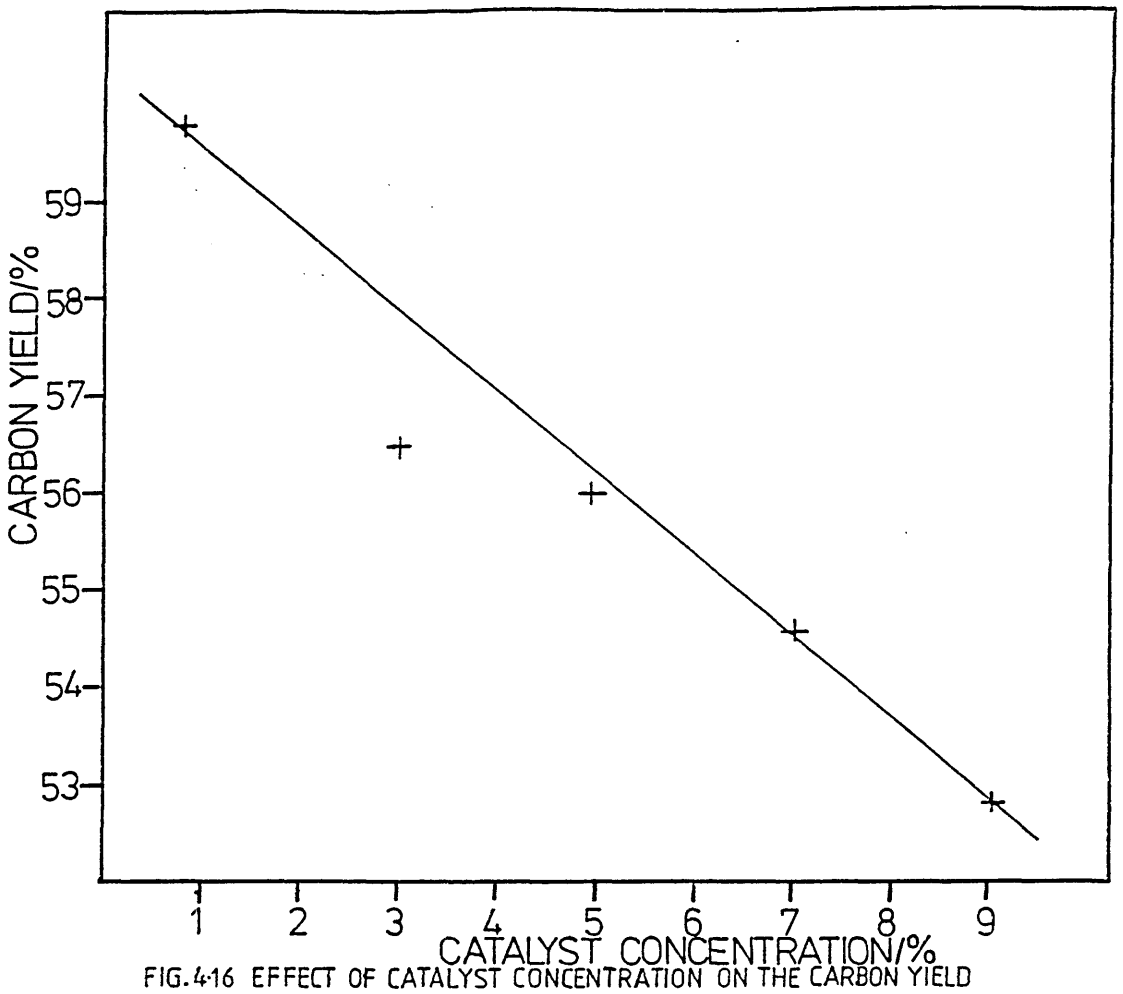


FIG.4·16 EFFECT OF CATALYST CONCENTRATION ON THE CARBON YIELD OBTAINED BY PYROLYSIS OF POLYFUFURYL ALCOHOL.

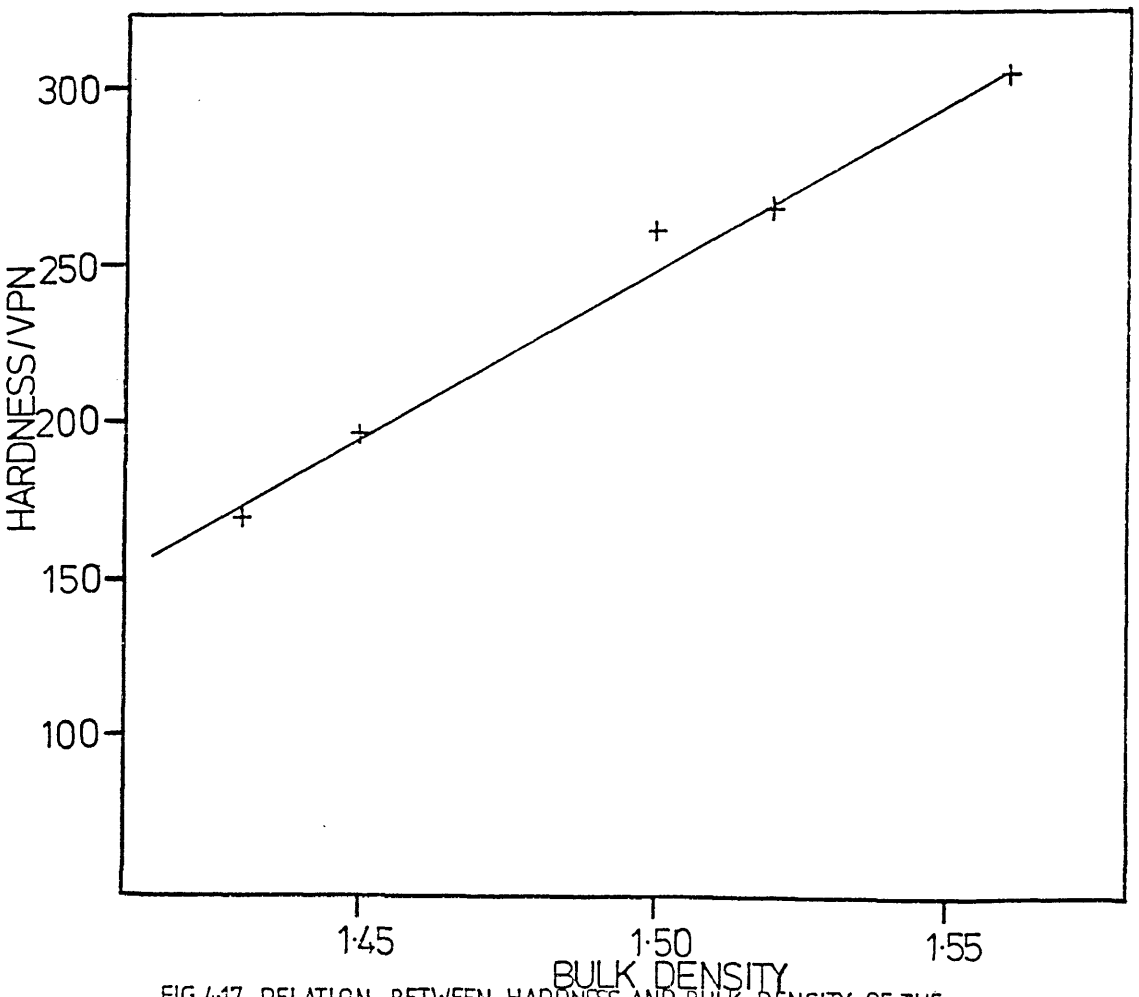


FIG.4·17 RELATION BETWEEN HARDNESS AND BULK DENSITY OF THE AMORPHOUS CARBON.

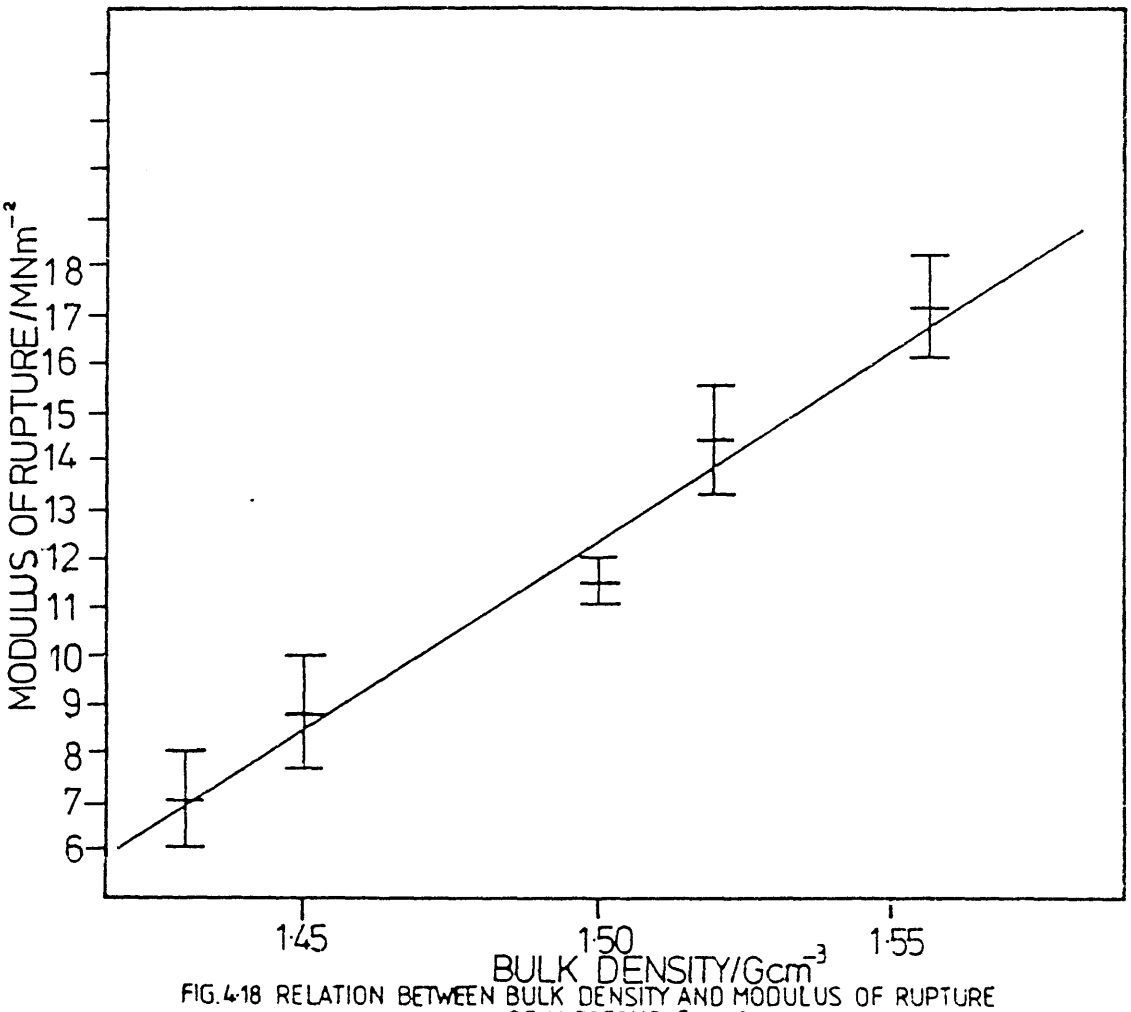


FIG. 4·18 RELATION BETWEEN BULK DENSITY AND MODULUS OF RUPTURE OF VITREOUS CARBON.

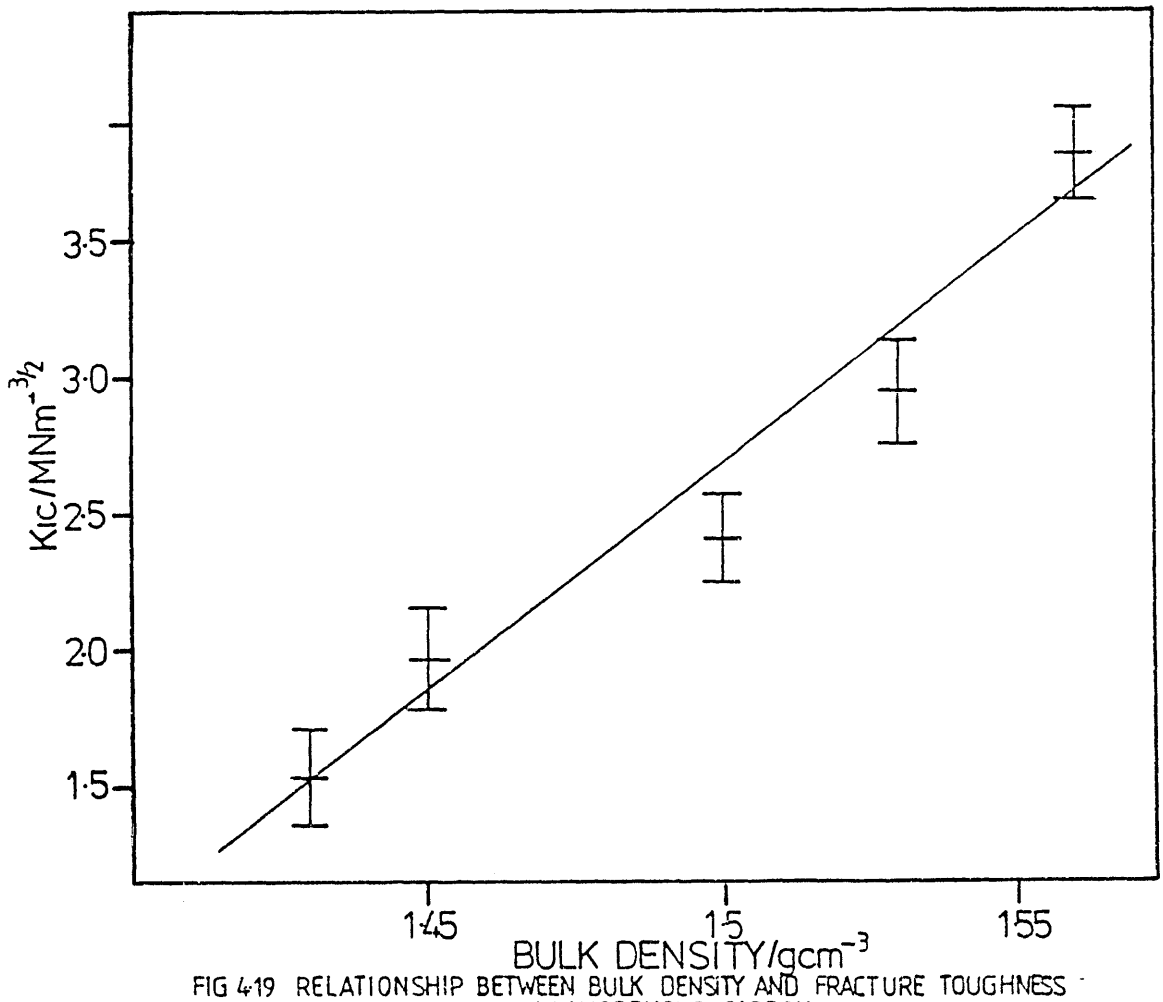
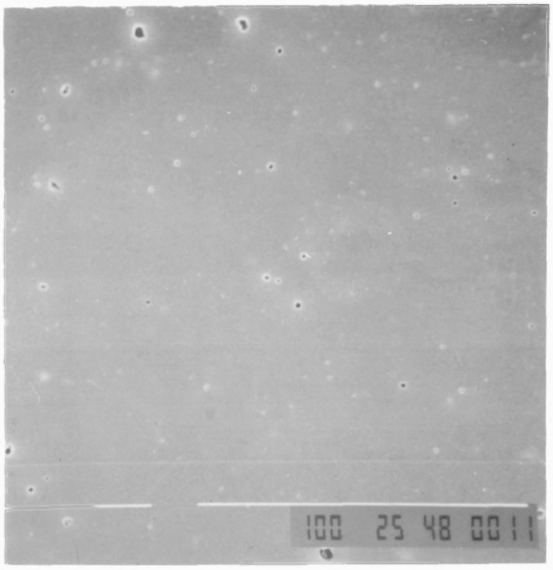
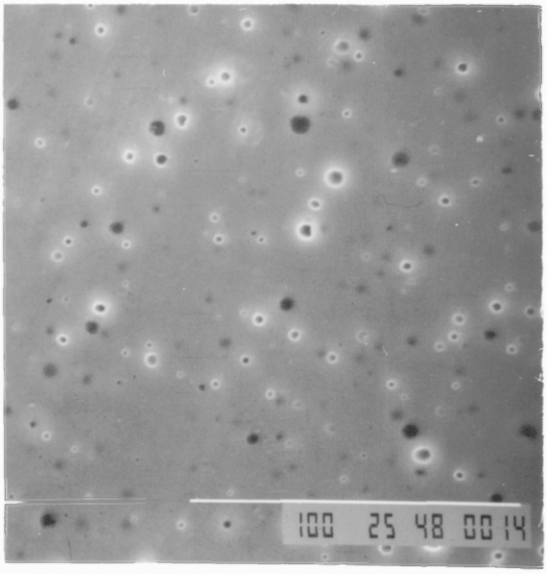


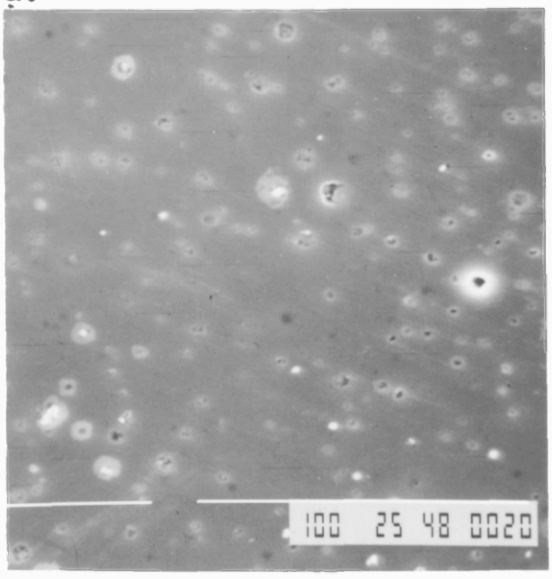
FIG 4·19 RELATIONSHIP BETWEEN BULK DENSITY AND FRACTURE TOUGHNESS IN AMORPHOUS CARBON.



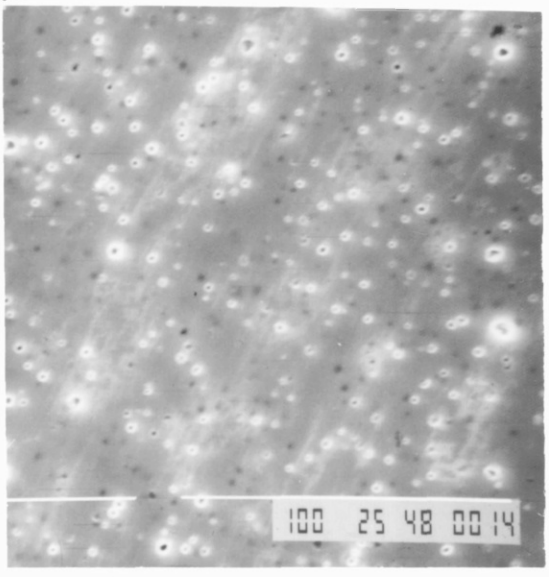
a.



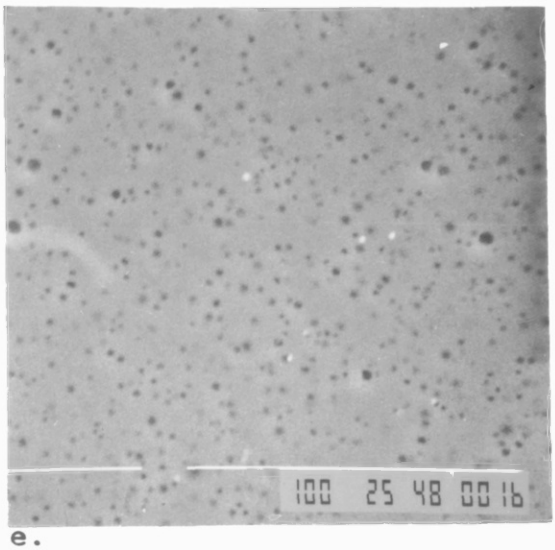
b.



c.



d.



e.

Key

a. = 1% catalyst
b. = 3% catalyst
c. = 5% catalyst
d. = 7% catalyst
e. = 9% catalyst

100μ

Fig. 4.20 Effect of catalyst concentration on the microstructure of pyrolysed polyfurfuryl alcohol.

4.7 Summary of experiments carried out on pure resin

a. Effect of curing time

The carbon yield, hardness, modulus of rupture and fracture toughness have all been observed to increase with increased time of curing of the resin at 80°C. The results would indicate that a minimum of 48 hours is required to obtain properties close to the optimum values.

b. Effect of varying the curing temperature

The carbon yield was found to be independant of curing temperature in the range 60 to 100°C. However, the hardness, modulus of rupture and fracture toughness all showed a maximum for samples cured at 80°C. Above 80°C the residual pores in the material increased in size which led to a decrease in the mechanical properties of samples cured above this temperature.

c. Effect of catalyst concentration

Increasing the amount of added aqueous $ZnCl_2$ catalyst increases the amount of water added to the system. This increased the porosity of the amorphous carbon with subsequent decreases to the carbon yield, bulk density, modulus of rupture and fracture toughness.

4.8 Vitreous Carbon - Graphite Composites

4.8.1 Introduction

Many ceramic materials of commercial importance comprise of a crystalline phase or phases embedded in a glassy matrix. These include, for example, debased aluminas ($\approx$85% Al_2O_3 in glass) and electrical porcelains. The factors which control the mechanical properties of such materials are known but not fully understood. Because of this a number of studies have been performed on 'model' systems, generally particles of a crystalline ceramic, often in spherical form, in various glassy matrices. The important factors which control the mechanical properties of these composite materials are (119) : (a) The expansion coefficients of the two phases, (b) the volume fraction of the crystalline phase, (c) the particle size of the crystalline phase and (d) the elastic properties of the two phases. In this work the effect of (b) and (c) have been investigated in a composite comprising natural graphite in a vitreous carbon matrix.

The incorporation of a strong second phase into a material to form a composite with superior mechanical properties is loosely termed 'dispersed phase toughening' Claussen (120) observed this effect in composites fabricated from Al_2O_3 and unstabilized ZrO_2 powder. The fracture toughness of these composites was shown to be dependent on the volume fraction of ZrO_2 particles. From these observations, Claussen deduced that the increase in toughness results from small matrix microcracks absorbing energy by controlled propagation. The cracks arise during fabrication

as a result of the different thermal expansion of the constituent phases. The generation of stable microcracks is not necessarily connected with an increase in fracture toughness but in a brittle composite with residual stress distribution (of which vitreous carbon/graphite is an example) this toughening mechanism is thought likely to occur.

Davidge and Green (121) experimented on the effect of the particle size of the dispersed phase on the strength of the composite. They studied the effect of thoria spheres of various diameters embedded in a glassy matrix and found that stresses occured around the spheres due to differences in the expansion coefficients on cooling from the fabrication temperature. Stress concentration occured near the spheres due to differences in elastic properties in the presence of an applied stress. Providing the expansion coefficient of the particles was greater than that of the glass (as in vitreous carbon/graphite) circumferential cracks formed around the spheres when the sphere diameter was greater than a critical value. This critical diameter arises when the size of the particles becomes greater than those of the inherent Griffith flaws already present in the matrix. Larger particles cause increased internal stress in the glass and are therefore more deleterous to the strength than small particles. The strongest composite, other things being equal, is likely to be one with the finest dispersed particle size.

There are various possible mechanisms for the increase in toughness by the inclusion of second phase particles. These mechanisms have been reviewed by Green (122). Firstly, the fracture energy may be increased by an augmentation in the surface area of fracture as follows:

$$\gamma_c = \gamma_m \left| \frac{A_t}{A_p} \right| \qquad (4.1)$$

where γ_c and γ_m are fracture energies of the composite and matrix respectively, A_t is the true surface area and A_p the planar surface area. This effect is, however, too small to account for the observed increases in toughness. Secondly, the fracture energy may be increased by the creation of fracture surface steps. These arise when the crack front is divided and forced into different planes. 'River' markings have been observed frequently on the surfaces of two phase materials (123). The additional energy depends on the volume fraction of the second phase (Vp).

$$\gamma_c = \gamma_m \left(1 - V_p \right) + S \left| \frac{h}{dc} \right| \qquad (4.2)$$

Where S is a constant, h the step height and dc the centre to centre interparticle spacing. Thirdly, the fracture toughness maybe increased by a bowing of the crack front between the particles. This mechanism was originally suggested by Lange (124) and is analagous to the line tension concept used in dislocation theory. A fourth

possible mechanism to account for the increase in toughness caused by dispersed phase inclusions is a decohesion of the particles from the matrix ahead of the crack tip giving rise to crack tip blunting. This phenonema was observed by Owen (125) in study of the fracture of epoxy resin filled with glass beads.

Maloney, Kausch and Stieger (126) measured the fracture properties of an epoxy resin filled with silica glass, alumina and dolomite particles and were able to produce some general conclusions about the effects of dispersed phase toughening: Glassy matrices may be toughened by the addition of rigid particulate fillers but the maximum increase in toughness may, however, only be obtained under certain conditions.

1. The particles must be stronger than the matrix; the mere presence of interfaces is insufficient to promote increased toughness.
2. A certain minimum adhesion between the filler and the matrix is necessary for toughening from crack bowing.
3. The particle shape plays an important role in determining the toughness of the composite. The theoretical work of Green and the experimental results of Maloney, et al showed that spheres are less effective in increasing toughness than irregularly shaped particles.

4.8.2 Effect of Volume Fractions of Graphite on the Properties of the Composite

Composites of vitreous carbon and natural graphite were formed by pyrolysing polyfurfuryl alcohol resin to which natural graphite powder had been added as a known weight % prior to curing. The amount of graphite added was varied from 0 to 40% and the curing conditions kept constant at 80°C for 24 hours with 3% (by weight) catalyst added. It was not possible to prepare test specimens containing more than 15% graphite because of the presence of air bubbles trapped during mixing. These air bubbles were formed because the vacuum equipment used was not powerful enough to remove them from the viscous green mixture. During heat treatment large thermal stresses were built up around the air bubbles and caused fracture of the specimens. The physical and mechanical properties of the composites produced are presented in tables 4.8 and 4.9.

The carbon yield increased with volume fraction of graphite in the composite (Fig. 4.21) because none of the graphite was lost during pyrolysis so the proportion of the material volatilised during pyrolysis was decreased. To prove that the graphite was unaffected by the heat treatment a small block of graphite was placed inside the furnace and subjected to the same heat treatment programme as the resin. The weight loss observed was negligible. The shrinkage during pyrolysis, shown in Fig. 2.22, was observed to decrease as the amount of graphite increased because the graphite flakes resist the movement of the glassy carbon ribbons during cooling. This, in turn, is responsible for

Batch Number	Amount of Graphite in Composite/%	Carbon Yield/%	Linear Shrinkage/%	Volume Shrinkage/%	Bulk Density/gcm^{-3}	Calculated Porosity/%	Hardness/VPN
3	0	56.48	19.74	48.32	1.52	6.85	264
14	2	58.25	19.27	48.11	1.53	8.50	250
15	5	59.10	18.55	47.19	1.54	9.74	232
16	7.5	61.51	18.02	46.40	1.55	10.32	204
17	10	62.56	17.05	46.77	1.57	10.83	178
18	12.5	62.88	16.61	41.93	1.58	11.39	161
19	15	64.90	15.53	40.78	1.60	11.88	139

Table 4.8 Effect of increasing the volume fraction of graphite on the properties of vitreous carbon/graphite composites.

Note: All samples cured for 24 hours at 80°C with 3% (by weight) catalyst added Graphite particle size constant at 'nominal' 10μm.

Batch Number	Amount of Graphite in Green Composite/wt%	Modulus of Rupture Strength/MNm^{-2}	Std. Dev. of MOR/MNm^{-2}	90% Conf. Int. of MOR/MNm^{-2}	K_{IC}/$MNm^{-3/2}$	Std. Dev. of K_{IC}/$MNm^{-3/2}$	90% Conf. Int. of K_{IC}/$MNm^{-3/2}$
3	0	14.42	3.56	± 1.01	0.293	0.033	± 0.012
14	2	15.54	3.89	± 1.33	0.316	0.036	± 0.013
15	5	15.75	3.77	± 1.23	0.359	0.039	± 0.013
16	7.5	18.15	4.39	± 1.41	0.390	0.040	± 0.014
17	10	25.95	5.75	± 1.97	0.511	0.055	± 0.018
18	12.5	31.48	6.63	± 2.22	0.553	0.054	± 0.017
19	15	31.88	6.37	± 1.98	0.662	0.066	± 0.021

Table 4.9 Mechanical properties of amorphous carbon/graphite composites.

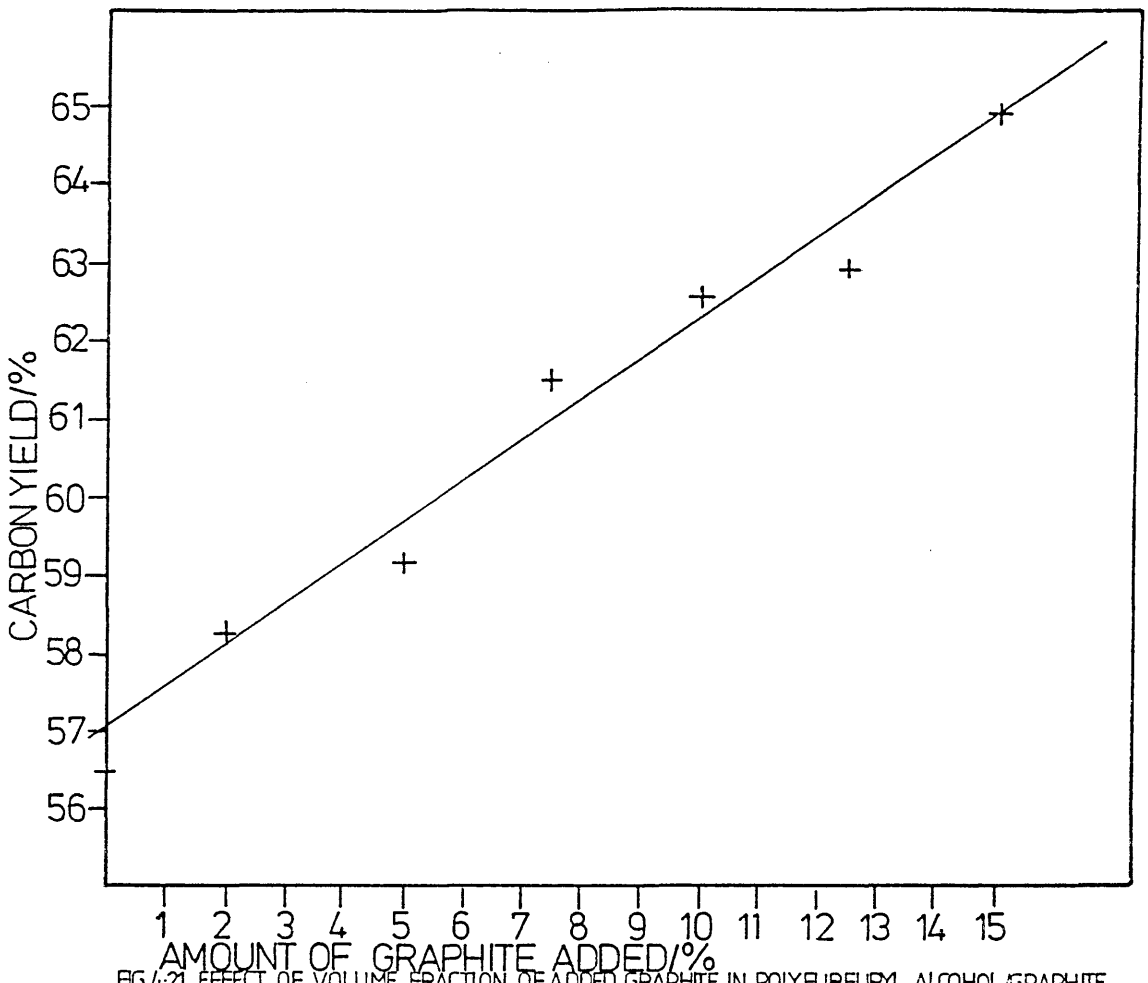


FIG 4·21 EFFECT OF VOLUME FRACTION OF ADDED GRAPHITE IN POLYFURFURYL ALCOHOL/GRAPHITE COMPOSITES ON THE CARBON YIELD OBTAINED ON PYROLYSIS

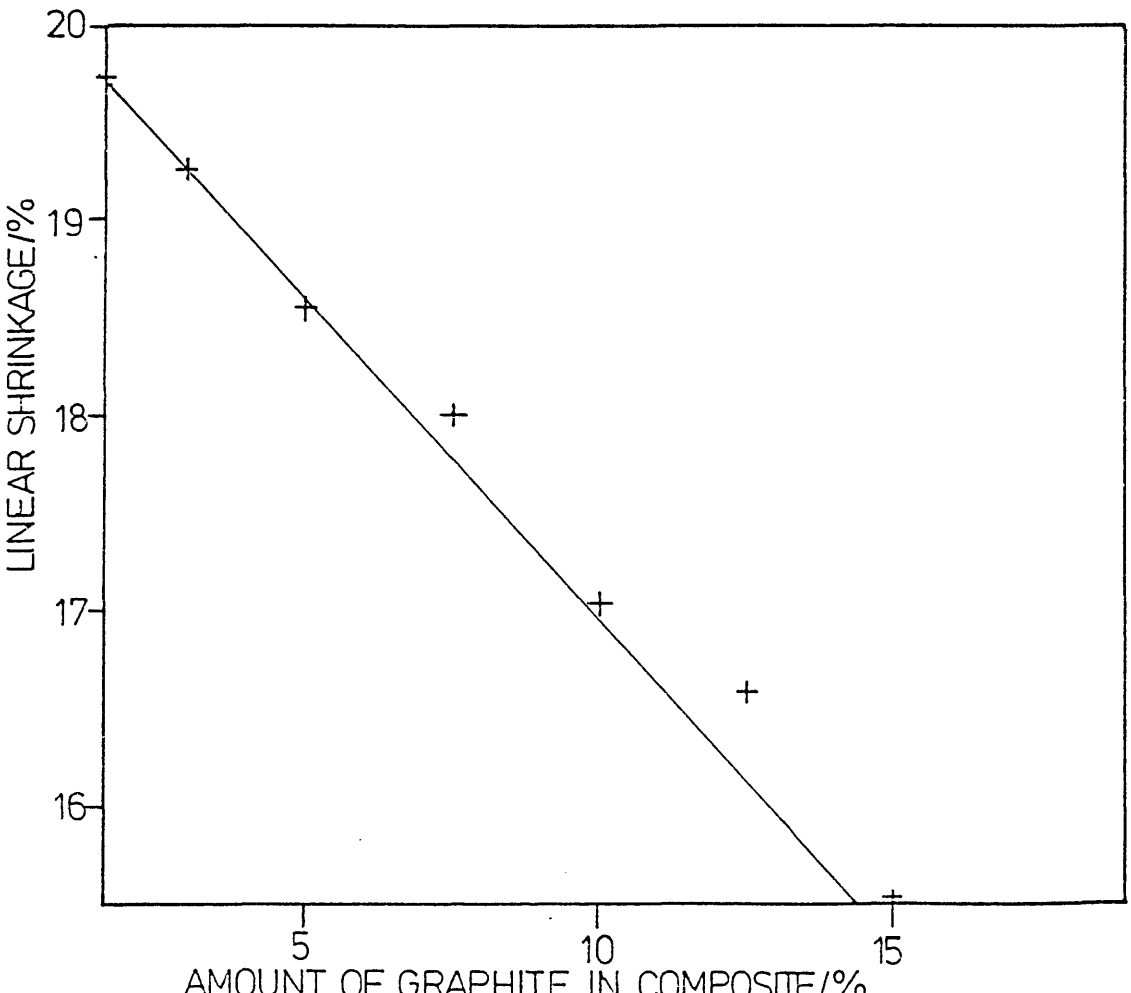


FIG 4·22 EFFECT OF GRAPHITE CONTENT ON THE LINEAR SHRINKAGE DURING PYROLYSIS OF VITREOUS CARBON/GRAPHITE COMPOSITES

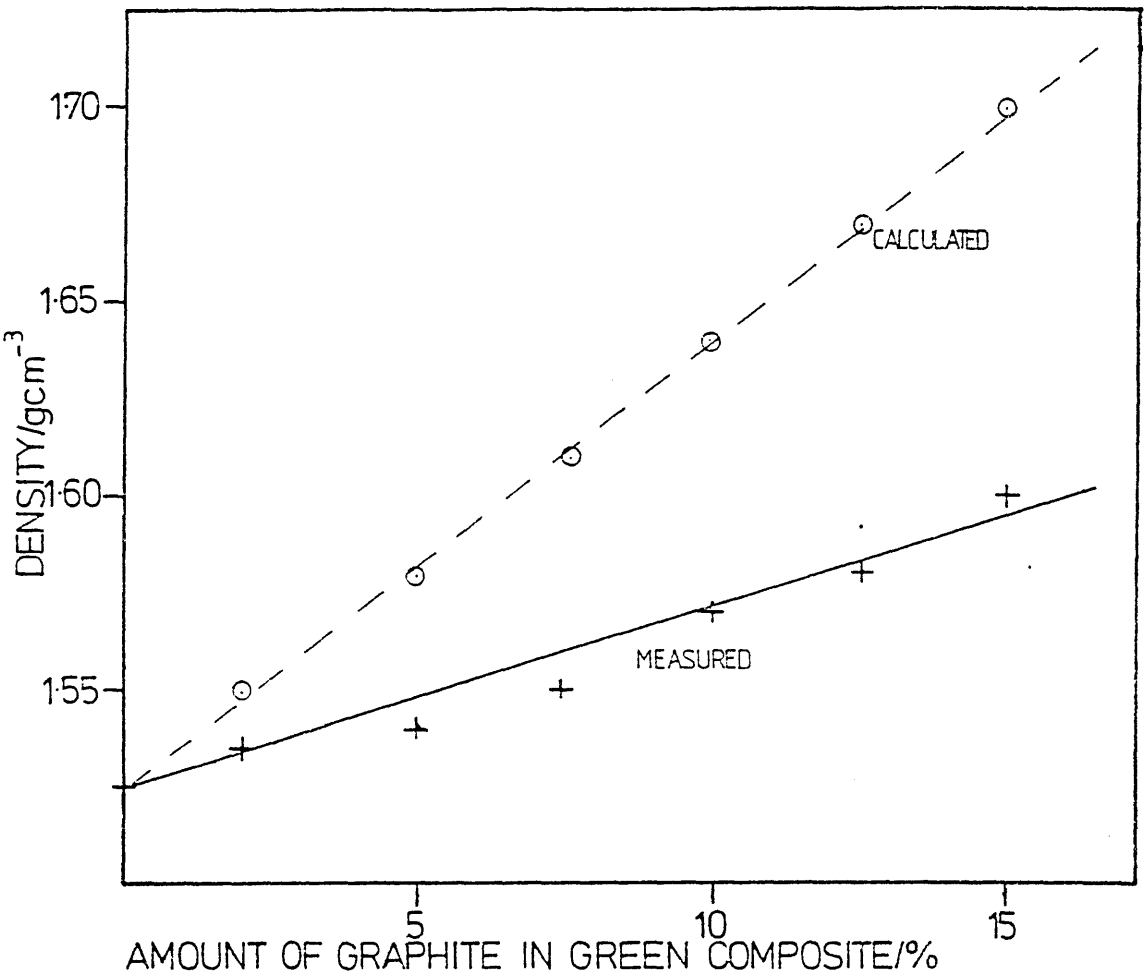


FIG 4·23 CALCULATED AND MEASURED DENSITIES OF AMORPHOUS CARBON/GRAPHITE COMPOSITES AS A FUNCTION OF GRAPHITE VOLUME FRACTION

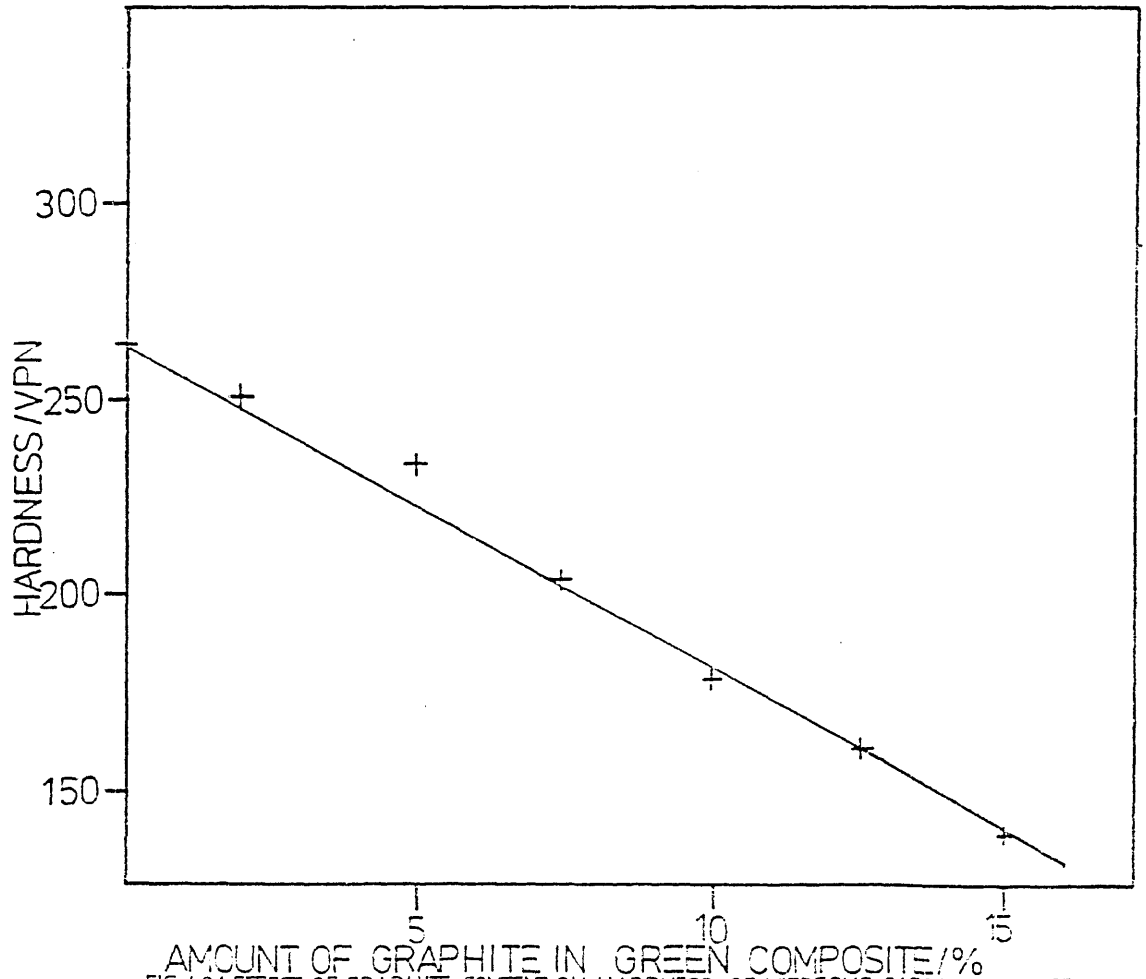


FIG 4·24 EFFECT OF GRAPHITE CONTENT ON HARDNESS OF VITREOUS CARBON/GRAPHITE COMPOSITES

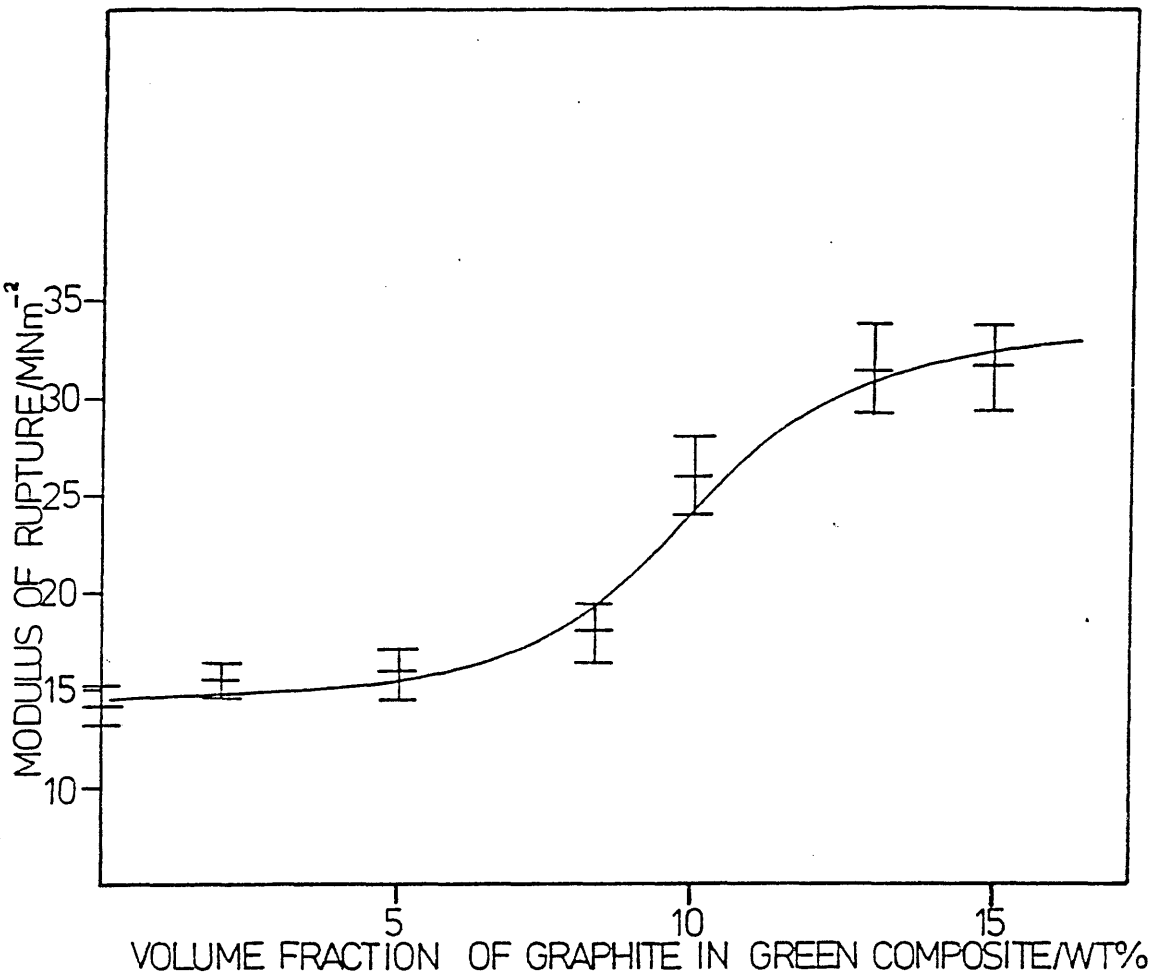


FIG 4·25 EFFECT OF GRAPHITE CONTENT ON THE MODULUS OF RUPTURE STRENGTH OF FIRED GRAPHITE/POLYFURFURYL ALCOHOL COMPOSITES.

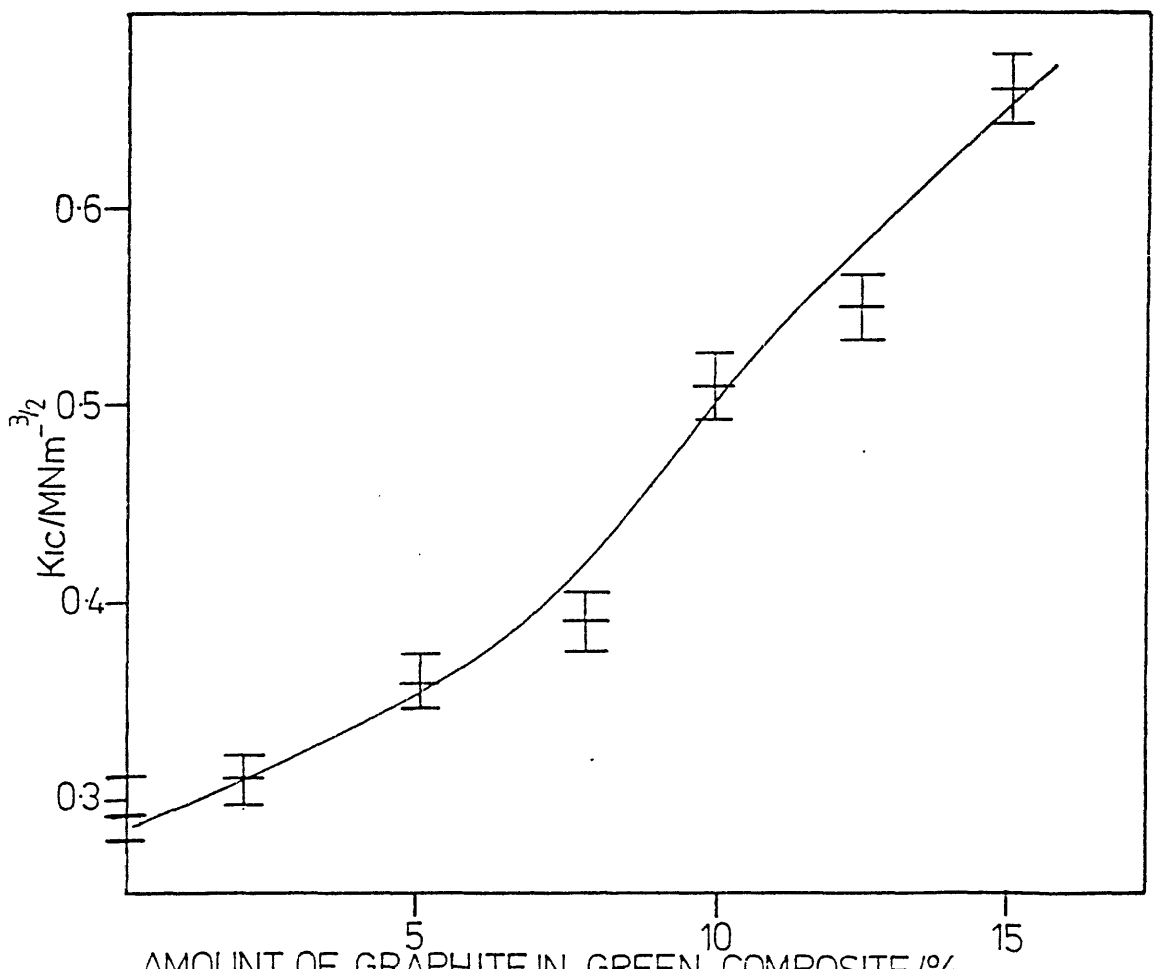


FIG 4·26 EFFECT OF GRAPHITE CONTENT ON THE FRACTURE TOUGHNESS OF FIRED GRAPHITE/POLYFURFURYL ALCOHOL COMPOSITES

the increase in calculated "porosity" since the stacking of ribbons is hindered making space filling less efficient.

The bulk density of the composites increased with graphite content due to the higher density of natural graphite. The percentage of graphite in the fired composite was calculated from the amount in the green composite using the following assumptions:

Let the amount of graphite in green composite = X%

then, amount of resin in green composite = $100 - X$.

Assuming that no graphite is lost in heat treatment, and the carbon yield of resin (from batch 3) is 56.5% then,

amount of amorphous carbon = $0.565\ (100 - X)$

amount of graphite in fired composite =

$$\frac{X}{X + 0.565\ (100 - X)} \times 100\% \qquad (4.3)$$

The theoretical density of the composite can then be estimated from the law of mixtures:

$$\rho_c = V_G \rho_G + V_{VC} \rho_{VC} \qquad (4.4)$$

where ρ_c = density of composite

ρ_G and ρ_{VC} are densities of graphite and vitreous carbon respectively and V_G and V_{VC} their volume fractions.

The increase in the amount of unfilled space is clearly illustrated by the difference between calculated and measured densities. Graphite is much softer than amorphous carbon (2 on Mohs' scale) and so the observed decrease in hardness when the amount of graphite was increased (Fig. 2.24) is to be expected.

The most obvious and important effect observed in the composites was the dramatic improvement in mechanical properties caused by increased additions of graphite. Electron micrographs of fracture faces (Figs. 4.28 and 4.29) show how the addition of graphite changed the material from a glassy carbon with its smooth, featureless, brittle fracture face to one which became gradually textured and tougher as the graphite content was increased. The graphite adhered well to the glassy carbon matrix and there were no obvious voids around particles. The strength and toughness increased slowly at first and then more rapidly as the effect of the graphite took control, with the result that for graphite loadings of 15% in the green composite ($\approx$ 24% in fired composite) the strength and toughness were more than doubled.

The increase in mechanical properties occured because the graphite flakes are able to blunt and deflect the advancing crack tip as shown in Fig. 4.27.

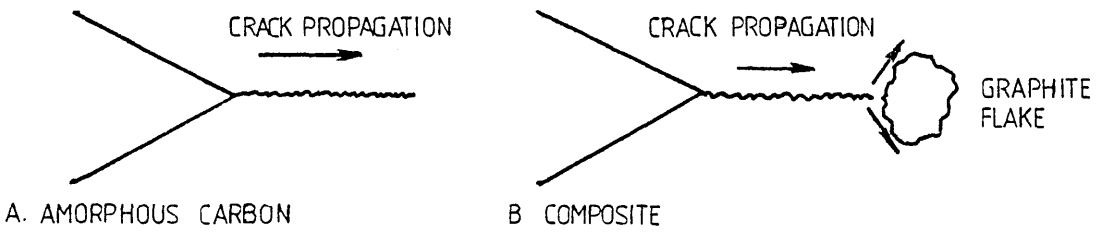
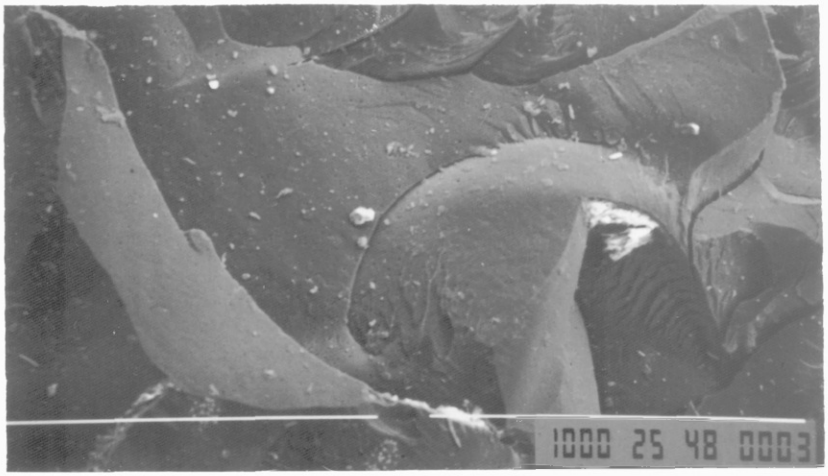
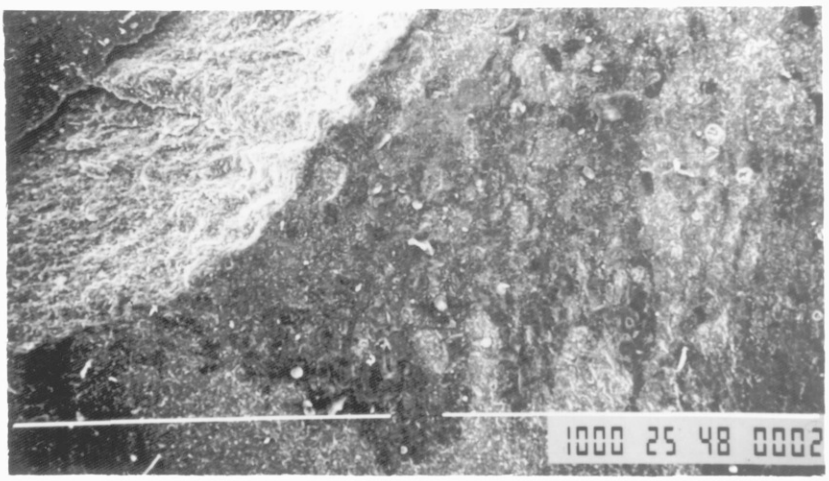


Fig. 2.27 Schematic diagram of dispersed phase toughening by graphite particles in amorphous carbon/graphite composites.



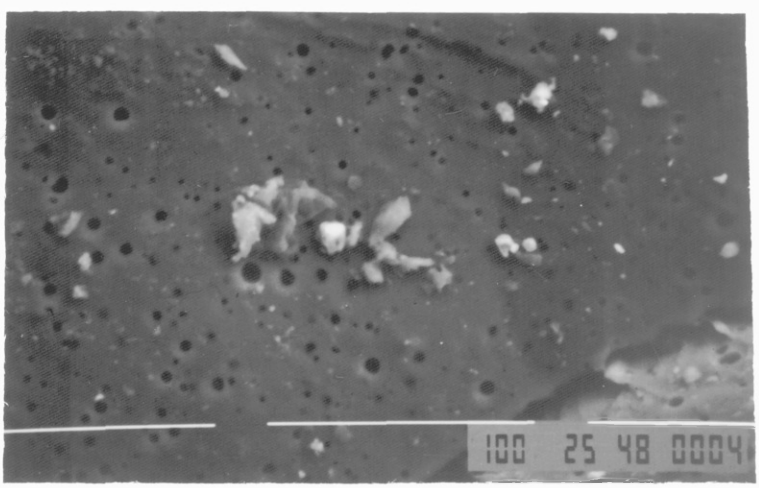
A.



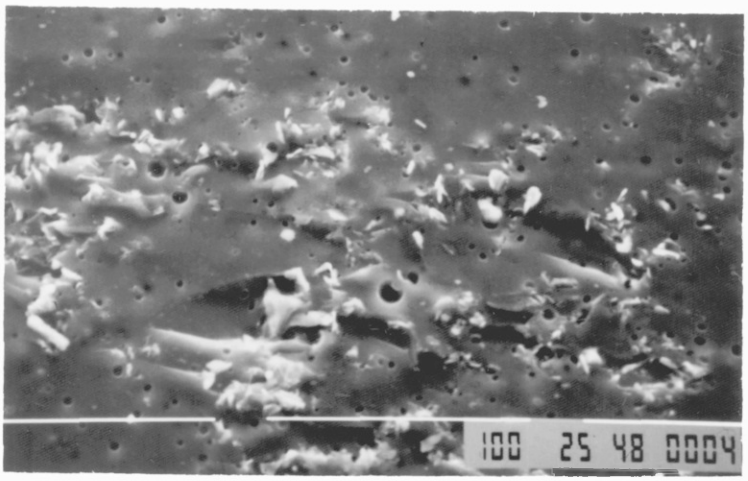
B.

1000μ

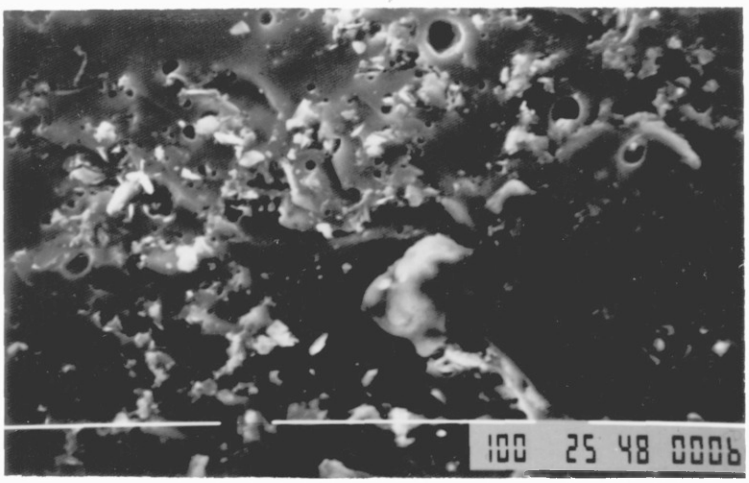
Fig. 4.28 Low magnification fracture faces of 'pure' amorphous carbon (A) and a composite with a loading of 15% graphite when green (B) showing the change from a very brittle and featureless to a textured and tougher material.



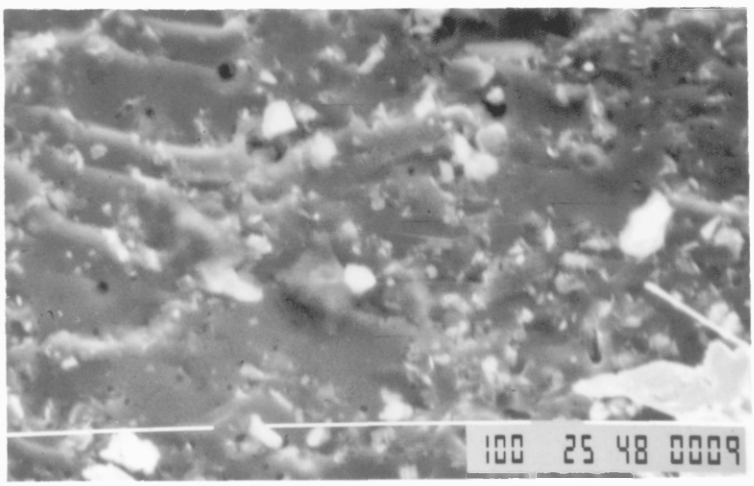
a. 0% graphite



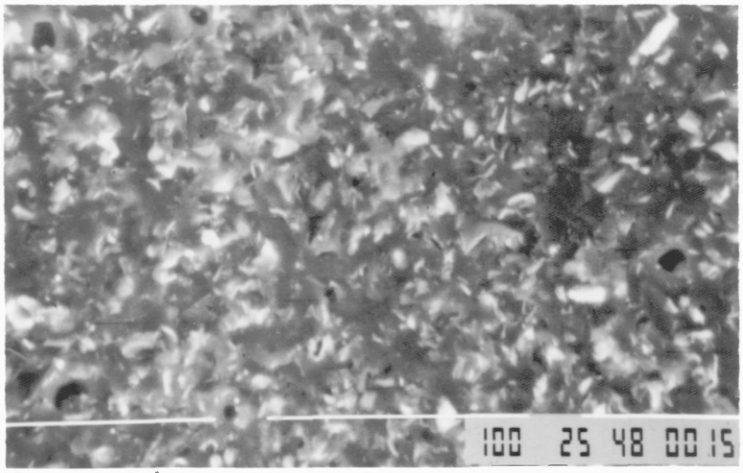
b. 2% graphite



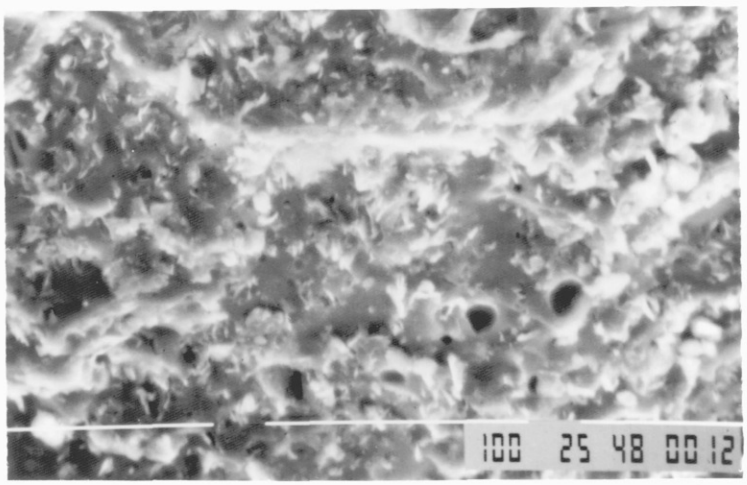
c. 5% graphite



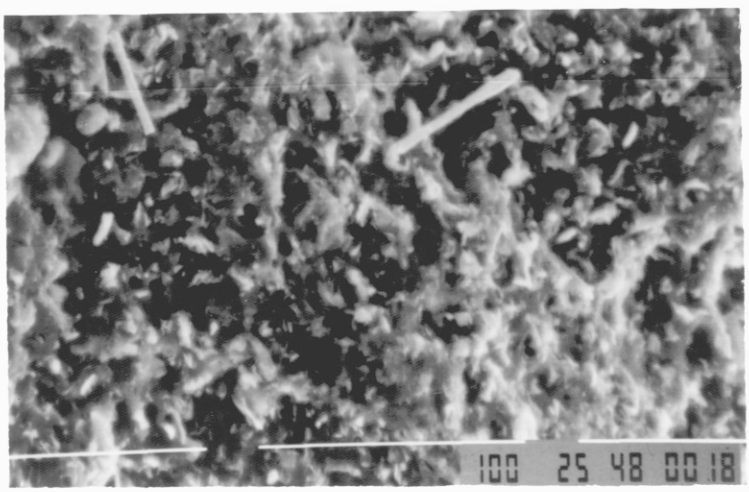
d. 7.5% graphite



e. 10% graphite



f. 12.5% graphite



g 15% graphite

100 μ

Fig. 2.29 Fracture faces of vitreous carbon/graphite composites showing the transition to a stronger and tougher material with increased graphite content.

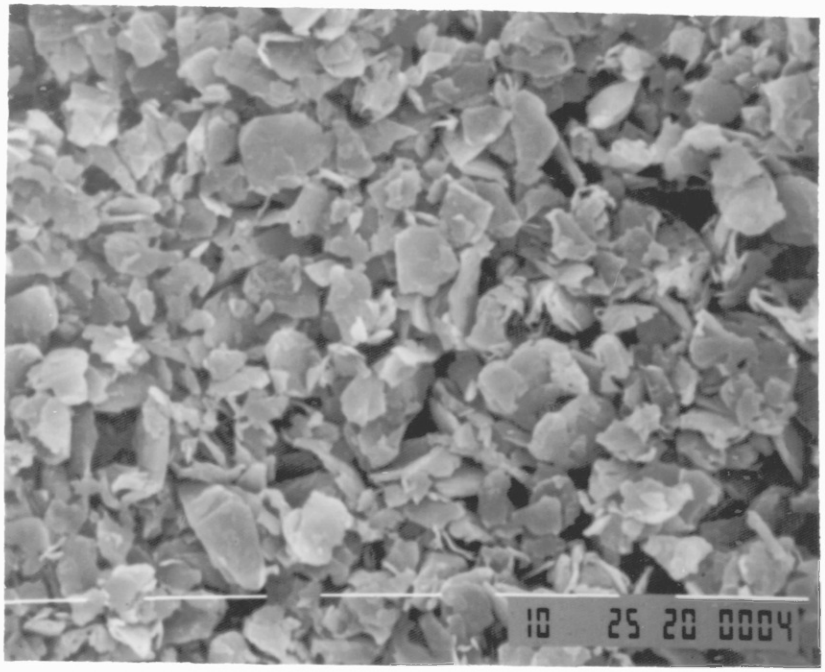
In a brittle material such as amorphous carbon there is no plastic deformation and blunting at the crack tip, so a crack can propagate quickly and easily as a result of the stress concentration effect at the tip. In the composite material the propagation of cracks is resisted by graphite flakes in their path with the result that the crack tip is blunted, and the crack deflected around the graphite, thus toughening the material. This phenomena is very well illustrated by Fig. 4.29 g. in which it can clearly be seen where the failure initiating crack has been deflected around the graphite flakes. A very simple but effective illustration of the increased toughness can be carried out by dropping a sample of 'pure' amorphous carbon and a composite containing 10% graphite both from a height of 1m onto a hard surface. The amorphous carbon will shatter on hitting the surface but the composite will remain intact.

4.8.3 Effect of graphite particle size on the properties of the composite

Five graphite powders from various commercial suppliers were analysed for particle size and distribution and found to fall into "nominal" sizes of 6, 10, 20, 25 and 100μm. The results of this analysis are presented in Figs. 4.30 - 4.34 in the form of scanning electron micrographs and particle size distribution histograms for each graphite in turn. A series of vitreous carbon/graphite composites were produced using constant curing conditions and a constant loading of 12.5% of each size of graphite in order to observe the effect of graphite particle size on the properties of the composite. The results are shown in tables 4.10 and 4.11.

The use of different graphite particle sizes in the composites appears to have had little or no effect on their physical properties. The hardness was observed to fall slightly with coarsening of the second phase, suggesting that a material with an irregularly shaped crystalline second phase can be included in Zarzycki's prediction (118). Increasing the graphite particle size caused a rapid decrease in the modulus of rupture strength of the composites. This occured because, as the particle size was increased, it became more and more difficult for the randomly oriented vitreous carbon ribbons to adhere uniformly to the graphite particles resulting in the formation of voids around the particles. A further factor leading to a fall in strength is the build up of internal stresses due to the different thermal expansions of graphite and vitreous carbon which would be expected to increase with increasing particle size.

The fracture toughness showed a definite maximum with respect to particle size at around 20μm such that there was something like a 250% increase in the toughness of a composite containing 12.5% of 20μm graphite compared with that of a "pure" vitreous carbon. A possible explanation of the effect observed is that the maximum toughening corresponds to the particle size at which it is preferential for the fracture initiating crack to pass through the particles rather than around them. This can be inferred from the micrographs in Fig. 4.38 as the fracture faces are flatter with no evidence of the crack having passed around the larger particles of graphite.



10μm

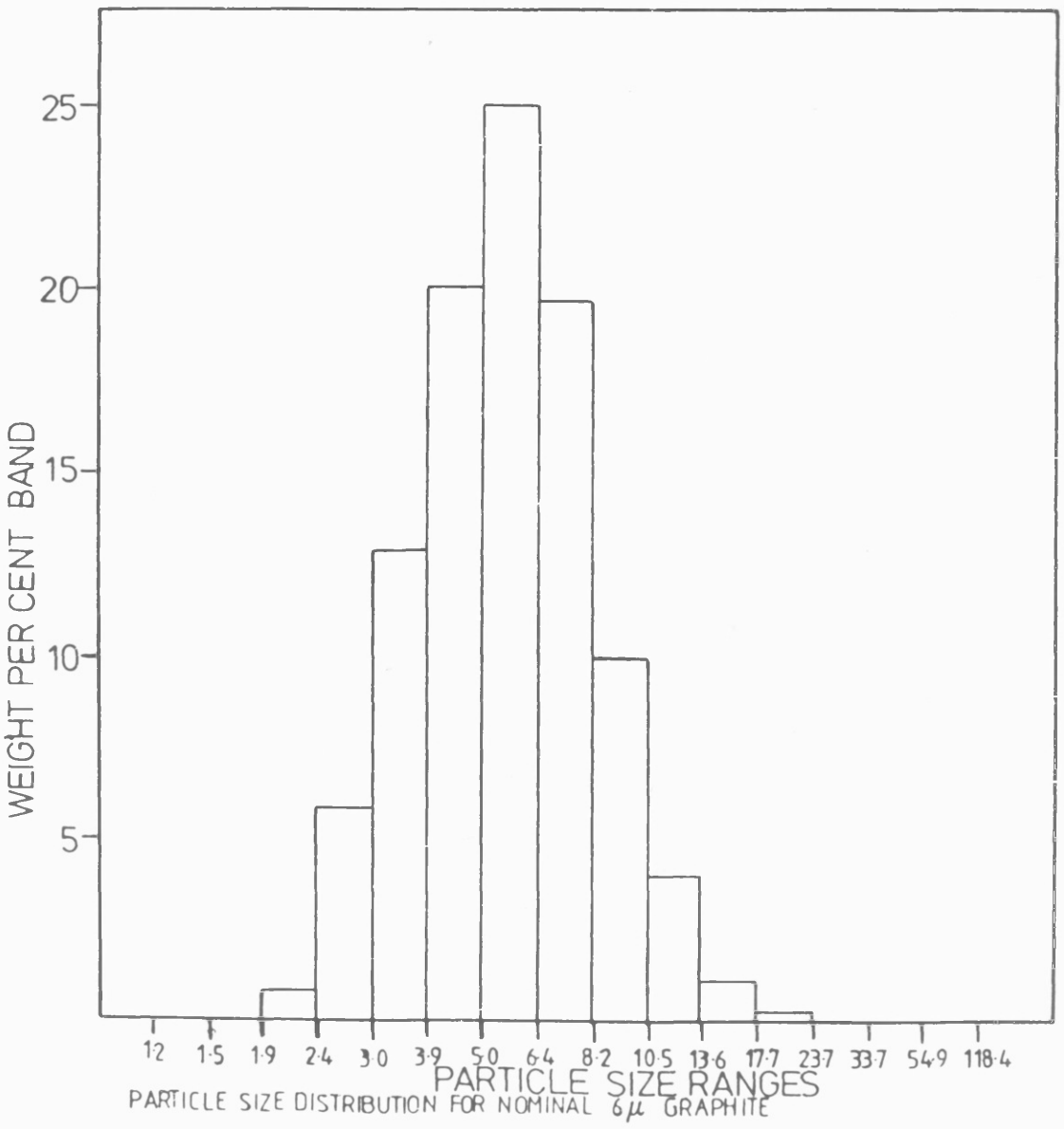
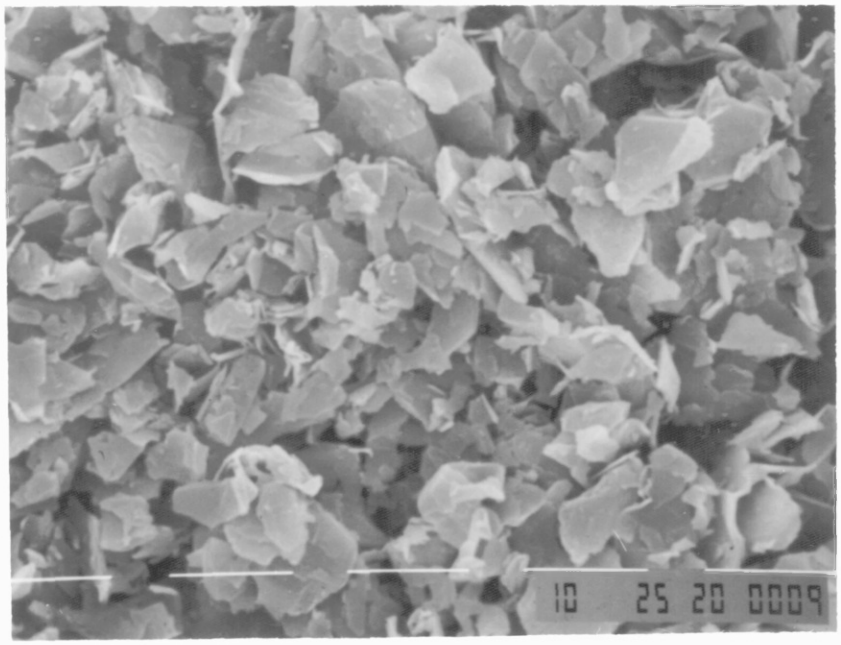


Fig. 4.30 "Nominal" 6μ graphite (P.S. Wilson & Co.).



10μm

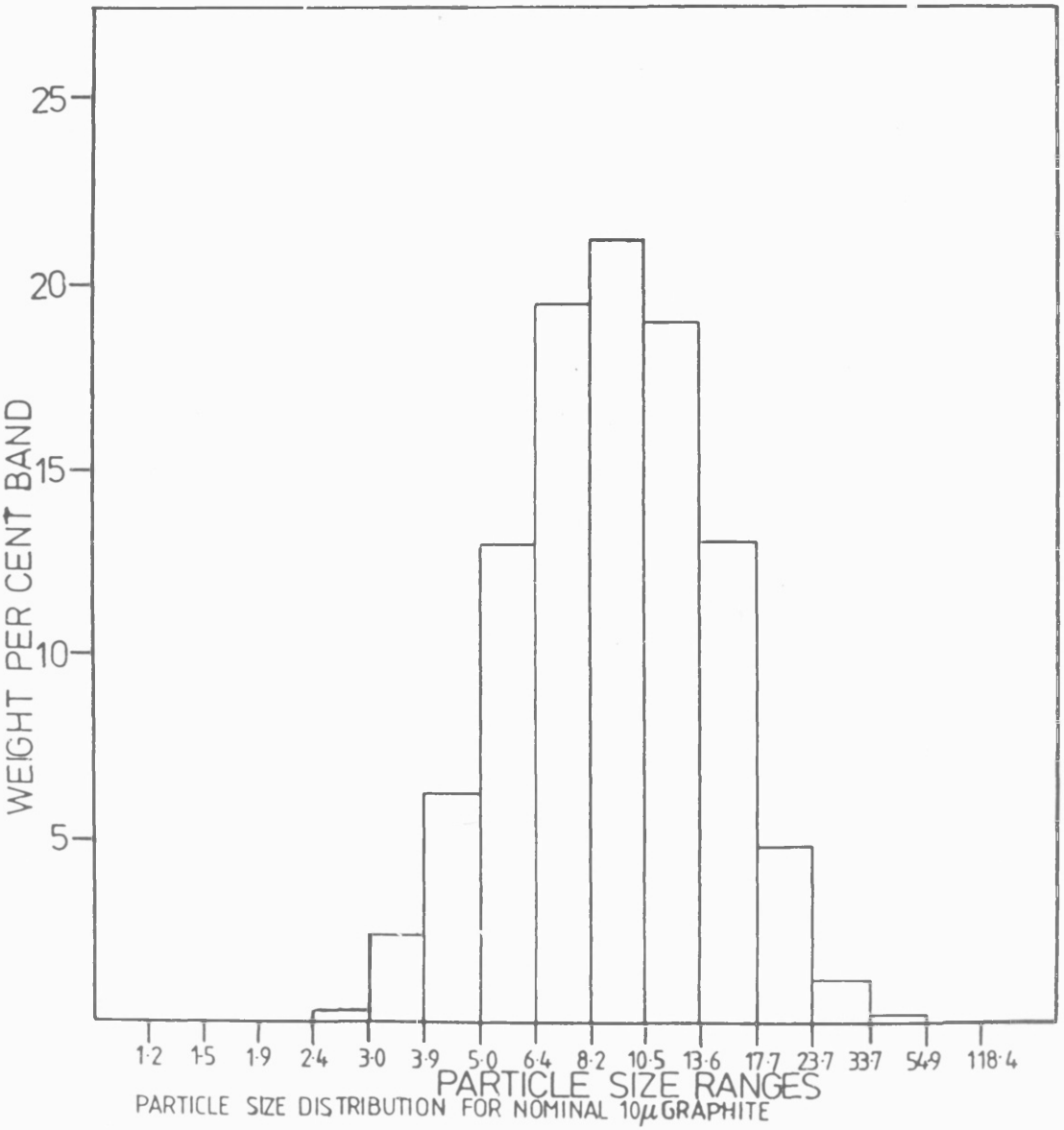
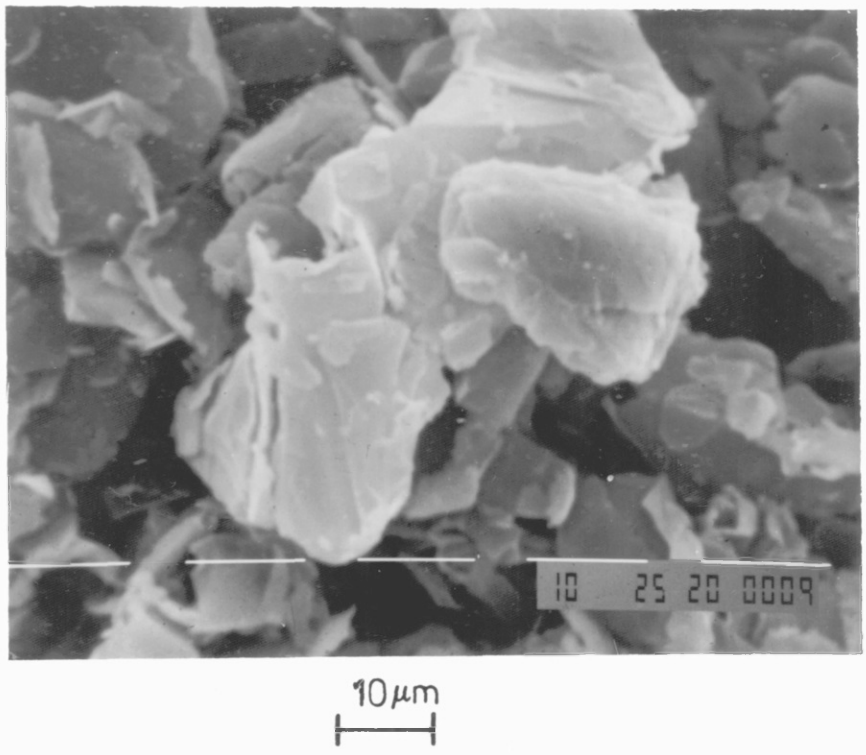


Fig. 4.31 "Micro 10" Graphite (James Durrans & Sons Ltd.) nominal 10μm.



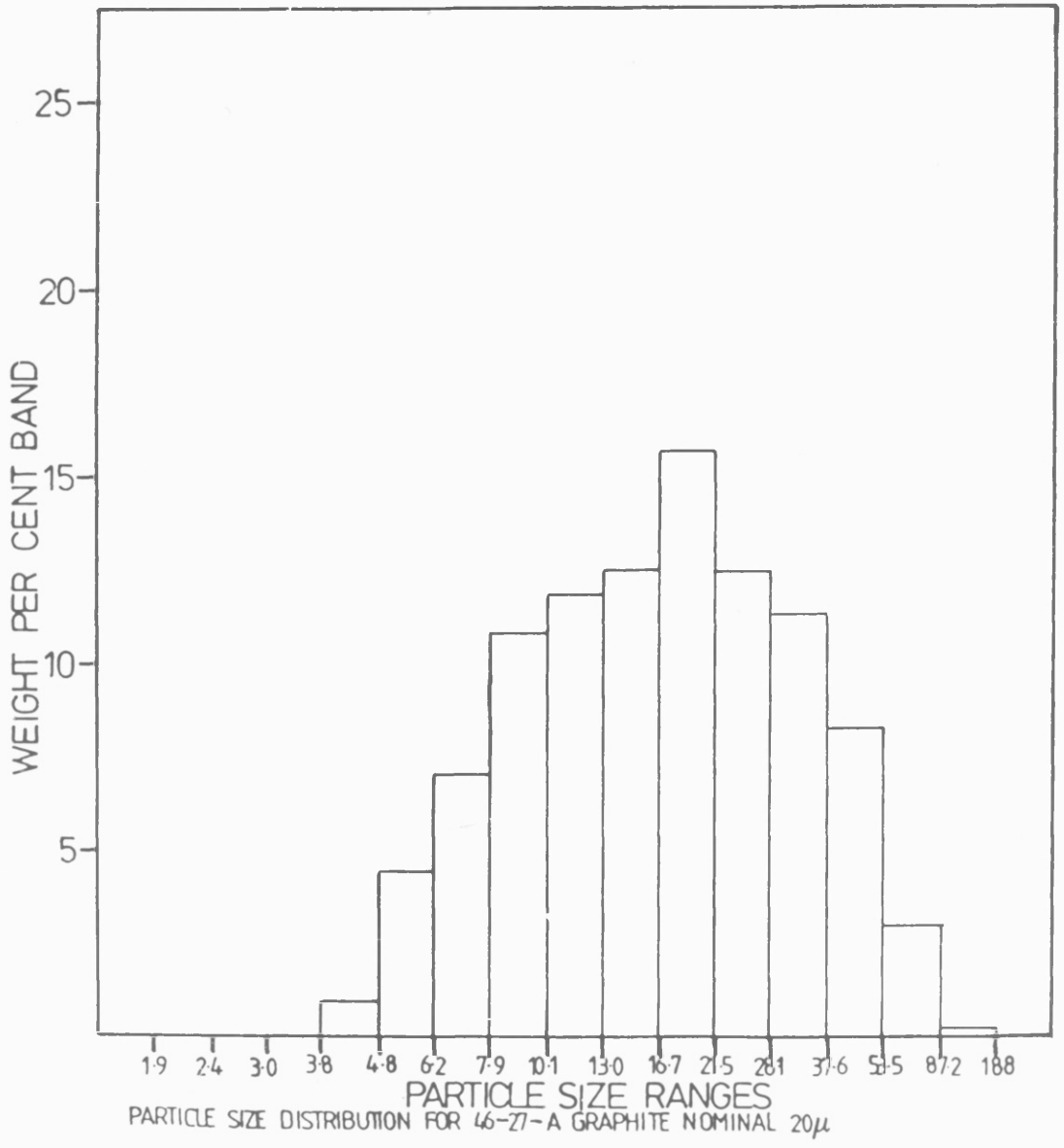
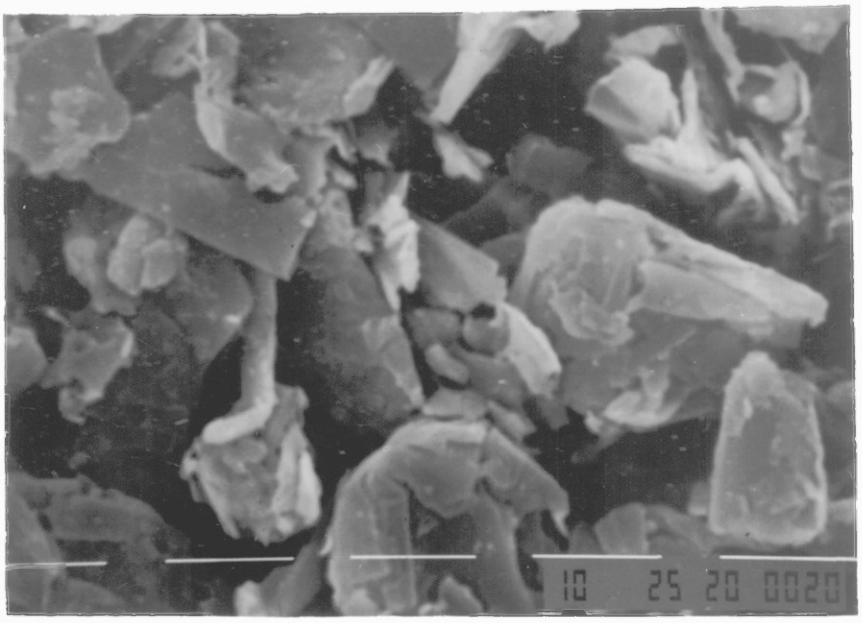


Fig. 4.32 46-27-A graphite (nominal 20μm, P.S. Wilson & Co.).



10μm

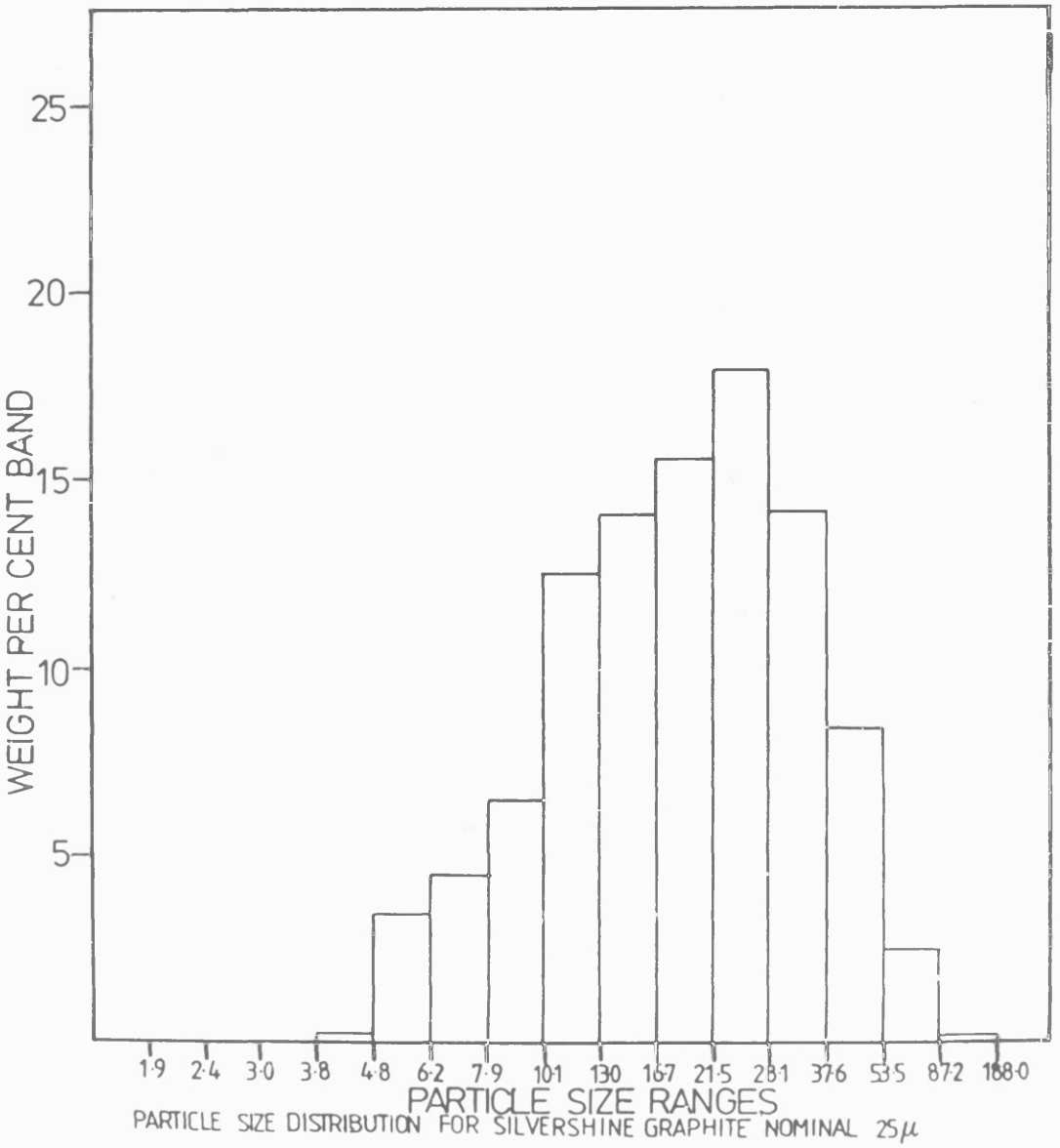
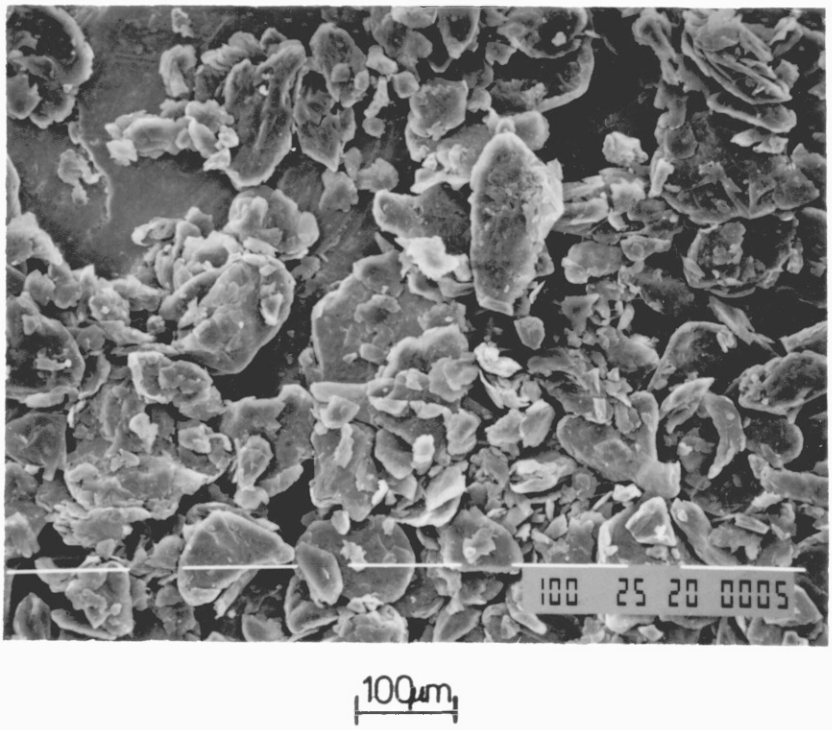


Fig. 4.33 Silvershine graphite (nominal 25μm Skaland Grafitverk Norway).



100μm

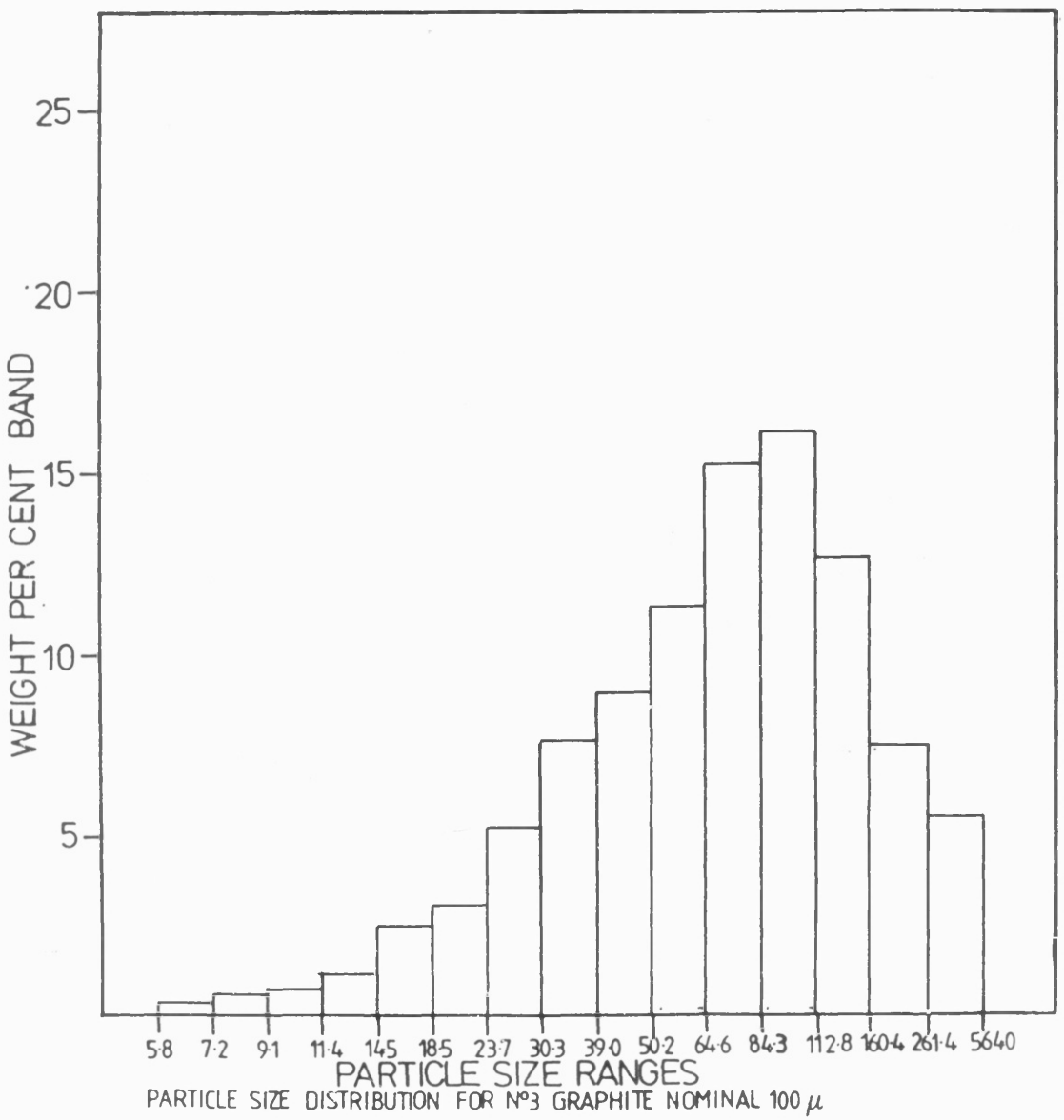


Fig. 4.34 No. 3 graphite (nominal 100μm P.S. Wilson & Co.).

Batch Number	Graphite Particle size (nominal)/μm	Carbon Yield/%	Linear Shrinkage/%	Volume Shrinkage/%	Bulk Density/ gcm^{-3}	Calculated Porosity/%	Hardness/VPN
24	6	62.37	16.55	42.07	1.59	10.83	161
18	10	62.88	16.61	41.93	1.58	11.39	161
25	20	60.41	17.08	43.45	1.59	10.84	158
26	25	62.41	16.82	42.61	1.58	11.53	157
27	100	60.99	16.64	44.19	1.58	11.53	151

Table 4.10 Effect of graphite particle size on the properties of amorphous carbon/graphite composites.

Note: All specimens cured for 24 hours at 80°C with 3% (by weight) catalyst added. Graphite loading in green composite constant at 12.5% (by weight).

Batch Number	Nominal Graphite Particle Size/μm	Modulus of Rupture Strength/ MNm^{-2}	Std. Dev. of MOR/MNm^{-2}	90% conf. int. of MOR/MNm^{-2}	K_{IC} /$MNm^{-3/2}$	Std. Dev. of K_{IC}/$MNm^{-3/2}$	90% Cont. Int. of K_{IC}/$MNm^{-3/2}$
24	6	32.81	7.79	± 2.40	0.457	0.050	± 0.018
18	10	31.48	6.63	± 2.22	0.553	0.054	± 0.017
25	20	23.50	6.15	± 2.10	0.759	0.041	± 0.014
26	25	17.34	4.76	± 1.56	0.702	0.044	± 0.015
27	100	15.51	4.82	± 1.69	0.295	0.046	± 0.015

Table 4.11 Effect of graphite particle size on the mechanical properties of vitreous carbon/graphite composites.

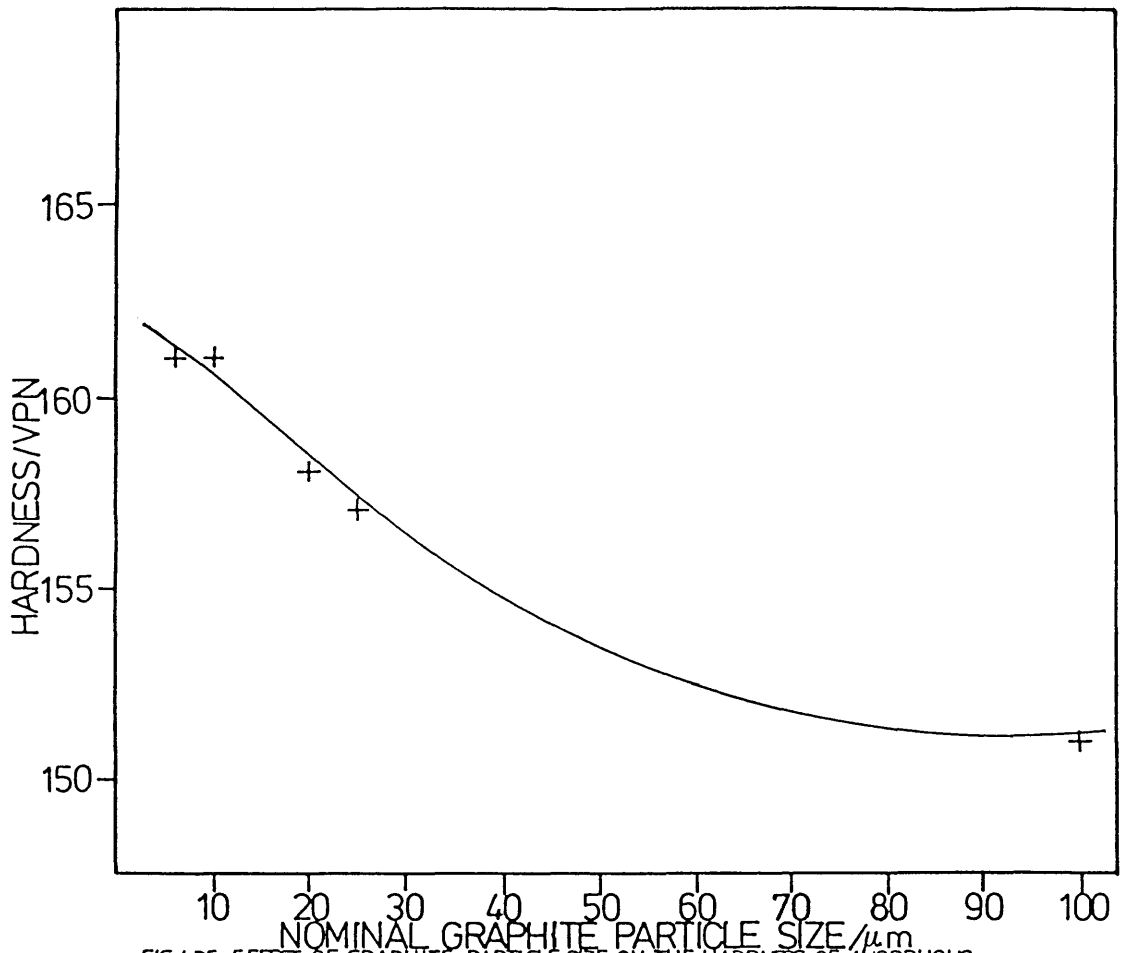


FIG 4·35 EFFECT OF GRAPHITE PARTICLE SIZE ON THE HARDNESS OF AMORPHOUS CARBON/GRAPHITE COMPOSITES

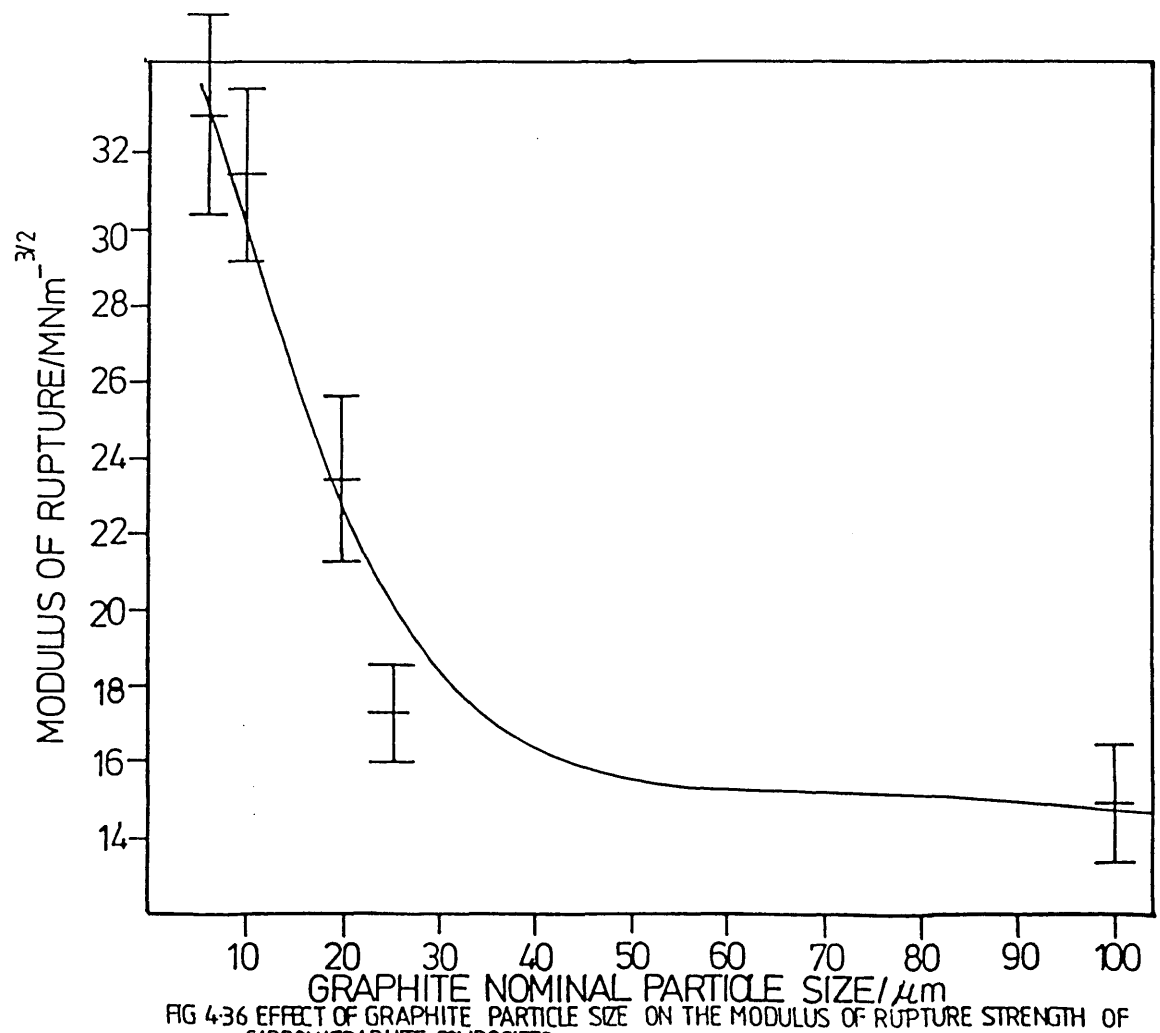


FIG 4·36 EFFECT OF GRAPHITE PARTICLE SIZE ON THE MODULUS OF RUPTURE STRENGTH OF CARBON/GRAPHITE COMPOSITES

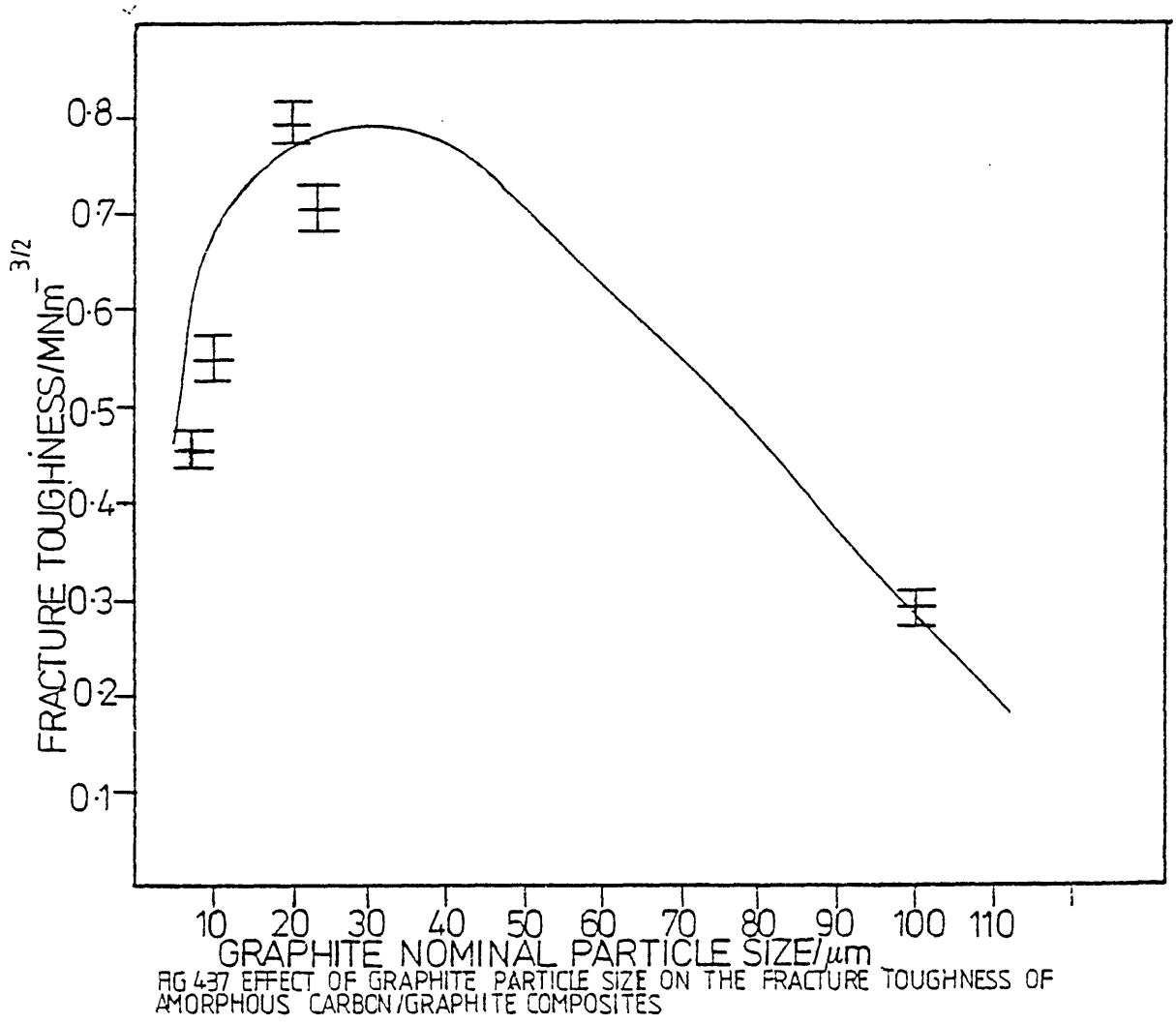
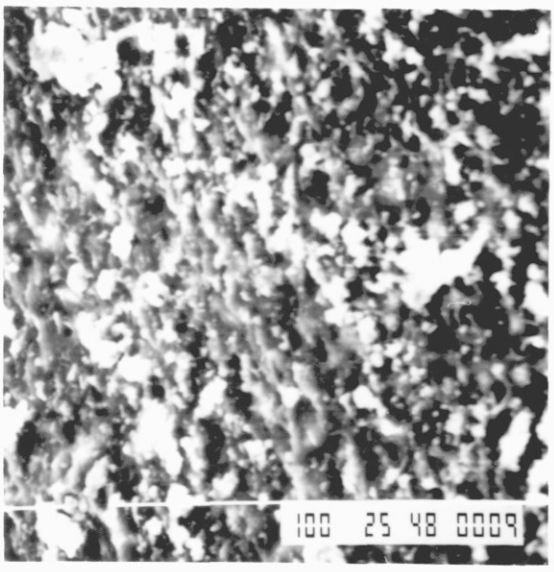
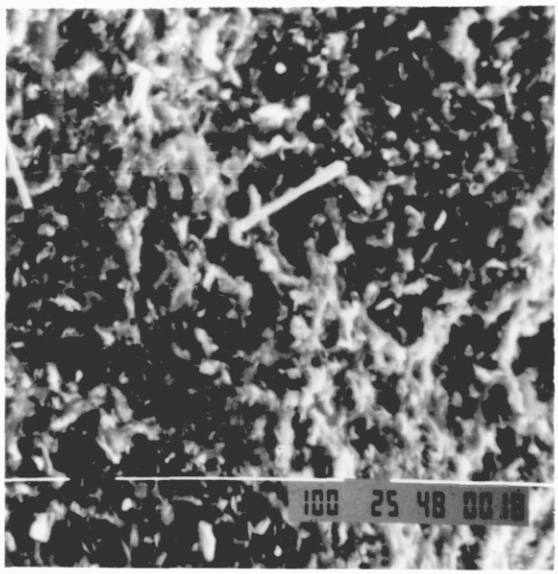


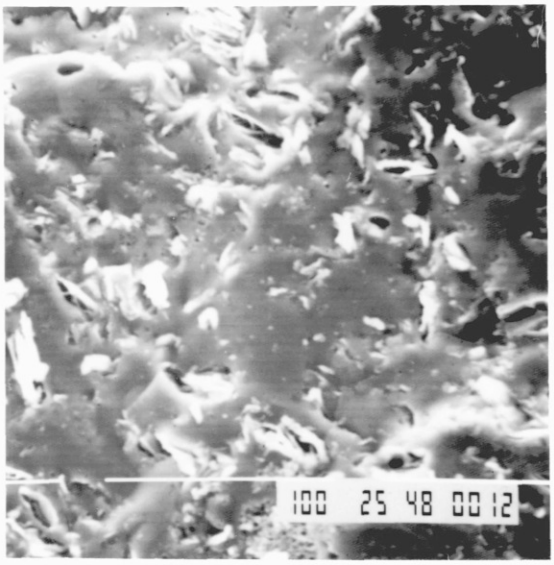
FIG 4.37 EFFECT OF GRAPHITE PARTICLE SIZE ON THE FRACTURE TOUGHNESS OF AMORPHOUS CARBON/GRAPHITE COMPOSITES



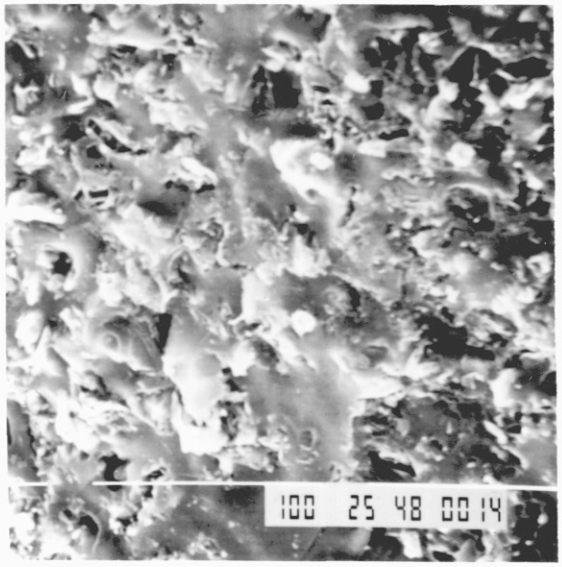
a.



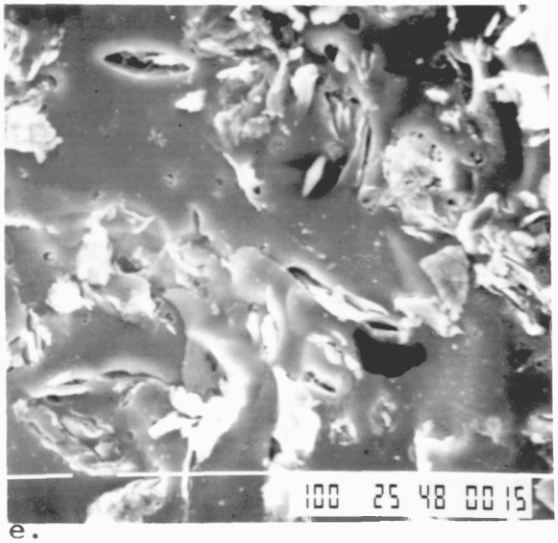
b.



c.



d.



e.

Key

a. 6 μm
b. 10 μm
c. 20 μm
d. 25 μm
e. 100 μm

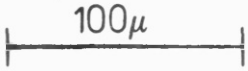


Fig. 4.38 Effect of changing the particle size of graphite on the microstructure of carbon/graphite composites containing 12.5% graphite.

4.9 Use of zinc oxide as a pore former in vitreous carbon

It was found that the softer grades of sub mm. pencil required leads with large amounts of porosity to enable them to deposit larger quantities of graphite during writing. This was attempted by the introduction of a pore forming material. The compound chosen for this task was zinc oxide which is reduced by the carbon to zinc and carbon monoxide at temperatures above 950°C.

$$ZnO_{(s)} + C_{(s)} \xrightarrow{>950^{\circ}} Zn_{(g)} \uparrow + CO_{(g)} \qquad (4.5)$$

Since the boiling point of zinc is 910°C (127) the reaction products volatilize at the amorphous carbon production temperature (1000°C) producing the required porosity. The micrograph and particle size distribution of zinc oxide (fig. 4.39) showed the material to be sub-micron. This small particle size made zinc oxide appear an ideal choice for dispersion in the resin as the extra porosity produced would tend to be very small and less detrimental to mechanical properties.

In fig. 4.39, the majority of the zinc oxide particles fall in the range 0 to 1.2 μm. If the particles are assumed to be spherical with a diameter of 0.6 μm (and knowing the density of zinc oxide to be 5.61 gcm^{-3}) then:-

vol. of ZnO particle = $4/3 \pi r^2 \cong 0.113\ \mu m^3$ (where r = radius of particle).

mass of ZnO particle = 0.634×10^{-12} g

This will react with

$$0.634 \times 10^{-12} \left(\frac{\text{Molecular weight of carbon}}{\text{Molecular weight of ZnO}} \right) = 9.35 \times 10^{-14} \text{ g of}$$

vitreous carbon according to eqn. (4.5). Assuming density of vitreous carbon = 1.52 gcm-3 (from batch 3), ZnO particle

will react with $6.15 \times 10^{-2}\ \mu m^3$ of vitreous carbon.

Volume of pores produced = $V_{ZnO} + V_{vc} = 0.175\ \mu m^3$ (where V_{ZnO} = volume of zinc oxide particle, Vvc = volume of carbon with which it reacts). Therefore, if the pores produced are assumed spherical, the diameter of pores produced using the ZnO pore former will be $0.7\ \mu m$. The carbon yield and bulk density of the amorphous carbon were observed to fall steadily with increasing additions of ZnO to the resin. For example, with no pore former added the carbon yield was 56.48% yielding a material with a bulk density of $1.52\ gcm^{-3}$. When 4 wt % ZnO was added the carbon yield fell to 52.76% and the bulk density to $1.45\ gcm^{-3}$. The theoretical carbon yield was calculated as follows and found to be in reasonable agreement with that observed experimentally with increasing pore former additions (Fig. 4.41).

Let amount of ZnO added = χ (wt %).

amount of carbon reacting =

$$\left(\frac{\text{Molecular wt of amorphous carbon}}{\text{Molecular wt of ZnO}}\right)\chi = \quad y\ (\text{wt \%})$$

Theoretical carbon yield =

(100 - (χ + y)) x fractional carbon yield when no pore former was added (= 0.565, from batch 3) (4.6)

The depreciation of mechanical properties observed as the pore former was added was much more drastic than expected. There are two observations which would appear to account for this. Firstly, the porosity produced was not sub-micron as predicted from the particle size of zinc oxide but was of the same order of magnitude as that produced by the evolution of water vapour (Fig. 4.46). Secondly, some of the pores produced were not spherical but of a more irregular

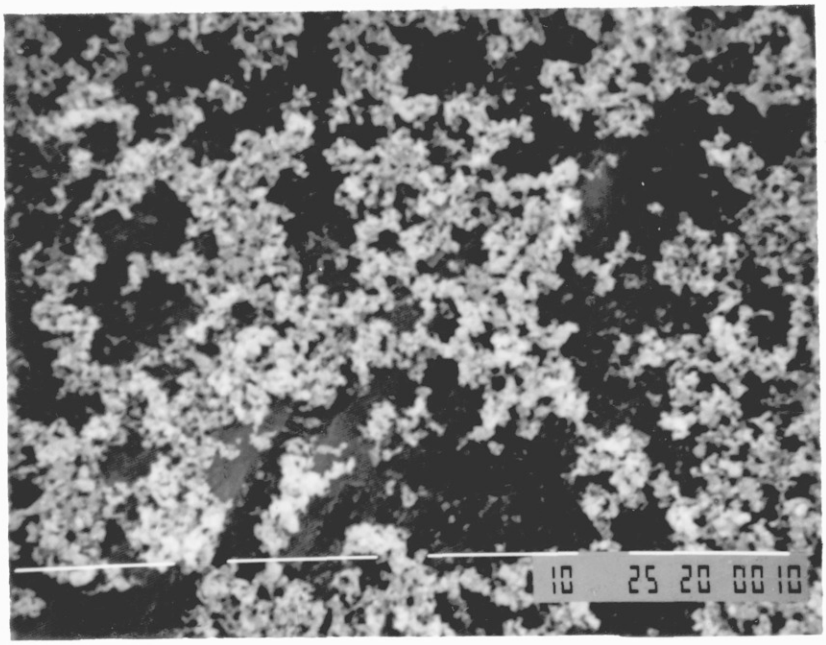
Batch Number	Amount of Zinc Oxide added Wt/%	Theoretical carbon yield/%	Observed Carbon Yield/%	Linear Shrinkage/%	Volume Shrinkage/%	Bulk Density/ gcm^{-3}	Calculated Porosity/%	Hardness/ VPN
3	0	56.48	56.48	19.74	48.32	1.52	6.85	264
28	1	55.85	56.13	19.05	49.49	1.52	6.85	258
29	2	55.20	55.39	19.95	52.41	1.49	9.31	240
30	3	54.55	54.14	19.02	48.63	1.48	9.75	237
31	4	53.91	52.76	19.39	49.21	1.45	11.32	211
32	6	52.61	52.41	19.67	51.10	1.41	14.27	174

Table 4.12 Effect of ZnO pore former additions on the properties of amorphous carbon.

Note: All samples cured for 24 hours at 80°C with catalyst concentration constant at 3% (by weight).

Batch Number	Amount of Zinc Oxide added/%	Modulus of Rupture Strength/MNm^{-2}	Std. Dev. of MOR/$MNm^{-3/2}$	90% Conf. Int. of MOR/$MNm^{-3/2}$	K_{1C} /$MNm^{-3/2}$	Std. Dev./ $MNm^{-3/2}$	90% Conf. Int. of K_{1C}/$MNm^{-3/2}$
3	0	14.42	3.56	± 1.21	0.293	0.029	± 0.009
28	1	14.12	4.02	± 1.32	0.289	0.037	± 0.013
29	2	13.29	4.71	± 1.61	0.281	0.041	± 0.014
30	3	11.02	3.58	± 1.10	0.264	0.046	± 0.015
31	4	8.27	3.08	± 0.99	0.213	0.038	± 0.012
32	6	5.87	2.41	± 0.82	0.131	0.028	± 0.010

Table 4.13 Effect of adding ZnO as a pore former on the mechanical properties of the pyrolysed polyfurfuryl alcohol resin.



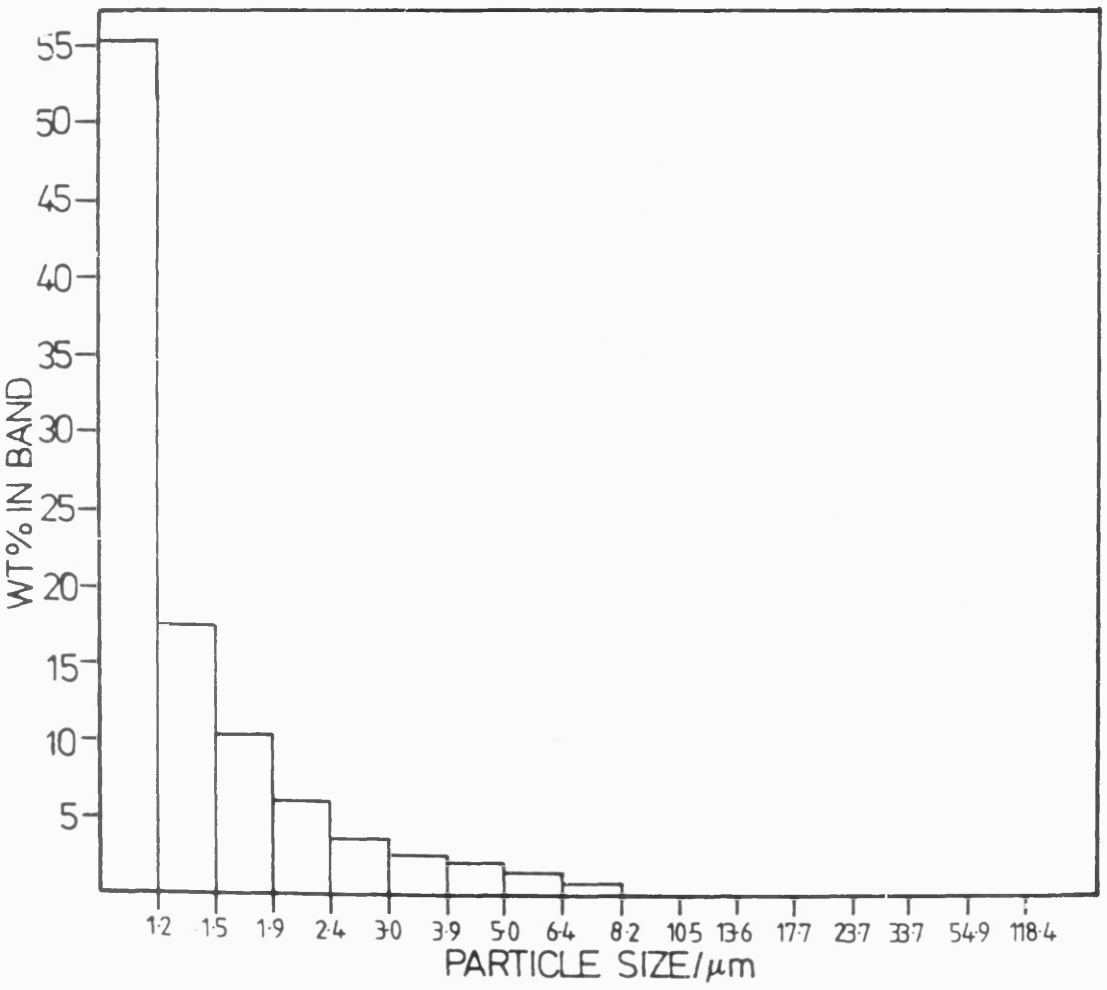


Fig. 4.39 Particle size distribution of ZnO powder ultrasonically dispersed in distilled water

shape which would result is an increased stress concentration. Although the particle size of the ZnO powder was sub-micron, a certain amount of agglomeration occurs in the powder. This is illustrated in Fig. 4.40 which shows a particle size distribution plot of zinc oxide dispersed by hand stirring with a spatula in distilled water rather than ultrasonically as in Fig. 4.39. In the manually dispersed sample agglomeration increased the average aggregate size to around 4.5 μm. If the same analysis as before is applied to these larger ZnO aggregates the predicted size of pores is 10 μm which is of the correct order of magnitude as those observed. Agglomeration of the ZnO particles must have occured in the carbon because the pore former was dispersed in this way by hand - in fact dispersion in the resin would probably be more difficult than in water because of the higher viscosity. The irregular shapes of some of the pores presumably arose because the agglomerations of ZnO particles were also irregularly shaped. During the manufacture of sub mm. pencil leads, acetone is used as a resin thinner to aid mixing so the agglomeration problem could be avoided by ultrasonically dispersing the pore former in the thinner before the mixing process.

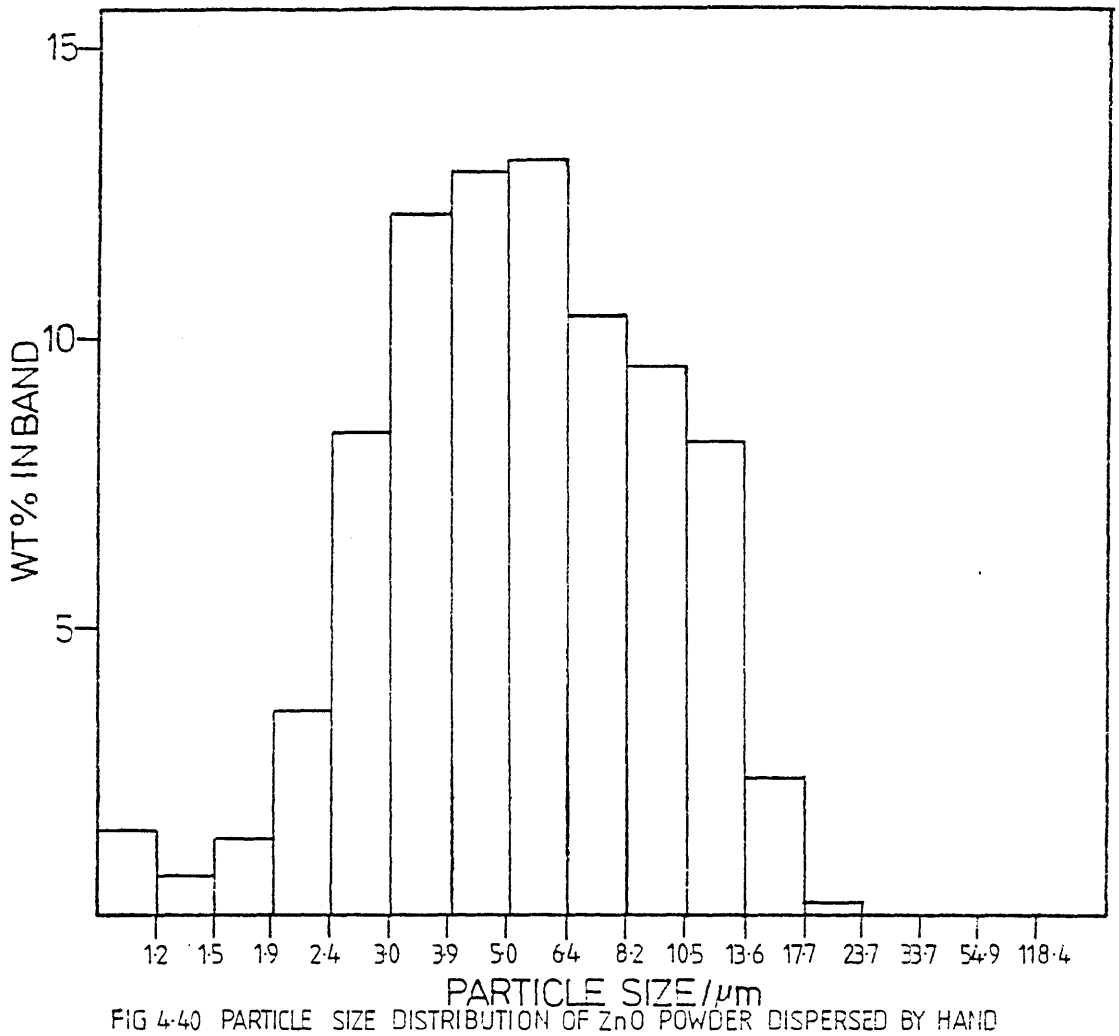


FIG 4·40 PARTICLE SIZE DISTRIBUTION OF ZnO POWDER DISPERSED BY HAND STIRRING IN DISTILLED WATER

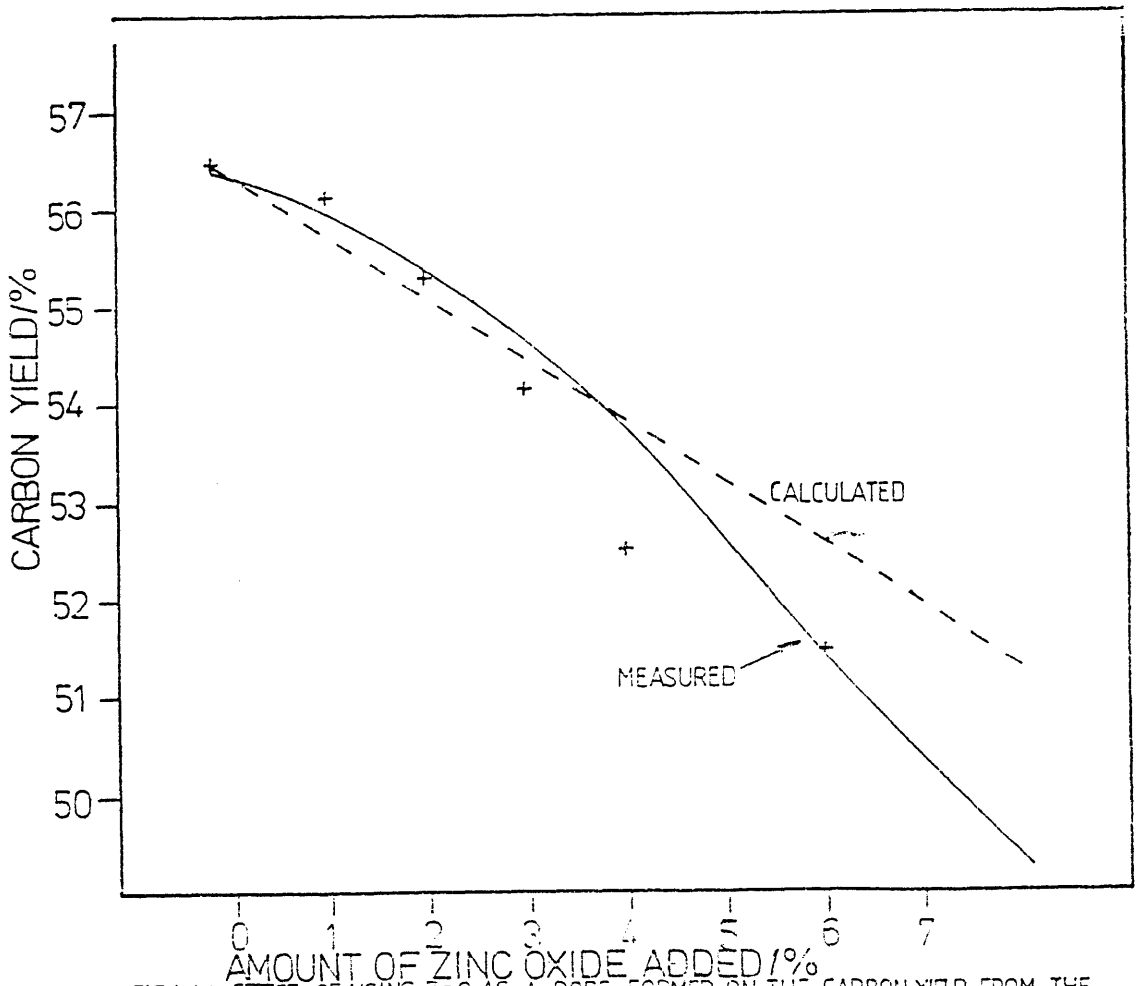


FIG 4·41 EFFECT OF USING ZnO AS A PORE FORMER ON THE CARBON YIELD FROM THE PYROLYSIS OF POLYFUFURYL ALCOHOL

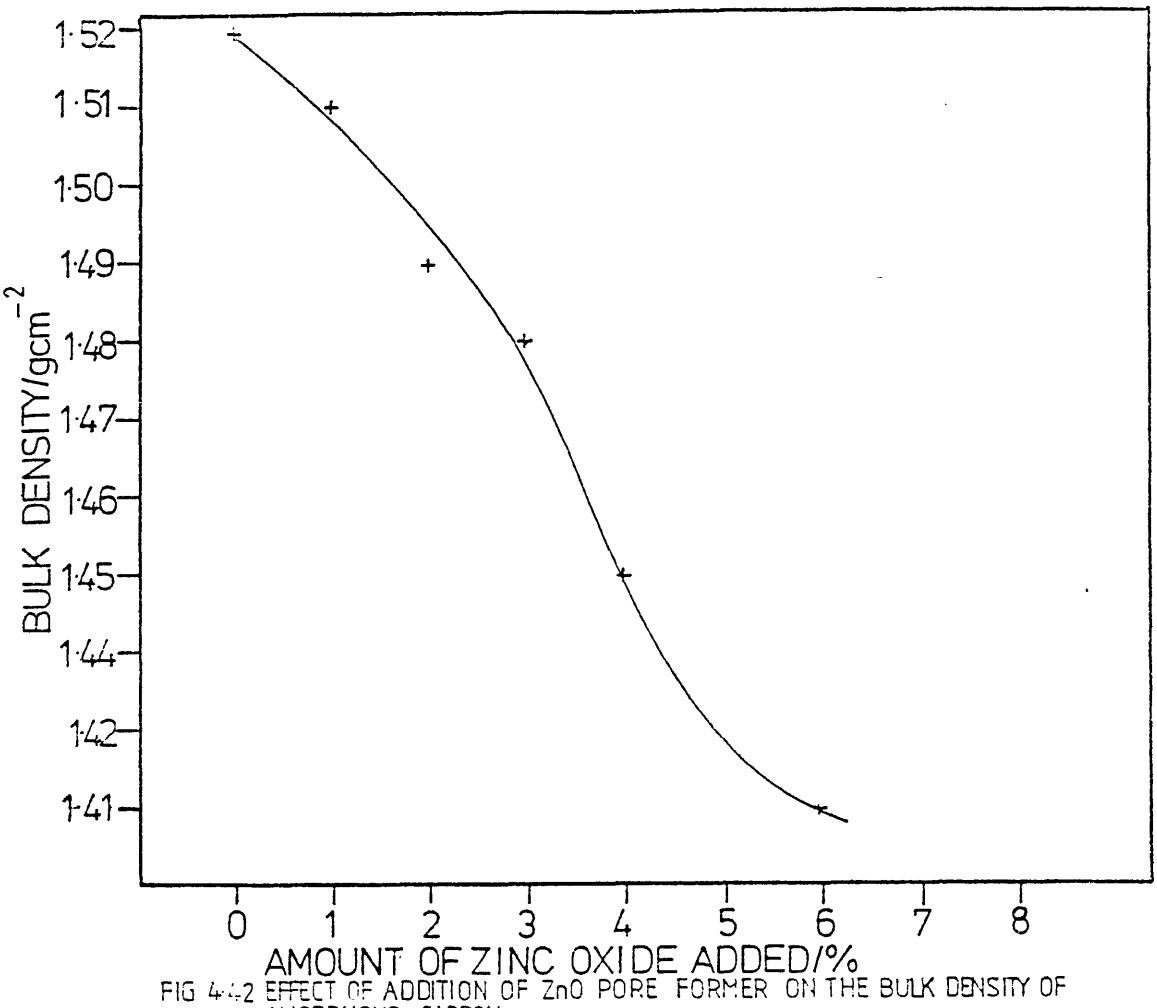


FIG 4.42 EFFECT OF ADDITION OF ZnO PORE FORMER ON THE BULK DENSITY OF AMORPHOUS CARBON

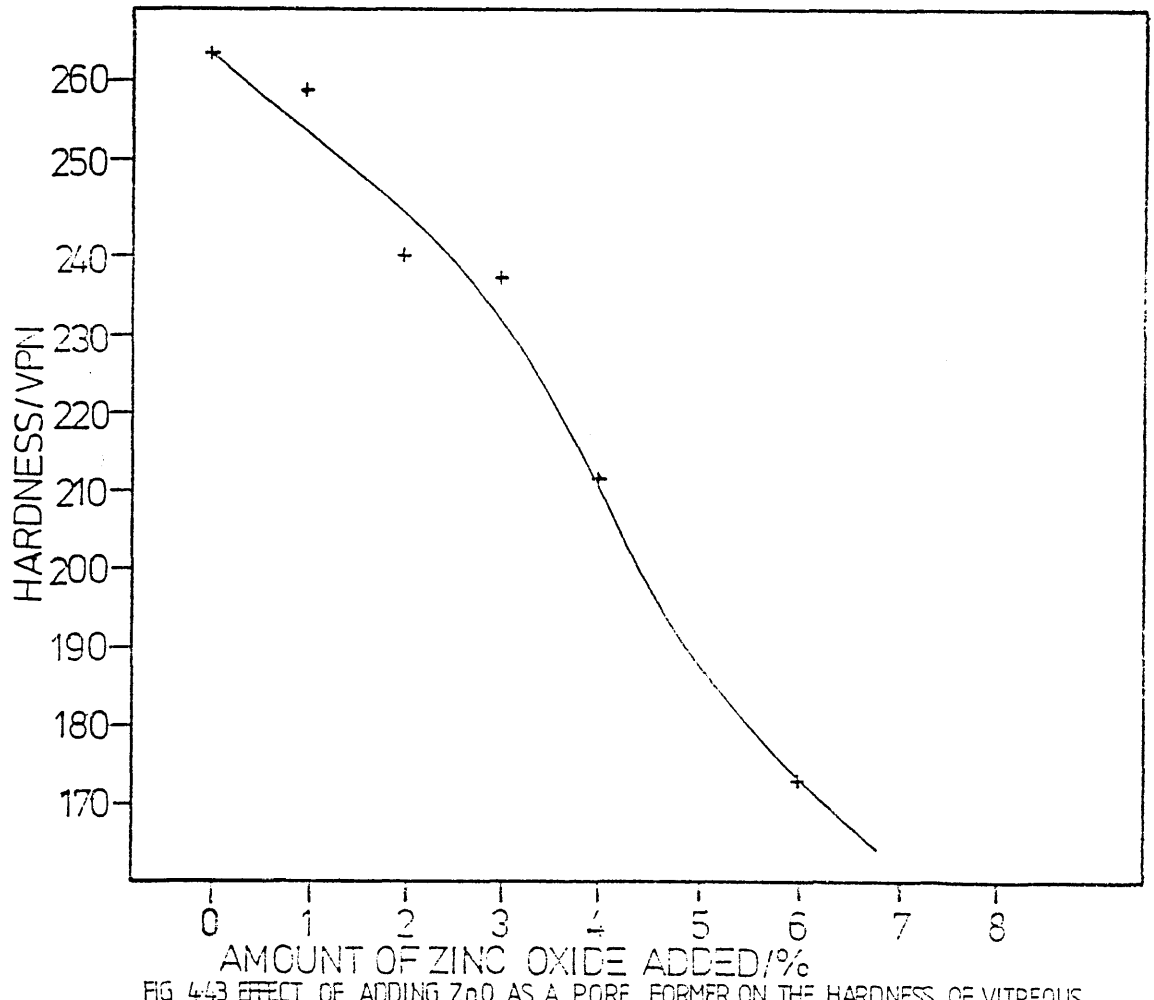


FIG 4.43 EFFECT OF ADDING ZnO AS A PORE FORMER ON THE HARDNESS OF VITREOUS CARBON

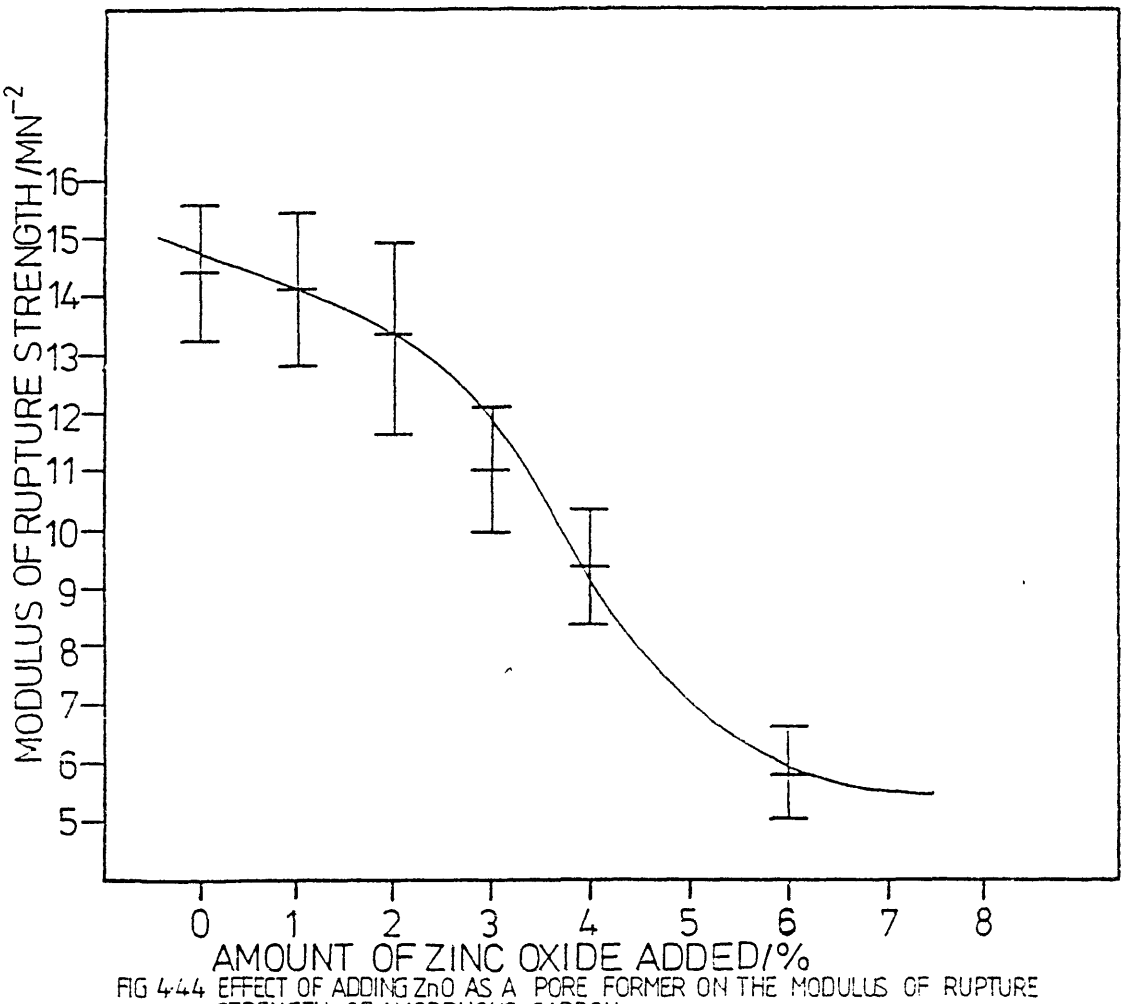


FIG 4·44 EFFECT OF ADDING ZnO AS A PORE FORMER ON THE MODULUS OF RUPTURE STRENGTH OF AMORPHOUS CARBON

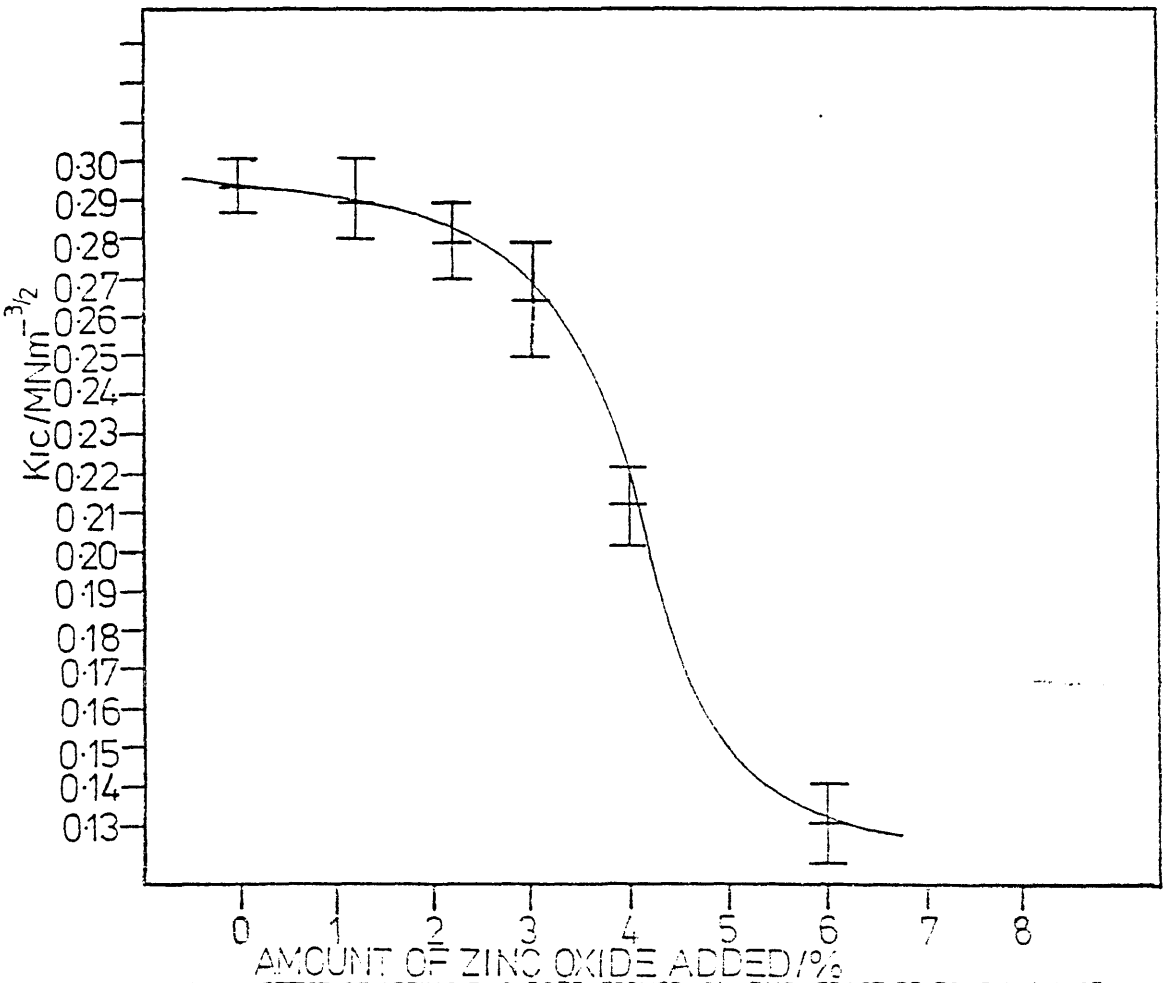
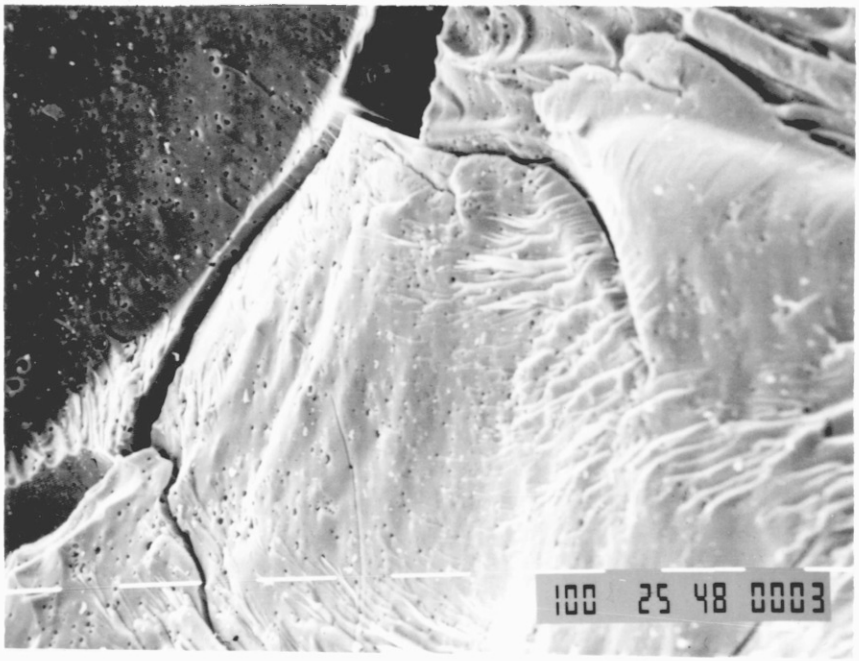
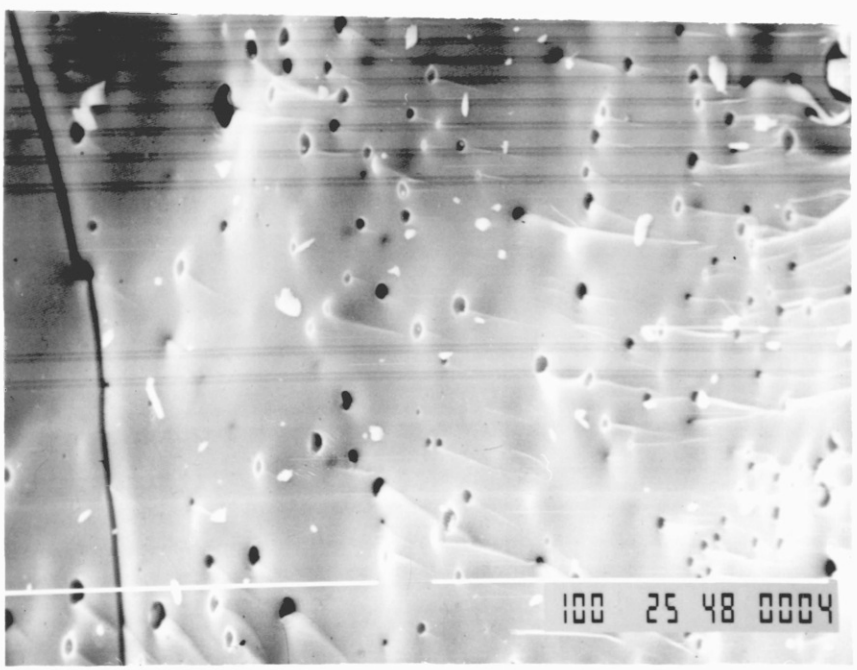


FIG 4·45 EFFECT OF ADDING ZnO PORE FORMER ON THE FRACTURE TOUGHNESS OF AMORPHOUS CARBON



a. 100μ



b. 100μ

Fig. 4.46 Effect of introduction of ZnO pore former on the Microstructure of amorphous carbon.

SECTION 5

OBJECTIVE, CONCLUSION AND SUGGESTIONS FOR FURTHER WORK

5.1.a Objective

The objective of the research programme was to obtain basic information on the properties of amorphous carbon/graphite composites which would be of value for the production of sub mm pencil leads based on furfuryl alcohol/graphite mixtures.

5.1.b Conclusions

(i) The strength and fracture toughness of the amorphous carbons were observed to increase with curing time of the resin up to a maximum at about 48 hours. Samples cured for longer periods were liable to fracture during firing, possibly due to thermal stress in resin with too high a degree of chemical cross-linking.

(ii) A uniformly distributed micron-scale porosity, spherical in shape, was produced by the evolution of water vapour during curing and the initial stages of firing.

(iii) Water in the resin was produced during the condensation polymerisation reaction and was also introduced by the aqueous acid catalyst. Curing at higher temperatures was seen to increase the rate of polymerisation but resulted in a coarsening of the porosity.

(iv) When the resin was cured at temperatures above 80°C, large pores grew at the expense of smaller ones resulting in an increase in the flaw size within the material and a consequent lowering of strength and fracture toughness. An optimum curing temperature of 80°C

for 24-48 hours was observed. This allowed for a reasonably fast cure with little pore ripening.

(v) The rate of polymerisation could be enhanced by increasing the catalyst concentration. This however introduced more water into the resin which, when driven off in curing, resulted in increased porosity and affected adversely the mechanical properties of the carbon.

(vi) By optimising the curing stage of fabrication, the strongest vitreous carbon was obtained by curing for a period of 48 hours at a temperature of 80°C using a catalyst concentration of 1% by weight.

(vii) Graphite and amorphous carbon can be formed into a composite material with mechanical properties superior to the resin alone. The graphite particles were seen to initiate a crack deflection and crack-tip blunting mechanism within the glass-like carbon.

(viii) The strength and fracture toughness of the composite were found to increase rapidly with volume fraction of added graphite. Samples containing up to 15 wt % graphite in the green form were prepared.

(ix) The properties of the composite could not be estimated using the law of mixtures because a simple relationship between each end member did not hold. This was because shrinkage of the glass-like carbon during heat treatment was restrained by the graphite particles.

(x) The highest composite strength (at a constant graphite loading) was obtained using the smallest graphite size, i.e.

6μm. This was because (a) voids can form round larger particles creating flaws, and (b) increased internal stress is created in the material by resistance to the thermal shrinkage of the vitreous carbon.

(xi) The fracture toughness of the composites exhibited a maximum with a graphite particle size of 20μm. this appeared to be the particle size which resulted in the maximum crack deflection. Above this size it was easier for cracks to pass through, rather than round, graphite flakes.

(xii) Zinc oxide can be introduced as a pore-forming material by virtue of being reduced to zinc vapour at high temperatures (i.e. above 950°C). The reaction products are volatilised at the production temperature (1000°C). Although the particle size of zinc oxide was seen to be sub-micron, the pores produced were much larger (i.e. in the range 1-10μm) due to an agglomeration of particles in the resin.

(xiii) Large pores with non-spherical symmetry gave a material with much reduced mechanical properties. For example, the addition of 6 wt % of ZnO to the resin reduced the strength by a factor of 2.

5.2 Suggestions for further work

High speed extrusion of batch materials for pencil lead production will affect markedly the mechanical properties of the fired leads. A logical extension of the present work would therefore include the following.

(i) An evaluation of the role of preferred orientation on the strength of carbon/graphite composites by

observing the relationship between extrusion speeds and modulus of rupture.

(ii) Examination of the microstructure with respect to MOR and extrusion speed.

(iii) The introduction of new fabrication techniques for composite production with the use of resin thinners to give a good homogeneous mix and allow an increase in graphite loadings of up to 50%.

(iv) Increase of the graphite particle size range to include powders with particle sizes $<6\mu m$ and also between 30 and 90 μm.

(v) Evaluation of methods to ensure a good dispersion of ZnO if this is used as a pore-former; for example, by ultra-sonic dispersion in the resin thinner prior to batch mixing.

APPENDIX

A. Statistical Analysis carried out on Mechanical Testing Results

The subject of statistics is generally concerned with inferring information about a parent (or theoretical) population using observations from a relatively small amount of data. Such a collection of data is called a sample. Suppose, in collecting the data, the statistical experiment is performed a total of n times. If the manner in which the experiment is performed each time is in no way influenced by previous results, the data is referred to as a random sample of size n. The definition implies that any sample of size n taken from a particular population has the same distribution as the population and that each value in the sample is independent of the others. The properties of the sample can therefore be used to estimate the properties of the parent population. The mean value ($\bar{X}$) of a random sample of n observations of a variable X can be found as follows:

$$\bar{x} = \frac{1}{n}(x_1 + x_2 + \ldots\ldots\ldots x_n)$$

$$\text{ie:} \quad x = \frac{1}{n}\sum_{i=1}^{n} x_i \qquad (A.1)$$

The spread of the observations about the mean is estimated using the standard deviation S_x .

$$S_x = \left(\frac{1}{n} \sum_{i=1}^{n} (x_i - \bar{x})^2 \right)^{1/2} \qquad (A.2)$$

One of the most important things to remember in statistical work is that estimates made from data are bound to be imprecise. It is part of the analyst's task to indicate the level of imprecision associated with an estimate. The generally accepted procedure for doing this is to state upper and lower limits within which the true value of the parameter is likely to lie. These limits are called confidence limits and the interval between them a confidence interval. It is assumed that the distribution of the mean values of random samples of size n from an arbitary population approaches a normal distribution of mean $\approx \bar{X}$ and standard deviation $\approx S_x$.

The confidence interval (t) is given by;

$$t = \bar{x} \pm \frac{\alpha S_x}{\sqrt{n}} \qquad (A.3)$$

---

where α is a constant depending on the number of degrees of freedom ν (= n - 1) in the sample and the % of confidence

required. The constant can be found from the "Cambridge Statistical Tables" (130). In the computer programme used to calculate the properties of the carbon in this work (cf. Section B) α was estimated graphically since it is known to be linear in $120/\nu$, providing the sample size is large enough. This is illustrated in Fig. A.1.

slope of the graph = 0.015

y axis intercept = 1.635

$y = mx + c$

$$\alpha = 0.015 \ \frac{120}{\nu} + 1.635 \qquad (A.4)$$

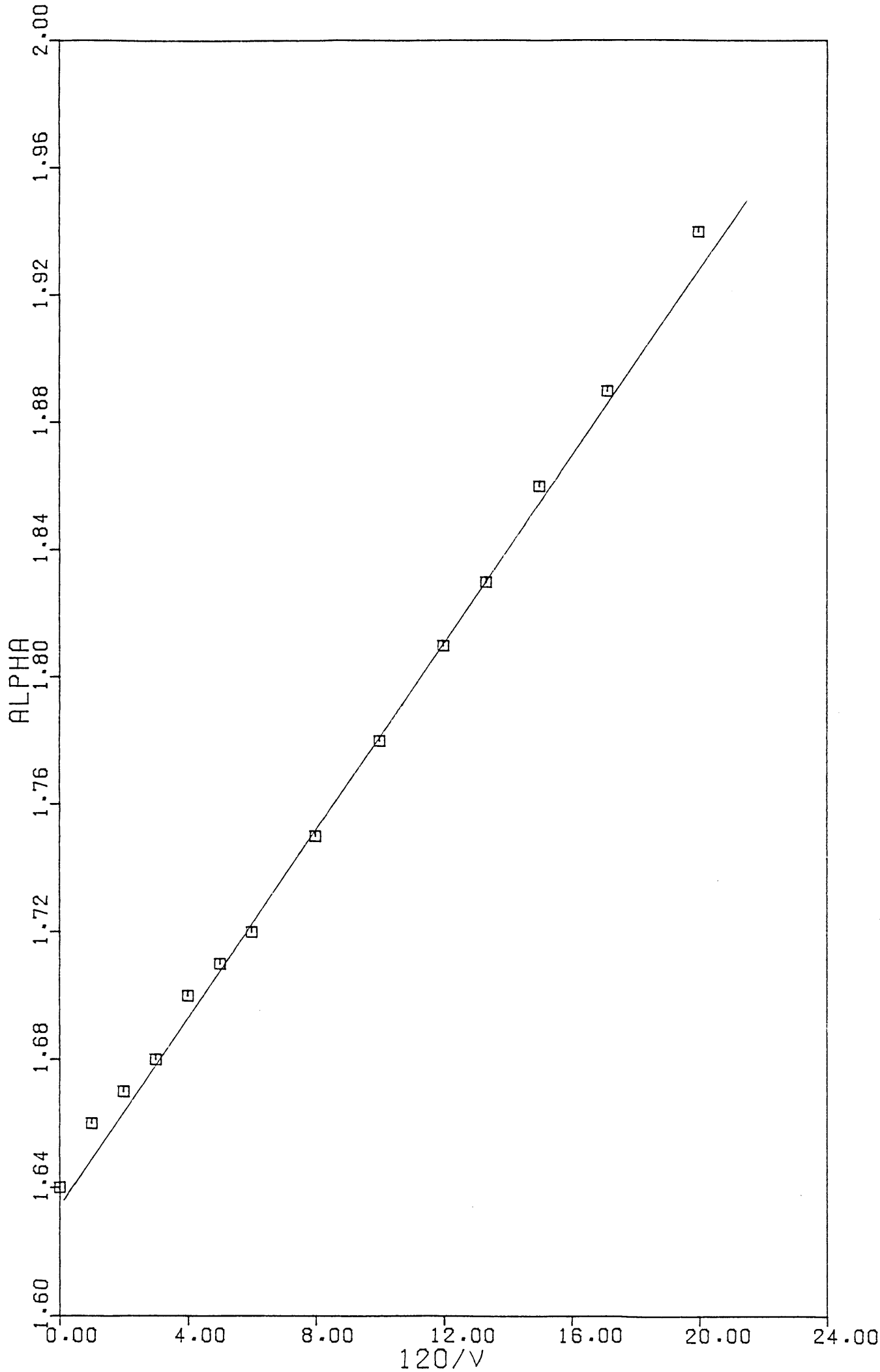


Fig. A.1. Calculation of t-test constant.

B. COMPUTER PROGRAM USED TO CALCULATE THE PROPERTIES OF AMORPHOUS CARBON

```
C              ********************************
C              *PROGRAM LOUISE BY GARY SAVAGE*
C              ********************************
C
C  A PROGRAM TO PROCESS RESULTS FROM RESEARCH WORK INTO THE
C  PRODUCTION AND PROPERTIES OF AMORPHOUS CARBON MADE BY
C  PYROLYSIS OF POLYFURFURYL ALCOHOL RESIN
C
C  THE CARBON YIELD,LINEAR AND VOLUME SHRINKAGE DURING
C  PYROLYSIS ALONG WITH THE BULK DENSITY,POROSITY AND THE
C  MODULUS OF RUPTURE AND FRACTURE TOUGHNESS STRENGTHS OF
C  THE RESULTING CARBON ARE MEASURED
C
C  THE RESULTS ARE PRESENTED ALONG WITH THE CURING CONDITIONS
C  OF THE POLYMER PRECURSOR
C
C  ************************************************
C  *                  VARIABLES USED                *
C  *                                                *
C  *SIMPLE VARIABLES                                *
C  *MINDY=NUMBER OF BATCHES TO BE PROCESSED         *
C  *IBN=BATCH NUMBER                                *
C  *ITEMP=RESIN CURING TEMP                         *
C  *LCURE=CURING TIME                               *
C  *ICAT=AMOUNT OF CATALYST                         *
C  *IPF=AMOUNT OF PORE FORMER                       *
C  *AG=AMOUNT OF GRAPHITE                           *
C  *PG=PERCENTPGE GRAPHITE IN GREEN COMPOSITE       *
C  *IPSG=PARTICLE SIZE OF GRAPHITE                  *
C  *N=NUMBER OF SAMPLES IN THE BATCH                *
C  *M=NUMBER OF MODULUS OF RUPTURE TESTS CARRIED    *
C  *  OUT                                           *
C  *L=NUMBER OF FRACTURE TOUGHNESS TESTS CARRIED    *
C  *  OUT                                           *
C  *                                                *
C  *DIMENSIONED VARIABLES                           *
C  *XL=LENGTH OF POLYMER SAMPLE                     *
C  *WA=WEIGHT OF POLYMER SAMPLE IN AIR              *
C  *WW=WEIGHT OF POLYMER SAMPLE IN WATER            *
C  *XC=WEIGHT OF SUPPORT CRADLE FOR POLYMER SAMPLES*
C  *VCXL=LENGTH OF CARBON SAMPLE                    *
C  *VCWA=WEIGHT OF CARBON SAMPLE IN AIR             *
C  *VCWW=WEIGHT OF CARBON SAMPLE IN WATER           *
C  *VCXC=WEIGHT OF SUPPORT CRADLE FOR CARBON        *
C  *     SAMPLES                                    *
C  *G(3,J)=INPUT DATA FOR MOR TESTS                 *
C  *       G(1,J)=FRACTURE LOAD(P)                  *
C  *       G(2,J)=BREADTH OF SPECIMEN(B)            *
C  *       G(3,J)=DEPTH OF SPECIMEN(D)              *
C  *Z(4,J)=INPUT DATA FOR K1C TESTS                 *
C  *       Z(1,J)=FRACTURE LOAD(P)                  *
C  *       Z(2,J)=CRACK LENGTH(A)                   *
C  *       Z(3,J)=BREADTH OF SPECIMEN(B)            *
C  *       Z(4,J)=DEPTH OF SPECIMEN(D)              *
C  ************************************************
```

```
C
      PROGRAM LOUISE(INPUT,OUTPUT,TAPE5=INPUT,TAPE6=OUTPUT)
      DIMENSION XL(30),WA(30),WW(30),XC(30)
      DIMENSION VCXL(30),VCWA(30),VCWW(30),VCXC(30)
      DIMENSION VVC(30),G(3,30),Z(4,30),SIG(30),XK1C(30)
      COMMON N,AG
C
C SET NUMBER OF BATCHES TO BE PROCESSED
      WRITE(6,10)
   10 FORMAT(1X,'HELLO GARY,HOW MANY BATCHES HAVE YOU TO ANALYSE?')
      READ(5,20)MINDY
   20 FORMAT(I1)
C
C  INPUT FORMATS
      PRINT*,'WOULD YOU LIKE HELP TO FORMAT YOUR INPUT DATA?'
      READ(5,30)PARISSG
   30 FORMAT(A2)
      IF(PARISSG.EQ.2HNO) GO TO 40
      PRINT*,'THE NUMBER OF SPECIMENS AND TESTS ARE INPUT AS (I2)'
      PRINT*,'THE BATCH CURING CONDITIONS ARE READ IN ACCORDING TO;'
      PRINT*,'(I3,1X,I2,1X,I1,1X,I2,1X,F4.1,1X,I2)'
      PRINT*,'SPECIMEN LENGTHS AND WEIGHTS ARE INSERTED '
      PRINT*,'IN THE ORDER REQUESTED,IN FREE FORMAT'
      PRINT*,'MODULUS OF RUPTURE DATA IS GIVEN IN THE FOLLOWING FORMAT;'
      PRINT*,'(F5.2,1X,F7.5,1X,F7.5)'
      PRINT*,'FRACTURE TOUGHNESS DATA IS WRITTEN IN THE FORMAT;'
      PRINT*,'(F5.2,1X,F7.5,1X,F7.5,1X,F7.5)'
   40 CONTINUE
C
C  INITIATE REPETITION ACCORDING TO THE NUMBER OF BATCHES
      DO 1 I1=1,MINDY
      WRITE(6,12)
   12 FORMAT(//)
C
C  CHOOSE WHICH PARTS OF THE PROGRAM ARE TO BE USED
      PRINT*,'DO YOU WANT TO USE ALL OF THE PROGRAM ON THIS BATCH?'
      READ(5,50)ANS
   50 FORMAT(A1)
      IF(ANS.EQ.1HY) THEN
      ANS1=ANS
      ANS2=ANS
      ANS3=ANS
      ANS4=ANS
      GO TO 60
      ELSE
      PRINT*,'DO YOU WANT A PRINT OUT OF THE BATCH CURING CONDITIONS?'
      READ(5,50)ANS1
      PRINT*,'DO YOU WANT TO USE THE PHYSICAL PROPERTIES'
      PRINT*,'PART OF THE PROGRAM?'
      READ(5,50)ANS2
      PRINT*,'WOULD YOU LIKE TO CALCULATE THE'
      PRINT*,' MODULUS OF RUPTURE OF YOUR SPECIMENS?'
      READ(5,50)ANS3
      PRINT*,'DO YOU REQUIRE THE K1C EVALUATION?'
      READ(5,50)ANS4
```

```
      END IF
   60 CONTINUE
C
C  SET CURING CONDITIONS OF BATCH
      IF(ANS1.EQ.1HN)THEN
      WRITE(6,13)
   13 FORMAT('IS THERE ANY GRAPHITE IN THIS BATCH?')
      READ(6,50)CR
      IF(CR.EQ.1HN)THEN
      AG=0.0
      ELSE
      WRITE(6,14)
   14 FORMAT('HOW MUCH GRAPHITE IS THERE?...ANSWER IN PARTS PER HUNDRED'
     +)
      READ(5,16)AG
   16 FORMAT(F4.1)
      END IF
      GO TO 70
      ELSE
      GO TO 71
      END IF
   71 CONTINUE
      PRINT*,'WHICH BATCH IS THIS?'
      READ(5,80)IBN
   80 FORMAT(I2)
      WRITE(6,90)
      WRITE(6,100)
      WRITE(6,110)
      WRITE(6,120)
   90 FORMAT(1X,'LIST THE BATCH CURING CONDITIONS IN THE FOLLOWING ORDER
     +,')
  100 FORMAT(1X,'CURING TEMPERATURE,LENGTH OF CURE,AMMOUNT OF CATALYST')
  110 FORMAT(1X,'AMMOUNT OF PORE FORMER ADDED,AMMOUNT OF GRAPHITE')
  120 FORMAT(1X,'IN COMPOSITE,PARTICLE SIZE OF GRAPHITE')
      READ(5,130)ITEMP,LCURE,ICAT,IPF,AG,IPSG
  130 FORMAT(I3,1X,I2,1X,I1,1X,I2,1X,F4.2,1X,I2)
   70 CONTINUE
C
C  READ IN DATA FOR ANALYSIS
      IF(ANS2.EQ.1HN) GO TO 140
C  INPUT SAMPLE LENGTHS & WEIGHINGS
      PRINT*,'HOW MANY SAMPLES ARE THERE IN THIS BATCH?'
      READ(5,80)N
C  INPUT DATA FROM POLYMER SAMPLES
      WRITE(6,150)
      WRITE(6,160)
      WRITE(6,170)
  150 FORMAT(1X,'SPECIFY THE LENGTH,WEIGHTS IN AIR AND WATER,&')
  160 FORMAT(1X,'THE WEIGHT OF THE SUPPORT CRADLE FOR POLYMER')
  170 FORMAT(1X,'SAMPLES IN THAT ORDER')
      READ(5,*)(XL(J),WA(J),WW(J),XC(J),J=1,N)
C  READ IN DATA FROM VITREOUS CARBON SAMPLES
      WRITE(6,180)
      WRITE(6,190)
  180 FORMAT('SPECIFY THE SPECIMEN LENGTHS & REQUIRED WEIGHTS')
```

```
  190 FORMAT('FOR ANALYSIS OF VITREOUS CARBON SAMPLES')
      READ(5,*)(VCXL(K),VCWA(K),VCWW(K),VCXC(K),K=1,N)
  140 CONTINUE
      IF(ANS3.EQ.1HN) GO TO 200
C  INPUT MODULUS OF RUPTURE DATA
      PRINT*,'HOW MANY MODULUS OF RUPTURE TESTS DID YOU CARRY OUT?'
      READ(5,80)M
      PRINT*,'SPECIFY VALUES OF P,B AND D IN THAT ORDER'
      READ(5,210)((G(I,J),I=1,3),J=1,M)
  210 FORMAT(F6.2,2F8.6)
  200 CONTINUE
      IF(ANS4.EQ.1HN) GO TO 220
C  INPUT FRACTURE TOUGHNESS DATA
      PRINT*,'HOW MANY FRACTURE TOUGHNESS TESTS DID YOU CARRY OUT?'
      READ(5,80)L
      PRINT*,'SPECIFY VALUES OF P,A,B AND D IN THAT ORDER'
      READ(5,230)((Z(I,J),I=1,4),J=1,L)
  230 FORMAT(F6.3,3F8.6)
  220 CONTINUE
C
C  WRITE OUT BATCH CURING CONDITIONS
      IF(ANS1.EQ.1HN) GO TO 240
      WRITE(6,61)
      WRITE(6,250)
      WRITE(6,260)IBN
      WRITE(6,250)
   61 FORMAT(/)
  250 FORMAT(1X,'*********')
  260 FORMAT(1X,'*BATCH',I2,'*')
      WRITE(6,270)ITEMP
  270 FORMAT(1X,'CURING TEMPERATURE',1X,I3,' DEGREES CENTIGRADE')
      WRITE(6,280)LCURE
  280 FORMAT(1X,'CURED FOR',1X,I2,'HRS')
      WRITE(6,290)ICAT
  290 FORMAT(1X,I1,1X,'PER-CENT CATALYST ADDED')
      IF(IPF.GT.0) GO TO 300
      WRITE(6,310)
  310 FORMAT(1X,'NO PORE FORMER ADDED')
      GO TO 320
  300 CONTINUE
      WRITE(6,330)IPF
  330 FORMAT(1X,I2,' PER-CENT PORE FORMER ADDED')
  320 CONTINUE
      IF(AG.GT.0) GO TO 340
      WRITE(6,350)
  350 FORMAT(1X,'NO GRAPHITE ADDED')
      GO TO 360
  340 CONTINUE
      PG=(AG/(AG+100.0))*100.0
      WRITE(6,370)PG
      WRITE(6,380)IPSG
  370 FORMAT(1X,F5.2,1X,'PER-CENT GRAPHITE(BY WEIGHT)IN GREEN COMPOSITE'
     +)
  380 FORMAT(1X,'GRAPHITE PARTICLE SIZE,NOMINAL ',I2,' MICRONS')
  360 CONTINUE
```

```
  240 CONTINUE
C
C  ANALYSE DATA AND PRINT RESULTS
      IF(ANS2.EQ.1HN) GO TO 390
      CALL CYIELD(WA,VCWA,CY)
      CALL LOOLOO(XL,VCXL)
      CALL VSHRINK(WA,WW,XC,VCWA,VCWW,VCXC)
      CALL MIURA(VVC,VCWA,VCWW,VCXC,WA)
  390 CONTINUE
      IF(ANS3.EQ.1HN) GO TO 400
      CALL MOR(G,M,SIG)
  400 CONTINUE
      IF(ANS4.EQ.1HN) GO TO 410
      CALL FTUFF(Z,L,XK1C)
  410 CONTINUE
    1 CONTINUE
      WRITE(6,61)
      WRITE(6,444)
  444 FORMAT(1X,'GOODBYE,HAVE A NICE DAY!')
      STOP
      END
C
      SUBROUTINE SUM(G,TG)
C  CALCULATES THE SUM TOTAL OF AN ARRAY OF N VALUES
C  ************************
C  *VARIABLE CREATED     *
C  *TG=SUM TOTAL OF ARRAY*
C  ************************
      DIMENSION G(30)
      COMMON N
C  SET COUNTER TO ZERO
      TG=0.0
      DO 2 J=1,N
      TG=TG+G(J)
    2 CONTINUE
      RETURN
      END
C
      SUBROUTINE AVE(G,AG)
C  CALCULATES AVERAGE VALUE OF AN ARRAY OF N VALUES
C  ***************************
C  *VARIABLE CREATED         *
C  *AG=AVERAGE VALUE OF ARRAY*
C  ***************************
      DIMENSION G(30)
      COMMON N
      CALL SUM(G,TG)
      AG=TG/FLOAT(N)
      RETURN
      END
C
      SUBROUTINE CYIELD(WA,VCWA,CY)
C  CALCULATES CARBON YIELD FROM PYROLYSIS
C  ********************
C  *VARIABLE PRODUCED*
```

```
C  *CY=CARBON YIELD  *
C  ********************
      DIMENSION WA(30),VCWA(30)
      CALL SUM(WA,TWA)
      CALL SUM(VCWA,TVCWA)
      CY=(TVCWA/TWA)*100.0
      WRITE(6,15)CY
   15 FORMAT(1X,'CARBON YIELD=',F5.2,1X,'PER-CENT')
      RETURN
      END
C
      SUBROUTINE LOOLOO(XL,VCXL)
C  CALCULATES LINEAR SHRINKAGE DURING PYROLYSIS
C  ***********************
C  *VARIABLE CREATED    *
C  *XLS=LINEAR SHRINKAGE*
C  ***********************
      DIMENSION XL(30),VCXL(30)
      CALL SUM(XL,TXL)
      CALL SUM(VCXL,TVCXL)
      XLS=100.0-(TVCXL/TXL)*100.0
      WRITE(6,25)XLS
   25 FORMAT(1X,'LINEAR SHRINKAGE=',F5.2,1X,'PER-CENT')
      RETURN
      END
C
      SUBROUTINE VOL(VX,XWA,XWW,XXC)
C  CALCULATES THE VOLUME OF A SPECIMEN USING
C  A WATER DISPLACEMENT METHOD
C  *******************************
C  *DIMENSIONED VARIABLE PRODUCED*
C  *VX(K)=VOLUME OF SPECIMEN     *
C  *******************************
      DIMENSION VX(30),XWA(30),XWW(30),XXC(30)
      COMMON N
      DO 3 K=1,N
      VX(K)=XWA(K)-(XWW(K)-XXC(K))
    3 CONTINUE
      RETURN
      END
C
      SUBROUTINE VSHRINK(WA,WW,XC,VCWA,VCWW,VCXC)
C  CALCULATES THE VOLUME SHRINKAGE DURING PYROLYSIS
C  *********************
C  *VARIABLE PRODUCED  *
C  *VS=VOLUME SHRINKAGE*
C  *********************
      DIMENSION VP(30),WA(30),WW(30),XC(30)
      DIMENSION VVC(30),VCWA(30),VCWW(30),VCXC(30)
      COMMON N
      CALL VOL(VP,WA,WW,XC)
      CALL VOL(VVC,VCWA,VCWW,VCXC)
      CALL SUM(VP,TVP)
      CALL SUM(VVC,TVVC)
      VS=100.0-(TVVC/TVP)*100.0
```

```
      WRITE(6,35)VS
   35 FORMAT(1X,'VOLUME SHRINKAGE=',F5.2,1X,'PER-CENT')
      RETURN
      END
C
      SUBROUTINE MIURA(VVC,VCWA,VCWW,VCXC,WA)
C  CALCULATES BULK DENSITY AND AVERAGE POROSITY
C  OF THE AMORPHOUS CARBON PRODUCED
C  ************************************************
C  *               VARIABLES PRODUCED             *
C  *                                              *
C  *SIMPLE VARIABLES                              *
C  *AD=AVERAGE BULK DENSITY OF BATCH              *
C  *AP=AVERAGE POROSITY                           *
C  *                                              *
C  *DIMENSIONED VARIABLES                         *
C  *D=BULK DENSITY                                *
C  *P=POROSITY                                    *
C  ************************************************
      DIMENSION VVC(30),VCWA(30),VCWW(30),VCXC(30),D(30),P(30),WA(30)
       COMMON N,AG
      PVC=1.635
      PGC=2.267
      IF(AG.EQ.0.0)THEN
      C=PVC
      ELSE
      CALL CYIELD(WA,VCWA,CY)
      PG=(AG/(AG+100.0))*100.0
      XBARG=PG/(PG+(100.0-PG)*CY)*100.0
      XBARVC=1.0-XBARG
      WRITE(6,37)PG
   37 FORMAT(1X,F5.2,1X,'PER-CENT GRAPHITE(BY WEIGHT)IN GREEN COMPOSITE'
     +)
      XG=XBARG*100.0
      WRITE(6,56)XG
   56 FORMAT(1X,'YIELDS ',F5.2,1X,'PER-CENT GRAPHITE IN FIRED COMPOSITE'
     +)
      C=(XBARVC*PVC)+(XBARG*PGC)
      END IF
      CALL VOL(VVC,VCWA,VCWW,VCXC)
      DO 4 L=1,N
      D(L)=VCWA(L)/VVC(L)
      P(L)=100.0*(C-D(L))/D(L)
    4 CONTINUE
      CALL AVE(D,AD)
      CALL AVE(P,AP)
      WRITE(6,45)AD
      WRITE(6,55)AP
   45 FORMAT(1X,'BULK DENSITY=',F4.2,1X,'GCM-3')
   55 FORMAT(1X,'AVERAGE POROSITY=',F5.2,1X,'PER-CENT')
      RETURN
      END
C
      SUBROUTINE MOR(G,M,SIG)
C  CALCULATES MODULUS OF RUPTURE
```

```
C  ******************************
C  *DIMENSIONED VARIABLE PRODUCED*
C  *SIG=MOR                     *
C  ******************************
      DIMENSION G(3,30),SIG(30),XSIG(30)
C  SET TEST RIG SPAN
      A=35E-3
      DO 5 J=1,M
      P=G(1,J)
      B=G(2,J)
      D=G(3,J)
      XSIG(J)=(3*P*A)/(2*B*(D**2))
      SIG(J)=XSIG(J)/1E6
    5 CONTINUE
C  WRITE OUT RESULTS
      CALL STATS(SIG,M,ZMSIG,SDSIG,T90SIG)
      WRITE(6,65)ZMSIG
   65 FORMAT(1X,'MODULUS OF RUPTURE=',F6.2,' MNM-2')
      IF(M.LT.6)GO TO 75
      WRITE(6,85)SDSIG
   85 FORMAT(1X,'STANDARD DEVIATION=',F4.2,' MNM-2')
      IF(M.LT.10) GO TO 95
      WRITE(6,96)T90SIG
   96 FORMAT(1X,'90 PER-CENT CONFIDENCE INTERVAL OF MOR=(+OR-)',F4.2,'MN
     +M-2  ')
   95 CONTINUE
   75 CONTINUE
      RETURN
      END
C
      SUBROUTINE FTUFF(Z,L,XK1C)
C  CALCULATES FRACTURE TOUGHNESS,K1C
C  ************************************
C  *DIMENSIONED VARIABLES PRODUCED     *
C  *XK1C=FRACTURE TOUGHNESS            *
C  *W(2,J)=PARAMETERS FOR K1C EVALUATION*
C  *       W(1,J)=A/D RATIO            *
C  *       W(2,J)=Y CONSTANT           *
C  ************************************
      DIMENSION Z(4,30),XK1C(30),W(2,30),YK1C(30)
C  SET TEST RIG SPAN
      S=24E-3
      DO 6 J=1,L
      W(1,J)=Z(2,J)/Z(4,J)
      R=W(1,J)
      W(2,J)=1.93-3.07*R+13.66*(R**2)-23.98*(R**3)+25.22*(R**4)
    6 CONTINUE
C  CALCULATE K1C
      DO 7 LOU=1,L
      P=Z(1,LOU)
      A=Z(2,LOU)
      B=Z(3,LOU)
      D=Z(4,LOU)
      Y=W(2,LOU)
      YK1C(LOU)=(3*P*S*Y*(SQRT(A)))/(2*B*D**2)
```

```
      XK1C(LOU)=YK1C(LOU)/1E6
    7 CONTINUE
C  OUTPUT RESULTS
      CALL STATS(XK1C,L,ZMFT,SDFT,T9ØFT)
      WRITE(6,1Ø5)ZMFT
  1Ø5 FORMAT(1X,'K1C=',F6.4,' MNM-3/2')
      IF(L.LT.6) GO TO 115
      WRITE(6,125)SDFT
  125 FORMAT(1X,'STANDARD DEVIATION=',F6.4,' /MNM-3/2')
      IF(L.LT.1Ø)GO TO 115
      WRITE(6,99)T9ØFT
   99 FORMAT(' 9Ø PER-CENT CONFIDENCE INTERVAL OF K1C=(+OR-)',F6.4,'MNM-
     +3/2  ')
  115 CONTINUE
      RETURN
      END
C
      SUBROUTINE STATS(X,K,ZMX,SDX,T9ØX)
C  CALCULATES MEAN,STANDARD DEVIATION AND 9Ø PER-CENT
C  CONFIDENCE INTERVAL OF MEAN FROM AN ARRAY OF K VALUES
C  *********************************
C  *VARIABLES PRODUCED             *
C  *ZMX=MEAN VALUE OF ARRAY        *
C  *SDX=STANDARD DEVIATION OF MEAN*
C  *T9ØX=CONFIDENCE INTERVAL       *
C  *********************************
      DIMENSION X(3Ø),B(3Ø)
C  CALCULATE MEAN
      SUMX=Ø.Ø
      DO 8 I=1,K
      SUMX=SUMX+X(I)
    8 CONTINUE
      ZMX=SUMX/FLOAT(K)
      IF(K.LT.6) GO TO 135
C  CALCULATE SUM OF SQUARES
      SUMSQ=Ø.Ø
      DO 9 J=1,K
      B(J)=(X(J)-ZMX)**2
      SUMSQ=SUMSQ+B(J)
    9 CONTINUE
C  CALCULATE STANDARD DEVIATION
      SDX=SQRT(SUMSQ/FLOAT(K))
      IF(SDX.GT.ZMX/2.Ø)THEN
      WRITE(6,145)
      WRITE(6,155)
  145 FORMAT(1X,'THE SCATTER IN YOUR RESULTS IS TOO LARGE')
  155 FORMAT(1X,'SUGGEST YOU REPEAT THIS BATCH')
      GO TO 135
      ELSE
      GO TO 165
      END IF
  165 CONTINUE
C  CALCULATE 9Ø PER-CENT CONFIDENCE INTERVAL
      IF(K.LT.1Ø)GO TO 175
      A=Ø.Ø15
```

```
      C=1.635
      V=12Ø/(FLOAT(K)-1)
      ALPHA=A*V+C
      T9ØX=(ALPHA*SDX)/SQRT(FLOAT(K))
  175 CONTINUE
  135 CONTINUE
      RETURN
      END
```

C. Calculation of Particle Size Distribution from a Distribution of Section Diameters

C. 1. Introduction

A knowledge of the distribution of particle sizes is often required in the study of materials' processes. The complete distribution curve is generally too complicated for practical characterization of a particulate material. Because of the opacity of many composite materials, particle size distribution curves must usually be obtained from a two-dimensional plane of polish. The distribution of particulate sections may then be converted into a distribution of particle sizes by a mathematical method.

The most effective conversion method, rather than considering the experimentally determined distribution of section diameters as a continuous function, breaks it up into discrete size groups (class intervals). This method is called "reconstruction" of the sphere size distribution (131). The profile and particle sizes are represented in the form of a histogram. The particles within each interval (bin) of the histogram are considered to have the same diameter. Saltykov recommended between 7 and 15 sub-divisions. In the present work the number was extended to include up to 20, to account for the bin sizes produced by the image analyser, and not found to be detrimental to the results.

The number and sizes of the sections on the plane of polish can be counted and measured. Then the probable number and size of the spheres that give rise to the observed section distribution can be deduced from this

information. To facilitate this calculation, the distribution of section diameters is broken down into discrete size groups. If all the spheres are the same size:

$$N_V = \frac{N_A}{D_j} \qquad (C.1)$$

where N_V = number of particles in unit volume

N_A = number of sections in unit area

D_j = diameter of spheres.

n.b : N_A involves the number of sections of all sizes in unit area.

When sections of only one particular size d are counted a probability factor, to account for the arbitrary restriction that is imposed, must be introduced. Under these conditions, Eqn. (C.1) becomes

$$N_V = \frac{N_A(i,j)}{p} \quad \frac{1}{D_j} \qquad (C.2)$$

where p is the probability of the plane intersecting a sphere of diameter D_j so as to yield sections of size d and $N_A(i,j)$ is the number of sections of diameter d_i per unit area obtained from spheres of diameter D .

The coefficients based upon the probability term in Eqn. (C.2) are used in order to speed the calculation. The values of the coefficients are obtained from the probabilities of a random plane intersecting a sphere to give the various sizes of sections. In general, if a sphere of diameter D is intersected between distances h_i and $h_{(i-1)}$

from the centre, circular sections with diameters between d_i and $d_{(i-1)}$ will result. The situation is illustrated by the diagram in Fig. C.1. The probability of intersection of a random plane between h_i and $h_{(i-1)}$ is equal to the thickness h of the circular slice divided by the particle radius i.e.

$$p = \frac{h}{D_j/2} = \frac{h_{(i-1)} - h_i}{D_j/2} \qquad (C.3)$$

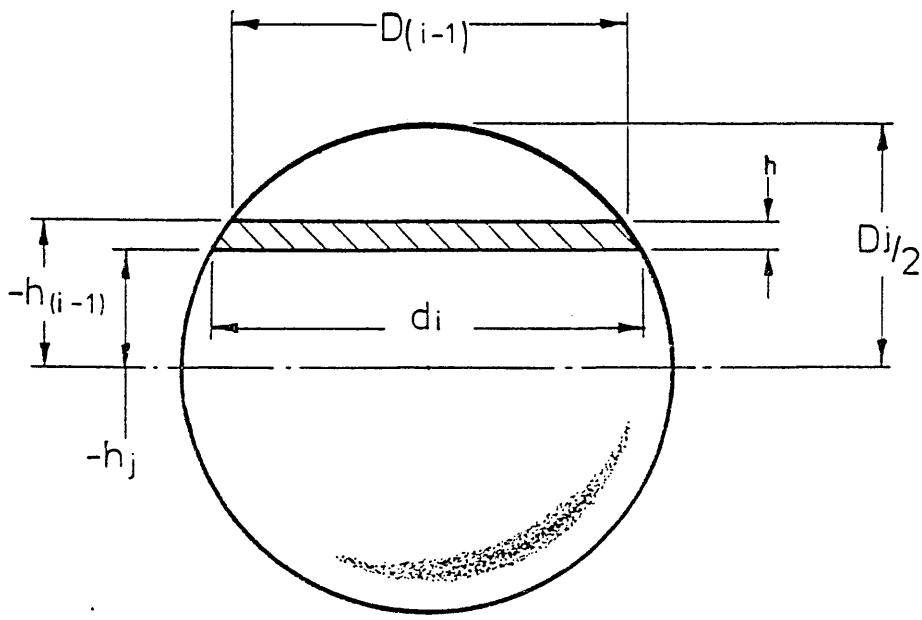


Fig. C.1 Intersection of a sphere by a random plane.

The conversion of particle sections to particle sizes involves a successive subtraction process. Consider a polydispersed system of spheres intersected by a plane. When the number of sections of the same diameter is counted, allowance must be made for the fact that some of the sections derive from spheres of larger diameters. The number of these latter sections must be subtracted from the total number in order to obtain those sections due only to spheres of one size. Fig. C.2 shows the problem involved here. The sections from spheres in the vertical columns have the same diameter, whereas the sphere diameters vary systematically between D_1 and D_5. The total number of sections of one size, for example the smallest size can be expressed as:

$$N_A(1) = N_A(1,1) + N_A(1,2) + N_A(1,3) + N_A(1,4) + N_A(1,5) \quad (C.4)$$

This equation states simply that the total number of sections of diameter d_1 per unit area consists of the sum of the separate contributions of this section size from spheres of the same size and all larger sizes. (nb. $N_A(i)$ is a measured quantity). Similar equations can be written for other sections and particle diameters.

It is desired to calculate the number of spheres of diameter D_5, D_4, D_3 etc. In order to do so, the number of sections of diameter d_5, d_4, d_3 etc., that arise only from the above spheres must be known. In this case Eqn. C.4 becomes:

$$N_A(5,5) = N_A(5)$$

$$N_A(4,4) = N_A(4) - N_A(4,5)$$

$$N_A(3\,3) = N_A(3) - N_A(4,3) - N_A(5,3)$$

and so on.

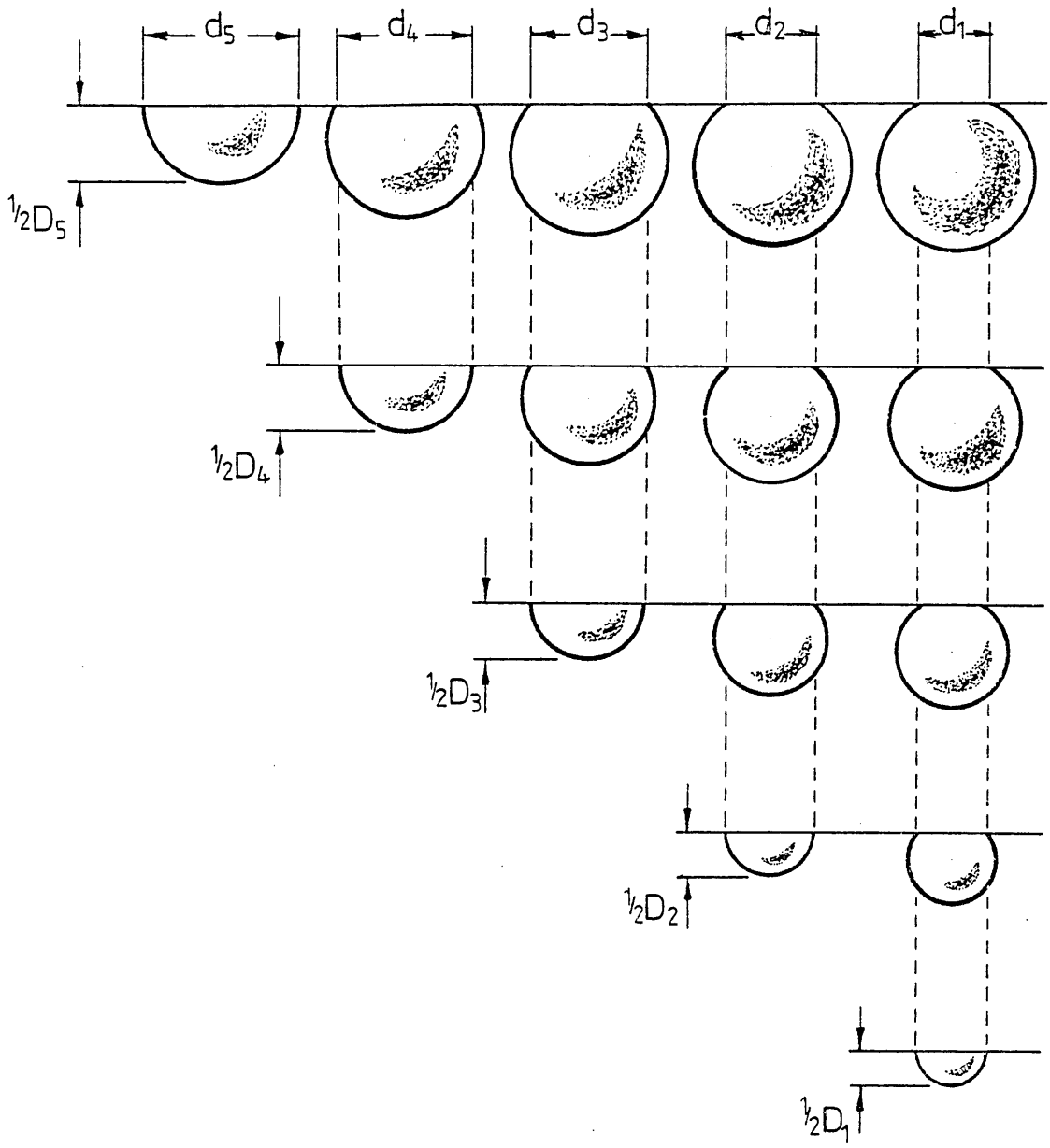


Fig. C.2 Schematic illustration of the contribution of spheres with diameters D_1 to D_5 to the total number of sections with diameters d_1 to d_5.

Since $N_A(5)$ is a measured quantity, $N_A(5,5)$ is known, and eqn. (C.2) gives N_V for the particles of the 5th size group. Continuing, since $N_V(5)$ is known, the value of $N_A(4,5)$ can be calculated. This number is then subtracted from $N_A(4)$, which gives $N_A(4,4)$ which in turn yields $N_V(4)$ via eqn. (C.2). The process can be continued down to the smallest particle size. It can be seen that each subtracted term depends on the previously calculated value of N_V and that the number of smallest particles may be inaccurate because of accumulated errors.

C. 2 Saltykov's Method

Saltykov's method makes two assumptions about the sphere diameters within the matrix. Firstly, that the largest diameter observed corresponds to that of the largest sphere present and, secondly, that there is a discrete distribution made up of m classes. The diameter of the largest spheres is D_m and the class width (Δ) introduced as

$$\Delta = D_m/m \qquad (C.5)$$

Table C.1 shows that the sphere diameters in each class are considered to assume a continuous distribution which is then broken up into classes. The numerical density of profiles in class i is

$$N_A(i) = \sum_{j=1}^{m} N_A(i,j) \qquad (C.6)$$

To find the dependence between the number of spheres in class j, $N_V(j)$ and the number of profiles that these spheres contribute to profile class i, $N_A(i,j)$, Saltykov put forward the following argument (Fig. C.3). Consider a sphere of diameter $j\Delta$. A section plane will generate a profile of diameter $i\Delta$ to $(i - 1)\Delta$, the range of profile class i, if the sphere centre is at a distance between h_i and $h_{(i-1)}$ from the section plane. Accordingly, all spheres of size class j having having their centre in a fictitious "slice" of thickness $(h_{(i-1)}-h_i)$ to either side of the section plane will contribute profiles to class i.

Class Number	Diameter	Numerical Density
	Particles	
1	Δ	$N_V(1)$
2	2Δ	$N_V(2)$
3	3Δ	$N_V(3)$
j	$j\Delta$	$N_V(j)$
m	$m\Delta$	$N_V(m)$
	Particles	
1	0 to Δ	$N_A(1)$
2	Δ to 2Δ	$N_A(2)$
3	2Δ to 3Δ	$N_A(3)$
i	$(i-1)\Delta$ to $i\Delta$	$N_A(i)$
m	$(m-1)\Delta$ to $m\Delta$	$N_A(m)$

Table C. 1. Definition of terms used in Saltykov method.

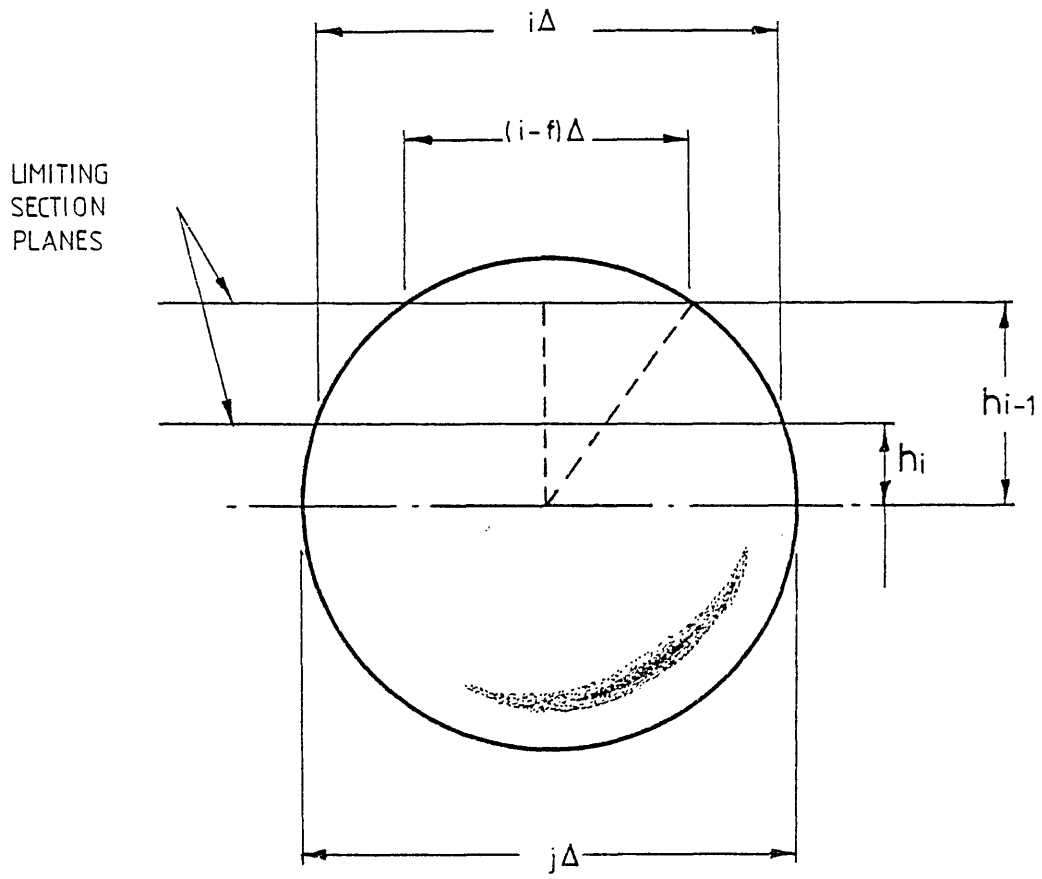


Fig. C. 3 Saltykov's model for deriving profile size frequency in class i.

Hence, $N_A(i,j) = N_V(j) \cdot 2(h_{i-1} - h_i)$ (C.7)

The factor 2 arises because each sphere has two regions from which profiles of this size can be cut. The volume between h_{i-1} and h_i can be expressed more conveniently in terms of particle diameter ($j\Delta$) and section diameters ($(i-1)\Delta$) to $i\Delta$

which gives:

$$N_{A(i,j)} = N_{V(j)}\,\Delta\left[\sqrt{j^2-(i-1)^2} - \sqrt{(j^2-i^2)}\right]$$
$$= \alpha_{ij}.\Delta.N_{V(j)} \qquad (C.8)$$

This is Saltykov's basic equation relating the number of sections in unit area to the number of particles in unit volume for spheres of one diameter. Equation (C.8) can be applied separately to each size group of spheres in the discrete distribution. The coefficients in the equation, relating the $N_{A's}$ to $N_{V's}$ are determined by successive substitution of integer values of i and j. Saltykov's procedure can be illustrated by considering a simple case where the particles are divided into three groups, that is j = 1, 2 and 3 where 3 is the largest and 1 the smallest. The equations for the three particle size groups can be written:

$$N_A(1) = N_A(1,1) + N_A(1,2) + N_A(1,3)$$
$$N_A(2) = N_A(2,2) + N_A(2,3)$$
$$N_A(3) = N_A(3,3)$$

substituting for eqn. (C.8):

$$N_A(1) = N_V(1)\Delta + K_{12}N_V(2)\Delta + K_{13}N_V(3)\Delta$$
$$N_A(2) = K_{22}N_V(2)\Delta + K_{23}N(2)\Delta$$
$$N_A(3) = K_{33}N_V(3)\Delta \qquad (C.9)$$

These three simultaneous linear equations may be solved for the unknowns ($N_V(1), N_V(2)$ and $N_V(3)$) in terms of the measured quantities ($N_A(1)$, $N_A(2)$ and $N_A(3)$):

$$N_V(1) = \frac{N_A(1)}{\Delta} - \alpha_{12}\frac{N_A(2)}{\Delta} - \alpha_{13}\frac{N_A(3)}{\Delta}$$
$$N_V(2) = \alpha_{22}\frac{N_A(2)}{\Delta} - \alpha_{23}\frac{N_A(3)}{\Delta}$$
$$N_V(3) = \alpha_{33}\frac{N_A(3)}{\Delta} \qquad (C.10)$$

This procedure can be followed for any desired number of groups. The general formula for $N_V(j)$ has the form

$$N_V(j) = \frac{\alpha_{j,i}\, N_A(i) - \alpha_{j,(i+1)}\, N_A(i+1) - \alpha_{j,(i+2)} N_{A(i+2)} - \ldots\ldots\ldots - \alpha_{j,m} N_{A(m)}}{\Delta} \quad (C.11)$$

where j = i and varies from 1 to m and m is equal to the total number of groups.

With this subtractive method, the errors tend to accumulate in the smaller particle size bins so the results for the small sizes will be inaccurate unless great care is taken with their measurement. In the computer program written to perform the Saltykov correction (section C.3) the section diameters were calculated from the areas of the circles measured. The bin sizes increase uniformly by area.

C.2 COMPUTER PROGRAM TO PERFORM SALTYKOV CORRECTION

```
      PROGRAM LOUISE2(INPUT,OUTPUT,TAPE5=INPUT,TAPE6=OUTPUT)
C
C
C  CONVERTS APARENT PORE SIZE TO TRUE PORE SIZE
C  USING SALTYKOV'S METHOD
      DIMENSION CELL(18),FREQ(18),PROBMA(18,18),SOLF(18)
      DIMENSION WSP1(18),FREQ1(18)
C  SET BIN SIZES
      DATA CELL/8.Ø6,7.81,7.57,7.31,7.Ø5,6.77,6.48,6.18,
     +        5.86,5.53,5.17,4.79,4.37,3.91,3.39,2.76,1.95,Ø.Ø1/
      M=17
       N=M+1
C READ IN DATA
      PRINT*,'TYPE IN FREQ VALUES STARTING WITH LARGEST CELL'
      READ(5,*)(FREQ1(I),I=1,M)
      DO 123 I=1,M
  123 FREQ(I)=FREQ1(I)
C  COMMENCE SALTYKOV CONVERSION
      CALL SALT(CELL,N,PROBMA)
      SUM2=Ø
      DO 4Ø I=1,M
      SUM2=SUM2+FREQ(I)
   4Ø WSP1(I)=FREQ(I)
      DO 6ØØ I=1,M
      FREQ(I)=FREQ(I)/SUM2
  6ØØ WSP1(I)=FREQ(I)
  5ØØ M1=M-1
      SUM1=Ø.Ø
      DO 3Ø J=1,M1
      SOLF(J)=WSP1(J)/PROBMA(J,J)
      SUM1=SUM1+SOLF(J)
      DO 1Ø I=1,M1
      WSP1(I)=WSP1(I)-PROBMA(I,J)*SOLF(J)
   1Ø CONTINUE
   3Ø CONTINUE
      SUM4=Ø.Ø
      SOLF(M)=1.Ø-SUM1
      DO 47 I=1,M
      WSP1(I)=SOLF(I)/(CELL(I)*CELL(I))
   47 SUM4=SUM4+WSP1(I)
      DO 48 I=1,M
   48 SOLF(I)=1ØØ.Ø*WSP1(I)/SUM4
      SUM3=Ø.Ø
C  CONVERT FROM NUMBER TO VOLUME WEIGHTED
      DO 124 I=1,M
      SOLF(I)=SOLF(I)*CELL(I)*CELL(I)*CELL(I)
  124 SUM3=SUM3+SOLF(I)
      DO 125 K2=1,M
  125 SOLF(K2)=SOLF(K2)*1ØØ.Ø/SUM3
C  CALCULATE MEAN PORE SIZE
      E=Ø.Ø
      DO 126 I=1,M
  126 E=CELL(I)*SOLF(I)+E
      E=E/1ØØ.Ø
C  OUTPUT RESULTS
```

```
      LU=5
  111 WRITE(LU,*)'SIZE DISTRIBUTION OF SPHERES CALCULATED BY'
      WRITE(LU,*)'            SALTYKOVS METHOD'
      WRITE(LU,800)
  800 FORMAT(//17X,'SIZE',18X,'INTERCEPTS',10X,'SPHERES %'/)
      WRITE(LU,900)(CELL(I),CELL(I+1),FREQ1(I),SOLF(I),I=1,M)
  900 FORMAT(13X,F8.3,' - ',F8.3,15X,F7.3,15X,F9.4)
      WRITE(LU,950)E
  950 FORMAT(//10X,'MEAN SIZE (VOLUME WEIGHTED) = ',F10.3//)
      IF(LU.NE.5)GO TO 75
      LU=6
      GOTO111
   75 CONTINUE
      WRITE(6,444)
  444 FORMAT(//33X,'FIN')
      END
C
      SUBROUTINE SALT(CELL,N,PROBMA)
C  CALCULATES PROBABILITY MATRIX
      DIMENSION CELL(18),PROBMA(18,18)
      M=N-1
      DO 12 I=1,M
      DO 12 J=1,M
   12 PROBMA(I,J)=0.0
      DO 20 J=1,M
      D=CELL(J)*CELL(J)
      DO 20 I=J,M
   20 PROBMA(I,J)=(CELL(I)*CELL(I)-CELL(I+1)*CELL(I+1))/D
      RETURN
      END
```

ACKNOWLEDGEMENTS

The author would like to express his thanks to all the members of the Department of Metallurgy and Materials Science at Imperial College who have assisted in various ways with this project. In particular the author wishes to thank his supervisor, Dr. J. Williamson, for his help and advice throughout the period of this work.

Thanks must also go to Mr. M. Janku of Berol Ltd., for his advice and the provision of the materials used in the work.

The author is extremely grateful to Mrs. A. Robinson (Angie) for fighting her way through my illegible scrawl and carefully typing this thesis. Thanks are due to Laurence Murray for his help with computing, Glenn Woodhead for his excellent draughting and stencil work and Steve Groves for reading and commenting on the text. The provision of a research studentship by the Science and Engineering Research Council and financial assistance from Berol Ltd., is gratefully acknowledged

Finally, I would like to thank my father Malcolm 'J.R.' Savage without whose help this would never have been finished.

REFERENCES

1. WILLIAMSON, J. Report on the development of sub. mm. pencil leads for Berol Ltd No.1, (1977).

2. JENKINS, G. M. and KAWAMURA, K. "Polymeric carbons, Carbon fibre, Glass and Char", Cambridge University Press (1976).

3. WILLIAMSON, J. Report on the development of sub. mm. pencil leads for Berol Ltd No.2, (1978).

4. SAVAGE, G. M. Progress Report to Berol Ltd. Oct. 1984.

5. GRIFFITH, A. A. Phil Trans. Roy. Soc. London, 221A (1920).

6. DALGLEISH, B. J. Dept. of Mat. Sci. and Min. Eng. University of California, Berkeley. Private Communication.

7. BILLMEYER, F. W. JR. Text Bk. of Polymer Science 2nd Ed. Wiley - Interscience p.486. (1970)

8. THE QUAKER OATS COMPANY, Technical Bulletin 131-A.

9. DELMONTE, J. "Furan Resins" p.138 "Modern Plastics Encyclopedia". McGraw-Hill Book Co., New Ycrk 1969.

10. DOWNING, P. A. The Chemical Engineer, p.272. (April, 1878).

11. BOQUIST, G. W. and BRADSTREET S. W. Project ARF. 6038.16 (Final Report) Armour Research Foundation, Illinois Institute of Technology (1961).

12. DUNLOP, A. P., and REINECK, E. A. Presented before the Organic Group at the Technical Conference of the American Chemical Society, Chicago Section, North Western University, (January 24 1947).

13. THE QUAKER OATS COMPANY, Technical Bulletin 205-B.

14. SAWYER, W. E. U.S. Patent 229, 335 (1880).

15. MANTELL, C. L., "Pyrolytic Graphite" p.162 in "Carbon and Graphite Handbook," Robert Krieger Publishing Company New York (1979).

16. HORTON, W. S. Proc. 5th. Conf. on Carbon Vol. 2, The MacMillian Co., New York, p.233. (1963).

17. BROWN, A. R. G. and WATT, W. "Industrial Carbon and Graphite." Society of Chemical Industry, pp. 86-100. (London 1958).

18. BROWN, A. R. G., HALL. A. R. and WATT. W. Nature, 172, 1145, (1953).

19. BROWN, A. R. G., WATT. W., POWELL. R. W. and TYE. R. P., Brit. J. appl. Phys., 7, 73 (1956).

20. PIRANI, M. and FEHSE, W. Z. Elektrochem, 29, 168 (1923).

21. FITZER, E., SCHAFER, W. and YAMADA, S. Carbon 7, 643. (1969).

22. YAMADA, S. and SATS, H. Nature 193, 162 (1964).

23. YAMADA, S., SATS, H. and ISHI, T. Carbon 2. (1964).

24. Belgian Patent No. 61 24 06.

25. Belgian Patent No. 62 03 81.

26. DAVIDSON, H. W., and LOSTY, H. W. GEC Journal 30, pp.22-30 (1963).

27. OTANI, S. Carbon 3, 31 (1965).

28. BRADSHAW, W., PINOLI, P., WATSEY, G. and WIGHT, H. 8th Carbon Conf., Buffalo p.80 (1967).

29. ISHIKAWA, T., TERANISHI, H. and HONDA, H. proc. 8th Carbon Conf. Buffalo (1967).

30. RIGGS, D. M. and DIFFENDORF. R. J. "Carbon '80" Preprints of the 3rd Int. Conf. on carbon, Baden-Baden, p.326 (1980).

31. MADORSKY, S. L. J., Res. Natl. Bur. Standards 51, 327 (1953).

32. MACKAY, H. A., Sandia Labs. Report SC-RR-68-651 (1969).

33. MADORSKY, S. L. J., "Thermal Degradation of Organic Polymers," Interscience, New York (1964).

34. FITZER, E. and SCHAFER, W. Carbon 8, 597 (1970).

35. OZANNE, N., Ph.D. Thesis, Grenoble (1968).

36. O'NEILL, H. J., BOQUIST, G. W., PUTCHER, R. E. and GRIFFITH, J. S., WADD TR.81-72 Vol. XL (1964).

37. BRAUN, W., Ph.D. Thesis, Institute fur Chem Technik, Universitat Karlsruke (1970).

38. YAMADA, S., SATS, H. and ISHI, T., Carbon 3, 253 (1965).

39. ROTHWELL, W. S., J. Appl. Phys. 39, 1840 (1968).

40. KLUG, H. P. and ALEXANDER, L. E. "X-Ray Diffraction procedures," Wiley, New York, (1954).

41. FISCHBACH, D. B., and KOTLEMSKY, W. V., Nasa. technical report 32, 842.

42. NODA, T. and INAGAKI, M., Carbon 1, 86 (1963).

43. NODA, T. and INAGAKI, M., Bull. Chem. Soc. Japan 37, 1534 (1964).

44. GUINIER, A. and FOURNET, G. "Small Angle Scattering of X-Rays," Wiley, New York, (1955).

45. RULAND, W. in "Chemistry and Physics of Carbon, Vol.4,"Ed. P. L. WALKER, DEKKER, New York (1969).

46. JENKINS, R. G. and WALKER, P. L., Jr. Carbon 14, 7 (1976).

47. ERGUN, S. and TIENSUU, V. H. Nature 183, 1668 (1959).

48. ERGUN, S. and ALEXANDER, L. E. Nature 195, 765 (1962).

49. KAKINOKI, T., KATADA, K., KARAWA, T. and IRO. J. Acta Cryst. 13, 171 (1960).

50. FURAKAWA, K. J., Acta Cryst. Japan 6, 107 (1964).

51. KAKINOKI, T. Acta Cryst. 18, 578 (1965).

52. TAKAHASHI, E., and WESTRUM, W. Proc. Tokyo Carbon Conf. (1970).

53. HALPIN, M. K. and JENKINS, G. M. Proc. Roy. Soc. London A313, 421 (1969).

54. JENKINS, G. M., KAWAMURA, K., and MAIN, L. Proc. Roy. Soc. London A327, 501 (1972)

55. SAXENA, R. R., and BRAGG, R. H. Carbon 16, 373 (1978).

56. BOSE, S., DAHMEN, U., BRAGG, R. H., and THOMAS J. J. Amer. Ceram. Soc. 61, 174 (1978).

57. FURUTA, T., SANADA, Y., and HONDA, H. Carbon 7, 510 (1969).

58. FISCHBACH, D. B., and RORABAUGH, M. E. High Temp. High Pressure 9, 199 (1977).

59. BOSE, S., and BRAGG, R. H. Carbon 19, 289 (1981).

60. NODA, T. and KATO, H. Carbon 3, 289 (1965).

61. FISCHBACH, D. B. Carbon 9, 193 (1971).

62. HALPIN, M. K. and JENKINS, G. M. Nature 218, 950 (1968).

63. DAS, S. Carbon 13, 33 (1975).

64. MEHROTRA, B., BRAGG, R. H. and RAO, A. S. J. Mat. Sci. 18, 2671 (1983).

65. HOLCOMBE, C. E. High Temp. Sci. 12, 63 (1980).

66. BHATIA, G. and AGGARWAL, R. K. J., Mat. Sci. 14, 1103 (1979).

67. OKADA, J. and TAKEWCHI, Y. Proc. 4th Conf. on Carbon, USA 1959, Pergamon Press. (1960).

68. WATT, W., BICKERDIKE, R. L., BROWN, A. R. G., JOHNSON, W. and HUGHES, G. Nuclear Power, p.86 (Feb. 1959).

69. YAMADA, S. "A Review of Glass like Carbons" Battelle Memorial Institute, Ohio (1968).

70. BOKROS, J. C. Carbon 15, 355 (1977).

71. BOKROS, J. C., LAGRANGE, L. D. and SCHOEN, F. J. "Chemistry and Physics of Carbon" 9, 103 WALKER. P. L. Jr., Ed. Dekker, New York (1972).

72. HAUBOLD, A. D., SHIM, H. S. and BOKROS, J. C. "Biocompatibility of Clinical implant materials" CRC Press. (1981).

73. MROZOWSKI, S. Proc. 1st and 2nd Carbon Conf. Univ. of Buffalo p.195 (1956).

74. SELDIN, E. J. Proc. 1st and 2nd Carbon Conf. Univ. of Buffalo p.217 (1956).

75. SELDIN, E. J. Proc. 3rd Carbon Conf. p.675, Pergamon Press. (1959).

76. COLLINS, F. M. Proc. 3rd Carbon Conf. p.659, Pergamon Press. (1959).

77. WEWERKA, E. M., WALTERS, K. L. and MOORE, R. H. Carbon 7 129 (1969).

78. DICKINSON, J. M. and WEWERKA, E. M. Carbon 8, 249 (1970).

79. DICKINSON, J. M. and WEWERKA, E. M. Carbon 11, 515 (1973).

80. RIESZ, C. H. and SUSMAN, S. Ex. Proc. 4th Conf. on Carbon (USA 1959) Pergamon, Press. (1960).

81. WINSLOW, F. H. MATRIYEK, W., and YAGER, W. A. "Industrial Carbon and Graphite" Soc. of Chem. Ind. London P.190 (1958).

82. KAMIYA, K. and INAGAKI, M. Carbon 11, 429 (1973).

83. KAMIYA, K., INAGAKI, M., MIZUTANI, M, and NODA, T. Bull. Chem. Soc. Japan; 41, 2169 (1968).

84. RICHERSON, D. W. "Modern Ceramic Engineering" Dekker, New York (1982).

85. MACKENZIE, J. K. Proc. Phys. Soc. (Lond.) B63, 2 (1950).

86. OROWAN, E. Rep. Prog. Phys. 12, 185 (1949).

87. DAVIDGE, R. W. "Mechanical Behaviour of Ceramics" Cambridge University Press. (1979).

88. GRIFFITH, A. A. Proc. 1st Int. Cong. on App. Mechanics p.55, J. Waltman, Delft (1924).

89. IRWIN, G. R. J. Appl. Mech. 24, 361 (1957).
OROWAN, E. Weld. S. London, 34, 1575 (1955).

90. MEREDITH, H., NEWEY, C. W. and PRATT. P. L. Proc. Br. Ceram. Soc. 20 229, (1972).

91. BENHAM, P. P. "Elementary Mechanics of Solids" Pergamon Press. (1965).

92. FELTHAM, P. "Deformation and Strength of Materials" (Butterworths, London 1966).

93. INGLIS, C. E. Trans. Inst. Nav. Archit. 55, 219 (1913).

94. HASHEMI, S. and WILLIAMS, J. G. J. Matt. Sci., 19, 3746 (1984).

95. PARIS, P. C. and SIH, G. C. ASTM Spc. Tech. Pub. No.381, 30-81.

96. EVANS, A. G. "Symp. on the Fracture Mechanics of Ceramics" Pennsylvania State Univ. Vol. 1 p.17 Plenum Press. New York (1973).

97. LEWIS, J.C., REDFERN, B. and COWLARD, F.C. Solid State Electronics 6, 251 (1963).

98. COWLARD, F.C., Design Eng 49. (March 1970),

99. BOKROS, J.C., AKINS, R.J., SHIM, H.S., HAUBOLD, A.D. and AGARWAL, N.K. "Carbon in Prosthetic Devices" P.237 in "Petroleum Derived Carbons" DEVINEY, M.L., and O'GRADY, T.M., Editors, American Chem. Sec. Soc. Washington D.C. (1976).

100. KAAE, J.L., Carbon 13, 246 (1975).

101. KAAE, J.L., J. Nucl Mater., 38, 42 (1971).

102. KAWAMURA, K. and JENKINS, G.M., J of Mats. Sci., 7, 1099 (1972).

103. KAAE, J.L., J. Biomed. Mat. Res. Vol. 6 P. 279 (1972).

104. STANITSKI, C.L. and MOONEY, V., J. Biomed. Mater. Res. Symp. 7, 97. (1973).

105. COWLARD, F.C. and LEWIS, J.C. J. of Mats. Sci. 2, 507, (1967).

106. FISCHBACH, D.B., Carbon 5, 565 (1967).

107. TAYLOR, R.E. and KLINE, D.E., Carbon 5, 607 (1967).

108. JENKINS, G.M. in 'Chemistry and Physics of Carbon, Vol. 11 ed. P.L. Walker, Dekker, New York (1973).

109. ANDREW, J.F. and SATO, S., Carbon 1, 225, (1964).

110. KAWAMURA, K. Ph.D. Thesis, University of Wales (1971).

111. BOKROS, J. C. In "Chemistry and Physics of Carbon," Vol. 5 Chap. 1 Ed. P. L. Walker, Dekker, New York (1969).

112. SATO, S. and ASAKURA, K. Private Communication to Yamada (1968).

113. JOHNSON, J. W. Appl. Polym. Symp. No. 9, 229 (1969).

114. SRAWLEY, J. E. and BROWN W. F. ASTM Spec. Tech. Pub. No. 410 (1966).

115. LEAKE, L. E. Met. and Mat. Sci. Dept. Imperial College (Private Communication).

116. SALTYKOV, S. A. "Stereometric Metallography" 2nd Ed. State Publishing House for Metals and Sciences. Moscow (1958).

117. RAUTAVUORI, J. and TORMALA, P. J. Mat. Sci. 14, 2020 (1979).

118. ZARZYCKI, J. C. R. Acad. Sci. Paris Ser. C. 278 (8), 487 (1974).

119. BINNS, D. B. "Science of Ceramics" Vol. 1 (G. H. STEWART Ed.) P.315 Academic Press., London (1962).

120. CLAUSSEN, N. J. Amer. Ceram. Soc. 59, 49 (1976).

121. DAVIDGE, R. W., and GREEN, T. J. J. Mat. Sci. 3, 629 (1968).

122. GREEN T. J. Ph.D Thesis, McMaster Univ. Hamilton Onterio, Canada. (1976).

123. PHILLIPS, D. C. and HARRIS, B., Ch. 2 in "Polymer Engineering Composites" (M. O. W. Richardson Ed.). Applied Science, London (1977).

124. LANGE, F. F. Phil. Mag. 22, 983 (1970).

125. OWEN, A. B. J. Mat. Sci. 14, 2523 (1979).

126. MOLONEY, A. C., KAUSCH, H. H. and STIEGER, H. R. J. Mat. Sci. 19, 1125 (1984).

127. MORGAN, S. W. K. "Zinc and its alloys" Macdonald and Evans (1977).

128. ROBBINS, J. M. and WEI, G. C. Am. Ceram. Soc. Bull. 64(5), 691 (1985).

129. MARKOVIC, V. and MARINKOVIC, S. Carbon 8, 329 (1980).

130. LINDLEY, D. V. and MILLER, J. C. P. "Cambridge Elementry Statistical Tables" Camb. Univ. Press., (1958).

131. WEIBEL, E. R. "Stereological Methods Vol. 2" Accad. Press. inc. (London Ltd.) (1980).

132. PERRET, R. and RULAND W. J. APPL. CRYST. 5, 183 (1972)

133. WIGNALLS, G. D. and PINGS, C. J. CARBON 12, 51 (1974)

134. SCHEHL, R.R. and ERGUN, S. CARBON 11, 127 (1973)

135. ERGUN, S. Chem. + Physics of Carbon vol 3. p. 211 Marcel Dekker, New York (1968)